VATTENFALL

KME 508 FURNACE WALL CORROSION IN BIOMASS FIRED BOILERS

U 12-62

2013-04-24 PR.263.1.9

Department: Chemistry and Materials technology
Author: Annika Stålenheim
Security class: None [C1]
Attention: Pamela Henderson, KME 508 Project group

ANALYSIS OF DEPOSITS FROM STEVEN'S CROFT

1 STEVEN'S CROFT BOILER

Stevens Croft is a 40 MWel bubbling fluidised bed boiler built by Kvaerner Power, operated by E.ON and located in Southern Scotland. The plant was taken into operation in 2007 and is the largest biomass power plant in Scotland. The steam data are 137 bar / 537℃ and the fuel consists of a mixture of forest fuel, saw-mill residues and waste wood.

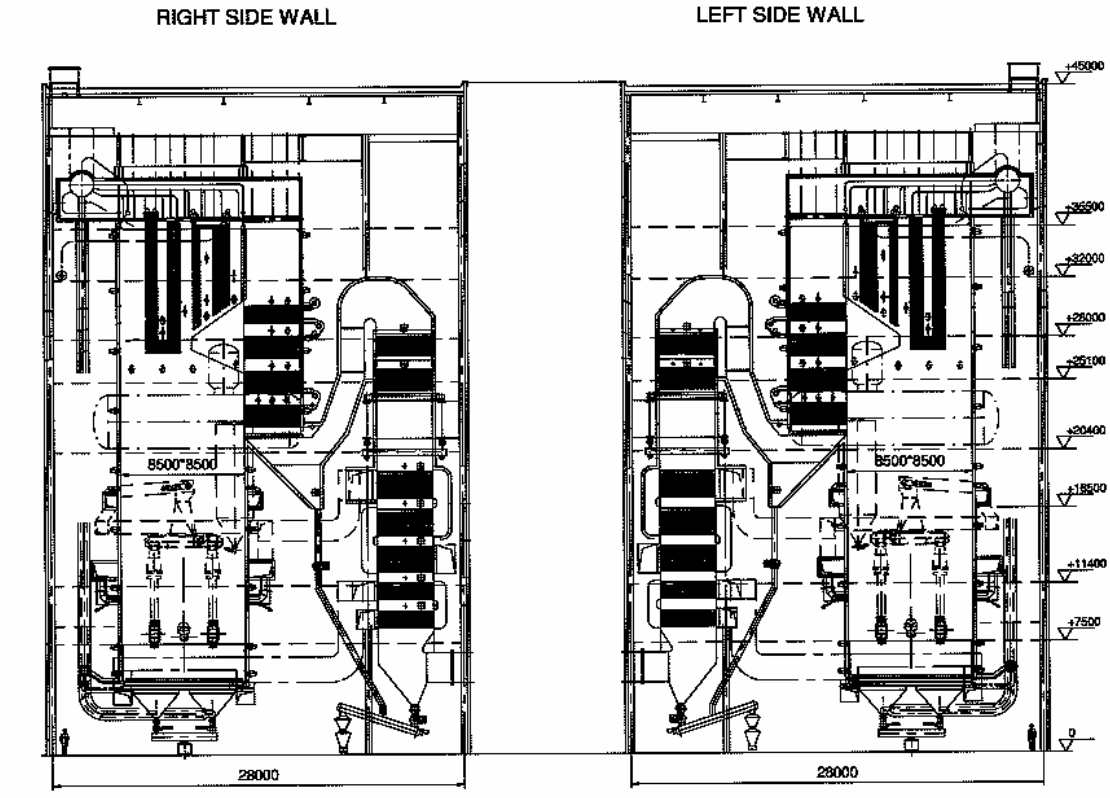

Figure 1 Schematic of Steven's Croft boiler

VATTENFALL RESEARCH AND DEVELOPMENT AB

ADDRESS
SE-814 26 Älvkarleby, Sweden

TELEPHONE
+46 26 835 00

VAT NUMBER
SE556390-5891

VISITING ADDRESS
Älvkarleby Laboratory

TELEFAX
+46 26 836 70

E-MAIL
utveckling@vattenfall.com

The boiler is similar to Idbäcken P3 which is also a bio fuelled BFB of the same size. However, the fuel used at Idbäcken is 100% waste wood, resulting in somewhat higher levels of contaminants in the fuel such as chlorine, alkali and heavy metals. Analysis of some selected elements in the fuels from the two plants is shown in Table 1 below. A full analysis for the Steven's Croft fuel is presented in Appendix A.

Table 1 Fuel analyses for Steven's Croft and Idäcken P3

	Steven's Croft	**Idbäcken P3**	
Al	1237	1700	mg/kg ts
K	1193	1330	mg/kg ts
Na	647	1180	mg/kg ts
Pb	127	156	mg/kg ts
Cu	12,5	39,6	mg/kg ts
Zn	83,5	107	mg/kg ts
Cl	0,09	0,07	% ts
S	0,04	0,125	% ts
Moisture 105℃	46,1	33,7	%
Ash 550℃	4,8	8,8	% ts

2 DESCRIPTION OF DEPOSIT SAMPLES

Samples have been taken from two levels in the boiler, level 1 at 3 m and level 5 at 25 m, from all four sides of the boiler. Level 5 is above the tertiary air inlets. Deposits have been scraped off the furnace walls giving fairly small pieces to analyse, most of them 2-10 mm. The samples have been analysed with SEM-EDX. Several pieces of deposit have been analysed for each sample and, when possible, both the brown bulk of the deposit as well as the black/red part that has been facing the tube has been investigated. The aim has been to analyse an area of ~2.5*2 mm, but in some cases, especially for the parts that have been facing the tube, the samples have been smaller than that. The magnification used has been 50X and the accelerating voltage has been 20kV for all samples.

Eleven samples were received from Steven's Croft: These were:

Level 1 – 3m

Sample 100	front wall above refractory
Sample 101	left wall above fuel inlet chute
Sample 102	rear wall above refractory
Sample 103	right wall above fuel chute

Level 5 - 25m (Above the tertiary air inlets)

Sample 1	right hand side
Sample 2	middle
Sample 5	left wall – middle
Sample 6	left wall – front wall side
Sample 8	front wall – left hand side
Sample 9	rear wall – left of nose tip
Sample 10	rear wall – middle o f nose tip

Figure 2 and Figure 3 shows typical appearance of the samples. In Figure 3 the composition of the surfaces analysed is also shown. As can be seen, the Fe content is high on the black/red part that has been facing the tube, indicating that this is mainly corrosion products from the tube.

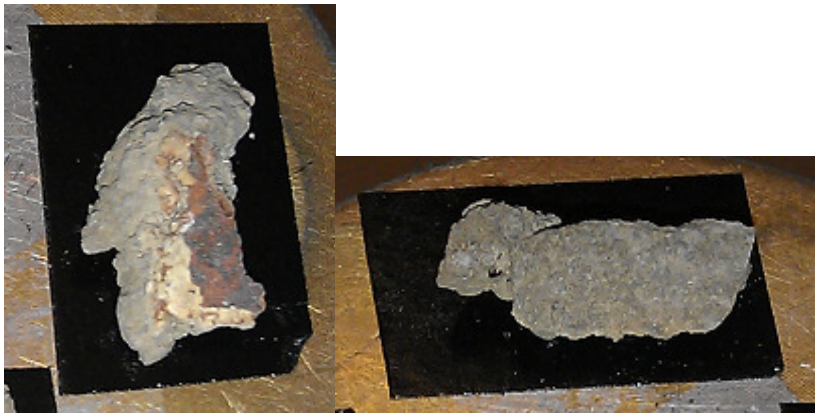

Figure 2 Sample 1 (level 5, 25 m right hand side) The image to the left is of a piece with oxide from tube (red/black) and the image to the right is of the side that has been facing the flue gases. The size of the black tape is ~1*1.5 cm

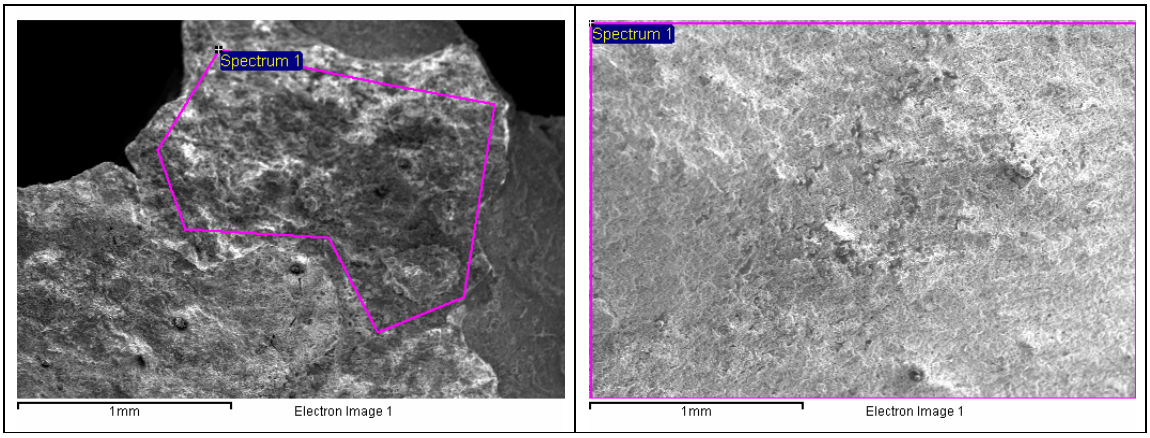

Figure 3 Sample 1 (level 5, 25 m right hand side) Pictures taken with the SEM. Surfaces analysed with EDX marked. The image to the left is of oxide that has been facing the tube and the image to the right is of the brown part that has been facing the flue gases. Composition of the surfaces indicated in the pictures is shown below.

Element	Weight%	Atomic%		Element	Weight%	Atomic%
O	40.49	66.24		O	45.52	63.97
Na	2.42	2.76		Na	6.87	6.72
Mg	0.56	0.60		Mg	1.01	0.94
Al	0.46	0.45		Al	1.26	1.05
Si	1.58	1.47		Si	3.62	2.90
P	-	-		P	0.74	0.54
S	4.38	3.57		S	12.50	8.77
Cl	0.18	0.13		Cl	0.40	0.25
K	5.39	3.61		K	13.46	7.74
Ca	1.51	0.98		Ca	8.47	4.75
Ti	0.23	0.12		Ti	1.36	0.64
Mn	0.45	0.22		Mn	-	-
Fe	42.36	19.85		Fe	1.49	0.60
Zn	-	-		Zn	3.28	1.13

3 OUTER LIGHT BROWN PART OF DEPOSIT

The dominating species in the outer, light brown part of the deposit are Ca, K, S, Na, Si, Zn and in some cases Pb. In the samples from level 1 there are also substantial amounts of Cl and more Zn than in the level 5 samples. (Figure 4, Figure 5, Table 2 and Table 3)

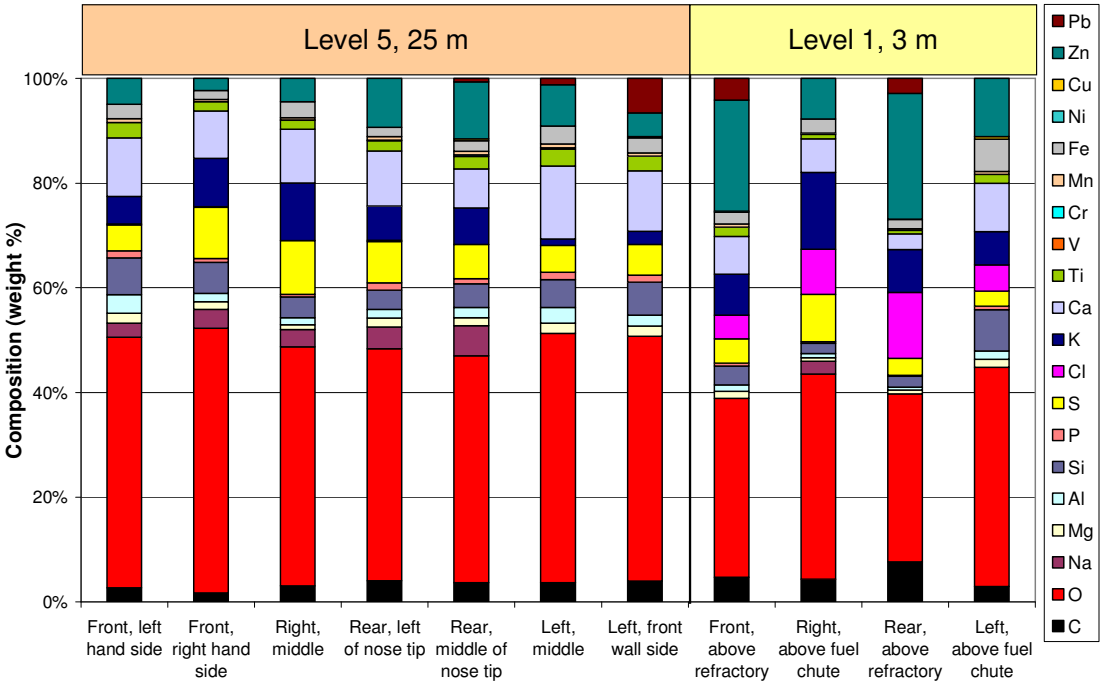

Figure 4 Composition of deposit samples from Steven's Croft, outer light brown part of deposit

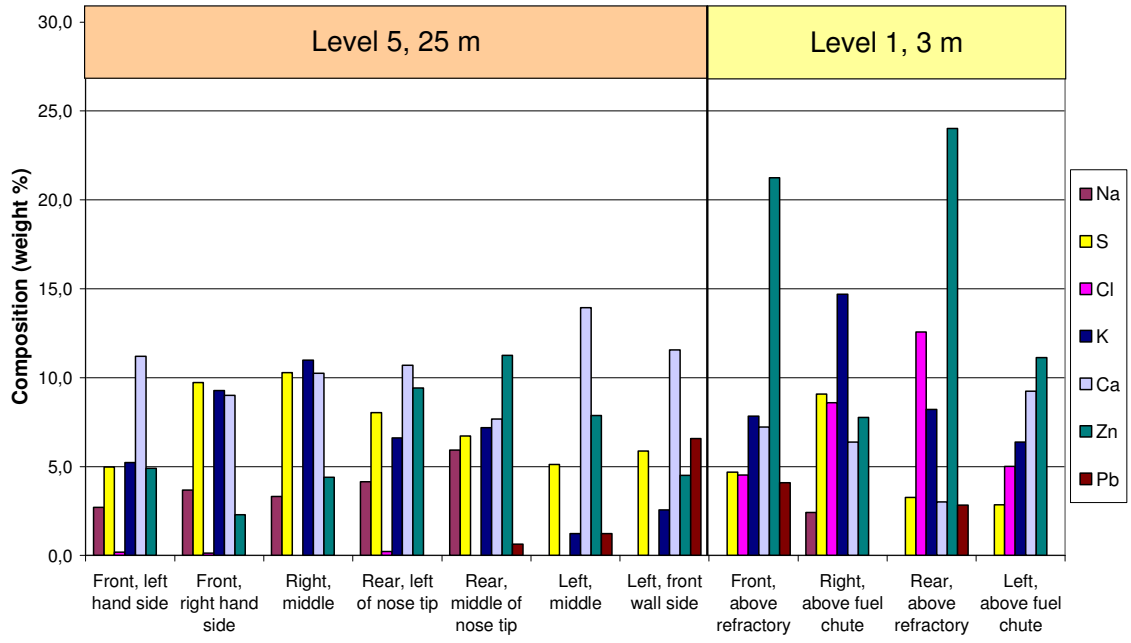

Figure 5 Content of some selected elements in deposit samples from Steven's Croft, outer, light brown part of deposit

Table 2 Average composition, weight %, level 5 (25 m), light brown part of deposit

	Front, left hand side	Front, right hand side	Right, middle	Rear, left of nose tip	Rear, middle of nose tip	Left, middle	Left, front wall side
C	2,7	1,7	3,1	4,1	3,8	3,6	4,0
O	47,9	50,5	45,7	45,0	44,7	47,7	46,8
Na	2,7	3,7	3,3	4,2	5,9	0,0	0,0
Mg	1,9	1,5	0,9	1,8	1,6	2,0	1,9
Al	3,6	1,6	1,3	1,7	2,0	2,9	2,1
Si	7,0	6,0	4,0	3,7	4,7	5,3	6,3
P	1,3	0,7	0,5	1,4	1,0	1,4	1,3
S	5,0	9,7	10,3	8,0	6,7	5,1	5,9
Cl	0,2	0,1	0,0	0,2	0,0	0,0	0,0
K	5,2	9,3	11,0	6,6	7,2	1,2	2,6
Ca	11,2	9,0	10,2	10,7	7,7	13,9	11,6
Ti	2,9	1,8	1,7	2,0	2,5	3,3	2,8
Cr	0,0	0,0	0,1	0,1	0,3	0,3	0,0
Mn	0,7	0,4	0,4	0,7	0,7	0,7	0,6
Fe	2,8	1,7	3,1	1,9	2,1	3,4	2,8
Cu	0,0	0,0	0,0	0,0	0,4	0,0	0,3
Zn	4,9	2,3	4,4	9,4	11,3	7,9	4,5
Pb	0,0	0,0	0,0	0,0	0,6	1,2	6,6

Table 3 Average composition, weight %, level 1 (3 m), outer light brown part of deposit

	Front, above refractory	Right, above fuel chute	Rear, above refractory	left, above fuel chute
C	4,7	4,3	7,7	3,0
O	34,2	39,2	32,1	41,9
Na	0,0	2,4	0,0	0,0
Mg	1,3	0,7	0,7	1,5
Al	1,2	0,8	0,6	1,6
Si	3,6	2,0	2,1	7,8
P	0,5	0,3	0,2	0,7
S	4,7	9,1	3,3	2,9
Cl	4,5	8,6	12,6	5,0
K	7,9	14,7	8,2	6,4
Ca	7,2	6,4	3,0	9,2
Ti	1,8	0,8	0,6	1,7
Cr	0,0	0,0	0,0	0,0
Mn	0,6	0,3	0,3	0,6
Fe	2,2	2,7	1,8	6,2
Cu	0,2	0,0	0,1	0,4
Zn	21,2	7,8	24,0	11,1
Pb	4,1	0,0	2,8	0,0

4 BLACK PART FACING WATERWALL TUBE

Black and in some cases partly rust red parts of the deposit have also been analysed. This is parts that have been facing the tube and that probably contain corrosion products and oxide from the tube surface. As for the outer part of the deposit, the chlorine content is higher in the samples from level 1 than in the samples from level 5.

On the samples from level 5, the dominating species except for Fe are S, K and Na, whereas on the samples from level 1, there is also a high content of Cl and less S.

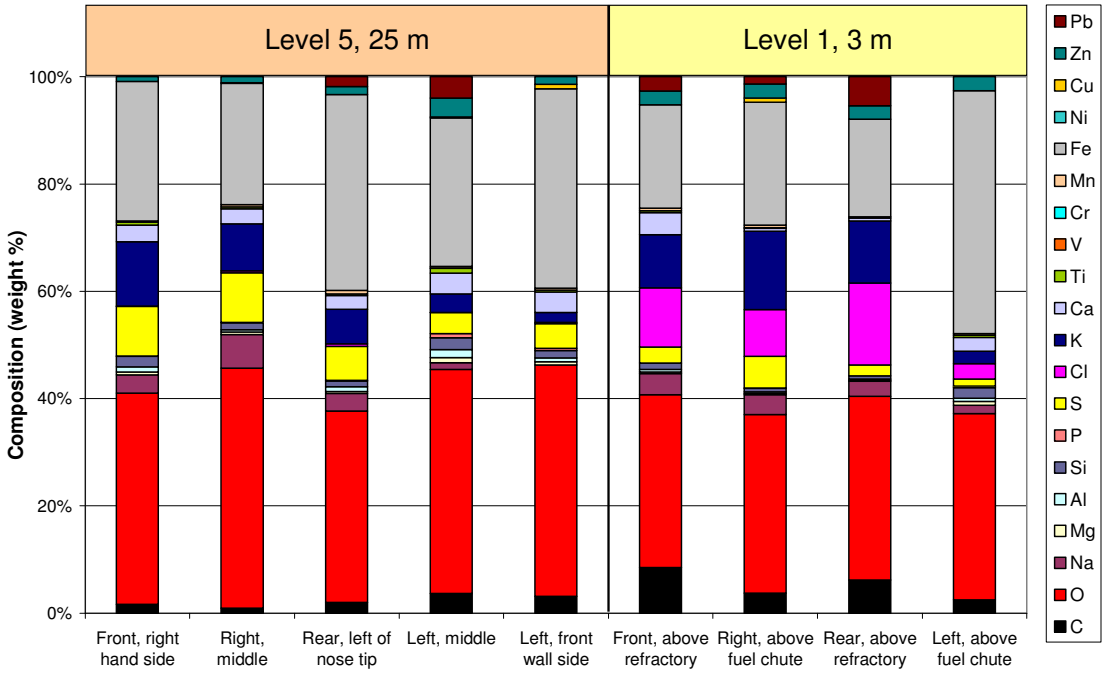

Figure 6 Composition of deposit samples from Steven's Croft, inner black part of deposit

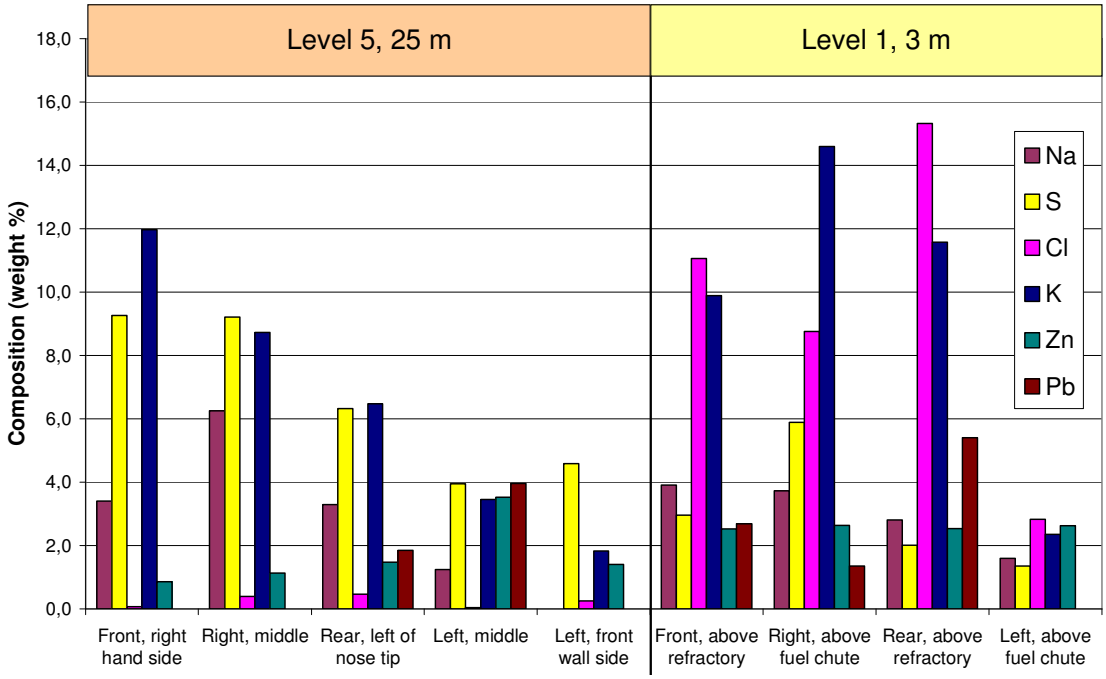

Figure 7 Content of some selected elements in deposit samples from Steven's Croft, inner, black part of deposit

Table 4 Average composition, weight %, levels 5 (25 m) and 1 (3 m), inner black part of deposit

	Level 5, 25 m					Level 1, 3 m			
	Front, right hand side	Right, middle	Rear, left of nose tip	Left, middle	Left, front wall side	Front, above refractory	Right, above fuel chute	Rear, above refractory	Left, above fuel chute
C	1,6	1,0	2,0	3,7	3,1	8,5	3,8	6,2	2,5
O	39,4	44,7	35,7	41,8	43,1	32,2	33,3	34,2	34,7
Na	3,4	6,3	3,3	1,2	0,0	3,9	3,7	2,8	1,6
Mg	0,6	0,5	0,4	1,0	0,6	0,3	0,2	0,2	0,7
Al	0,9	0,4	0,8	1,5	0,7	0,5	0,3	0,3	0,6
Si	2,0	1,3	1,1	2,2	1,4	1,2	0,7	0,6	2,0
P	0,1	0,1	0,1	0,8	0,4	0,0	0,1	0,0	0,3
S	9,3	9,2	6,3	3,9	4,6	3,0	5,9	2,0	1,4
Cl	0,1	0,4	0,5	0,0	0,3	11,1	8,8	15,3	2,8
K	12,0	8,7	6,5	3,5	1,8	9,9	14,6	11,6	2,3
Ca	3,1	2,8	2,6	3,9	3,8	4,1	0,6	0,5	2,5
Ti	0,5	0,3	0,3	0,9	0,4	0,4	0,1	0,2	0,4
Cr	0,0	0,0	0,0	0,1	0,0	0,0	0,0	0,0	0,0
Mn	0,2	0,4	0,7	0,3	0,3	0,5	0,5	0,0	0,3
Fe	26,0	22,6	36,5	27,7	37,2	19,3	22,9	18,2	45,3
Cu	0,0	0,1	0,0	0,2	0,9	0,0	0,7	0,0	0,0
Zn	0,9	1,1	1,5	3,5	1,4	2,5	2,6	2,5	2,6
Pb	0,0	0,0	1,8	4,0	0,0	2,7	1,4	5,4	0,0

5 COMPARISON OF INSIDE AND OUTSIDE OF DEPOSIT

The inside of the deposit clearly contains more iron than the outside. The outer part of the deposit contains more Ca, Zn and Si and the level 5 samples also contain some more Al, Mg, Ti, P and Mn on the outside than on the inside.

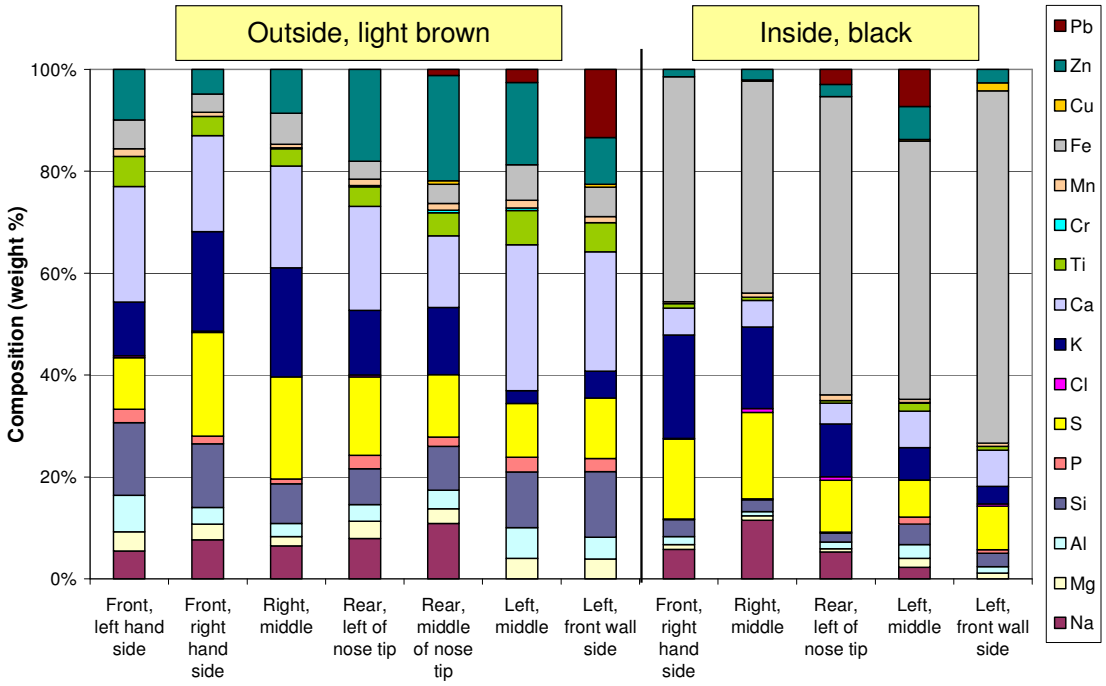

Figure 8 Composition in weight % of deposit samples from Steven's Croft, level 5, 25m

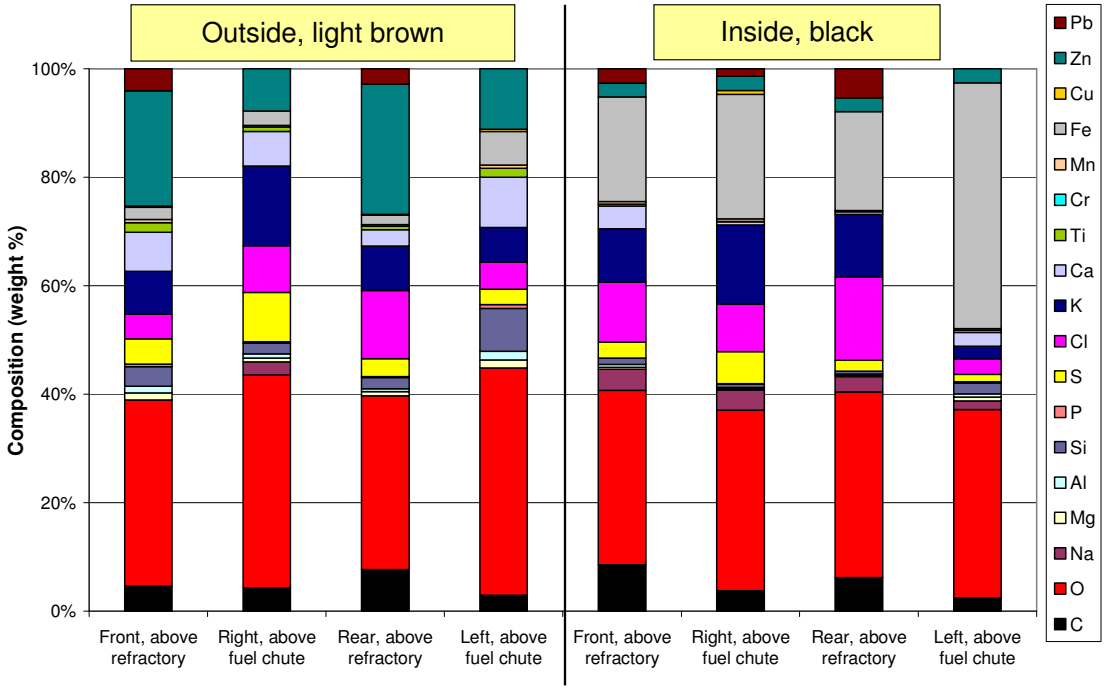

Figure 9 Composition in weight % of deposit samples from Steven's Croft, level 1, 3 m

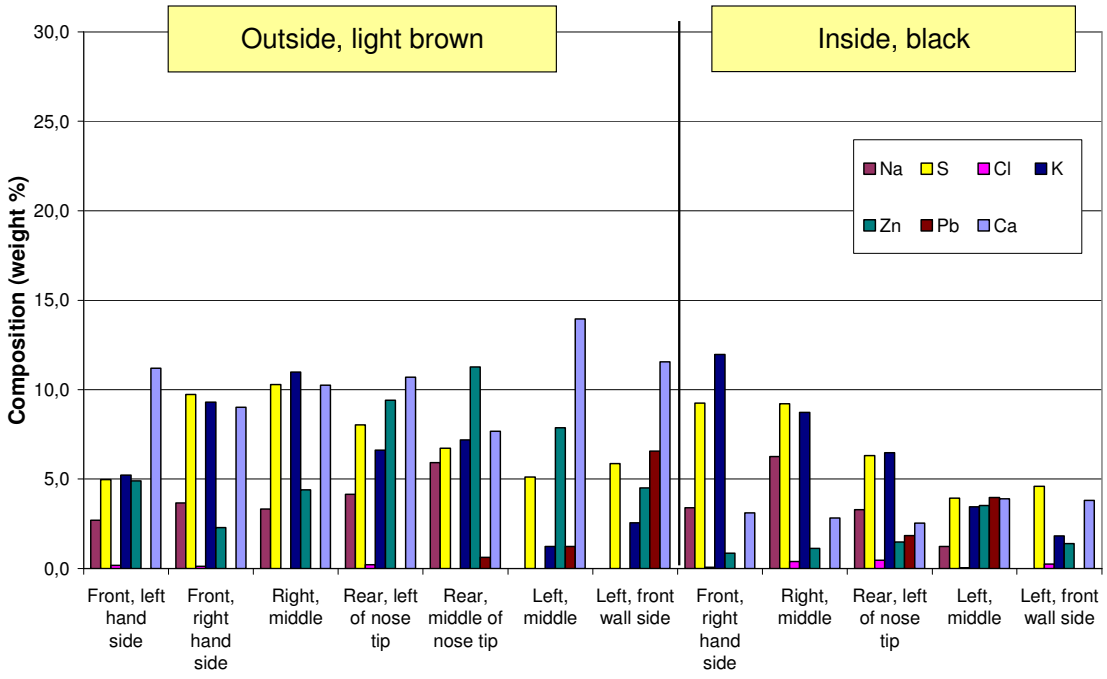

Figure 10 Content of some selected elements in deposit samples from Steven's Croft, level 5, 25m

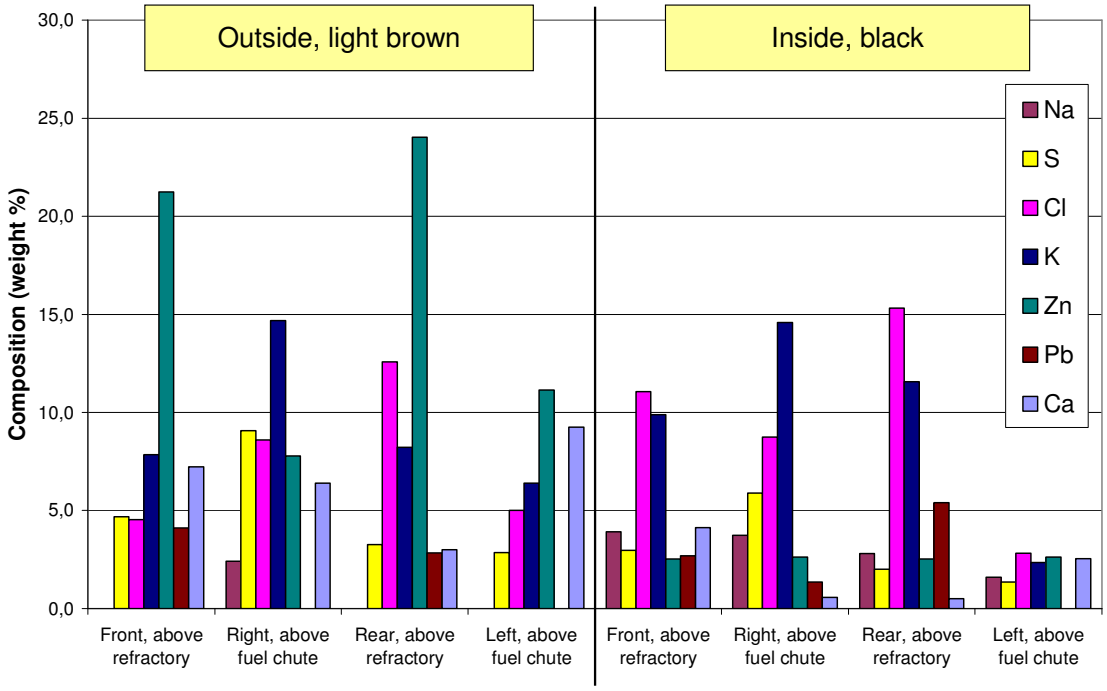

Figure 11 Content of some selected elements in deposit samples from Steven's Croft, level 1, 3 m

6 DETAILED STUDY OF INNER PART OF DEPOSIT

In some positions, areas that looked like melts were found. These melts had different compositions, mainly Na and Cl (Figure 12), mainly K and Cl (Figure 15), or mainly Al (Figure 13 and Figure 14). In one sample, a particle of crystallised KCl was identified. (Figure 16)

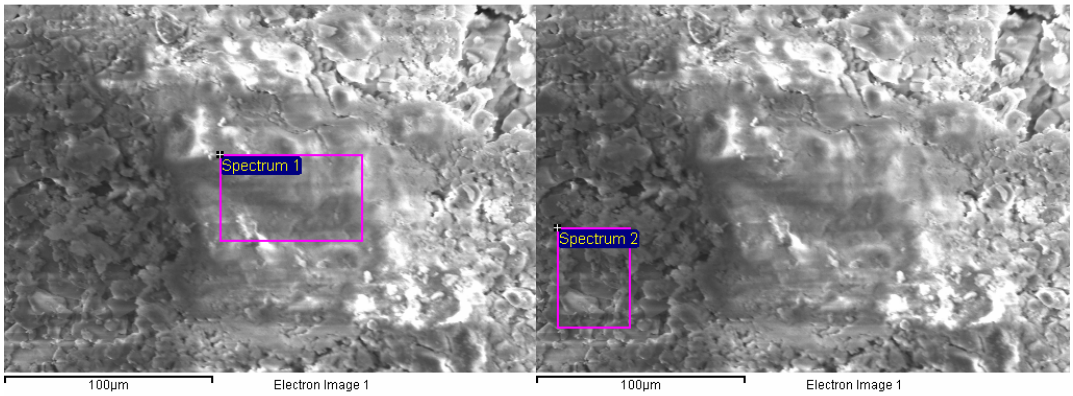

Figure 12 Sample 100 (level 1, 3 m front wall above refractory), black part of deposit that was facing tube

Element	Weight%	Atomic%
O	9.71	16.88
Na	30.79	37.27
Si	0.26	0.26
S	3.49	3.03
Cl	47.30	37.13
K	5.38	3.83
Ca	1.07	0.74
Zn	2.00	0.85

Element	Weight%	Atomic%
C	2.76	5.35
O	35.49	51.74
Na	9.26	9.39
Mg	0.15	0.14
Al	0.21	0.18
Si	0.43	0.36
S	14.23	10.36
Cl	9.55	6.29
K	23.81	14.20
Ca	2.08	1.21
Ti	0.17	0.08
Fe	0.48	0.20

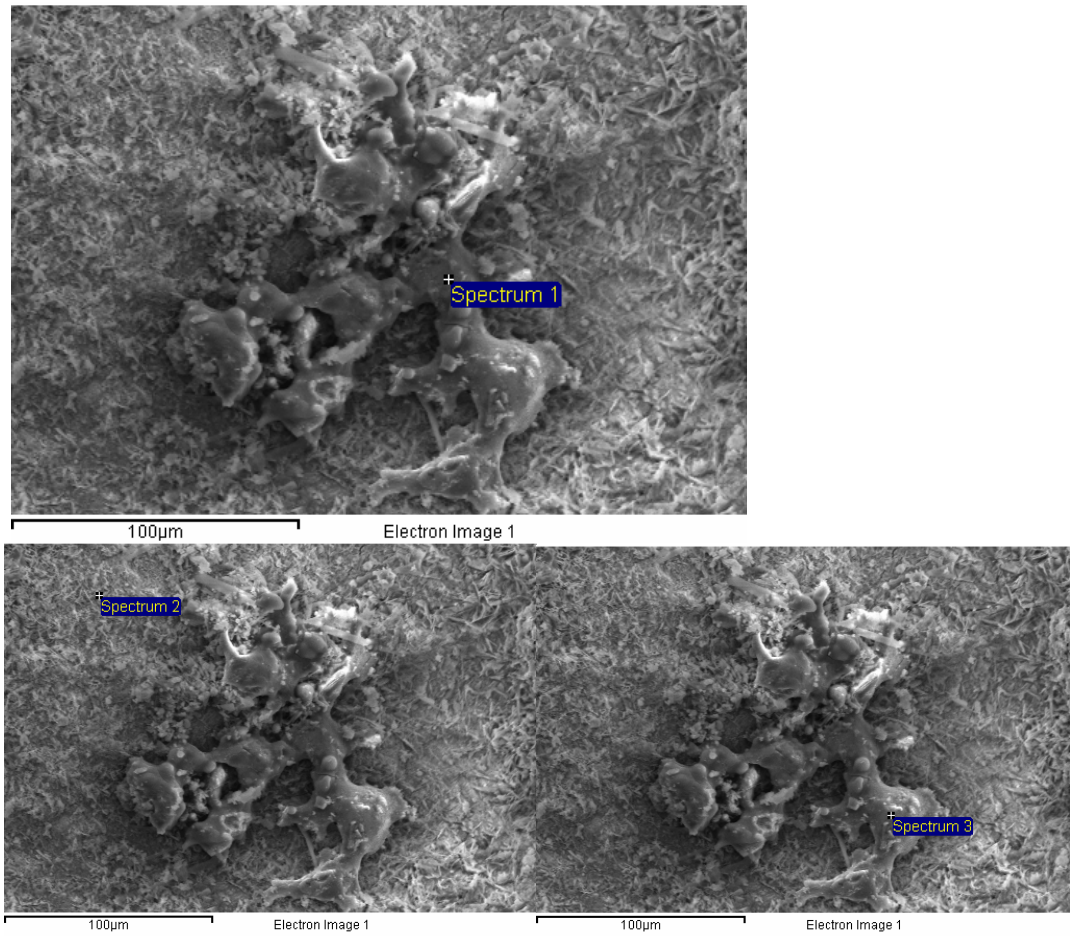

Figure 13 Sample 9 (level 5, 25m rear wall – left of nose tip) red/black part of deposit that was facing tube

	Spectrum 1	
Element	Weight%	Atomic%
C	9.40	16.78
O	22.25	29.82
Na	0.44	0.41
Al	64.77	51.47
Si	0.33	0.25
S	0.50	0.33
Cl	0.57	0.35
K	0.17	0.09
Ca		
Cr		
Mn		
Fe	0.98	0.38
Zn		
Ag L	0.58	0.12

Spectrum 2	
Weight%	Atomic%
4.24	9.11
39.32	63.38
0.65	0.73
0.31	0.28
1.51	1.22
0.46	0.34
0.61	0.40
0.94	0.61
0.22	0.11
1.27	0.60
49.46	22.84
1.00	0.39

Spectrum 3	
Weight%	Atomic%
9.75	18.34
12.58	17.77
0.18	0.18
74.67	62.53
0.41	0.33
0.18	0.13
1.32	0.53
0.90	0.19

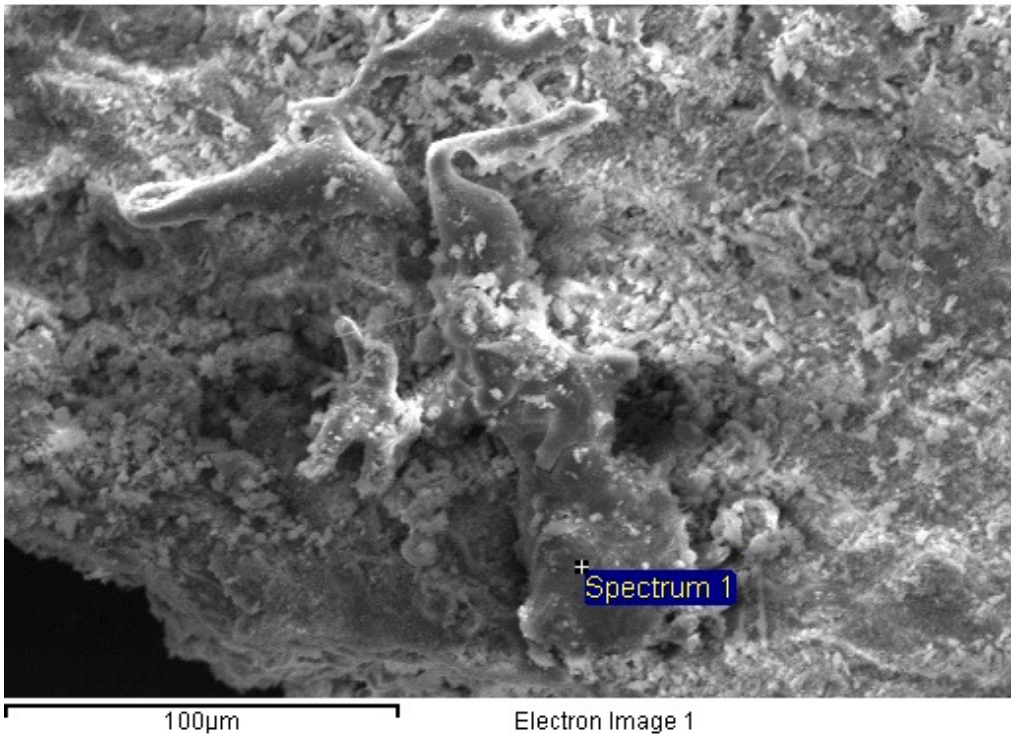

Figure 14 Sample 9 (level 5, 25m rear wall – left of nose tip) red/black part of deposit that was facing tube

Element	Weight%	Atomic%
C	8.56	15.83
O	18.16	25.19
Na	0.69	0.67
Al	67.41	55.45
Si	0.31	0.25
S	1.82	1.26
Cl	0.32	0.20
K	0.38	0.22
Ca	0.86	0.48
Fe	0.87	0.35
Ag L	0.62	0.13

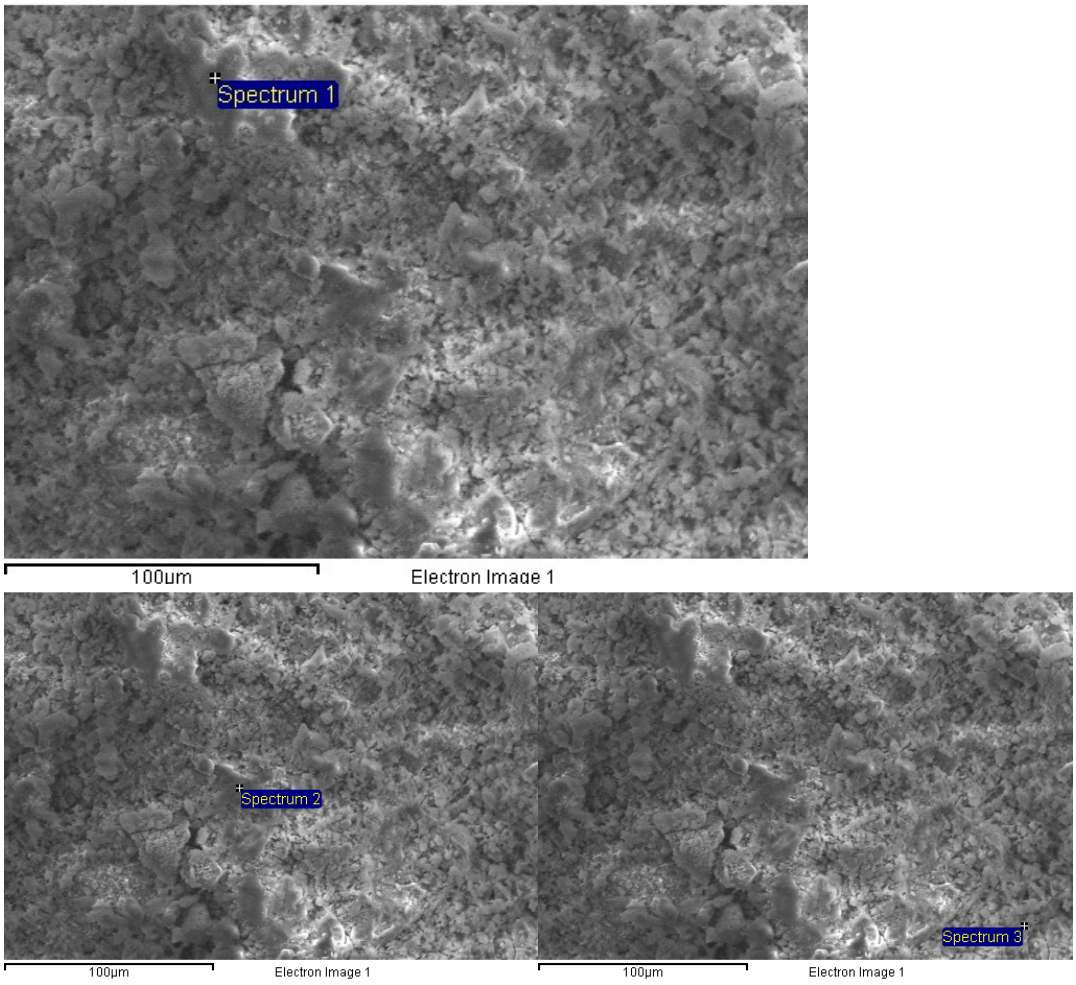

Figure 15 Sample 101 (level 1, 3 m left wall above fuel inlet chute), black/red part

	Spectrum 1	
	Weight%	Atomic%
C	12.58	28.22
O	9.32	15.70
Mg	0.37	0.41
Si	0.54	0.52
P	0.32	0.27
S	0.28	0.24
Cl	36.31	27.61
K	37.11	25.59
Ca		
Ti	0.42	0.24
Cr		
Mn	0.58	0.29
Fe	0.27	0.13
Zn	1.91	0.79

Spectrum 2	
Weight%	Atomic%
2.28	7.03
3.81	8.81
0.31	0.47
0.85	1.11
0.30	0.36
0.84	0.97
31.39	32.77
36.04	34.11
0.54	0.42
0.69	0.49
0.80	0.54
3.93	2.60
18.22	10.32

Spectrum 3	
Weight%	Atomic%
2.38	4.73
40.42	60.19
0.32	0.31
14.75	12.51
0.44	0.32
3.61	2.42
2.38	1.45
21.42	12.73
0.30	0.15
0.29	0.12
1.06	0.45
12.65	4.61

The square shapes seen in the picture below indicate crystallisation of KCl or NaCl. The EDX analysis shows that the main constituents are K and Cl.

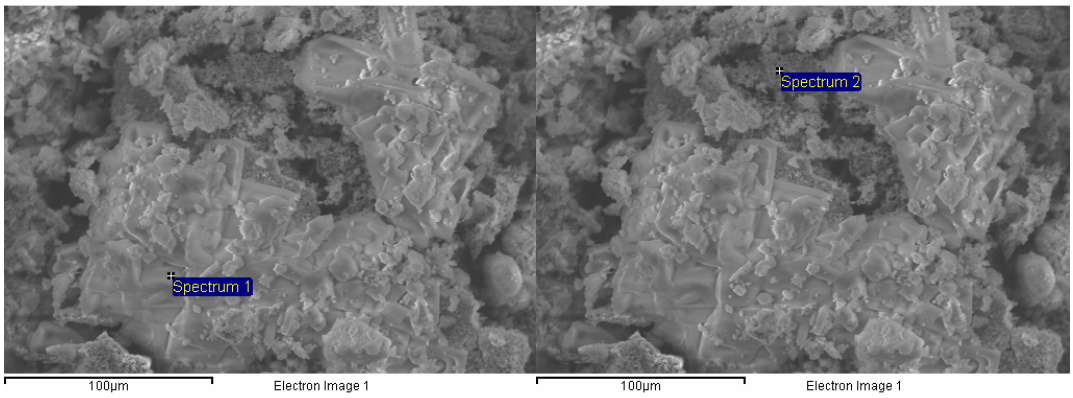

Figure 16 Sample 100 (level 1, 3 m front wall above refractory) black part of deposit that was facing tube

Element	Weight%	Atomic%
C	8.72	22.21
O	2.41	4.60
Si	0.13	0.14
Cl	47.06	40.61
K	40.93	32.03
Fe	0.75	0.41

Element	Weight%	Atomic%
O	17.77	41.41
Na	1.64	2.67
Si	0.21	0.28
S	0.53	0.62
Cl	3.38	3.56
K	1.10	1.05
Ca	0.61	0.57
Mn	1.34	0.91
Fe	72.88	48.65
Zn	0.53	0.30

7 SUMMARY AND DISCUSSION

Deposits from the waterwalls of Steven's Croft BFB have been studied. Samples have been taken from two levels in the furnace, level 1 (3 m) and level 5 (25 m). The outer parts of the deposits that were facing the flue gases as well as the inner parts that were facing the tubes have been analysed.

Studying the inner part of the deposit can give an indication on the corrosion process as they often contain corrosion products from the tube.

The dominating species in the outer, light brown part of the deposit are Ca, K, S, Na, Si, Zn and in some cases Pb. In the samples from level 1 there are also substantial amounts of Cl and more Zn than in the level 5 samples.

In the inner, black part of the deposit, the chlorine content is also higher in the samples from level 1 than in the samples from level 5. In the samples from level 5, the dominating species except for Fe are S, K and Na, whereas on the samples from level 1, there is also a high content of Cl and less S.

The inside of the deposit clearly contains more iron than the outside. This could come from the tubes if they were corroding. Stevens Croft wall tubes are either carbon steel or 15Mo3 and are not currently coated. Magnetite (Fe_3O_4) is black and hematite (Fe_2O_3) is reddish brown which ties in with appearance of the inside of the deposit.

In the level 5 samples there is an enrichment in alkali and sulphur at the tube surface, whereas there is an enrichment of alkali and chlorine in the level 1 samples at the tube surface. For effective sulphation of chlorides to occur (i.e to convert KCl into K_2SO_4) sufficient oxygen needs to be present to react with the sulphur in the fuel or the sulphur dioxide in the flue gases. The excess chlorine is probably converted into HCl(g) and does not remain in the deposit. This reaction can explain why alkali sulphates are found predominantly at level 5, which is above the tertiary air, and why alkali chlorides are found lower down in the furnace, where there is a lack of oxygen.

In some positions, areas that looked like melts were found. These melts had different compositions, mainly Na and Cl, mainly K and Cl, or mainly Al. In one sample, a particle of crystallised KCl was identified. The melting point for Al is 660°C, for KCl 770°C and for NaCl 801°C. This is far above the surface temperature of the waterwalls, but below the flue gas temperature in the furnace. This means that when deposited on the waterwalls these species will probably be solid, but when transported in the flue gases they will be liquid or partly liquid, making them sticky and prone to attach to surfaces.

8 ACKNOWLEDGEMENTS

Thank you to Colin Davis and Pamela Henderson for their additional comments.

Appendix A

APPROVED SIGNATORY

Technology Centre
Ratcliffe on Soar
Nottingham, NG11 0EE
Tel: 02476 192900
Fax: 0115 936 2711
www.eon.com/technology

D.R. Credland
Team Leader

CERTIFICATE OF ANALYSIS

ISSUED BY: **E.ON New Build & Technology Ltd**

DATE OF ISSUE: **04 November 2011**

PAGE 1 OF 5

CERTIFICATE NUMBER: **11-457**

Title	STEVEN'S CROFT: ANALYSIS OF STEVENS CROFT BIOMASS SAMPLES
To	MCCOLE, K Steven's Croft Stevens Croft Biomass Power Plant, Johnstonebridge Lockerbie Dumfries & Galloway DG11 2SQ
FAO	
Other Distribution	File (STC)
Date Received	11 October 2011
Date Of Analysis	11 October 2011 - 03 November 2011
Our Reference	A2011-457
Job Number	2122.C10436.001
Description	Sample(s) have been analysed in accordance with documented in-house methods. Results are provided on the attached sheet(s).

CERTIFICATE OF ANALYSIS

ISSUED BY: **E.ON New Build & Technology Ltd**

DATE OF ISSUE: **04 November 2011**

PAGE 2 OF 5

CERTIFICATE NUMBER: **11-457**

A2011-457-001 - Wood Composite September 2011

Activity	Analyte	Result	Unit
ICP-OES	*Al*	1237	mg/kg
ICP-OES	*Co*	2.87	mg/kg
ICP-OES	*Cr*	11.9	mg/kg
ICP-OES	*Cu*	12.5	mg/kg
ICP-OES	*K*	1193	mg/kg
ICP-OES	*Mn*	135	mg/kg
ICP-OES	*Na*	647*	mg/kg
ICP-OES	*Ni*	4.73	mg/kg
ICP-OES	*Pb*	127	mg/kg
ICP-OES	*Sn*	<1	mg/kg
ICP-OES	*Tl*	<2	mg/kg
ICP-OES	*V*	2.10	mg/kg
ICP-OES	*Zn*	83.5	mg/kg
ICP-OES Hydride	*As*	5.59	mg/kg
ICP-OES Hydride	*Sb*	4.26*	mg/kg

Determinations marked $ were sub-contracted.

Unless otherwise stated, E.ON New Build & Technology was not responsible for sampling.

CERTIFICATE OF ANALYSIS

ISSUED BY: **E.ON New Build & Technology Ltd**

DATE OF ISSUE: **04 November 2011**

PAGE 3 OF 5

CERTIFICATE NUMBER: **11-457**

A2011-457-001 - continued...

Activity	Analyte	Result	Unit
GFAAS	*Cd*	0.47*	mg/kg
CVAAS.	*Hg*	0.031	mg/kg
ISE	*F*	8.35	mg/kg
IC Anions.	*Br*	<2.1	mg/kg
Ash composition	*Al2O3*	6.56	% w/w
Ash composition	*BaO*	0.48	% w/w
Ash composition	*CaO*	16.9	% w/w
Ash composition	*Fe2O3*	4.34	% w/w
Ash composition	*K2O*	3.96	% w/w
Ash composition	*MgO*	4.35	% w/w
Ash composition	*Mn3O4*	0.56	% w/w
Ash composition	*Na2O*	2.54	% w/w
Ash composition	*P2O5*	1.26	% w/w
Ash composition	*SiO2*	39.2	% w/w
Ash composition	*SO3*	4.04	% w/w

Determinations marked $ were sub-contracted.

CERTIFICATE OF ANALYSIS

ISSUED BY: **E.ON New Build & Technology Ltd**

DATE OF ISSUE: **04 November 2011**

PAGE 4 OF 5

CERTIFICATE NUMBER: **11-457**

A2011-457-001 - continued...

Activity	Analyte	Result	Unit
Ash composition	*TiO2*	4.27	% w/w
ICP-OES (Total)	*Al (metallic)*	74.5	mg/kg
CSL	*ash*	4.8	% w/w dry.
CSL	*Cl*	0.09	% w/w dry.
CSL	*Gross CV*	10.5	Mj/Kg
CSL	*Moisture Content*	46.1	%
CSL	*N*	see monthly ROC report	N/A
CSL	*Nett Cv*	8.6	Mj/Kg
CSL	*S*	0.04	% w/w dry.

Determinations marked $ were sub-contracted.

Unless otherwise stated, E.ON New Build & Technology was not responsible for sampling.

CERTIFICATE OF ANALYSIS

ISSUED BY: **E.ON New Build & Technology Ltd**

DATE OF ISSUE: **04 November 2011**

PAGE 5 OF 5

CERTIFICATE NUMBER: **11-457**

Key to activities:

CSL	*Internal Subcontracting*	*BE/WI/0.11*
CVAAS.	*Cold Vapour Atomic Absorption Spectroscopy*	*0083*
GFAAS	*Graphite Furnace Atomic Absorption Spectroscopy*	*0012*
IC Anions.	*Ion Chromatography*	*0013*
ICP-OES	*ICP optical Emission Spectroscopy*	*0006*
ICP-OES (Total)	*ICP Emission Spectroscopy*	*0006*
Ash composition	*acid dissolution + emission spectroscopy*	*ASTM D6349-09*
ICP-OES Hydride	*ICP-OES Hydride*	*0106*
ISE	*ISE*	*0014/0049*

Determinations marked $ were sub-contracted.

Unless otherwise stated, E.ON New Build & Technology was not responsible for sampling.

VATTENFALL

MEMO NO U 13-18

2013-03-28 PR.263.1.9

Department: Chemistry and Materials Technology
Author: Annika Stålenheim, Mattias Mattsson, Pamela Henderson,
Security class: Internal Vattenfall [S2] plus KME 508 project group
Attention: KME 508 project group

EVALUATION OF WATERWALL MATERIALS FROM TEST PANELS 2012

Summary

During the summer of 2008 test panels were installed in the waterwalls of the Idbäcken P3 boiler. In 2011 parts of the furnace walls were exchanged and some new test panels were installed. The test panels are installed on the right wall (motorway side) of the boiler. Amstar AMS 888, one of the coatings installed in 2008, was consumed during the first firing season and this coating is not included in this report. Tube specimens were cut out from the test panels in the summer 2012. This memo presents results from investigation of these samples. Samples have previously been taken out and analysed in 2009, 2010 and 2011. [1], [2], [3]

The coatings on the test panels were:

Coating	Tube nr
Arc welded hard facing by Burmeister and Wain Energy A/S, BWE, consisting of Inconel 625. The intended thickness is > 1,5 mm (2008)	39-42
A metal sprayed coating using HVOF (High Velocity OxyFuel) applied by Sulzer Metco. The alloy is SumeBoil70C (Inconel625 + carbides) with an intended thickness of 0,3 mm (2008)	45-48
FlameSpray, FlameSeal WW (a ceramic seal on top of a thermal sprayed coating). The thermal sprayed alloy is Alloy C-276 (Ni16Cr16Mo5Fe4W) with the intended thickness 0,3 mm (2008)	52-54
A coating that was plasma sprayed in workshop by Häuser [4]. The alloy used is HS4, Häuser's own corrosion erosion resistant Ni-alloy (NiCrWBSi). Intended thickness 0.4 mm. (2011)	55-58
Coating plasma-sprayed in workshop by MH engineering. The alloy used was TP316 stainless steel. (2011)	59-60, 62-63
Coating applied by MH engineering on site. Material used is CorrEr (A variation of Alloy 625). Only one tube coated. (2011)	65
Coating applied by MH engineering on site. Material used is alloy 625. Only one tube coated. (2011)	67

VATTENFALL RESEARCH AND DEVELOPMENT AB

ADDRESS
SE-814 26 Älvkarleby, Sweden

TELEPHONE
+46 26 835 00

VAT NUMBER
SE556390-5891

VISITING ADDRESS
Älvkarleby Laboratory

TELEFAX
+46 26 836 70

E-MAIL
utveckling@vattenfall.com

All coatings except the overlay weld were damaged. The two thermally sprayed coatings (Sulzer and FlameSpray) applied in 2008 were mainly intact, but were damaged in the area near the weld repair after last year's sampling. Except for these holes the coatings do not seem to have suffered any thickness loss.

The coatings that were installed in 2011 (all thermally sprayed) were all severely damaged and in one case, MH Engineering alloy 625, the coating was lost completely. The other two coatings, Häuser HS4 and MH Engineering 316, also have areas in good condition, indicating that the break down is not caused by corrosion of the coating, but rather physical damage, such as cracking and delamination. This could indicate that stainless steel might be an alternative to Ni-base.

The reference sample analysed in 2011 experienced a maximum metal loss of 2mm (0.65 mm per year) during the three year period 2008-2011 and an average metal loss of 1.65 mm (0.55mm per year). The maximum metal loss of the reference sample analysed this year was about 1 mm after one firing season and the average was 0.65mm, indicating a marginally higher corrosion rate.

The average metal loss of all the nickel-based coatings (where the coating had not delaminated) was negligible, regardless of alloy chemistry or application method. The metal loss of the 316 stainless steel was less than 0.1 mm after one year and the average metal loss of 16Mo3 was 0.65 mm.

1 EXPERIMENTAL

1.1 Installation and materials

During the summer 2008 test panels were installed in the waterwalls of the Idbäcken P3 boiler. In 2011 parts of the furnace walls were exchanged and some new test panels were installed. The test panels were installed on the right wall (motorway side) of the boiler and the positions of the coatings on the boiler wall are shown in Figure 1.

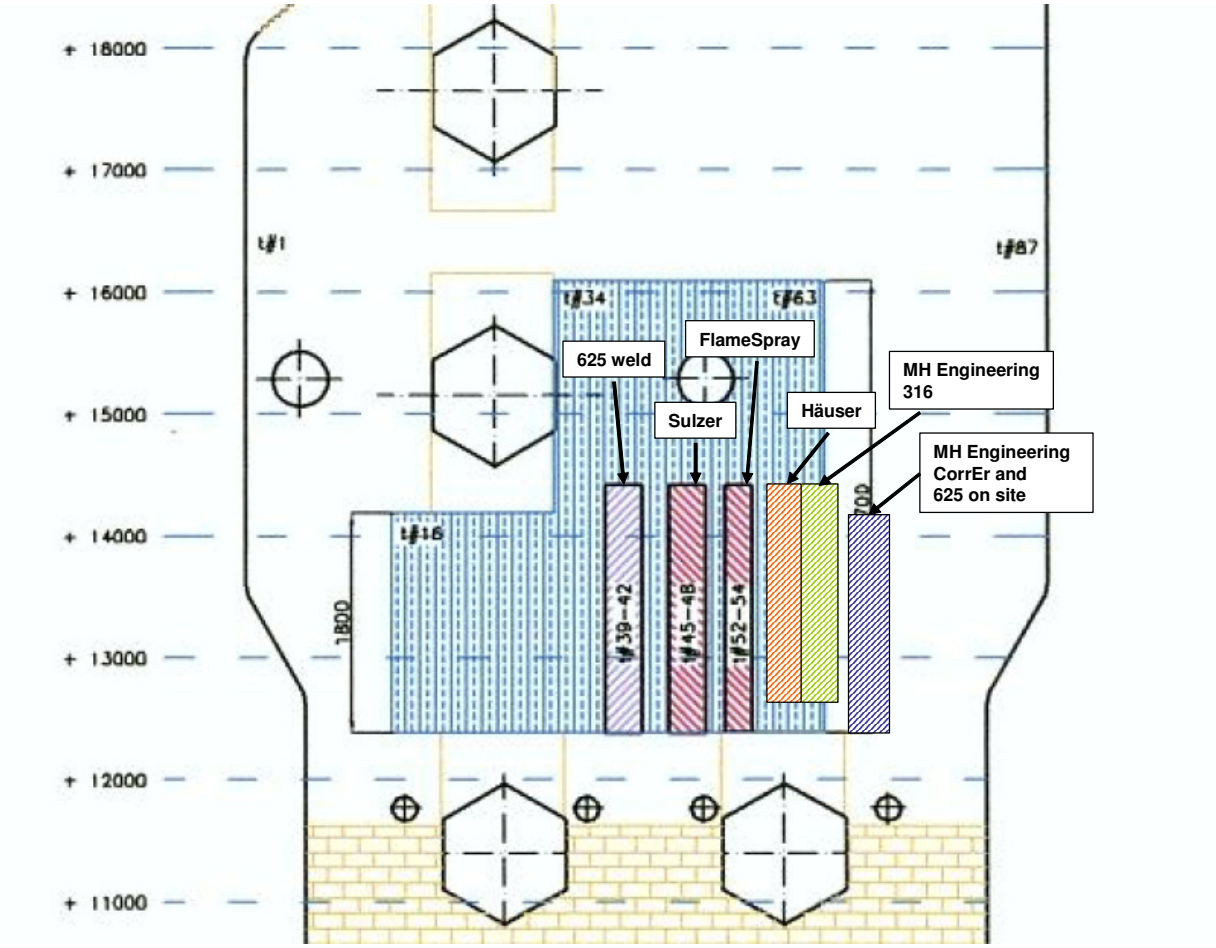

Figure 1 Positions of the coatings. The test panels are installed on the right wall of the boiler.

Details of the test panels are given in Table 1 and the specimens taken for analysis are given in Table 2.

Tube specimens (after 4 years' and one year's exposure) were cut out from the test panels in the summer of 2012. Samples had previously been taken out and analysed in 2009, 2010 and 2011. [1], [2], [3]. A reference sample of 16Mo3, without a coating, was also analysed.

Table 1 Test panels and coatings

Coating	Tube nr
Arc welded hard facing by Burmeister and Wain Energy A/S, BWE, consisting of Inconel 625. The intended thickness is > 1,5 mm (2008)	39-42
A metal sprayed coating using HVOF (High Velocity OxyFuel) applied by Sulzer Metco. The alloy is SumeBoil70C (Inconel625 + carbides) with an intended thickness of 0,3 mm (2008)	45-48
FlameSpray, FlameSeal WW (a ceramic seal on top of a thermal sprayed coating). The thermal sprayed alloy is Alloy C-276 (Ni16Cr16Mo5Fe4W) with the intended thickness 0,3 mm (2008)	52-54
A coating that was plasma sprayed in workshop by Häuser [4]. The alloy used is HS4, Häuser's own corrosion erosion resistant Ni-alloy (NiCrWBSi). Intended thickness 0.4 mm. (2011)	55-58
Coating plasma-sprayed in workshop by MH engineering. The alloy used was TP316 stainless steel. (2011)	59-60, 62-63
Coating applied by MH engineering on site. Material used is CorrEr (A variation of Alloy 625). Only one tube coated. (2011)	65
Coating applied by MH engineering on site. Material used is alloy 625. Only one tube coated. (2011)	67

The alloy 625 coating applied by MH Engineering on site had been lost completely during the firing season and no sample could be analysed.

Sample P1, P2, P3 and P7 were situated at the same height on the waterwall. The rest, Ref, P5 and P6, were situated one level higher. (Figure 2 and Figure 3)

Table 1 Samples analysed

Sample	Tube	Material	Position
P1	41	Alloy 625 weld, installed 2008	Low
P2	47	Sulzer, Sumeboil 70C, installed 2008	Low
P3	52	Flamespray,Flameseal WW, installed 2008	Low
Ref	61	16Mo3 (no coating), installed 2011	High
P5	56	Häuser, alloy 625, installed 2011	High
P6	60	MH engineering, TP 316 stainless, installed 2011	High
P7	65	MH engineering, CorEr, installed 2011	Low

Figure 2 Samples P1, P2 and P3. Sample P7 is situated somewhat further to the right. (Out of the picture)

Figure 3 Sample P5, P6 and Ref.

1.2 Coating methods

1.2.1 Arc welding. (P1).

Gas metal arc welding (GMAW), sometimes known as metal inert gas (MIG) welding is a process in which an electric arc forms between the consumable alloy wire electrode and the tube wall which heats them, causing them to melt, and join. This is the most common process and the method by which the rest of the furnace walls in Idbäcken are coated. Along with the wire electrode, an inert gas feeds through the welding gun, which shields the process from contaminants in the air. The process can be semi-automatic or automatic and the welding is longitudinal. The thickness is at least 2 mm and depends on the number of welding strings, in the case of the welded test panel at least 4 mm. This method gives the best adhesion between the coating and the tube.

1.2.2 HVOF High Velocity oxyfuel (P2)

A mixture of propane and oxygen is used to give a high temperature flame of around 2700℃ The metal alloy powder is mixed with nitrogen and sprayed into the flame which rotates to evenly heat the particles. Compressed air accelerates the particles to a velocity of 600-900 m/s (the gas velocity reaches 1300m/s) and the particles impact the substrate with a temperature of 150-160 ℃. This is a relatively low temperature which means that the particles are not highly oxidised.

If the particles are too large or the speed too high, poor adhesion to the substrate may occur. HVOF- coatings are sensitive to internal stress, which is why they are limited in thickness.

1.2.3 Flame-spraying (P3)

The metal alloy in powder or wire form is fed into a an explosive mixture of acetylene and oxygen, with a temperature up to 3000℃ . The material melts and compressed air breaks the melt up in to small particles which are transported to the substrate at a velocity of 150 – 200 m/s.

1.2.4 Plasma spraying (P5)

An electric arc is formed between two fixed electrodes and an inert gas (argon or nitrogen) is then fed through the arc and becomes a plasma. (A plasma is a gas which has been raised to such a high temperature that it ionizes and becomes electrically conductive.) The alloy coating in form of a power is fed into the plasma. The powder melts and is projected towards the surface to be coated. The temperature of the plasma can be up to 16 000℃, but the temperature of the particles that impact the surface is only 150℃. The velocity of the particles, however is high, is 240 – 600 m/s. The high particle velocity results in a lower porosity in plasma-sprayed coatings compared to flame-sprayed and the use of an inert gas protects the particles from oxidation.

2 INSPECTION OF TEST PANELS IN BOILER

Before the samples were taken out, but after sand blasting of the waterwalls, the test panels were inspected in the boiler, both by Vattenfall and by MH Engineering. The test panels were photographed and MH Engineering also performed a measurement of the coating thickness on some of the coatings with a digital thickness measuring instrument, Elcometer® 456.

Figure 4 Waterwalls after sand blasting

2.1 Sample P1: IN 625 Arc welded

The coating was applied during summer 2008 by Burmeister and Wain Energy. The intended thickness was > 1.5 mm. The sample was taken from tube number 41.

Figure 5 Sample P1: IN625 Arc welded. The coating was applied during summer 2008 by Burmeister and Wain Energy. The sample was taken from tube number 41.

2.2 Sample P2: Sulzer Sumeboil 70C HVOF

A metal sprayed coating using HVOF (High Velocity OxyFuel), applied by Sulzer Metco. The alloy is SumeBoil70C (Inconel625 + carbides) with an intended thickness of 0.3 mm. The coating was applied in summer 2008.

The coating on tube no 46 is damaged above and below the weld repair and in a position approximately 3 dm below the weld repair, as can be seen in Figure 6. These damages were also noted by MH Engineering on their inspection.

Figure 6 Sample P2: Sumeboil 70C (625 + C) HVOF. The coating was applied in summer 2008 on tubes 45-48.. The sample was taken from tube number 47.

2.3 Sample P3: Alloy C-276 Flame Spray

FlameSeal WW is a coating with a ceramic seal on top of a thermal sprayed coating. The thermal sprayed alloy is Alloy C-276 (Ni16Cr16Mo5Fe4W) with the intended thickness 0.3 mm. The coating was applied in summer 2008 by FlameSpray on tubes 52-54.

MH Engineering noted loss of the coating on all three tubes on their inspection. In Figure 7 damages can be seen on tubes 53 and 54.

Figure 7 Sample P3: Alloy C-276 Flame Spray. The coating was applied in summer 2008 on tubes 52-54. The sample was taken from tube number 52.

2.4 Reference sample

This sample has been taken from the middle tube (without any coating) of the test panel installed by MH Engineering. Hence, it has only been exposed for one firing season. The material is 16Mo3 and the original wall thickness was 7 mm.

Figure 8 Sample Ref: Un-coated sample from 2011, base material 16Mo3. The sample was taken from tube number 61.

2.5 Sample P5: HS4 plasma sprayed

Sample P5: The coating was plasma sprayed in workshop by Häuser and installed in the boiler in 2011. The alloy used is HS4, Häuser's own corrosion erosion resistant Ni-alloy (NiCrWBSi). The coating was severely damaged in some areas.

MH Engineering noted delamination of the coating on their inspection.

Figure 9 Sample P5: HS4 coating plasma sprayed in workshop by Häuser and installed in the boiler in 2011. The coating was severely damaged in some areas. The sample was taken from tube number 56. The coating was applied on tubes 55-58.

2.6 Sample P6 MH Engineering 316

TP316 stainless steel coating was applied in summer 2011. It was plasma-sprayed in workshop by MH engineering. Large areas had delaminated and were missing coating and after less than one year of exposure, most of the coating was lost. However, the remaining area was in good condition. The areas without coating are on the upper part of the panels near the welds. Two of the tubes (62 and 63) had lost all the 316 coating.

MH Engineering noted loss of much of the coating on their inspection.

Figure 10 Sample P6: TP316 stainless steel coating plasma-sprayed in workshop by MH Engineering and installed in the boiler in summer 2011. Large areas had delaminated and were missing, but the remaining area was in good condition. The coating was applied on tubes 59, 60, 62 and 63. The sample was taken from tube number 60.

2.7 Sample P7 CorrEr

The CorrEr coating (only one tube) was applied on site by MH engineering in summer 2011. The coating had delaminated at the top.

MH Engineering noted delamination of the coating on their inspection.

Figure 11 Sample P7: CorrEr The coating (only one tube) was applied during summer 2011 by MH engineering on site. The coating had delaminated at the top. The sample was taken from tube number 65.

3 MATERIAL THICKNESS

Small specimens were cut from the samples, mounted in resin, ground and polished. The thickness of the coating layers was measured as well as the wall thickness of the reference sample (Figure 12, Table 2). Only one, fairly small sample has been taken out from every test panel and it is not certain that this is representative of the entire test panel. This means that one shouldn't draw too far going conclusions from the investigation. Sample P7 had unfortunately been taken from a part of the tube that had lost all of its coating.

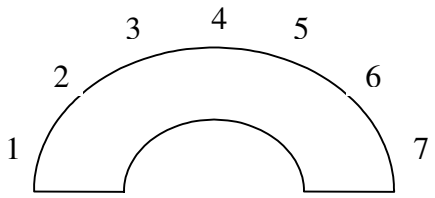

Figure 12 Measurement positions on samples, results shown in table below.

Table 2 Thickness measurement of samples

Position	**P1** (BWE, weld)	**P2** (Schulzer)	**P3** (Flamespray)	**Ref** (16Mo3)	**P5** Hauser 625	**P6** TP 316	**P7** CorEr	
	Coating (mm)	**Coating** (mm)	**Coating** (mm)	**Wall** (mm)	**Coating** (mm)	**Coating** (mm)	**Coating** (mm)	**Wall** (mm)
1	4,09	0,255	0,337	6,93	0,469	0,325	0	5,47
2	4,34	0,257	0,338	6,46	0,354	0,344	0	5,17
3	4,41	0,262	0,396	6,53	0,319	0,437	0	4,95
4	3,79	0,276	0,359	6,27	0,342	0,387	0	5,00
5	3,18	0,311	0,288	6,14	0,393	0,509	0	5,52
6	3,77	0,303	0,198	5,97	0,486	0,462	0	5,45
7	3,66	0,222	0,226	6,12	0,453	0,297	0	5,87
Average	**3,89**	**0,269**	**0,306**	**6,35**	**0,402**	**0,394**	**0**	**5,35**

For the tubes installed in 2008, the previous measurements performed in 2009, 2010 and 2011 are also given and show similar values.

P1: Coating thickness 2009 ~4mm, 2010 ~6 mm, 2011 ~4 mm, 2012 ~4 mm

P2: Coating thickness 2009 ~250 µm, 2010 ~275 µm, 2011 ~300 µm, 2012 ~270 µm

P3: Coating thickness: 2009 ~380µm, 2010 ~390µm, 2011 ~390 µm, 2012 ~310 µm

(The coatings do not actually increase in thickness with time. These results reflect the difference in coating thickness on different parts of the tube and show that corrosion has been negligible on the coatings.)

The original coating thickness of sample P6 was measured by MH Engineering (Table 3). This indicates that sample P6, stainless steel 316 had lost 35-90 µm during the operating year.

Table 3 Original coating thickness of MH Engineering 316 coating

	Average (mm)	Std dev (mm)
Tube 59-60	0.429	0.046
Tube 62-63	0.212	0.030

The original wall thickness of the 16Mo3 tube was 7 mm. The maximum reduction in wall thickness on the reference sample is about 0.9 mm, whereas it is about 2 mm on sample P7, the CorEr sample that had lost its coating. Both samples had been in the boiler for one firing season, but they were taken from different parts of the furnace wall (different heights).

MH Engineering also measured the coating thickness of the CorEr coating immediately after installation. The result was an average thickness of 0.520 mm with a standard deviation of 0.063.

3.1 Comparison with results from MH Engineering

In addition to Vattenfall's inspection and measurement of samples taken out from the boiler, MH Engineering also made an inspection and an on site measurement of the thickness of the coating layers. A visual inspection was carried out, where a digital camera was used for photographic documentation. Thickness measurements were conducted on coated surfaces with a digital thickness measuring instrument, Elcometer® 456. The P7 sample received by Vattenfall had lost all coating and was also severely corroded, whereas MH Engineering could perform a measurement in a position where the coating had not been lost. A comparison between Vattenfall´s and MH Engineering's measurements is given in Table 5.

Table 4 Comparison between results from Vattenfall and MH Engineering

	P1 (BWE, weld)	**P2** (Schulzer)	**P3** (Flamespray)	**Ref** (16Mo3)	**P5** Hauser 625	**P6*** TP 316	**P7** CorEr	
	Coating (mm)	**Coating** (mm)	**Coating** (mm)	**Wall** (mm)	**Coating** (mm)	**Coating** (mm)	**Wall** (mm)	**Coating** (mm)
Vattenfall average	3,89	0,269	0,306	6,35	0,402	0,394	5,35	0
Vattenfall std dev	0,43	0,030	0,072	0,32	0,067	0,078	0,33	-
MHE average	-	0,303	0,322	-	0,416	0,340	-	0,525
MHE std dev	*	0,061	0,103	-	0,126	0,159	-	0,120

*MH Engineering measured the coating thickness of tubes 59-60.

4 METALLOGRAPHIC INVESTIGATION

4.1 Sample P1: IN625 Arc welding (2008)

No visible corrosion of the base material has occurred. It is not possible to see any corrosion or other damages on the coating surface.

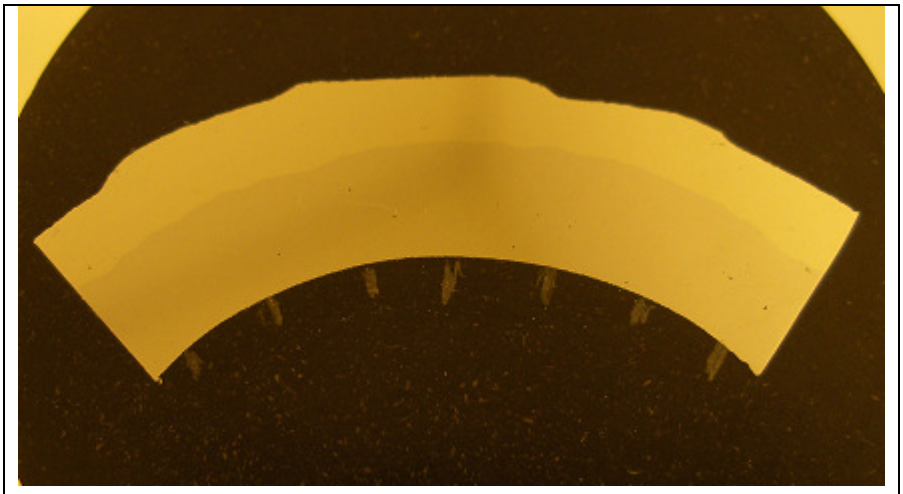

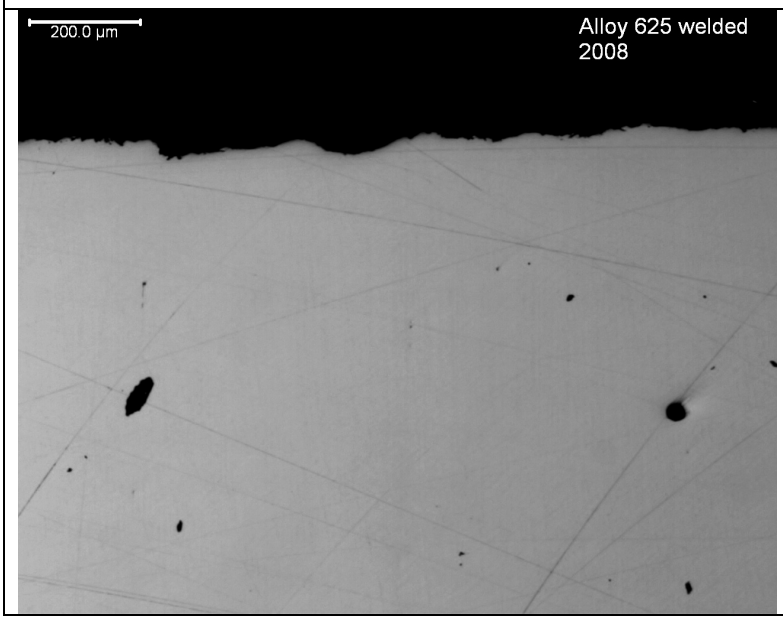

4.2 Sample P2: Sulzer Sumeboil 70C HVOF (2008)

No visible corrosion of the base material has occurred (Figure 13). The porosity of the interface between coating and substrate was observed in previous years as well. No cracks through the coating as those that were observed in 2010 and 2011 (Figure 15) could be seen in the 2012 sample.

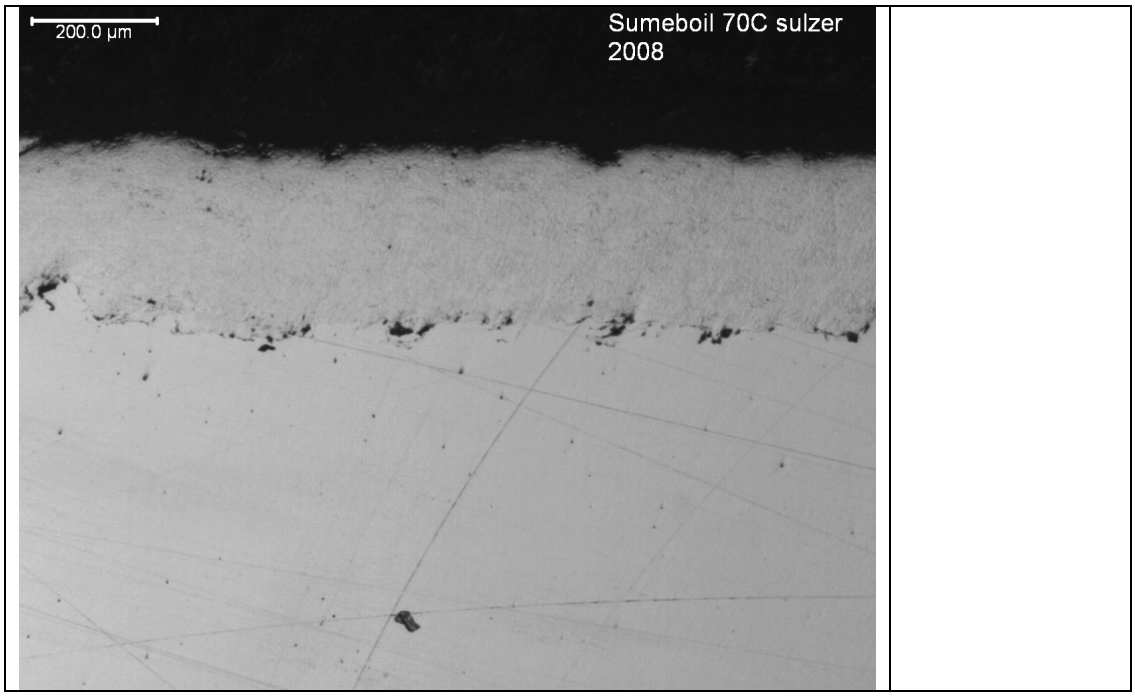

Figure 13 Sample P2: Sulzer Sumeboil 70C HVOF, (applied in 2008) result from 2012.

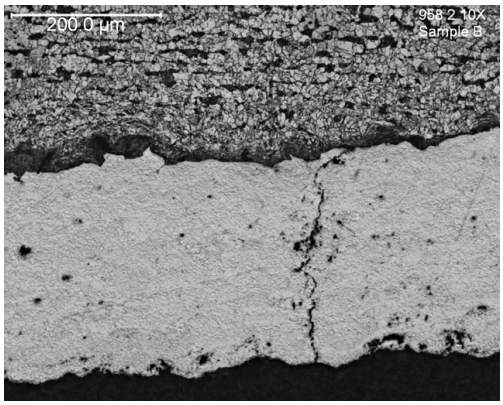

2010

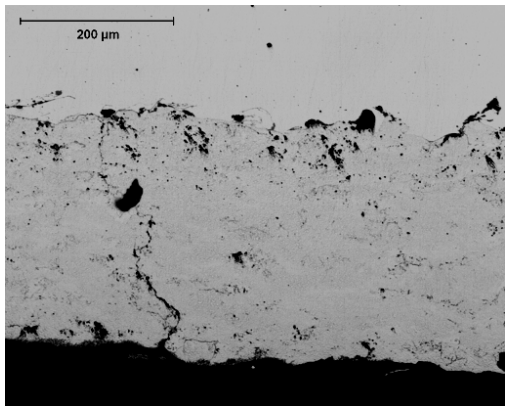

2011

Figure 14 Results from 2010 and 2011. Sample P2: Sulzer Sumeboil 70C HVOF.

4.3 Sample P3: Alloy C-276 Flame Spray (2008)

No visible corrosion of the base material has occurred. The porosity of the interface between coating and substrate was observed in previous samples as well. The surface of the coating does not appear to have more defects this year (Figure 15) than previously (Figure 16).

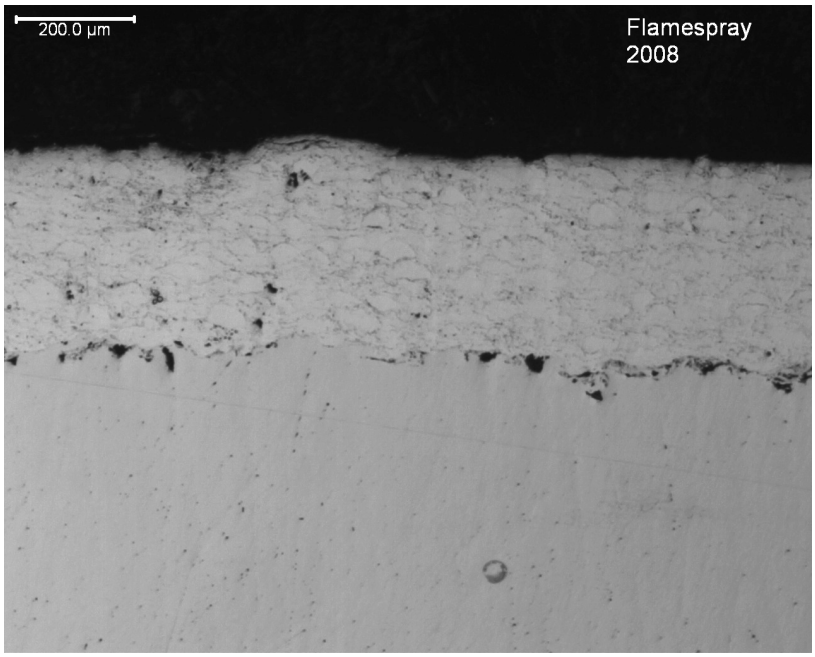

Figure 15 Sample P3: Alloy C-276 Flame Spray

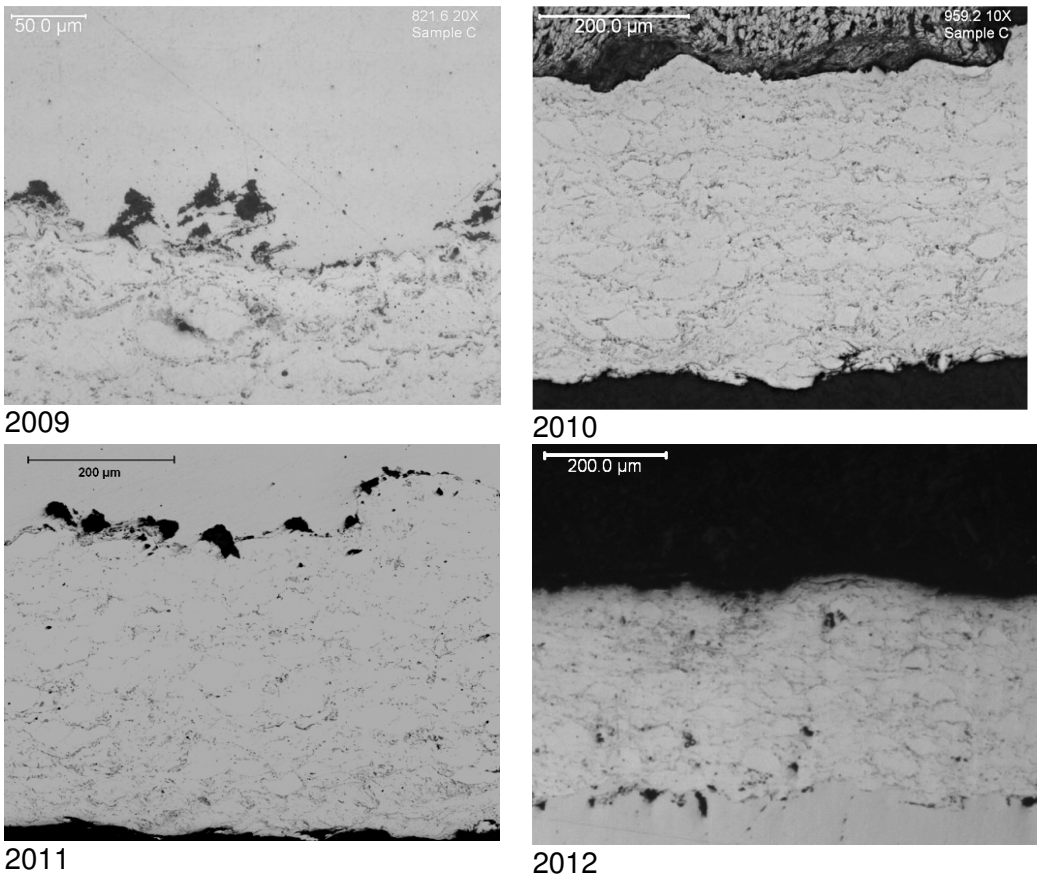

Figure 16 Results from 2009, 2010, 2011 and 2012. Sample P3: Alloy C-276 Flame Spray

4.4 Reference sample (2011)

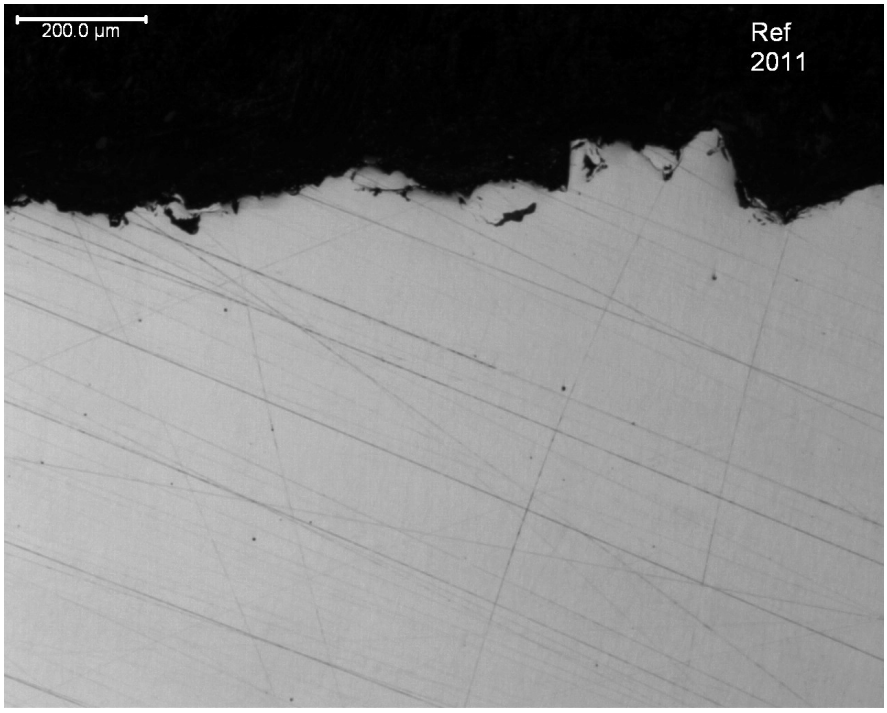

Figure 17 Reference sample 16Mo3 installed in 2011, no coating

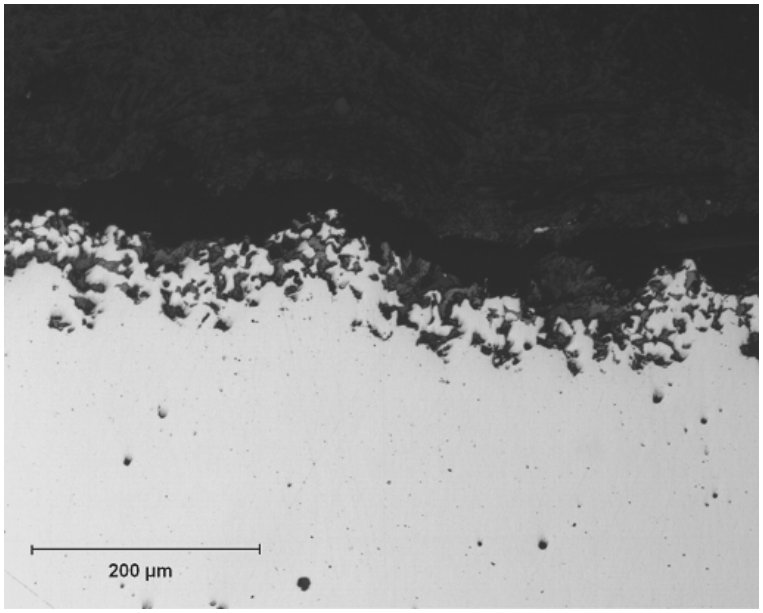

Figure 18 Reference sample 2011, tube was installed in 2008

4.5 Sample P5: HS4 plasma sprayed (2011)

No visible corrosion of the base material has occurred. Some pores can be seen in the interface between coating and substrate.

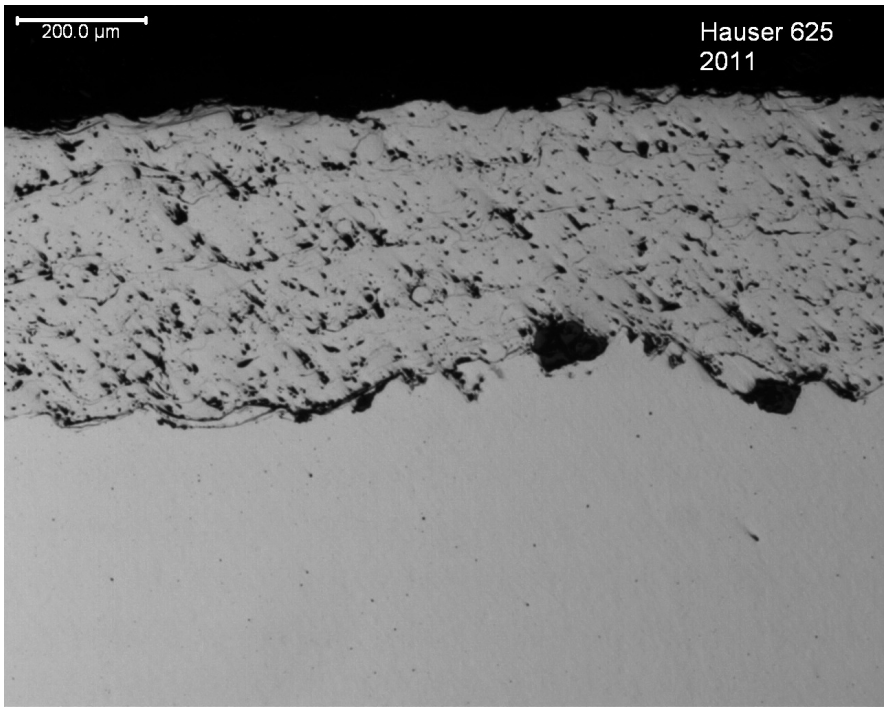

Figure 19 Sample P5: HS4 plasma sprayed

4.6 Sample P6 MH Engineering 316 (2011)

No visible corrosion of the base material has occurred.

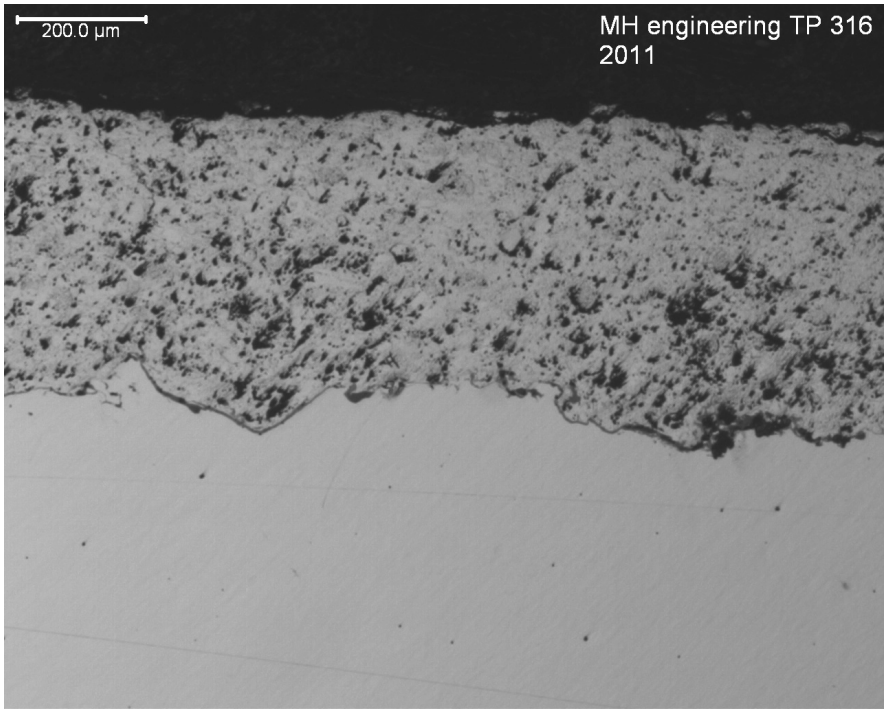

Figure 20 Sample P6 MH Engineering 316

4.7 Sample P7 CorrEr (2011)

No traces of the coating can be seen on the sample.

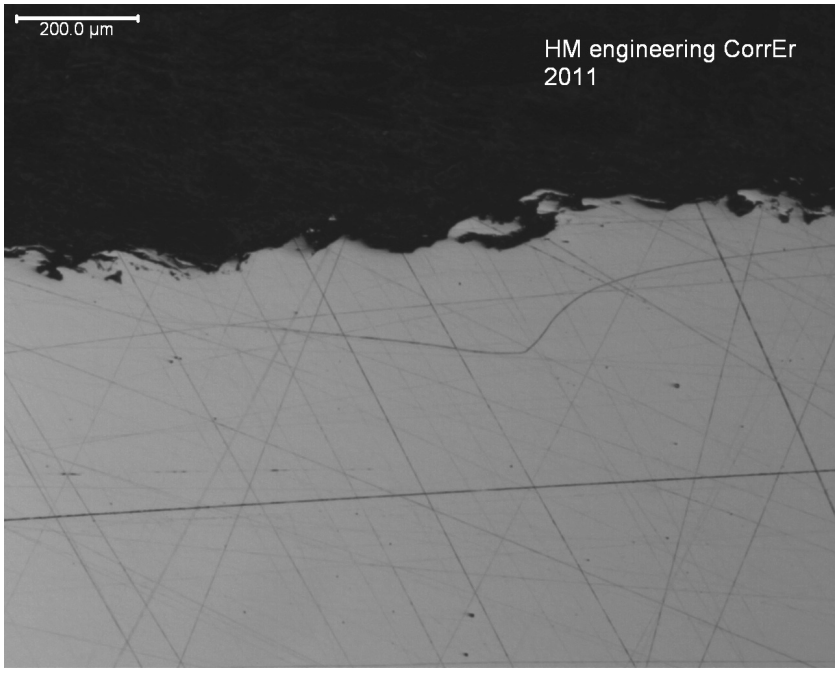

Figure 21 Sample P7 CorrEr

5 DISCUSSION AND CONCLUSIONS

All coatings except the overlay weld were damaged. The two thermally sprayed coatings (Sulzer and FlameSpray) applied in 2008 were mainly intact, but were damaged in the area near the weld repair after last years sampling. There was also one large hole in the coating of each of these panels one or a few decimetres from the weld repair. The cause of these holes is not known, but the local nature of the damages indicates that they are caused by some external factor, rather than deterioration of the material from corrosion caused by the flue gases and deposits. Except for these holes the coatings do not seem to have suffered any thickness loss.

The coatings that were installed in 2011 (all thermally sprayed) were all severely damaged and in one case, MH Engineering CorrEr , the coating was lost completely. The other two coatings, Häuser HS4 and MH Engineering 316, also have areas in good condition, indicating that the break down is not caused by corrosion of the coating, but rather physical damage, such as cracking and delamination. This could indicate that stainless steel might be an alternative to Ni-base.

As regards metal loss (corrosion), the nickel-based alloys showed negligible loss (too small to be measured accurately) and the stainless steel showed a loss of 35-90 µm per year (less than 0.1 mm), also very small.

The reference sample analysed in 2011 experienced a maximum metal loss of 2 mm (0.65 mm per year) during the three year period 2008-2011 and an average metal loss of 1.65 mm (0.55mm per year). The maximum metal loss of the reference sample analysed this year was about 1 mm after one firing season and the average was 0.65mm, indicating a marginally higher corrosion rate.

6 ACKNOWLEDGEMENTS

We thank Seppo Simola, Carl Nordenskjöld, Christer Forsberg and Yousef Alipour for the help given to us during the investigation.

7 REFERENCES

[1] Westberg S-B, “Utvärdering av panelväggsmaterial I eldstaden i Idbäcken”, PM U 10-142, Memo, Vattenfall Research and Development, 2010

[2] Westberg S-B, Stålenheim A, ”Corrosion test no 4, Evaluation of furnace tube wall materials at the Idbäcken plant”, NGBW D2.4.10, 2010

[3] Annika Stålenheim, Mattias Mattsson, “Evaluation of waterwall materials from test panels 2011”, Memo U 11-119, Vattenfall Research and Development, 2011

[4] http://www.haeuser-co.de/pages/de/home.php

[5] MH Engineering, Private Communication, (2012).

MEMO NO U13-03

2013-02-06 PR.263.1.9

Department: Chemistry and Materials Technology
Author: Annika Stålenheim and Pamela Henderson
Security class: Internal [S2]
Attention: KME 508 project group

MEASUREMENT CAMPAIGN, NOVEMBER 2011

KME 508 FURNACE WALL CORROSION IN BIOMASS FIRED BOILERS WITH HIGHER STEAM TEMPERATURE AND PRESSURE

Summary

Within KME 508 a measurement campaign was performed at Idbäcken with waste wood in November 2011. The measurements were made during the period 8-10 November with the boiler running at 65-80% of full load. This memo summarises the results of this measurement campaign. Flue gas composition, temperature and impactor measurements were made at the furnace wall and 1 m from the wall. Deposit probe measurements were made at the wall.

Very low O_2 levels were detected, sometimes below 0.5%, and the fluctuation over time was large. The fluctuation was greatest at the back wall and least on the right wall. The temperatures were lower close to the wall than 1 m into the furnace. The CO levels were high. When the ChlorOut system was turned off the KCl level near the superheaters was 19-28 ppm.

Average values of flue gas at the furnace wall, about + 16 m, were as follows :-

SICK O_2 0.9%, CO (out of range for many readings, i.e. > 1.3%)

FTIR, average values: CO 1.7%, SO_2 46 ppm, HCl 15 ppm, HF 1 ppm, CH_4 (methane) 1360 ppm, NOx 96 ppm, H_2O 19.6 %, CO_2 8.9%

IACM (with no ChlorOut additive) at superheaters: KCl 19-28 ppm, SO_2 32-49 ppm

K, Cl, S, Pb and Zn were found in the deposits. The levels varied considerably and in a seemingly random manner.

The chlorine content varied between 2 and 14 wt % , zinc 5-15 wt%, lead up to 6.8 wt%, potassium 2-9 wt% , sodium up to 6.6 wt% and sulphur 4-11 wt%. There was no correlation between Cl content, measuring position (back wall or side wall), substrate temperature or alloy, but a high S content correlated with a low Cl content.

Impactor measurements showed that Cl, K, Pb and Zn and S were found in sub-micron particles. Si and Ca were found in particle sizes 1-10µm.

1 EXPERIMENTAL

A measurement campaign was performed at Idbäcken in boiler P3 with waste wood in November 2011. Flue gas composition and temperature were measured and impactor measurements were made near the furnace wall and at a distance of 0.8-1 m from the wall. Deposit probes were also exposed at the wall.

1.1 Measurement positions

The measurement positions in the boiler are shown in Figure 1, Figure 2 and Figure 3. The flue gas composition has been investigated in seven positions in the boiler, positions A, J and K on the back wall, positions B-C and D on the side wall and positions F and G on the front wall of the furnace. These are at a height of 16 m in the boiler. Deposit probes have been inserted at three different positions in the furnace, positions A, B-C and B-C left.

Impactor measurements were made in positions A and B.

During the campaign, the ChlorOut was turned off for a period of time and a reading from the plant's IACM of the KCl and SO_2 contents of the flue gases in the superheater region was made.

During the summer stop in 2010, the wall thickness of the waterwall tubes was measured, showing that parts of the furnace walls experienced severe corrosion. In position A, on the back wall, the corrosion rate of the waterwalls is especially high (see Figure 4). In the other measurement positions the corrosion rate is more moderate (see Figure 5 and Figure 6).

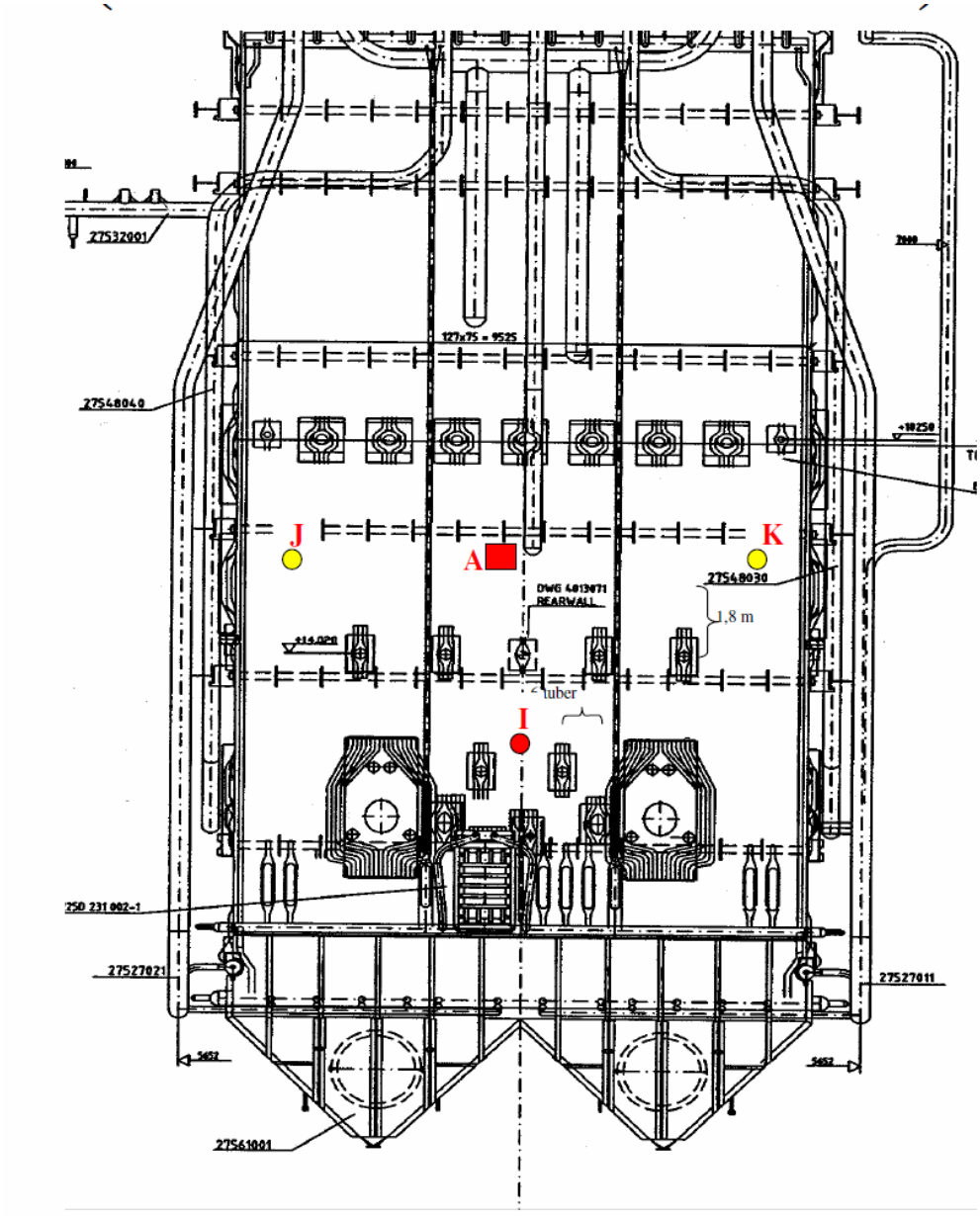

Figure 1 Back wall of furnace, with measurement positions marked. View from inside of boiler.

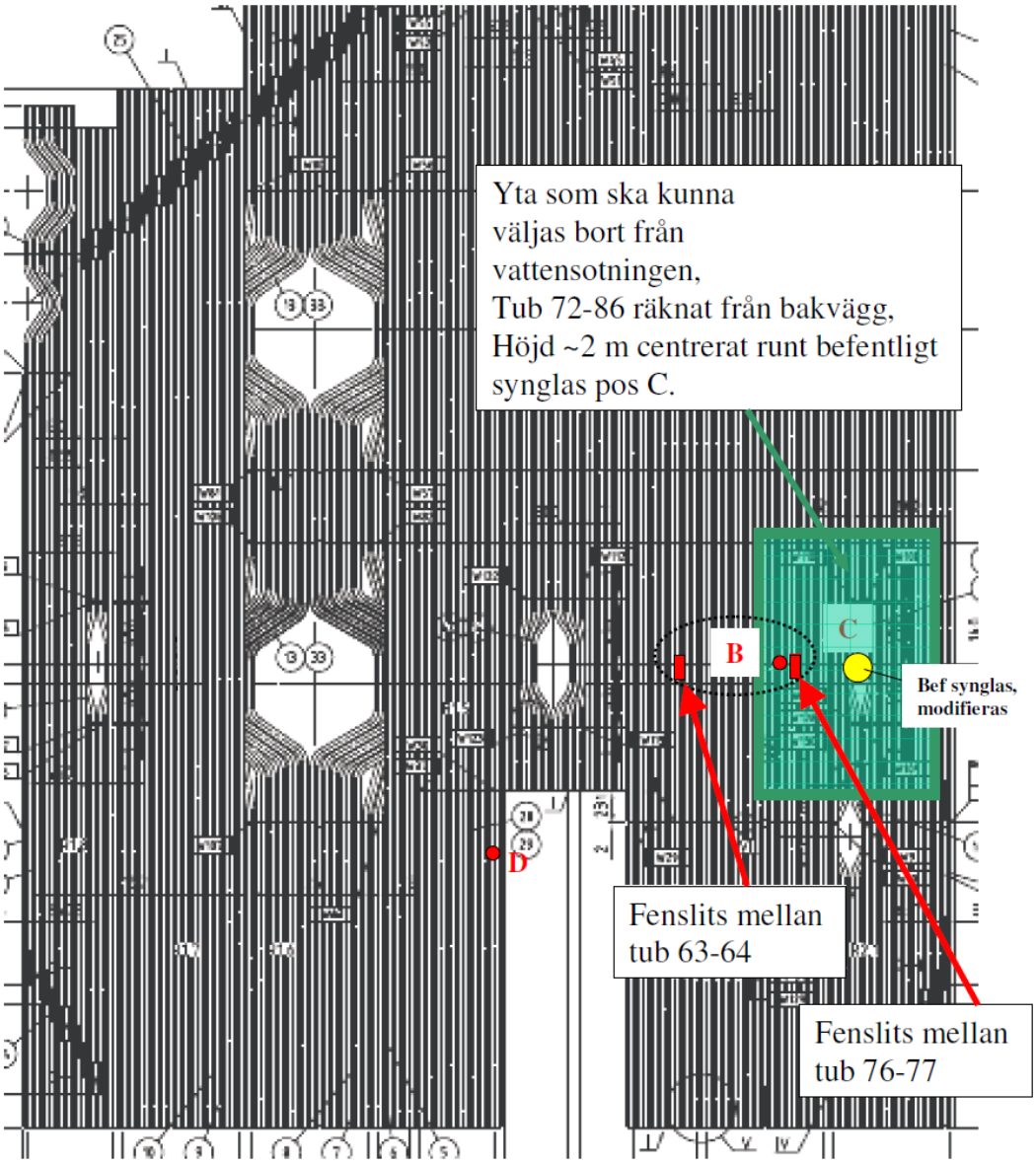

Figure 2 Side wall of furnace, with measurement positions marked. View from inside of boiler. The red arrows point at the positions for the deposit probes. Position B-C left is to the left seen from the outside of the boiler (to the right in this picture).

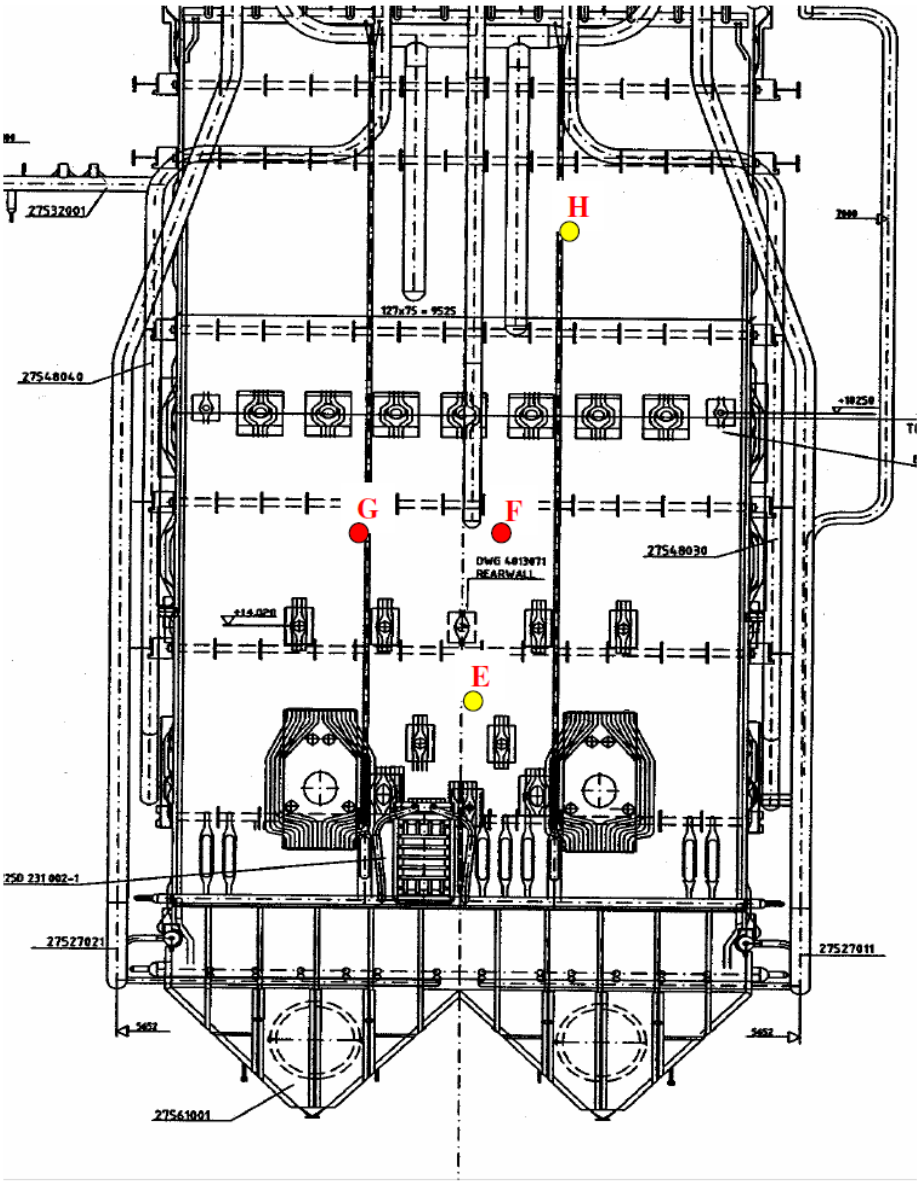

Figure 3 Front wall of furnace, with measurement positions marked. View from inside of boiler. Flue gas measurements have been made in positions F and G.

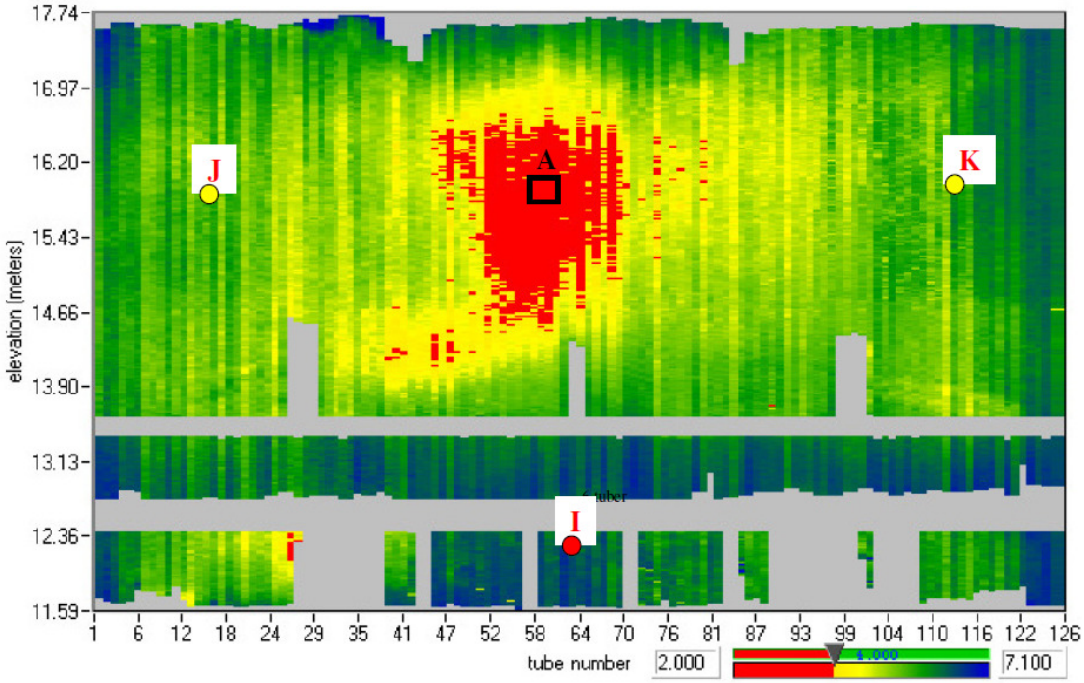

Figure 4 Tube thickness measurement of furnace back wall made during the summer 2010. In the red parts, the wall thickness of the tubes is less than 4 mm. (View from inside of boiler.)

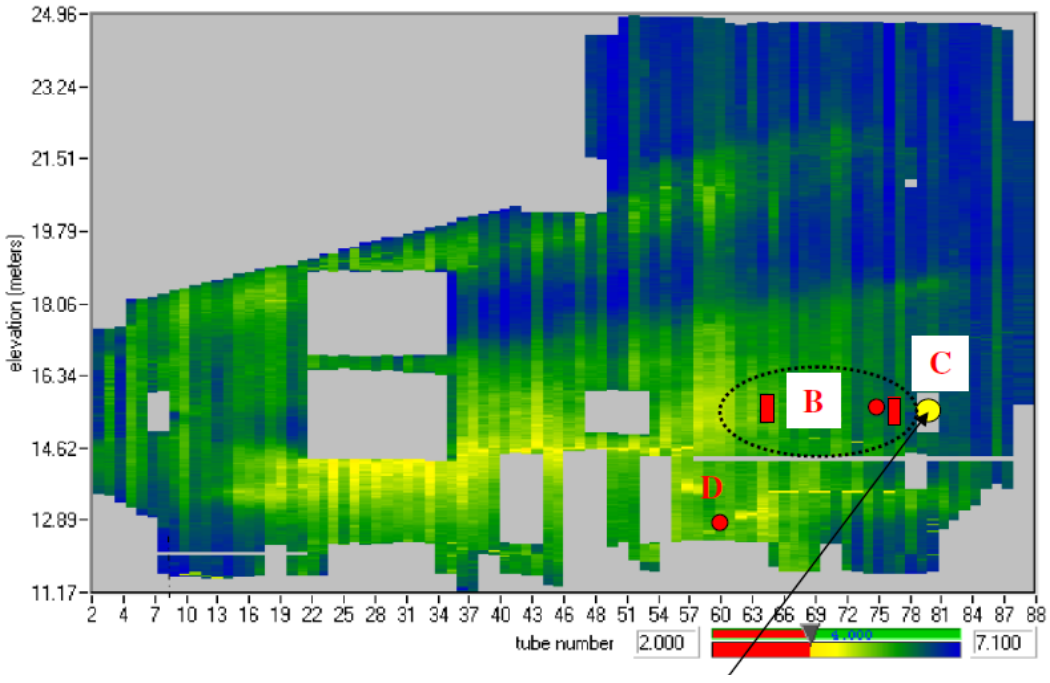

Figure 5 Tube thickness measurement of furnace side wall. The red squares mark the positions of the deposit probes. (View from inside of boiler.)

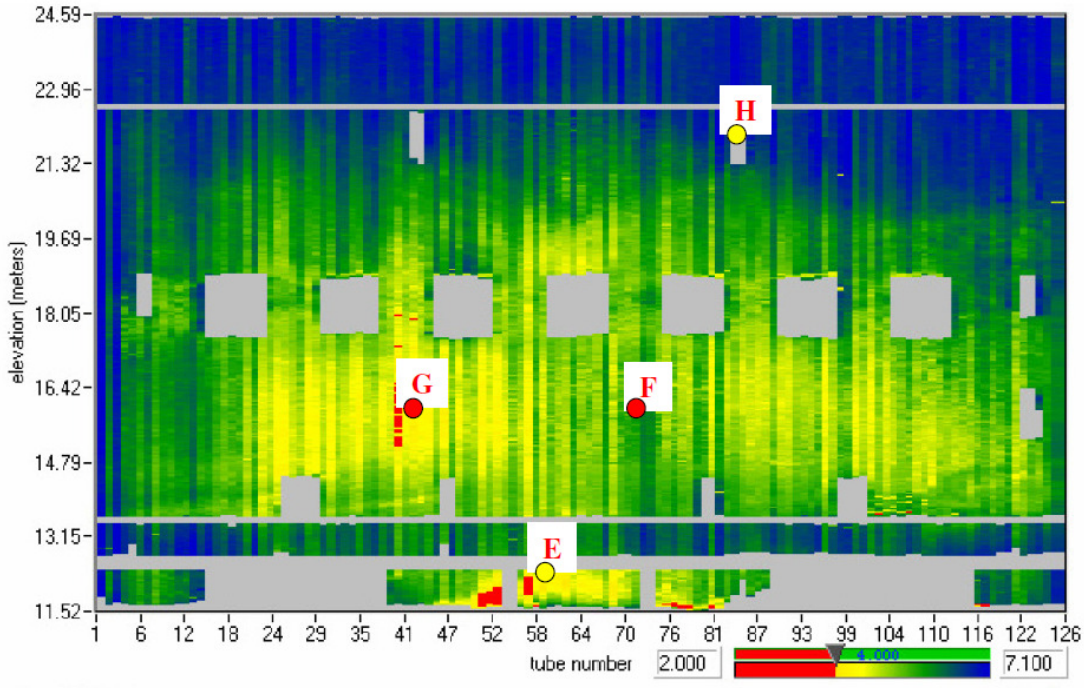

Figure 6 Tube thickness measurement of furnace front wall. In the red parts, the wall thickness of the tubes is less than 4 mm. (View from inside of boiler.)

1.2 Deposit probes

Six deposit probe exposures have been performed. The deposit probe is mounted with four cooled specimens where the deposits are collected. Probe specimens were 48 mm long, 7 mm wide and 6 mm thick. The temperature was measured by a thermocouple placed centrally at the back of each specimen. A picture of the probe after exposure is shown in Figure 7a. The probe is inserted in a slit in the fin between two tubes in the furnace wall. The exposure time was 12-15h. Two alloys have been used, 13CrMo4-5 (ferritic steel) and 310 (austenitic stainless steel). The composition of these alloys is shown in Table 1. The probes were inserted at three different positions in the furnace, positions A, B-C and B-C left (see Figure 1 and Figure 2 above). Position B-C left is to the left when seen from outside the furnace.

The cooling of the probes was adjusted to give a temperature gradient so that a number of different material temperatures could be investigated.

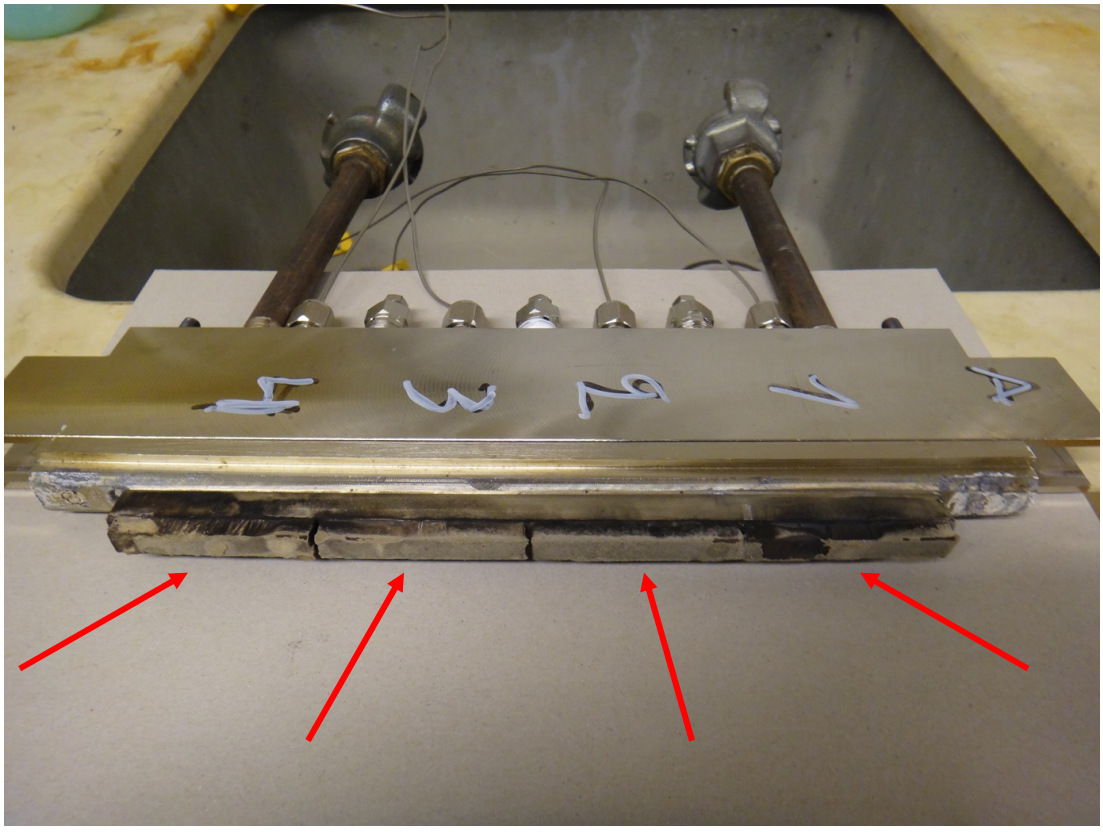

Figure 7a Deposit probe after exposure with four samples (indicated by red arrows)

Table 1 Composition of alloys used for deposit probe samples

Alloy	Fe	Cr	Ni	Mn	Mo	Si	C
13CrMo4-5	Bal.	0.7-1.15	<0.3	0.4 - 1.0	0.4- 0.6	≤ 0.35	0.08 - 0.18
310S	Bal.	25	20	1.5	<0.5	<0.5	<0.08

The sample specimens were weighed before and after exposure to establish the amount of deposit collected.

The composition of the deposits was analysed by SEM-EDX. 10 different areas approximately on the middle of each specimen have been analysed and the average composition has been calculated. (Figure 7b) The size of each area was ~2x2.5mm. The magnification used was 50X and the accelerating voltage was 20kV for all samples.

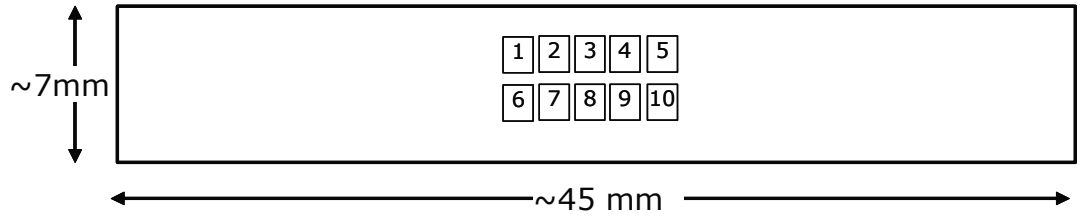

Figure 7b Schematic of deposit sample with areas for SEM-EDX analysis indicated.

1.3 Flue gas measurements

The flue gas composition and temperature has been investigated in seven positions in the boiler, positions A, J and K on the back wall, positions B-C and D on the side wall and positions F and G on the front wall of the furnace. (See Figure 1, Figure 2 and Figure 3.). The measurements were taken at a distance of 10 cm and 80 cm from the boiler wall on 8 and 10 November 2011 between 11:00h and 17:00h. During this time the boiler was running at 65-80% of full load.

An FTIR has been used to measure the flue gas content of CO, SO_2, NH_3, HF, CH_4, NOx, H_2O and CO_2.

A Sick-May instrument has been used the measure the O_2 content and flue gas temperature.

1.4 Impactor measurements

Impactor measurements were made by SP at positions A (on 8th Nov) and postion B (on 9th Nov). The measuerments were made at the wall and 80 cm from the wall, using a Dekati low pressure impactor. The impactor has 13 stages ranging from

0.03 to 10 µm and is shown in Figure 8. The principle of operation is shown in Figure 9.

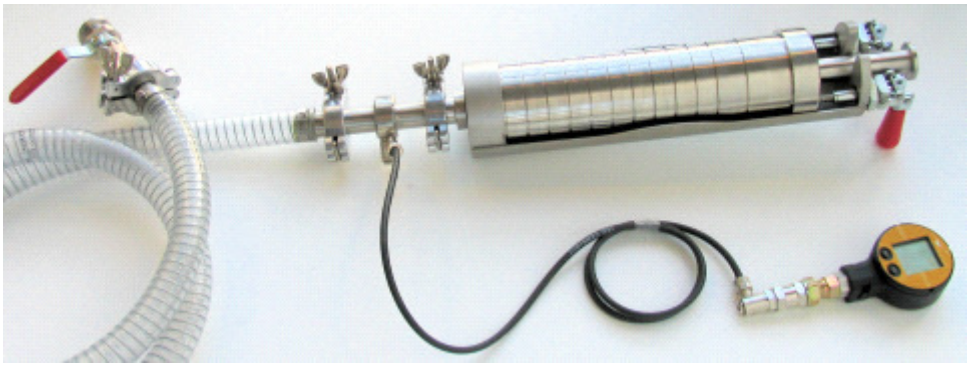

Figure 8 Low pressure impactor used for ash particle size measurements.

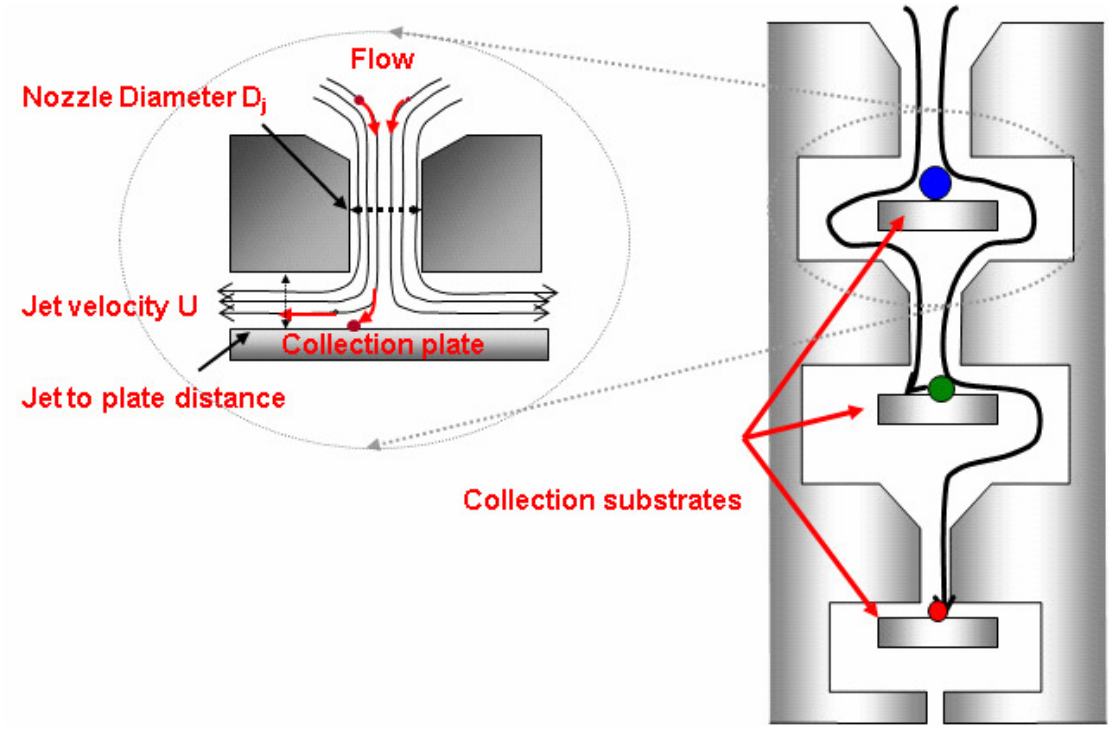

Figure 9 Schematic diagram showing principle of operation of an impactor

2 RESULTS

2.1 Deposit probes

The cooling of the probes was adjusted to give different temperatures on different samples. The sample with the regulating thermocouple has had a stable temperature on all probes, but the temperatures of the other samples fluctuated somewhat. Only the probes in case 2 (position B-C and B-C left) and some of the samples of probe B-C, case 3 has had reasonably stable temperatures. Examples of temperature curves for the deposit probes are shown in Figure 9 and Figure 10.

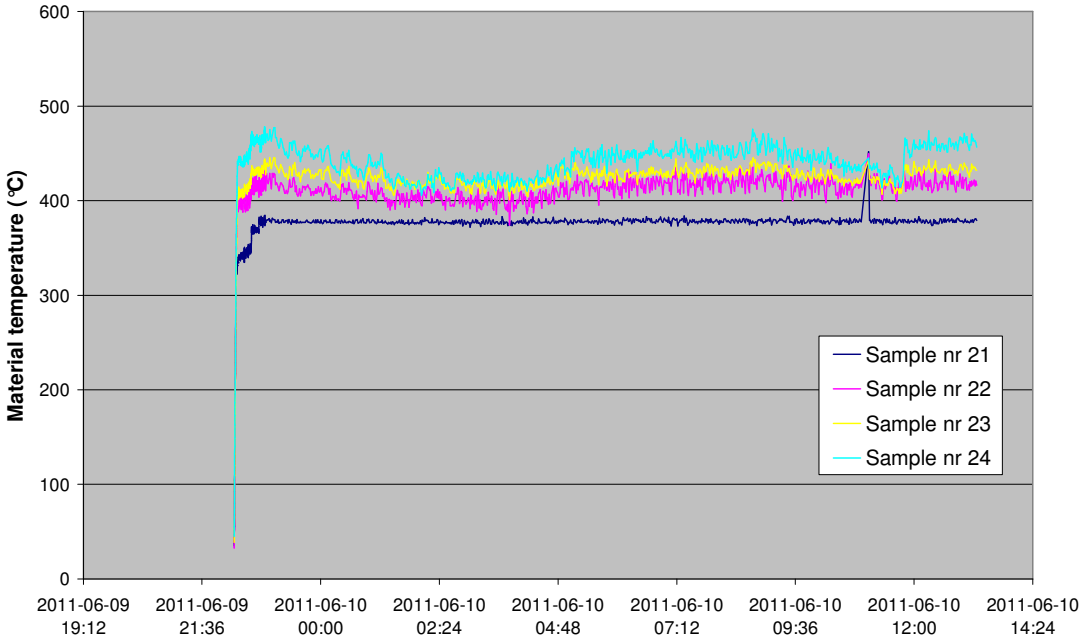

Figure 9 Material temperatures of samples on probe in position B-C, case 2. (Note, the month should be 11(November) and not 06 (June). Days and time is correct.). The cooling of the probe was altered to give a temperature gradient. It was not intended that all specimens should have the same temperature.

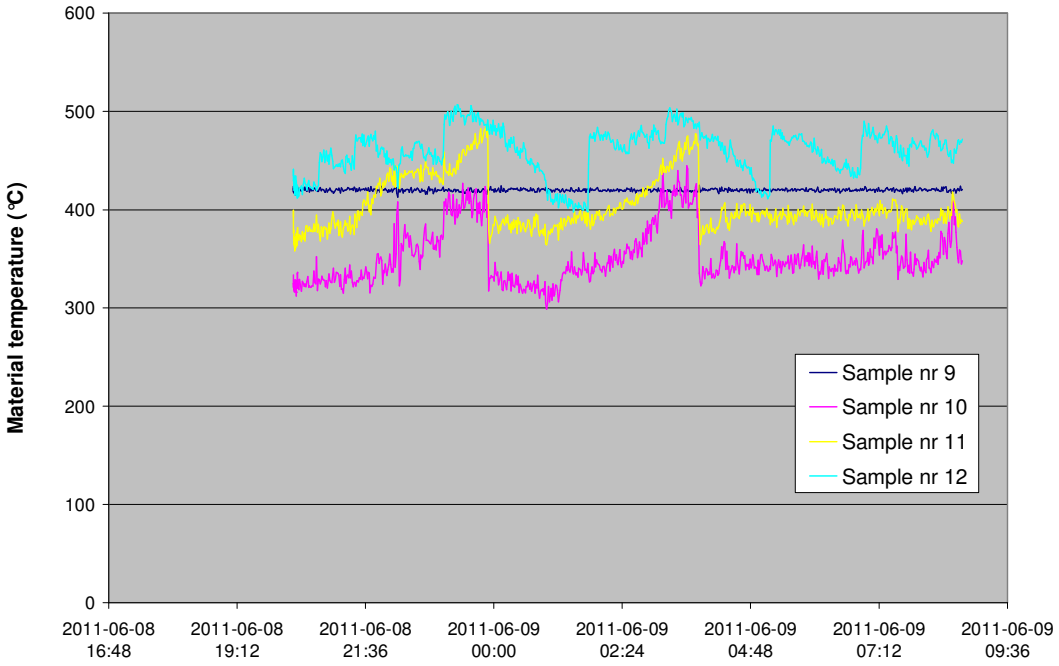

Figure 10 Material temperatures of samples on probe in position A, case 3. (Note, the month should be 11 (November) and not 06 (June). Day and time is correct)

The average material temperature of the samples and the weight gain are presented in Table 2. Since the fluctuation in temperature was so large, the average temperature cannot be used to any large extent in the evaluation of the results, but gives an indication of the temperature. The samples on one of the probes, case 2, position B-C left, had significantly larger weight gain than the rest of the samples. No explanation to this has been found.

Table 2 Average material temperature and weight gain of deposit probe samples

Exposure	Position	Sample no	Material	Average temp (℃)	Temp std dev (℃)	Weight gain (mg/mm2/h)
1	A	1	13CrMo4-5	399	2	0.0116
1	A	2	13CrMo4-5	342	17	0.0108
1	A	3	310	344	35	0.0071
1	A	4	310	398	25	0.0077
1	B-C	5	13CrMo4-5	399	6	0.0075
1	B-C	6	13CrMo4-5	298	22	0.0118
1	B-C	7	310	317	25	0.0169
1	B-C	8	310	375	15	0.0110
3	A	9	13CrMo4-5	420	1	0.0104
3	A	10	13CrMo4-5	352	28	0.0172
3	A	11	310	405	27	0.0093
3	A	12	310	460	24	0.0085
3	B-C	13	13CrMo4-5	419	2	0.0074
3	B-C	14	13CrMo4-5	395	10	0.0120
3	B-C	15	310	349	30	0.0135
3	B-C	16	310	418	9	0.0155
2	B-C left	17	13CrMo4-5	254	16	0.0263
2	B-C left	18	13CrMo4-5	334	21	0.0242
2	B-C left	19	13CrMo4-5	371	14	0.0443
2	B-C left	20	13CrMo4-5	370	5	0.0544
2	B-C	21	13CrMo4-5	377	13	0.0112
2	B-C	22	13CrMo4-5	412	10	0.0106
2	B-C	23	13CrMo4-5	425	9	0.0112
2	B-C	24	13CrMo4-5	442	15	0.0140

The composition of the deposit samples in weight % is presented in Table 3 and in Figure 11 and Figure 12. (The composition in atomic % can be seen in appendix A.) Information on the bed temperature and flue gas temperature at the top of the furnace during probe exposures can be found in Appendix B.

No clear differences in composition can be seen between the different positions in the furnace.

In Figure 13. the correlation between Cl and S content is shown. Samples with high S content (>8 weight %) have a fairly low Cl content (< 5 weight %).

Table 3 Composition of deposit samples in weight %

	Run 1, position A				Run 1, position B-C				Run 3, position A				Run 3, position B-C				Run 2, position B-C left				Run 2, position B-C			
	13CrMo44		310		13CrMo44		310		13CrMo44		310		13CrMo44		310		13CrMo44				13CrMo44			
	1	2	3	4	5	6	7	8	9	10	11	12	13	14	15	16	17	18	19	20	21	22	23	24
C	-	-	-	-	-	-	-	-	-	-	-	-	-	-	-	-	-	-	-	-	-	-	-	-
O	41,9	33,7	41,0	38,3	45,0	40,4	40,9	43,6	25,9	25,4	34,2	26,3	35,7	35,6	37,2	38,2	31,6	28,0	27,2	39,0	35,3	36,9	32,0	35,4
Na	6,1	6,6	5,5	6,6	4,7	3,8	-	1,7	5,3	4,6	3,3	6,6	4,3	4,6	3,2	2,9	4,9	5,8	5,7	2,5	3,6	2,9	4,4	4,2
Mg	1,4	1,4	1,5	1,1	1,9	1,8	1,6	1,2	1,5	1,4	1,6	1,5	1,7	1,7	1,7	1,8	1,4	1,4	1,4	1,8	1,4	1,6	1,5	1,6
Al	1,2	1,1	1,0	1,5	1,4	1,7	2,5	2,1	1,3	1,3	1,3	1,2	1,2	1,3	2,0	1,4	2,1	1,9	1,7	3,1	1,6	1,9	1,7	2,7
Si	2,4	2,2	2,0	1,8	2,8	3,3	5,5	5,6	2,5	2,8	2,6	2,3	2,5	2,6	4,6	2,9	5,1	4,2	3,6	8,3	3,1	3,9	3,5	6,0
P	0,6	0,6	0,7	0,6	0,8	0,7	0,8	0,7	0,4	0,2	0,4	0,5	0,4	0,4	0,3	0,5	0,4	0,4	0,4	0,4	0,4	0,5	0,5	0,5
S	10,3	6,4	10,2	9,9	9,9	7,0	5,2	4,5	5,5	6,3	10,3	5,6	10,7	10,3	8,0	10,1	4,9	3,7	3,9	4,6	10,4	9,2	7,5	6,0
Cl	2,3	9,5	2,3	1,3	1,8	7,3	5,1	5,0	13,4	13,8	3,5	13,2	2,4	2,6	2,1	1,6	1-	13,7	14,5	2,4	4,1	3,5	7,2	2,1
K	8,4	5,8	8,2	8,9	6,9	4,4	2,4	2,4	7,0	6,5	8,1	8,7	7,8	6,9	5,0	7,1	6,9	7,8	7,9	2,6	7,6	5,5	6,5	4,8
Ca	11,0	9,2	9,9	9,4	13,9	14,4	16,3	15,0	11,6	12,0	13,1	11,0	13,5	13,4	14,8	15,9	13,0	11,3	12,3	17,3	13,8	16,2	13,1	12,1
Ti	2,4	1,9	1,9	1,6	2,6	3,0	3,4	3,3	2,6	2,7	2,9	2,5	2,9	3,0	3,9	3,4	3,3	2,6	2,7	3,7	2,9	3,2	2,7	3,2
V	-	-	-	-	-	-	-	-	-	-	-	-	-	-	-	-	-	-	-	-	-	-	-	-
Cr	-	-	-	-	-	-	0,2	-	-	-	-	-	-	-	-	-	-	-	-	-	-	-	-	-
Mn	0,4	0,6	0,3	0,3	0,5	0,5	0,5	0,5	0,5	0,6	0,4	0,4	0,5	0,4	0,5	0,5	0,4	0,4	0,4	0,4	0,4	0,4	0,6	0,6
Fe	2,6	7,8	1,6	1,5	2,8	2,3	2,9	2,9	3,5	4,0	1,7	1,5	4,1	4,4	3,0	2,1	3,1	2,6	2,5	4,7	3,4	3,4	6,8	9,7
Ni	-	-	-	-	-	-	-	-	-	-	-	-	-	-	-	-	-	-	-	-	-	-	-	-
Cu	-	-	-	-	-	-	0,4	0,4	0,8	0,2	0,3	0,3	0,2	0,2	0,5	0,3	0,4	0,5	0,2	0,1	0,3	0,3	0,3	0,1
Zn	8,6	6,8	6,8	10,9	5,1	5,3	9,4	8,6	14,3	12,6	11,8	14,9	8,6	8,7	6,6	8,3	9,6	12,9	13,0	7,9	6,4	6,9	7,6	9,0
Pb	-	6,5	6,8	6,4	-	4,1	2,9	2,5	4,0	5,6	4,3	3,3	3,4	3,9	6,5	2,8	2,9	2,7	2,7	1,1	5,3	3,6	4,1	1,9
As*	0,4	-	-	-	-	-	-	-	-	-	-	-	-	-	-	-	-	-	-	-	-	-	-	-

* note : Lα for Pb is similar to Kα for As = 10.5 keV. Therefore sample 1 may contain Pb instead of As.

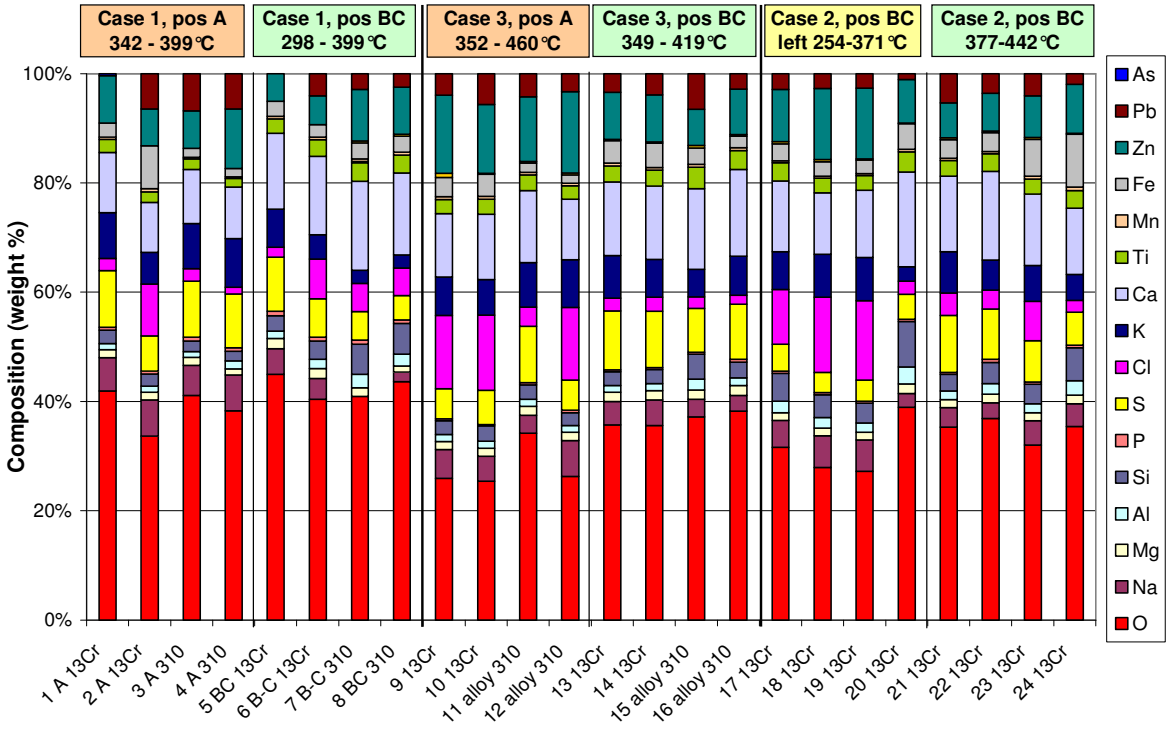

Figure 11 Deposit composition in weight %

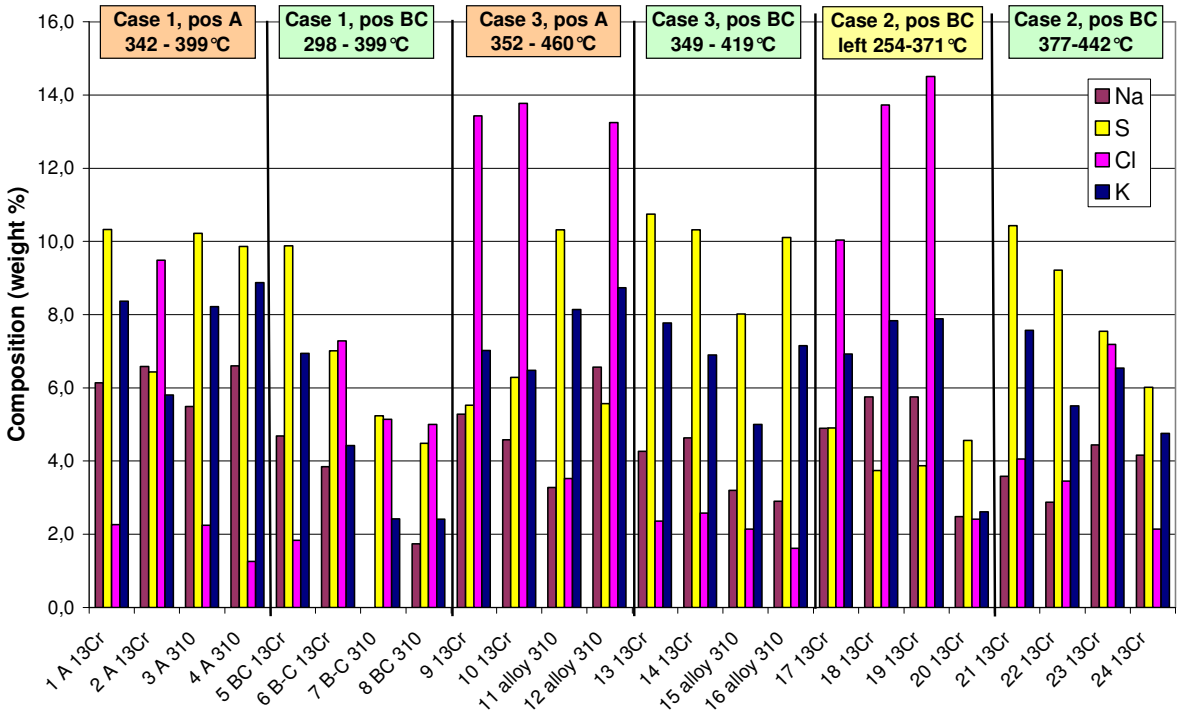

Figure 12 Content of some selected elements in deposit in weight %

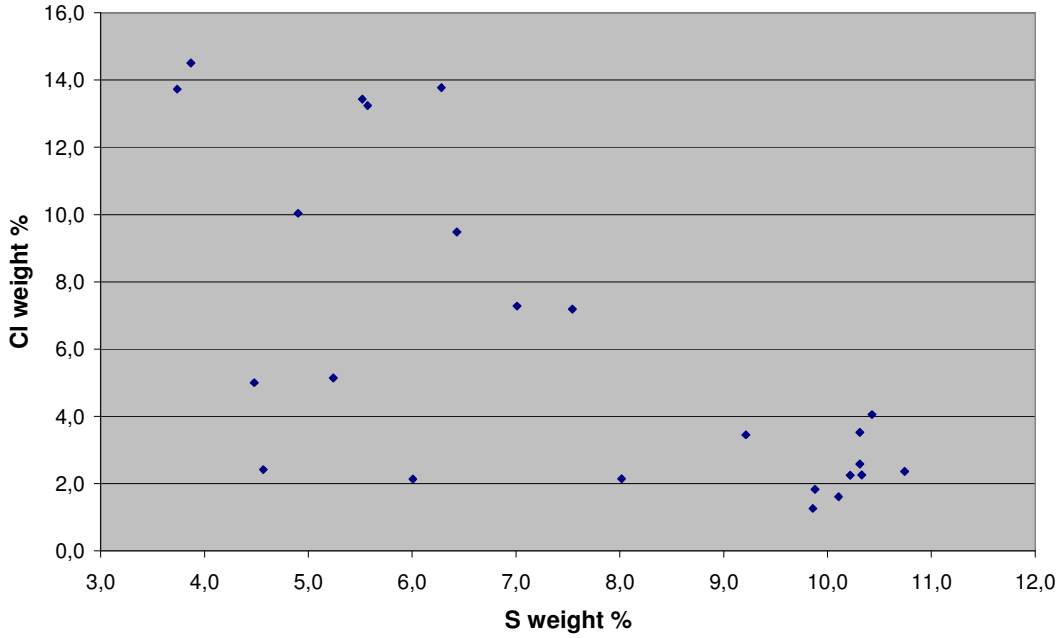

Figure 13 Correlation between Cl and S content of deposits

2.2 Flue gas measurements

The results of the flue gas measurements are presented in Table 4. Measurements at positions D, F, G and K were made on 8 November and repeated on 10 November. Measurements at position A were made only on 10 November and at B-C on 8 November, because impactor measurements were being made at these positions at other times. The bed and flue gas temperatures were higher on 10 Nov, see operational data in Appendix B

Very low O_2 levels were detected, sometimes below 0.5%, and the fluctuation over time was large. The fluctuation was greatest at the back wall and least on the right wall. (Figure 14 and Figure 15) The temperatures were lower close to the wall than 1 m into the furnace. (Figure 16) The CO levels were high. When the ChlorOut system was turned off the KCl level near the superheaters was 19-28 ppm. (Figure 17)

Average values of flue gas in furnace, about + 16 m

SICK O_2 0.9%, CO (out of range for many readings, i.e. > 1.3%)

FTIR, average values: CO 1.7%, SO_2 46 ppm, HCl 15 ppm, HF 1 ppm, CH_4 (methane) 1360 ppm, NOx 96 ppm, H_2O 19.6 %, CO_2 8.9%

IACM (with no ChlorOut additive) at superheaters: KCl 19-28 ppm, SO_2 32-49 ppm

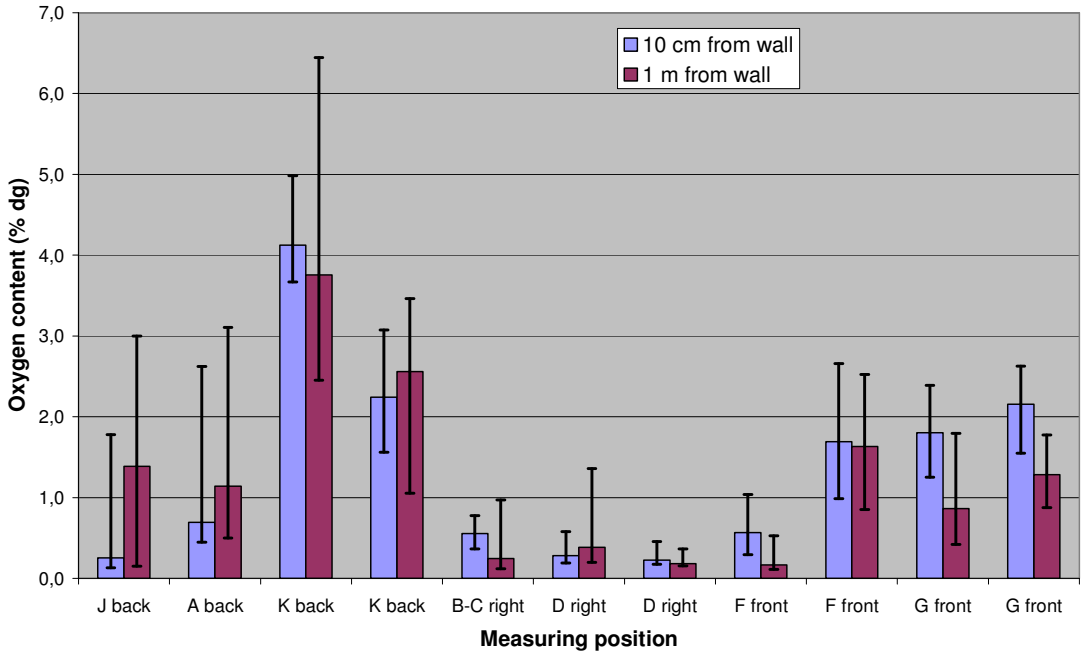

Figure 14 Oxygen content, measured with Sick instrument, average, minimum and maximum values. Measurements at K, D, F and G were made on 8 Nov and repeated on 10 Nov.

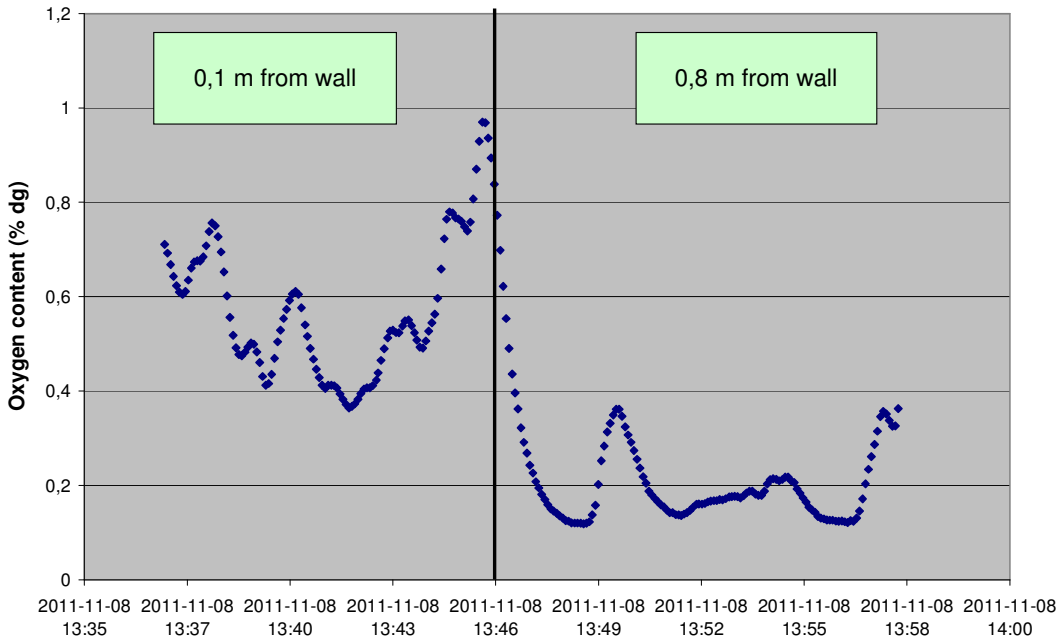

Figure 15 Oxygen measurement in position B-C.

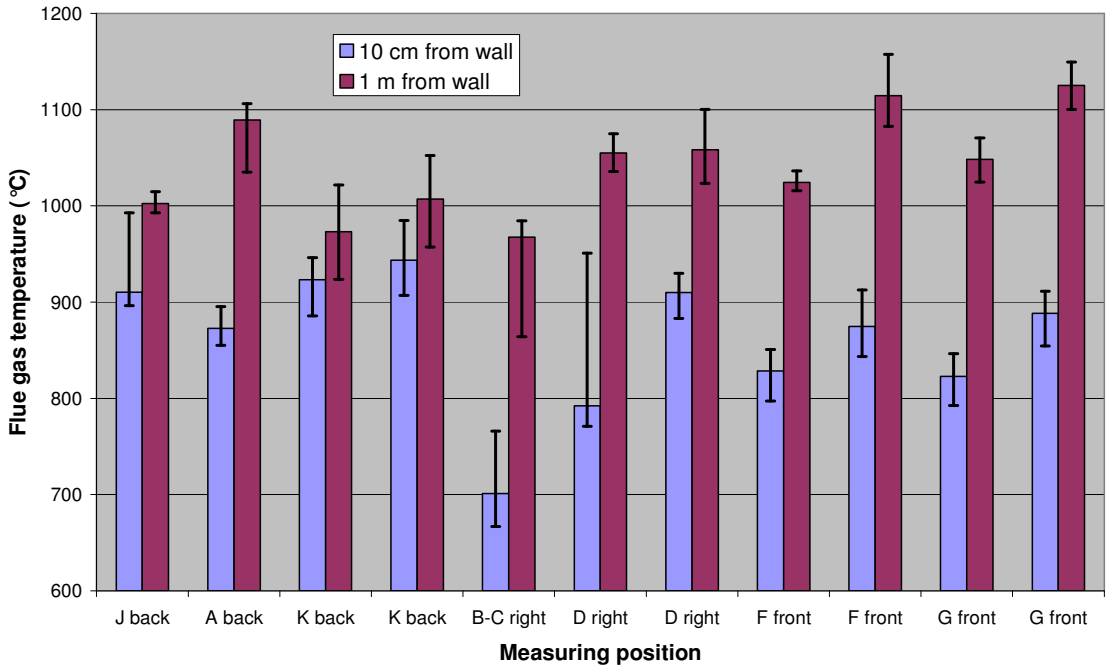

Figure 16 Flue gas temperature, measured with Sick instrument, average, minimum and maximum values

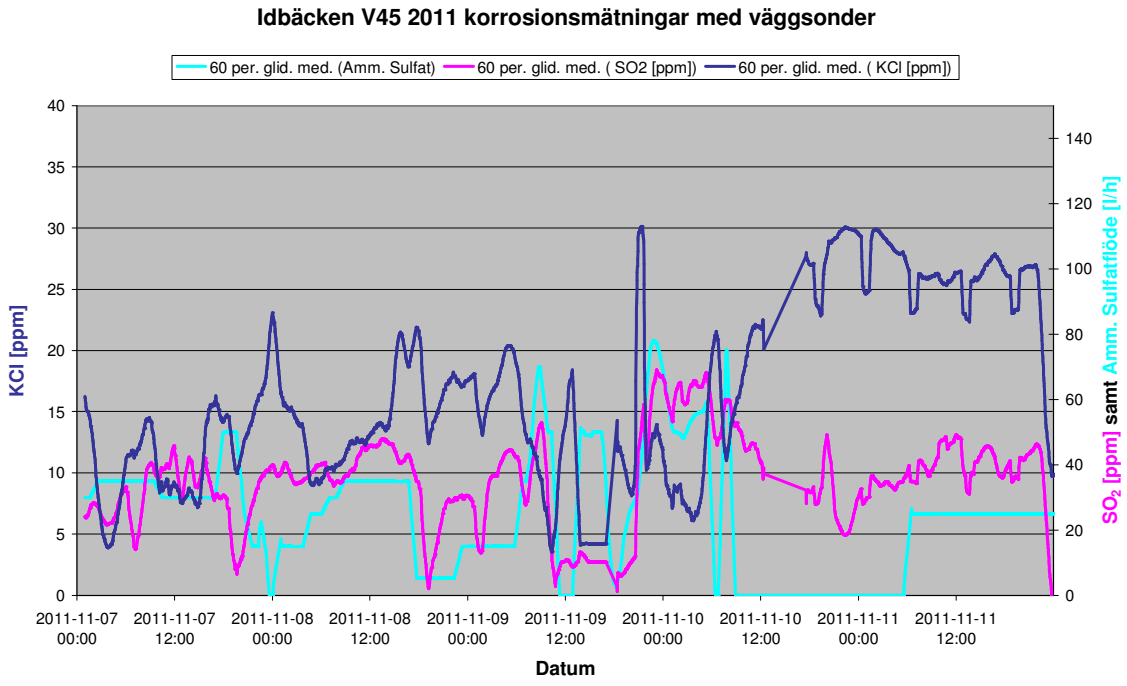

Figure 17 IACM measurement of KCl in flue gases

Table 4 Results from flue gas measurements, average content/temperature

Pos	Distance from wall	FTIR										Sick	
		CO	NO	SO2	NH3	HCl	HF	CH4	NOx	H2O	CO2	O2	Temp
	(m)	(ppm)	(ppm)	(ppm)	(ppm)	(ppm)	(ppm)	(ppm)	(ppm)	(%)	(%)	(% tg)	(°C)
A	0,1	17436	50	24	277	7,9	0,8	931	51	18	3	0,7	873
	0,8	18760	10	15	207	9,0	0,7	876	11	17	3	1,1	1089
B-C	0,1	19035	88	76	438	0,1	1,2	2497	85	26	5	0,6	701
	0,8	19179	88	67	408	3,7	1,1	2544	86	24	5	0,2	968
D	0,1	37702	81	74	1090	42,2	1,1	2578	104	22	26	0,3	792
	0,8	35811	21	53	876	16,8	1,0	2838	22	25	-3	0,4	1055
D	0,1	39663	42	56	1182	47,2	2,0	2497	62	18	25	0,2	910
	0,8	29793	10	17	845	12,4	1,5	2963	9	18	0	0,2	1058
F	0,1	6991	126	46	102	7,5	0,7	401	127	22	9	0,6	829
	0,8	22279	7	26	440	1,0	0,4	1896	7	21	3	0,2	1024
F	0,1	874	167	58	35	22,7	0,9	38	171	16	11	1,7	875
	0,8	1393	175	74	56	20,2	1,1	65	178	17	11	1,6	1115
G	0,1	1862	170	30	80	4,4	0,9	135	173	21	13	1,8	823
	0,8	3723	188	52	59	7,3	0,8	269	190	21	11	0,9	1049
G	0,1	315	179	76	14	21,5	1,0	29	182	16	11	2,2	888
	0,8	1524	181	92	15	23,8	1,0	119	184	17	10	1,3	1125
J	0,1	20941	45	33	400	3,7	1,0	1618	46	18	2	0,3	910
	1,2	23234	2	18	462	2,7	1,1	2153	1	19	1	1,4	1002
K	0,1	35	184	26	50	8,7	0,7	0	188	18	16	4,1	923
	1,2	155	169	39	42	22,1	0,5	8	174	20	15	3,8	973
K	0,1	38237	42	55	1178	44,1	2,0	2626	59	18	23	2,2	943
	1,2	30233	7	13	822	10,9	1,4	2884	4	18	-1	2,6	1007

2.3 Impactor measurements

Impactor measurements were made at :

- Position A, close to membrane wall
- Position A, 80 cm from membrane wall
- Position B, close to membrane wall
- Position B, 80 cm from membrane wall

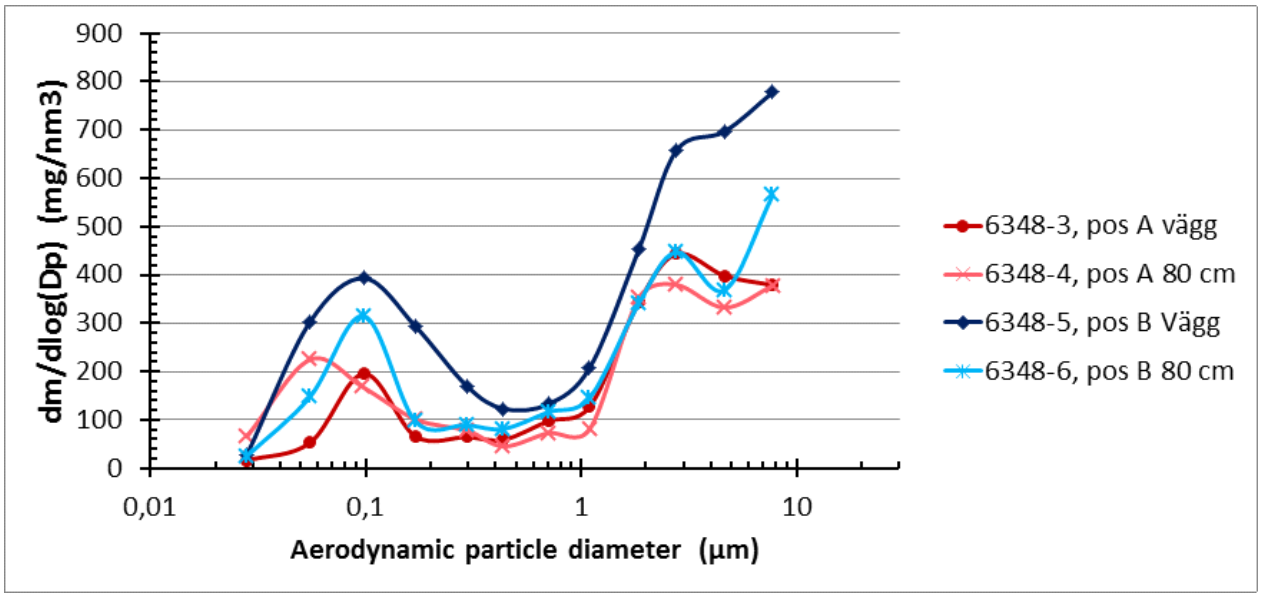

Figure 18 Size distribution of particles from impactor measurements

The overall size distribution is given in Fig. 19, which shows that in all categories there are more particles at the wall in position B (approximately twice as much as the wall in position A). This is not shown in the deposit growth measurements, apart from the probe in position B-C left hole (see Table 2). The most reasonable explanation of the results is that the rate of particle deposition varies considerably even locally on the wall and that particle flows are not homogeneous.

The chemical compositions in weight % for different size fractions are shown in Figures 20-26. Cl, K, Pb and Zn and S are found in sub-micron particles and are enriched in position B. Si and Ca are found in particle sizes 1-10µm.

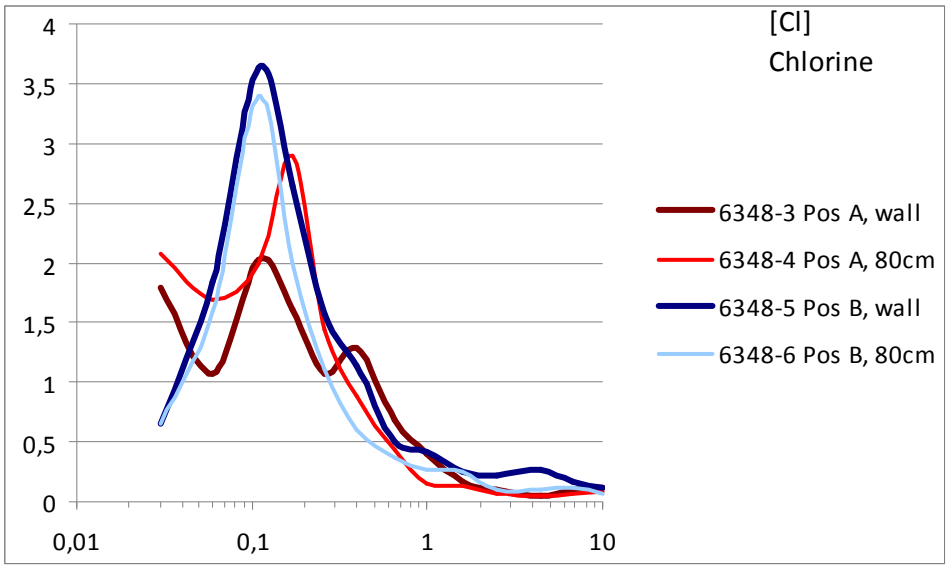

Figure 20 Chlorine content in weight % for each size fraction from the impactor measurements

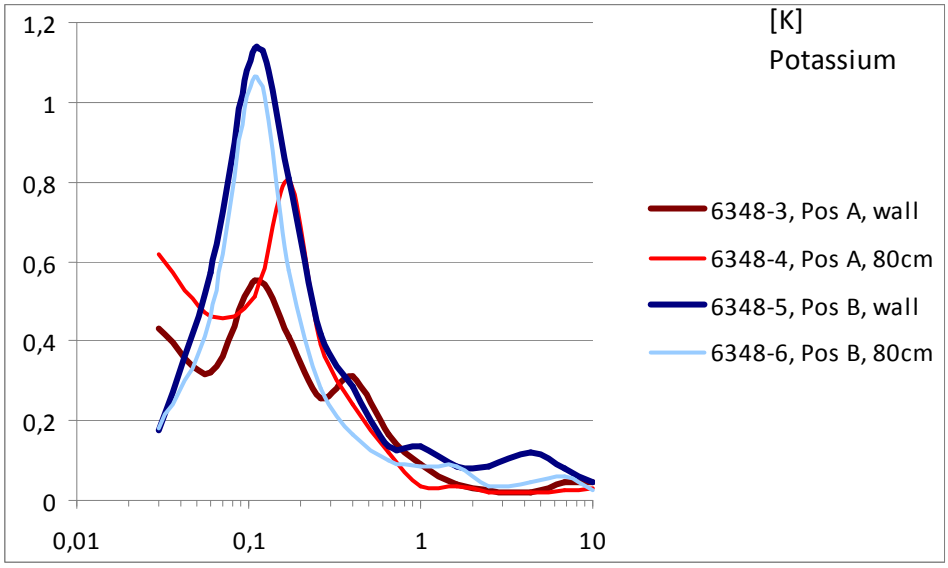

Figure 21 Potassium content in weight % for each size fraction from the impactor measurements

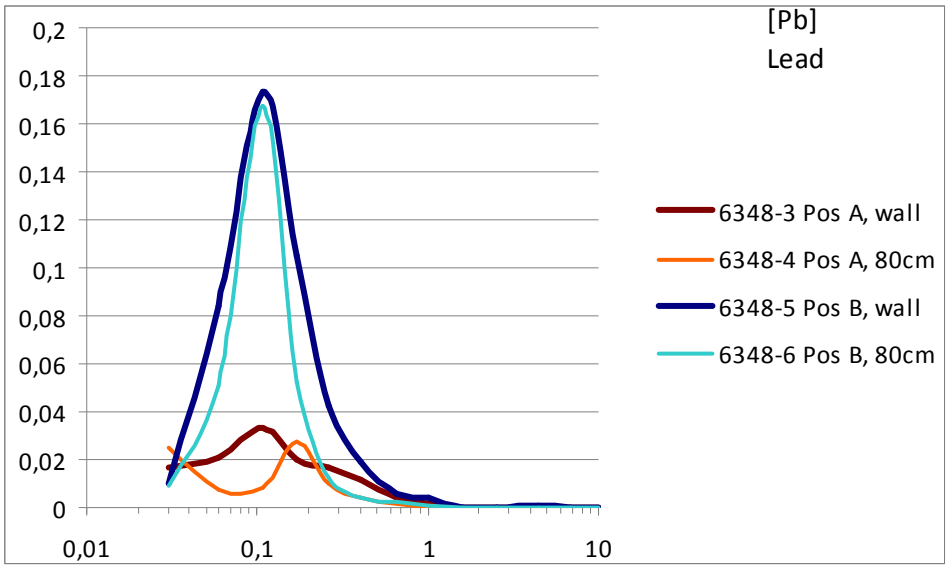

Figure 22 Lead content in weight % for each size fraction from the impactor measurements

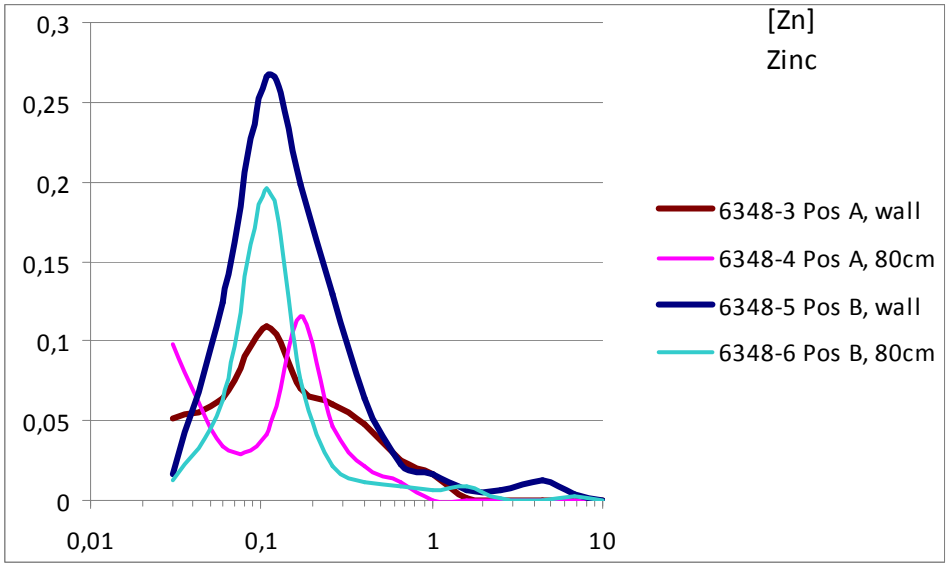

Figure 23 Zinc content in weight % for each size fraction from the impactor measurements

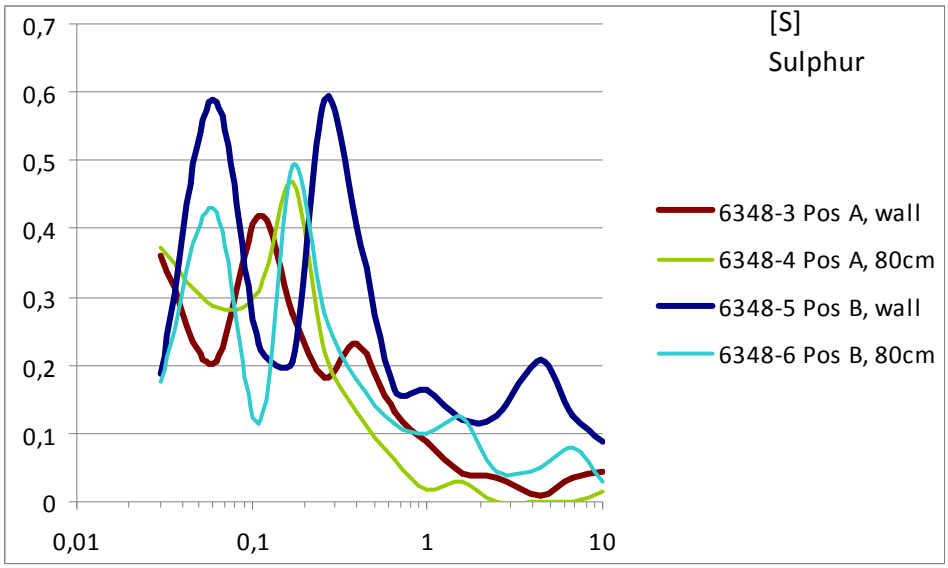

Figure 24 Sulphur content in weight % for each size fraction from the impactor measurements

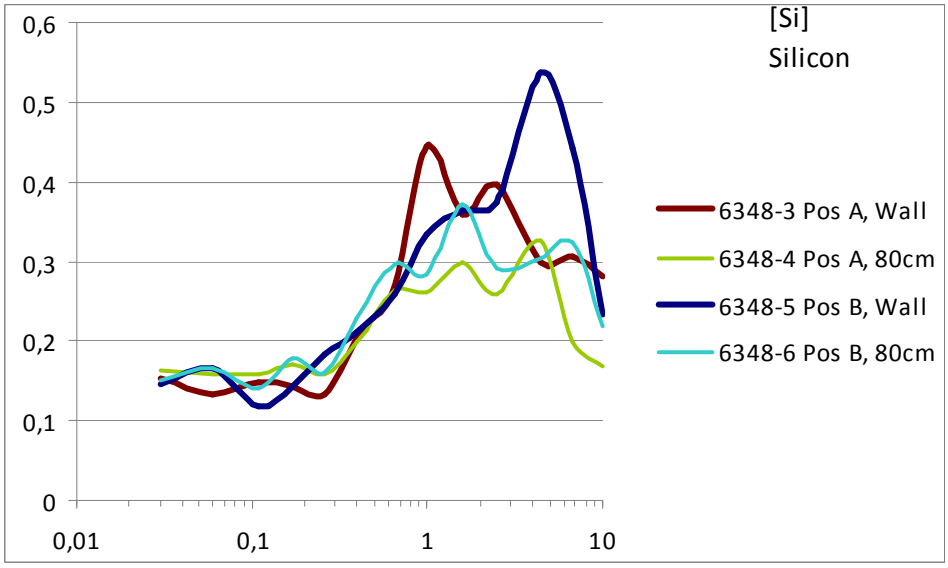

Figure 25 Silicon content in weight % for each size fraction from the impactor measurements

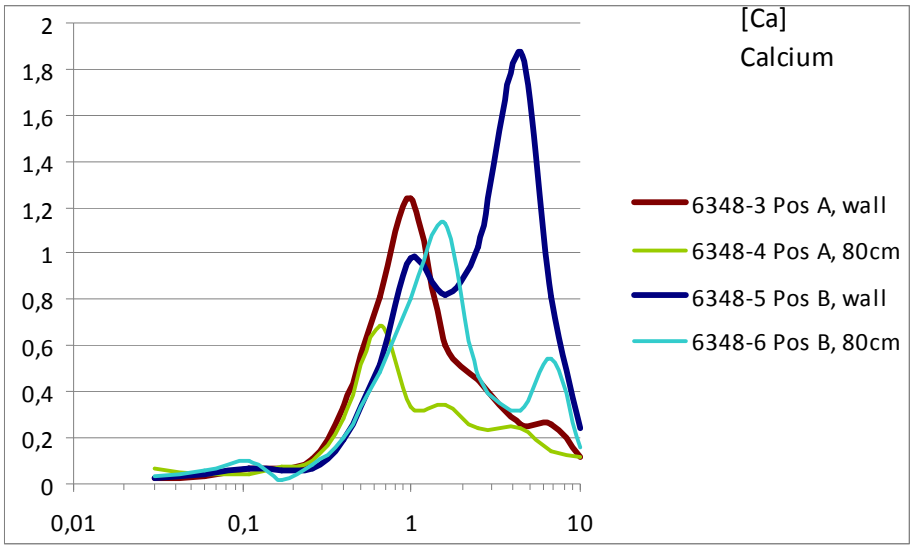

Figure 26 Calcium content in weight % for each size fraction from the impactor measurements

2.4 Fuel

Table 5 Fuel used during measurement campaign Nov 2011 compared to average values for wood chips and waste wood taken from Värmeforsk's fuel handbook. Only key elements shown

Parameter	Wood chips	Waste wood	Waste wood 113151 2011-11-10
Total moisture (weight %)	41,1	33,7	30,7
Total ash (weight %)	3 (d)	4,8 (d)	5,8 (d)
C (weight %) dry sample	51	51,7	46,9
N (weight %)	0,4 (d)	0,8	2,0
S (weight %)	0,03 (d)	0,07 (daf)	0,1 (d)
Cl (weight %)	0,03 (d)	0,05 (daf)	0,06 (d)
K (mg/kg) in ash	72000	22000	16240
Na (mg/kg) in ash	7000	16500	28694
Pb (mg/kg) in ash	63	560	3539
Zn (mg/kg) in ash	2047	6310	8490

d = dry sample , daf = dry & ash free sample

Table 5 shows the key elements which form corrosive salts in the waste wood which was fired during the treting campaign. The key elements for wood chips and waste wood from Värmeforsk's fuel handbook are shown for comparison. It can be seen that the levels of S, Cl, Na ,Pb and Zn are much higher in the waste wood than in forest fuel/wood chips.

3 DISCUSSION AND CONCLUSIONS

The lower furnace region of a boiler, where combustion is occurring, is a difficult area to make tests in. The combustion conditions fluctuate rapidly leading to a heterogeneous distribution of flue gases and particles landing on the furnace walls. Additionally, the operating conditions are not constant with time leading to a variation in bed and flue gas temperature in the furnace over the measurement period.

It was expected that the deposit composition might vary with metal substrate temperature, type of steel, or position in boiler. However, no such correlation could be found.

The back wall of the boiler, particularly position A , experiences a higher corrosion rate than the right wall, position B-C. The main differences between these two positions seemed to be a higher flue gas temperature and a greater fluctuation in the oxygen content at the back wall.

Very low O_2 levels were detected, sometimes below 0.5%, and the fluctuation over time was large. The fluctuation was greatest at the back wall and least on the right wall. The temperatures were lower close to the wall than 1 m into the furnace. The CO levels were high. When the ChlorOut system was turned off the KCl level near the superheaters was 19-28 ppm.

Average values of flue gas at the furnace wall, about + 16 m

SICK O_2 0.9%, CO (out of range for many readings, i.e. > 1.3%)

FTIR, average values: CO 1.7%, SO_2 46 ppm, HCl 15 ppm, HF 1 ppm, CH_4 (methane) 1360 ppm, NOx 96 ppm, H_2O 19.6 %, CO_2 8.9%

IACM (with no ChlorOut additive) at superheaters: KCl 19-28 ppm, SO_2 32-49 ppm

K, Cl, S, Pb and Zn were found in the deposits. The levels varied considerably and in a seemingly random manner.

The chlorine content varied between 2 and 14 wt % , zinc 5-15 wt%, lead up to 6.8 wt%, potassium 2-9 wt% , sodium up to 6.6 wt% and sulphur 4-11 wt%. There was no correlation between Cl content, measuring position (back wall or side wall), substrate temperature or alloy, but a high S content correlated with a low Cl content.

Impactor measurements showed that Cl, K, Pb and Zn and S were found in sub-micron particles. Si and Ca were found in particle sizes 1-10µm.

4 ACKNOWLEDGEMENTS

We thank Mattias Mattsson and Tomas Leffler (VRD) for making the flue gas and probe measurements, Anders Hjörnhede (SP) for organising the impactor measurements, Peter Viklund (KIMAB) and Yousef Alipour (KTH) for the deposit chemical analyses and Seppo Simola (Idbäcken) for his constant help during our time spent at the plant.

5 FUTURE WORK

Given the fluctuations and variations in combustion conditions it is desirable to repeat measurements in positions A and B-C with waste wood. A new measurement campaign with waste wood and an additive which reduces the corrosive nature of the fuel should be performed.

Given the increasing price of waste wood, the diminishing price gap between virgin and recycled wood, and the lower Cl and heavy metal content of virgin wood it would be interesting to perform a campaign with virgin wood.

Appendix A, Deposit composition in atomic %

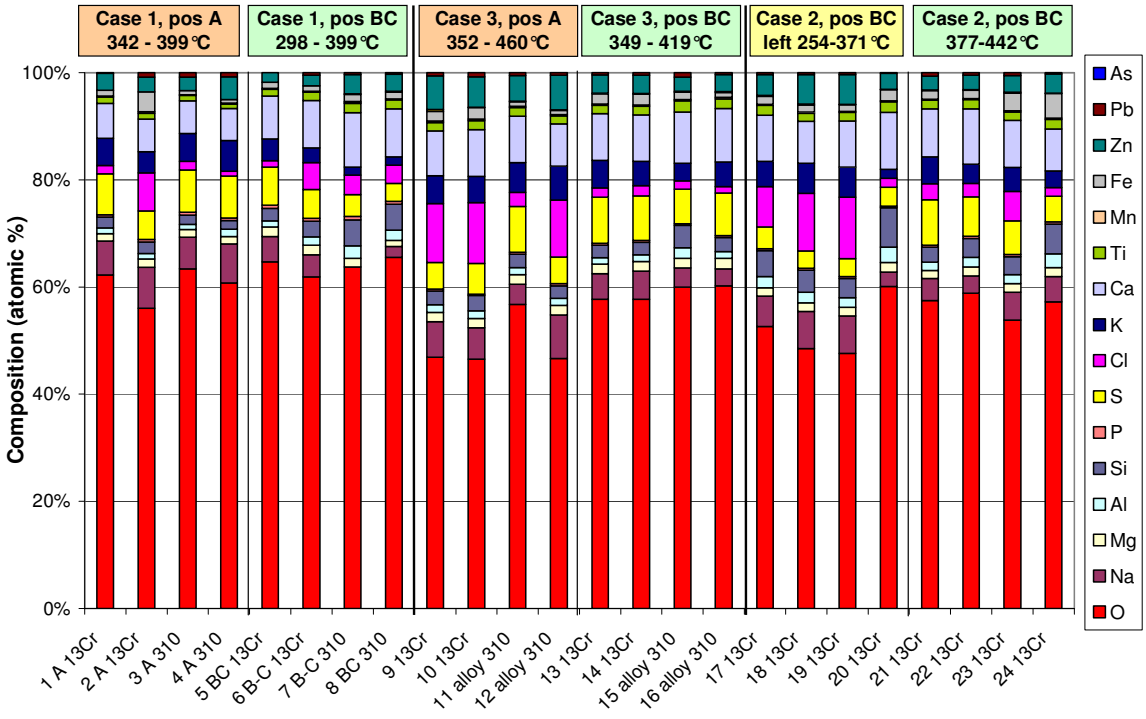

Figure A1 Composition of deposit samples in atomic %,

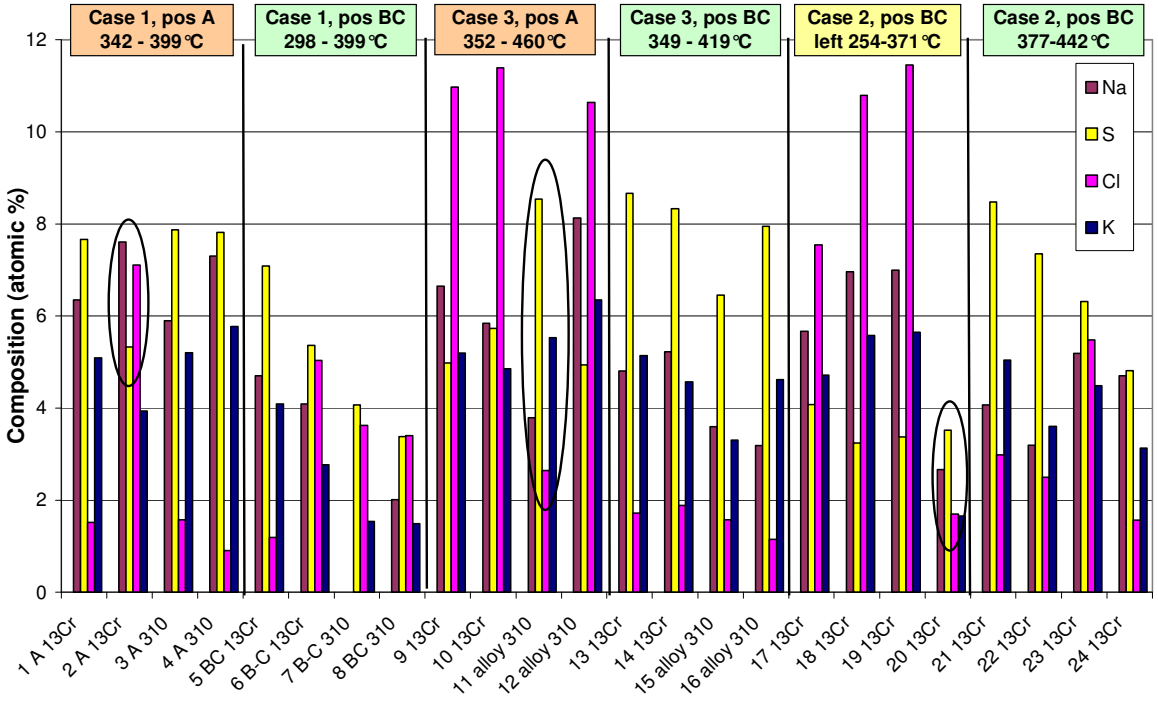

Figure A2 Content of some key elements in deposit samples (in atomic %)

Table A1 Deposit composition in atomic %

	Run 1, position A				Run 1, position B-C				Run 3, position A				Run 3, position B-C				Run 2, position B-C left				Run 2, position B-C			
	13CrMo44		310		13CrMo44		310		13CrMo44		310		13CrMo44		310		13CrMo44				13CrMo44			
	1	2	3	4	5	6	7	8	9	10	11	12	13	14	15	16	17	18	19	20	21	22	23	24
C	-	-	-	-	-	-	-	-	-	-	-	-	-	-	-	-	-	-	-	-	-	-	-	-
O	62,2	56,1	63,3	60,9	64,7	61,9	63,8	65,6	46,9	46,5	56,7	46,6	57,7	57,7	60	60,2	52,6	48,5	47,6	60,1	57,5	58,9	53,8	57,3
Na	6,4	7,6	5,9	7,3	4,7	4,1	-	2,0	6,6	5,8	3,8	8,1	4,8	5,2	3,6	3,2	5,7	7,0	7,0	2,7	4,1	3,2	5,2	4,7
Mg	1,4	1,6	1,5	1,4	1,8	1,8	1,6	1,2	1,7	1,7	1,8	1,8	1,8	1,8	1,8	1,9	1,6	1,6	1,6	1,8	1,5	1,7	1,6	1,7
Al	1,0	1,1	0,9	1,4	1,2	1,6	2,3	1,9	1,4	1,4	1,3	1,3	1,2	1,2	2,0	1,3	2,1	2,0	1,8	2,9	1,5	1,8	1,7	2,6
Si	2,1	2,1	1,7	1,6	2,3	2,9	4,9	4,8	2,6	2,9	2,5	2,4	2,3	2,4	4,2	2,6	4,8	4,1	3,6	7,3	2,8	3,5	3,4	5,6
P	0,4	0,5	0,6	0,5	0,6	0,6	0,6	0,5	0,3	0,2	0,3	0,4	0,3	0,3	0,3	0,4	0,4	0,3	0,4	0,3	0,3	0,4	0,4	0,4
S	7,7	5,3	7,9	7,8	7,1	5,4	4,1	3,4	5,0	5,7	8,5	4,9	8,7	8,3	6,5	8,0	4,1	3,2	3,4	3,5	8,5	7,3	6,3	4,8
Cl	1,5	7,1	1,6	0,9	1,2	5,0	3,6	3,4	11,0	11,4	2,6	10,6	1,7	1,9	1,6	1,1	7,5	10,8	11,5	1,7	3,0	2,5	5,5	1,6
K	5,1	3,9	5,2	5,8	4,1	2,8	1,5	1,5	5,2	4,9	5,5	6,4	5,1	4,6	3,3	4,6	4,7	5,6	5,6	1,7	5,0	3,6	4,5	3,1
Ca	6,5	6,1	6,1	6,0	8,0	8,8	10,1	9,0	8,4	8,8	8,7	7,8	8,7	8,6	9,5	10	8,6	7,8	8,6	10,7	9,0	10,3	8,8	7,8
Ti	1,2	1,1	1,0	0,9	1,3	1,5	1,8	1,7	1,6	1,7	1,6	1,5	1,6	1,6	2,1	1,8	1,8	1,5	1,6	1,9	1,6	1,7	1,5	1,7
V	-	-	-	-	-	-	-	-	-	-	-	-	-	-	-	-	-	-	-	-	-	-	-	-
Cr	-	-	-	-	-	-	0,1	-	-	-	-	-	-	-	-	-	-	-	-	-	-	-	-	-
Mn	0,2	0,3	0,1	0,1	0,2	0,2	0,2	0,2	0,3	0,3	0,2	0,2	0,3	0,2	0,2	0,2	0,2	0,2	0,2	0,2	0,2	0,2	0,3	0,3
Fe	1,1	3,7	0,7	0,7	1,1	1,0	1,3	1,3	1,8	2,1	0,8	0,8	1,9	2,1	1,4	0,9	1,5	1,3	1,2	2,1	1,6	1,6	3,3	4,6
Ni	-	-	-	-	-	-	-	-	-	-	-	-	-	-	-	-	-	-	-	-	-	-	-	-
Cu	-	-	-	-	-	-	0,1	0,1	0,4	0,1	0,1	0,2	0,1	0,1	0,2	0,1	0,2	0,2	0,1	0,1	0,1	0,1	0,1	0,1
Zn	3,1	2,8	2,6	4,2	1,8	2,0	3,6	3,2	6,3	5,7	4,8	6,5	3,4	3,4	2,6	3,2	3,9	5,5	5,5	3,0	2,5	2,7	3,1	3,6
Pb	-	0,8	0,8	0,8	-	0,5	0,4	0,3	0,6	0,8	0,5	0,5	0,4	0,5	0,8	0,4	0,4	0,4	0,4	0,1	0,7	0,4	0,5	0,2
As	0,1	-	-	-	-	-	-	-	-	-	-	-	-	-	-	-	-	-	-	-	-	-	-	-

Appendix B Operating conditions

Table B1 Emissions report of 2011-11-08

Idbäcksverket - P3

Dygnsrapport

Datum: 2011-11-08

Utskriven: 2012-02-07 12:57

Timme	Drifttid panna h	Skattad timmar	Nyttig energi MWh	O2 tg vol%	H20 vol%	CO tg mg/m3	CO tg 6% O2 mg/m3	NO2 tg mg/m3	NOx tg 6% O2 mg/m3	NO2 utsläpp mg/MJ	SO2 tg mg/m3	SO2 tg 6% O2 mg/m3	Stoft fg mg/m3	Stoft tg 6% O2 mg/m3	NH3 tg mg/m3	NH3 tg 6% O2 mg/m3	N2O tg mg/m3	N2O tg 6% O2 mg/m3	HCl tg mg/m3	HCl tg 6% O2 mg/m3	TOC tg mg/m3	TOC tg 6%O2 mg/m3	Rökgas-temp °C	Rökgas-flöde tg Nm3/h
00:00-01:00	1,0	0	57	4,7	13,5	49	45	157,0	144,1	53,8	55,1	50,5	0,0	0,0	0,7	0,6	0,0	0,0	5,1	4,6	0,0	0,0	56	75233
01:00-02:00	1,0	0	53	4,3	12,2	187	168	138,6	124,3	46,4	51,4	46,1	0,0	0,0	0,4	0,4	0,1	0,1	3,9	3,5	2,7	2,4	54	69183
02:00-03:00	1,0	0	53	4,2	9,4	87	78	144,3	129,1	48,2	46,1	41,3	0,0	0,0	0,0	0,0	0,0	0,0	2,7	2,4	0,1	0,1	50	68508
03:00-04:00	1,0	0	53	4,3	9,5	85	77	141,4	127,2	47,4	48,1	43,3	0,0	0,0	0,0	0,0	0,0	0,0	2,3	2,0	0,1	0,1	49	69074
04:00-05:00	1,0	0	53	4,6	9,7	49	45	152,9	140,2	52,3	54,3	49,7	0,0	0,0	0,0	0,0	0,0	0,0	2,7	2,5	0,1	0,1	50	70336
05:00-06:00	1,0	0	53	4,7	9,7	39	36	156,5	143,7	53,6	56,4	51,7	0,0	0,0	0,0	0,0	0,0	0,0	3,0	2,8	0,1	0,1	50	70813
06:00-07:00	1,0	0	59	4,4	10,0	59	53	144,3	130,6	48,7	59,8	54,2	0,0	0,0	0,1	0,0	0,0	0,0	3,4	3,1	0,4	0,3	50	76607
07:00-08:00	1,0	0	60	4,3	8,9	51	46	136,8	122,9	45,8	55,6	49,9	0,0	0,0	0,1	0,1	0,0	0,0	3,6	3,2	0,0	0,0	48	78426
08:00-09:00	1,0	0	63	4,2	8,7	58	52	138,6	124,0	46,3	56,2	50,3	0,0	0,0	0,1	0,1	0,0	0,0	3,7	3,3	0,2	0,2	48	81615
09:00-10:00	1,0	0	65	4,2	8,7	66	59	142,2	126,9	47,3	57,2	51,0	0,0	0,0	0,1	0,1	0,0	0,0	3,2	2,9	0,2	0,1	48	83857
10:00-11:00	1,0	0	65	4,2	8,4	45	40	140,4	125,4	46,8	61,9	55,3	0,0	0,0	0,2	0,1	0,0	0,0	3,0	2,7	0,0	0,0	47	83659
11:00-12:00	1,0	0	65	4,1	8,4	75	67	143,3	127,4	47,5	61,9	55,1	0,1	0,1	0,3	0,2	0,0	0,0	3,3	2,9	0,5	0,4	47	83903
12:00-13:00	1,0	0	65	4,1	8,4	87	77	140,2	124,0	46,3	61,0	54,0	0,1	0,1	0,3	0,3	0,0	0,0	3,1	2,8	0,1	0,1	47	83869
13:00-14:00	1,0	0	65	4,1	8,4	96	85	140,6	124,6	46,5	62,0	55,0	0,1	0,1	0,3	0,3	0,0	0,0	3,4	3,0	0,3	0,3	47	83764
14:00-15:00	1,0	0	69	3,9	8,5	98	86	146,2	128,1	47,8	67,0	58,7	0,2	0,2	0,3	0,3	0,0	0,0	3,4	3,0	0,3	0,3	47	86682
15:00-16:00	1,0	0	74	4,1	9,0	50	45	171,0	151,9	56,7	99,2	88,1	0,7	0,7	0,1	0,1	0,0	0,0	3,5	3,1	0,0	0,0	48	94436
16:00-17:00	1,0	0	74	4,2	9,3	33	30	184,8	164,9	61,5	97,1	86,7	0,7	0,7	0,0	0,0	0,0	0,0	3,2	2,8	0,0	0,0	49	95325
17:00-18:00	1,0	0	74	4,2	9,3	39	35	214,4	190,8	71,2	75,6	67,3	0,4	0,4	0,0	0,0	0,0	0,0	2,7	2,4	0,0	0,0	49	95040
18:00-19:00	1,0	0	74	4,1	9,7	58	52	187,0	166,0	62,0	68,6	60,9	0,9	0,9	0,1	0,1	0,0	0,0	3,0	2,7	0,0	0,0	50	95088
19:00-20:00	1,0	0	74	4,2	9,5	55	49	170,7	152,1	56,8	48,1	42,9	0,3	0,3	0,8	0,7	0,0	0,0	3,9	3,5	0,1	0,0	50	95128
20:00-21:00	1,0	0	74	4,1	9,4	59	52	167,7	149,1	55,6	45,4	40,4	0,3	0,3	1,2	1,0	0,0	0,0	4,4	3,9	0,0	0,0	49	94927
21:00-22:00	1,0	0	74	4,2	9,5	54	48	165,2	147,8	55,2	17,4	15,6	0,3	0,3	2,4	2,2	0,0	0,0	5,9	5,3	0,0	0,0	50	95923
22:00-23:00	1,0	0	75	4,2	9,5	116	104	159,8	142,3	53,1	7,0	6,3	0,4	0,4	3,3	3,0	0,0	0,0	6,3	5,6	0,8	0,7	50	96312
23:00-00:00	1,0	0	75	4,1	9,6	65	58	149,2	132,8	49,6	3,6	3,2	0,3	0,3	4,5	4,0	0,0	0,0	6,9	6,1	0,0	0,0	50	96200
Summa:	24,0	0	1567																					2023709
Medelvärde:			65	4,2	9,5	69	62		140,3	52,3		48,9	0,2	0,2		0,6		0,0		3,4		0,2	49	
Max:																								
Min:																								
Summa mån:	192,0	0	10515																					
Mån medelv:									122,7	45,8		60,4				1,7		0,8						
Summa år:			310311																					
Års medelv:									107,0	39,9		27,7												
Kommentar:							Dygn		År			År		Dygn		Månad		Månad						

Villkor:		Villkor:	
Stoft: Riktvärde, dygnsmedel [mg/m3 vid 6%O2]	15	CO: Riktvärde, dygnsmedel [mg/m3 vid 6%O2]	270
NH3: Riktvärde, månadsmedel [mg/m3 vid 6%O2]	10	N2O: Riktvärde, månadsmedel [mg/m3 vid 6%O2]	30
NOx: Begränsningsvärde, årsmedel [mg/m3 vid 6%O2]	200	SO2: Begränsningsvärde, årsmedel [mg/m3 vid 6%O2]	75

Table B2 Emissions report of 2011-11-10

Idbäcksverket - P3

Dygnsrapport

Datum: 2011-11-10

Utskriven: 2012-02-07 12:58

Timme	Drifttid panna h	Skattad timmar	Nyttig energi MWh	O2 tg vol%	H20 vol%	CO tg mg/m3	CO tg 6% O2 mg/m3	NO2 tg mg/m3	NOx tg 6% O2 mg/m3	NO2 utsläpp mg/MJ	SO2 tg mg/m3	SO2 tg 6% O2 mg/m3	Stoft fg mg/m3	Stoft tg 6% O2 mg/m3	NH3 tg mg/m3	NH3 tg 6% O2 mg/m3	N2O tg mg/m3	N2O tg 6% O2 mg/m3	HCl tg mg/m3	HCl tg 6% O2 mg/m3	TOC tg mg/m3	TOC tg 6%O2 mg/m3	Rökgas-temp °C	Rökgas-flöde tg Nm3/h
00:00-01:00	1,0	0	59	4,5	8,8	114	104	117,0	106,8	39,8	70,4	64,1	0,1	0,1	2,4	2,2	0,0	0,0	8,5	7,8	0,8	0,7	48	77670
01:00-02:00	1,0	0	59	4,5	8,8	150	136	115,3	104,7	39,1	74,0	67,2	0,1	0,1	3,0	2,7	0,1	0,0	9,7	8,9	2,1	1,9	48	76876
02:00-03:00	1,0	0	59	4,7	8,9	67	61	119,9	110,4	41,2	70,6	65,0	0,1	0,1	3,0	2,8	0,0	0,0	9,7	8,9	0,2	0,2	48	78018
03:00-04:00	1,0	0	59	4,7	9,0	58	53	113,4	104,6	39,0	75,1	69,2	0,1	0,1	3,3	3,0	0,0	0,0	10,5	9,7	0,0	0,0	48	78085
04:00-05:00	1,0	0	61	4,6	9,1	55	50	119,8	109,6	40,9	93,1	85,2	0,3	0,3	3,5	3,2	0,0	0,0	11,5	10,5	0,0	0,0	48	81278
05:00-06:00	1,0	0	77	4,3	9,6	107	96	160,4	143,9	53,7	130,7	117,2	1,5	1,5	3,5	3,2	0,0	0,0	11,7	10,5	0,8	0,5	50	99321
06:00-07:00	1,0	0	80	4,4	9,9	35	32	193,4	174,9	65,3	83,0	75,1	1,9	1,9	5,4	4,9	0,0	0,0	14,1	12,7	0,0	0,0	51	104201
07:00-08:00	1,0	0	80	4,1	9,7	130	115	165,8	147,4	55,0	162,3	144,2	1,5	1,4	5,1	4,6	0,0	0,0	15,1	13,4	0,7	0,6	50	102246
08:00-09:00	1,0	0	80	4,0	9,7	74	65	193,8	171,4	64,0	127,1	112,5	0,9	0,9	2,6	2,3	0,0	0,0	9,8	8,7	0,1	0,1	50	101795
09:00-10:00	1,0	0	80	4,2	9,8	64	57	186,3	166,2	62,0	69,9	62,3	1,2	1,2	3,7	3,3	0,0	0,0	10,3	9,2	0,2	0,2	51	102504
10:00-11:00	1,0	0	79	4,1	9,4	80	71	174,7	155,4	58,0	64,0	57,0	0,6	0,6	4,1	3,6	0,0	0,0	11,2	9,9	0,1	0,1	50	102017
11:00-12:00	1,0	0	79	4,1	9,4	105	93	178,1	158,0	59,0	57,3	50,8	0,8	0,8	3,7	3,3	0,0	0,0	10,4	9,2	0,7	0,6	50	101713
12:00-13:00	1,0	0	80	4,2	9,6	52	46	186,8	166,5	62,1	56,0	49,9	1,2	1,2	2,8	2,5	0,0	0,0	8,6	7,6	0,1	0,1	50	102492
13:00-14:00	1,0	0	79	4,2	9,4	63	56	178,8	159,4	59,5	60,0	53,5	0,5	0,5	3,3	2,9	0,0	0,0	9,3	8,3	0,2	0,2	50	102226
14:00-15:00	1,0	0	79	4,1	11,3	89	79	182,0	170,5	63,6	66,2	58,8	0,4	0,4	3,4	3,0	0,0	0,0	9,3	8,3	0,3	0,3	53	101516
15:00-16:00	1,0	0	79	4,3	14,6	50	45	219,4	197,2	73,6	65,1	58,5	0,8	0,9	4,2	3,8	0,0	0,0	9,4	8,5	0,0	0,0	58	102587
16:00-17:00	1,0	0	79	4,2	14,4	123	110	214,3	190,8	71,2	72,5	64,6	0,6	0,6	3,1	2,7	0,0	0,0	8,3	7,4	0,6	0,5	58	101675
17:00-18:00	1,0	0	79	4,2	14,5	109	97	215,5	192,5	71,8	75,2	67,1	0,5	0,5	2,6	2,3	0,0	0,0	7,9	7,1	0,3	0,3	59	101871
18:00-19:00	1,0	0	77	4,2	14,7	135	121	212,6	190,0	70,9	87,5	78,2	0,7	0,7	2,0	1,8	0,0	0,0	7,5	6,7	0,6	0,6	59	99909
19:00-20:00	1,0	0	75	4,4	15,1	195	176	181,1	163,7	61,1	173,9	157,2	1,7	1,8	1,3	1,2	0,0	0,0	7,6	6,8	2,0	1,8	59	98520
20:00-21:00	1,0	0	75	4,5	15,1	101	92	185,2	167,8	62,6	114,9	104,1	0,6	0,7	0,7	0,7	0,0	0,0	6,7	6,1	0,8	0,7	60	97737
21:00-22:00	1,0	0	74	4,4	13,0	41	37	192,5	173,7	64,8	55,1	49,7	0,3	0,3	0,6	0,5	0,0	0,0	6,1	5,5	0,0	0,0	56	96682
22:00-23:00	1,0	0	74	4,4	11,8	57	51	173,8	157,4	58,7	51,3	46,5	0,5	0,5	0,7	0,6	0,0	0,0	6,4	5,8	0,0	0,0	54	97333
23:00-00:00	1,0	0	75	4,5	11,9	58	53	171,2	155,9	58,2	59,9	54,6	0,5	0,5	2,1	1,9	0,0	0,0	8,5	7,8	0,0	0,0	54	98184
Summa:	24,0	0	1776																					2306456
Medelvärde:			74	4,3	11,1	88	79		158,4	59,1		75,8	0,7	0,7		2,6		0,0		8,5		0,4	53	
Max:																								
Min:																								
Summa mån:	240,0	0	13646																					
Mån medelv:									128,2	47,8		58,2				2,0		0,7						
Summa år:			313442																					
Års medelv:									107,3	40,1		27,9												
Kommentar:							Dygn		År			År		Dygn		Månad		Månad						

Villkor:		Villkor:	
Stoft: Riktvärde, dygnsmedel [mg/m3 vid 6%O2]	15	CO: Riktvärde, dygnsmedel [mg/m3 vid 6%O2]	270
NH3: Riktvärde, månadsmedel [mg/m3 vid 6%O2]	10	N2O: Riktvärde, månadsmedel [mg/m3 vid 6%O2]	30
NOx: Begränsningsvärde, årsmedel [mg/m3 vid 6%O2]	200	SO2: Begränsningsvärde, årsmedel [mg/m3 vid 6%O2]	75

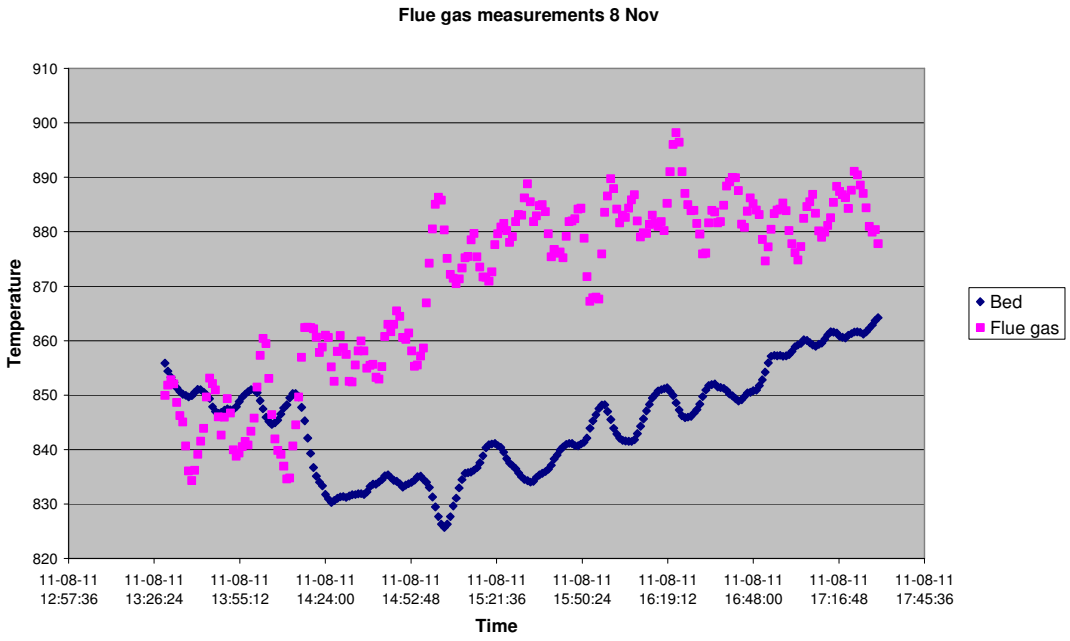

Fig. B1 **Bed temperature and flue gas temperature at the top of the furnace during the flue gas measurement campaign on November 8.**

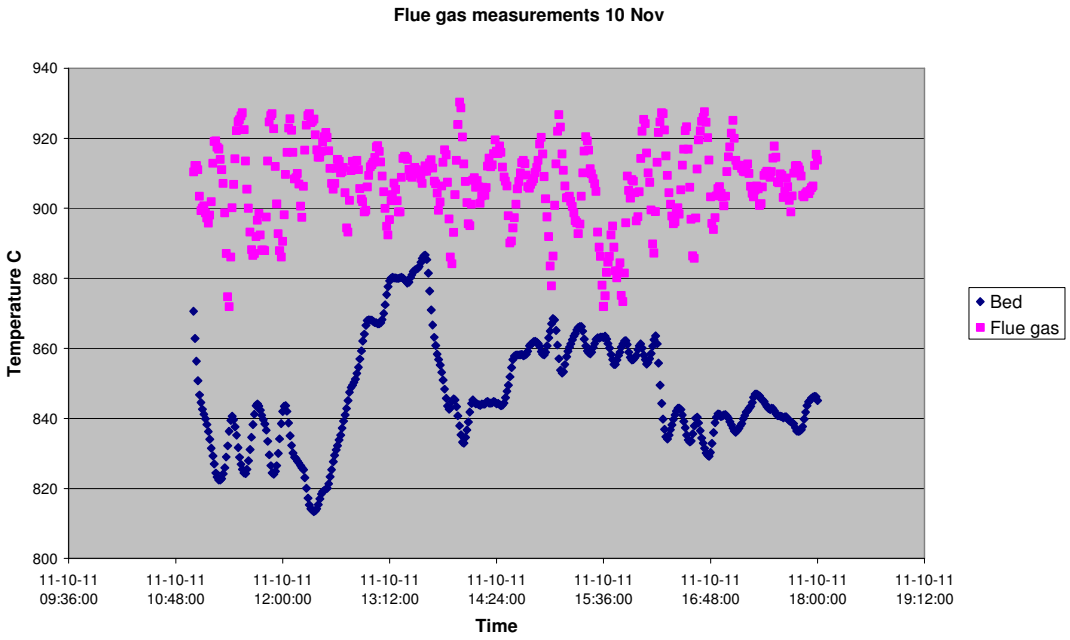

Fig. B2 **Bed temperature and flue gas temperature at the top of the furnace during the flue gas measurement campaign on November 10.**

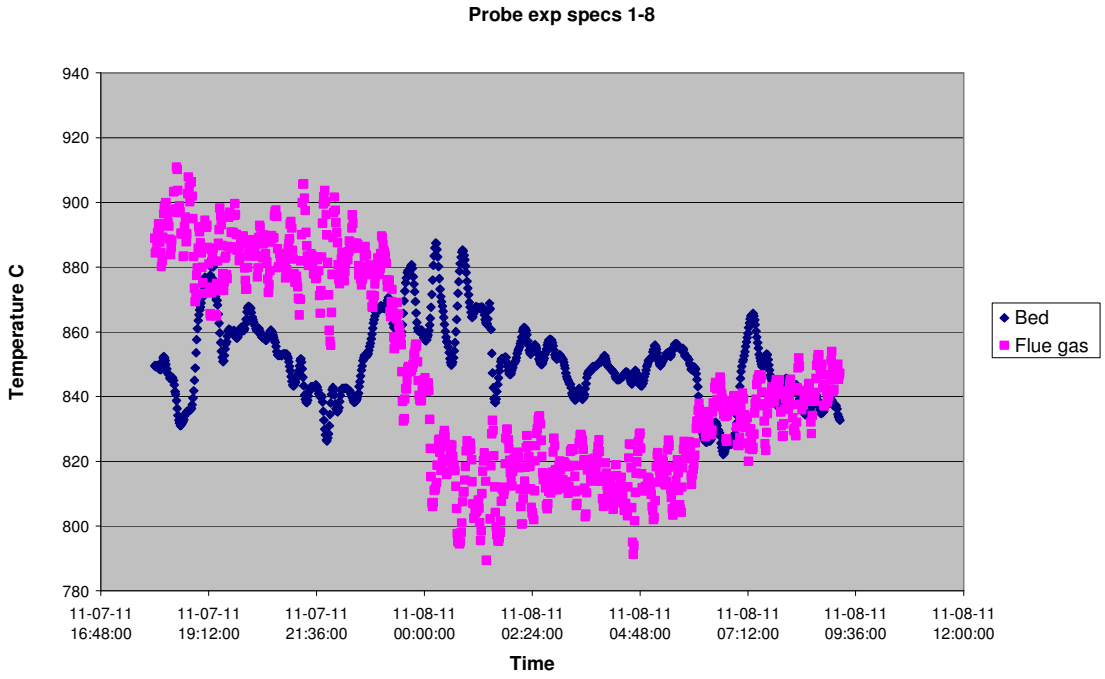

Fig. B3 **Bed temperature and flue gas temperature at the top of the furnace during the deposit probe exposure of specimens 1-8.**

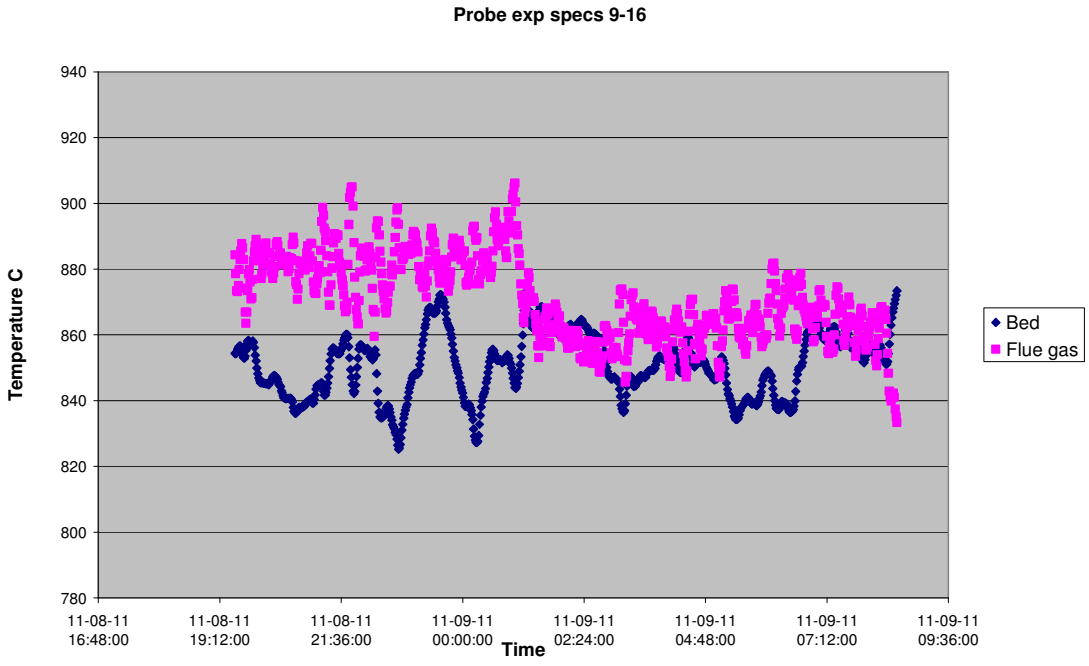

Fig. B4 **Bed temperature and flue gas temperature at the top of the furnace during the deposit probe exposure of specimens 9-16.**

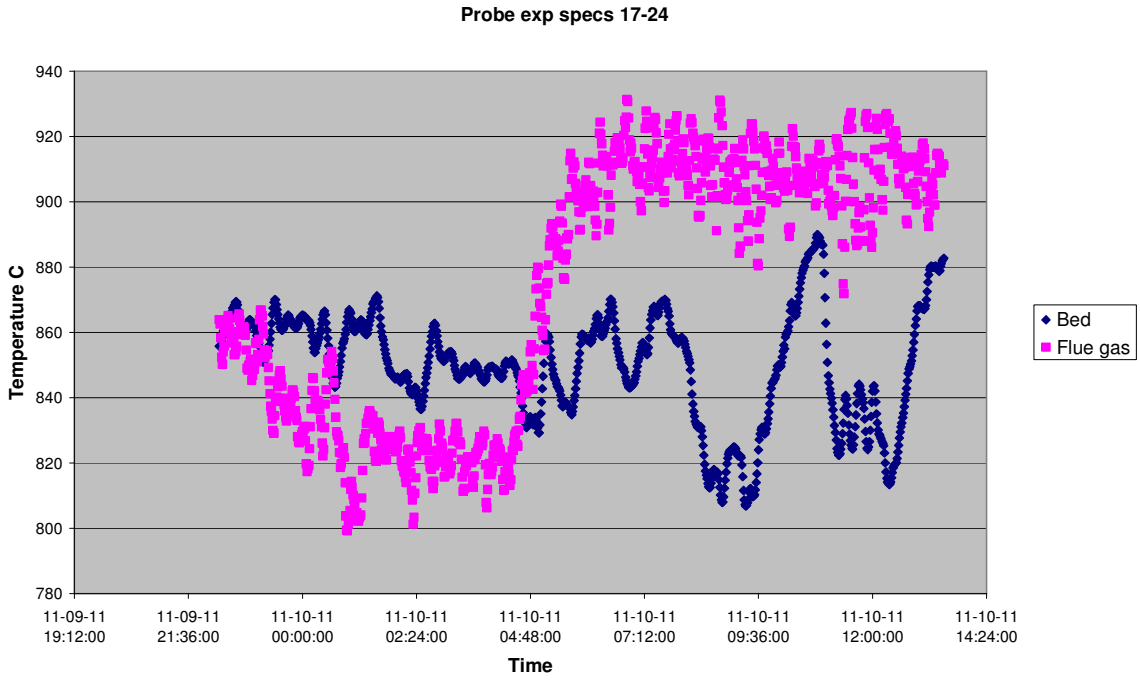

Fig. B5 **Bed temperature and flue gas temperature at the top of the furnace during the deposit probe exposure of specimens 17-24.**

The effect of co-firing of sewage sludge with waste wood on furnace wall corrosion

Yousef Alipour [1,*], and Pamela Henderson [1, 2]

[1] Surface and Corrosion Science Division, School of Chemical Science and Engineering, KTH Royal Institute of Technology, Drottning Kristinas väg 51, 10044, Stockholm, SWEDEN
[2] Vattenfall Research and Development AB, Stockholm, SWEDEN

e-mail: yousefa@kth.se

1. INTRODUCTION

The combustion of waste wood (recycled wood), which contains high amounts of chlorine, alkali and heavy metals [1-2], leads to severe corrosion problems in the furnace wall area of power plants [3-4]. Furnace walls are usually made of the low alloy carbon steel 16Mo3, with a coating of more corrosion resistant materials [5], for example nickel-base alloys, or high chromium-containing alloys.

It has been suggested that a fuel additive, such as sewage sludge, can change the flue gas chemistry and deposit composition, and consequently reduce high temperature corrosion problems [6-7]. Corrosion mechanisms are often studied in a simulated environment, where interpretation of the results is less complicated. However, in this study all the tests were made in a real environment. The samples were then studied under SEM/EDS, XRD and the thermodynamic stability of the corrosion product was also simulated.

2. EXPERIMENTAL

To study the effect of co-firing of sewage sludge, two air-cooled probes were exposed at the furnace wall in a bubbling fluidised bed boiler for 14.25 hours. Both probes contained low alloy steel 16Mo3 (the usual base of furnace walls), nickel-base alloy Alloy 625, iron-chromium-aluminium alloy APMT and stainless steel 310S. The Alloy 625 and APMT had previously been shown to have very good corrosion resistance to waste wood and together with 310S could be used for furnace wall coatings, [8]. The APMT sample was pre-oxidised by the supplier for 8 hours in air at 1050˚C to produce a protective 1 µm thick alumina layer on the sample surface. The temperature of the probes was controlled to 400˚C which is assumed to be the metal temperature of furnace walls. The power plant was operated on 100% waste wood during exposure of one probe, and then 8.4 wt% (1.7 vol%) of sewage sludge, as received, was added when testing the second probe. This corresponded to 3.5 dry wt% or 1.5% of the total energy. The chemical compositions of the samples are given in Table 1.

Table 1. Measuring Chemical compositions of coupons

Material	Wt%
Kanthal APMT	**Cr** 21.0, **Mo** 3.0, **Al** 5.0, **C** 0.08, **Si**0.7, **Mn** 0.4, **Fe** balance
16Mo3	**Mn** 0.55, **Si** 0.22, **Mo** 0.3, **Cu** 0.3, C **0.16**, **Fe** balance
310S	**Ni** 19.2, **Cr** 25.4, **Mo** 0.11, **Mn** 0.84, **Si** 0.55, **Ti** 0.001, **S** 0.001, **C** 0.046, **Cu** 0.08, **P** 0.015, **Ce** 0.004, **N** 0.04, **Fe** balance
Alloy 625	**Ni** 63, **Cr** 21, **Mo** 9.0, **Mn** 0.35, **Si** 0.2, **Ti** 0.25, **Al** 0.19, **Nb** 3.5, **Fe** balance

Deposits formed on the samples were chemically analysed under scanning electron microscopy (SEM)/energy dispersive spectroscopy (EDS) with 20 kV acceleration voltage. Fig. 1 shows the analysing protocol for all samples' deposits.

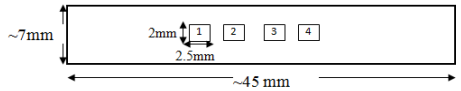

Fig. 1. Sketch of the sample, top side exposed into the finwalls between two tubes at furnace walls area. 4 different areas on the middle of each specimen were analysed under SEM/EDS.

The samples were dry polished by soft papers at the edge to facilitate the study of the interface between oxide layer and the substrate base metal, (see Fig. 2). Dry polishing avoided washing away the deposit, especially chlorine products which are soluble in water.

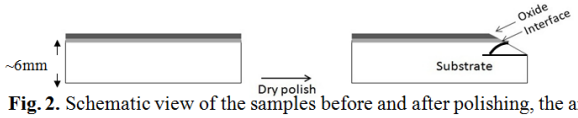

Fig. 2. Schematic view of the samples before and after polishing, the angle shown at the right figure was between 30˚ and 45˚.

X-ray diffraction (XRD) was performed on two nickel-base alloy samples. Specimens were first analysed on the deposit side. The deposit was then scraped off and the underneath layers were investigated separately.

3. RESULTS AND DISCUSSION

Average chemical compositions for 4 different areas on deposits are separately shown in Tables 2 and 3 for all the samples. The results show less chlorine, potassium and sodium in the deposits when burning sewage sludge along with waste wood, while deposits contain more aluminium, phosphorus and silicon.

Table 2. Average chemical composition results on waste wood samples

wt%	O	Na	Mg	Al	Si	P	S	Cl	K	Ca	Ti	Mn	Fe	Cu	Zn	Pb
APMT	40.4	6.4	1.3	1.5	1.5	0.5	11.3	5.0	7.5	8.9	2.6	0.2	1.6	0.3	2.5	8.1
16Mo3	31.8	8.9	1.1	1.7	1.6	0.4	6.0	15.4	8.4	6.7	2.0	0.8	5.5	0.1	4.9	4.4
310S	38.8	5.8	1.3	0.9	1.5	0.6	10.1	4.9	8.6	9.0	2.7	0.4	3.7	0.5	4.6	6.1
Alloy 625	40.8	4.5	1.5	1.0	1.9	0.7	10.6	4.0	8.5	10.7	3.2	0.2	1.1	0.2	4.2	6.6

Table 3. Average chemical composition results on waste wood + sewage sludge samples

wt%	O	Na	Mg	Al	Si	P	S	Cl	K	Ca	Ti	Mn	Fe	Cu	Zn	Pb
APMT	44.7	3.7	1.6	2.7	3.5	1.8	7.1	2.3	5.05	12.3	3.2	0.2	4.4	0.0	3.6	3.3
16Mo3	46.1	3.2	1.8	2.4	4.7	1.6	5.2	3.7	3.3	14.1	3.9	0.2	4.2	0.0	3.2	1.9
310S	43.7	4.2	1.4	3.4	3.6	1.7	6.6	2.7	4.4	11.2	3.0	0.2	4.8	0.2	3.6	4.7
Alloy 625	42.1	4.0	1.2	4.5	3.5	1.8	6.6	3.1	5.0	10.8	2.9	0.2	4.3	0.2	3.3	6.0

The sewage sludge contains aluminosilicates, phosphorus and sulphur. The interaction of alkali and aluminosilicates can probably reduce the deposition of potassium, sodium and chloride [9]. Sulphation was not expected because of reducing conditions in the furnace region.

The interface between oxide and metal base (initial corrosion front) was investigated by mapping under SEM/EDS. The 16Mo3 had corroded rapidly under both conditions so that it was difficult to say how much effect the sewage sludge had had. However it could be clearly seen that the chloride layer at the corrosion front was considerably reduced in thickness by use of the sludge, which implies a reduced corrosion rate. It could also be seen that the sludge lowers the initial corrosion in the other samples. The corrosion product in 16Mo3 samples was mainly iron chloride, Fig. 3.

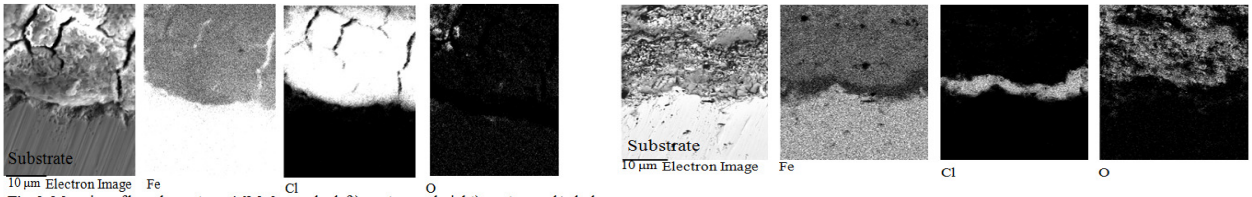

Fig. 3. Mapping of key elements on 16Mo3 samples left) waste wood right) waste wood+ sludge

The result shows that oxygen and chlorine barely overlap at the corrosion front, which leaves an iron chloride at the corrosion front. Chlorine in hydrated form [10], or via the ionic transport of Fe and Cl [11], has been suggested to govern the chlorine-induced corrosion under an oxide layer of a steel, rather than by gaseous chlorine [12,13].

Co-firing of sewage sludge in 310S reduced the initial corrosion as can be seen in Fig. 4 which shows a reduced migration of nickel, chromium and iron into the deposit. It has been proposed that the protective chromia layer can be attacked by molten chloride-containing salts, e.g. KCl, to form a non-protective chromate [14]. The results (Fig. 4) imply that reducing the amount of potassium and chlorine in the deposit has helped to maintain the chromia layer.

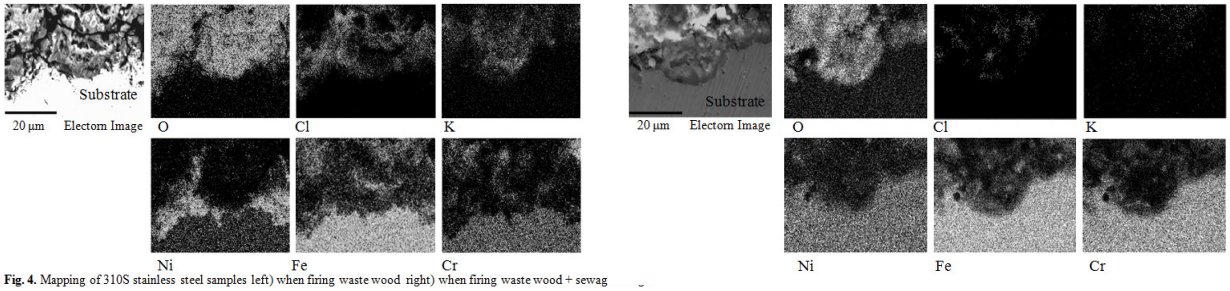

Fig. 4. Mapping of 310S stainless steel samples left) when firing waste wood right) when firing waste wood + sewag

Co-firing sewage sludge had a positive effect on retaining the alumina layer in FeCrAl alloy APMT (see Fig. 5). Figure 5 shows that initial corrosion in APMT samples is less when burning sewage sludge along with waste wood and the alumina layer has not been destroyed.

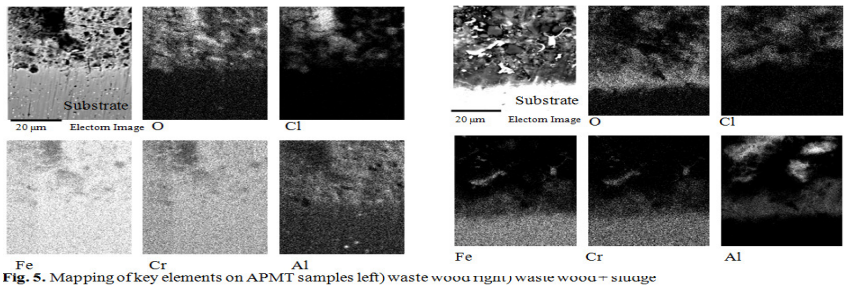

Fig. 5. Mapping of key elements on APMT samples left) waste wood right) waste wood + sludge

Alloy 625 overlay coating is reported to be acceptable in waste-burning power plants [15] and it can reduce the furnace wall corrosion attack [16]. The corrosion mechanism of Alloy 625 in biomass-fired boilers is a difficult issue and different corrosion mechanisms can occur simultaneously. It has been reported that lead oxide can attack protective chromia and reduce the corrosion resistance of nickel-based alloys by the formation of lead chromate [17], and it has been recently found that potassium can also attack the alloy by forming potassium chromate [14]. The XRD results, (Table 4) from this work are in agreement with those above and show the formation of $K_2Pb(CrO_4)_2$, even in this short 14.25 hours period, when burning waste wood This unprotective compound is also reported in some other works [18]. On the other hand the combination of potassium and lead doesn't seem to appear when burning 12% sewage sludge, leaving the protective chromia intact, Table 5.

Table 4. Compound found under XRD in Alloy 625, when burning waste wood

Strong intensity	Medium intensity	Weak intensity
NiO	(Na,K)2SO4	K2SO4, Pb, K2Pb(CrO4)2

Table 5. Compound found under XRD in Alloy 625, when burning waste wood + sewage sludge

Strong intensity	Medium intensity	Weak intensity
K2Ca2(SO4)3, Cr2O3	PbSiO3	Fe2O3, PCl3

Mapping of nickel-based Alloy 625, Fig. 6, shows that adding sewage sludge to the waste wood reduces the corrosion, as evidenced by the reduced spreading of nickel from the metal into the deposit.

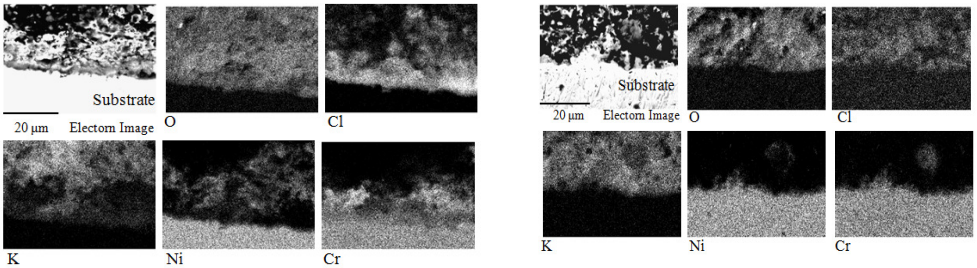

Fig. 6. Mapping of Alloy 625 nickel-based samples right) when firing waste wood left) when firing waste wood + sewage sludge

4. CONCLUSION

The results from this work showed that the co-firing of sewage sludge with recycled wood reduced the amounts of K, Na and Cl on the furnace wall deposits. This led to a reduction in the corrosion of Alloy 625 nickel-based alloy, 310S stainless steel, APMT FeCrAl alloy and the low alloy steel 16Mo3 during short-term tests. The dominant mechanism in the 16Mo3 was chlorine-induced corrosion. Attack by a potassium-lead combination appeared to be the main corrosion mechanism in the Alloy 625 during waste wood combustion. This resulted in the formation of a non-protective potassium-lead chromate. The addition of sewage sludge suppressed this attack and the protective chromia layer was maintained.

Acknowledgements

Financial support from Swedish Energy Agency and Vattenfall are gratefully thanked. The authors acknowledge Mattias Mattsson, and other colleagues at Vattenfall who have helped with the plant testing.

References

[1] Strömberg, B., Herstad, S.S., Bränslehandboken, Värmeforsk, (Stockholm, 2012).
[2] Krook, J., Mårtensson, A., Eklund, M., "Metal Contamination in Recovered Waste Wood Used as Energy Source in Sweden", *Resour. Conserv, Recycl.*, Vol. 41, No. 1, (2004), pp. 1-14.
[3] Andersson, C., Högberg, J. Fouling and Slagging Problems at Recovered Wood Fuel Combustion, Värmeforsk, (Stockholm, 2001), available at: www.varmeforsk.se/rapporter .
[4] Hohmann, U., Mohr, G., "High Temperature Corrosion in Biomass-Fired Boilers", *VGB PowerTech*, Volume 85/2005, No. 6, (2005), pp. 38-47.
[5] Kahawara, Y., "High Temperature Corrosion Mechanisms and Effect of Alloying Elements for Materials Used in Waste Incineration Environment", *Corros. Sci.,* Vol. 44, No. 2, (2002), pp. 223-245.
[6] Karlsson, S., Åmand, L., E., Pettersson, J., "Reducing High Temperature Corrosion when Burning Waste by Adding Digested Sewage Sludge", *Proc Swedish-Finish Flame Days*, Piteå, January,(2011), pp. 1-19.
[7] Davidsson, K.O., Åmand, L. E., Elled, A. L., Leckner, B., "Effect of Co-firing Coal and Biofuel with Sewage Sludge on Alkali Problems in a Circulating Fluidized Bed Boiler", *Energy Fuels*, Vol. 21, No. 4, (2007), pp. 3180-3188.
[8] Alipour Y., Henderson, P., "Corrosion of Furnace Wall Materials in a Waste-wood Fired Power Plant", **Submitted Paper**, KTH Royal Institute of Technology, Corrosion Science, Stockholm, Sweden.
[9] Yrjas, P., Aho, M., Zevenhoven, M., Taipale, R., Silvennoinen, J., Hupa, M., "Co-firing of Sewage Sludge with Bark in a Bench-scale Bubbling Fluidized Bed – a Study of Deposits and Emissions", *Proc of the 20th International Conference on Fluidized bed Combustion*, Xi'an, May, (2009), pp. 922-929.
[10] Szakalos, P., Henderson, P., Pettersson, R., "Mechanisms of chlorine induced corroson and effect of sulphur additive in superheater corrosion in biomass- and waste fired boilers", *Proc 16th International Corrosion Conference,* Beijing, September, (2005).
[11] Folkesson, N., Johansson, L. G., Svensson, J. E., "Initial Stages of the HCl-induced High Temperature Corrosion of Alloy 310", *J. Electrochem. Soc.*, Vol. 154, No. 9, (2007), pp. 515-521.
[12] Zahs, A., Spiegel, M., Grabke, H. J., "Chloridation and Oxidarion of Iron, Chromium, Nickel and Their Alloys in Chloridizing and Oxidizing Atmospheres at 400-700˚C", *Corros. Sci.*, Vol. 42, (2000), pp. 1093-1122.
[13] Reese, E., Grabke, H. J., "Einflu von Chloriden auf die Oxidation des 2¼ Cr-1 Mo-Stahls", *Werkst. Korros*, Vol. 43, (1992), pp. 547-557.
[14] Pettersson, J., Asteman, H., Svensson, J. E., Johansson, L. G., "KCl Induced Corrosion of a 304-type Austenitic Stainless Steel at 600˚C: The Role of Potassium", *Oxid. Met.*, Vol. 64, No. 112, (2005), pp. 23-41.
[15] Pettersson, R., Flyg, J., Viklund, P., "Materials Performance in Simulated Waste Combustion Environment", *Corros. Eng. Sci. Technol.*, Vol. 43, No.2, (2008), pp. 123-128.
[16] Viklund, P. PhD Thesis, Superheater Corrosion in Biomass and Waste Fired Boilers, KTH Royal Institute of Technology, (Stockholm, 2013).
[17] Chatterji, D., McKee, D.W., Romeo, G., Spacil, H.S., "The Effect of Lead on the Hot Corrosion of Nickel-base Alloys", *J. Electrochem, Soc.*, Vol. 122, (1975), pp. 941-952.
[18] Alipour, Y., Viklund, P., Henderson, P., "The Analysis of Furnace Wall Deposits in a Low-NOx Waste Wood- fired Bubbling Fluidised bed Boiler", *VGB PowerTech, Vol. 12, (2012), pp. 96-100.*

The effect of a nickel alloy coating on the corrosion of furnace wall tubes in a waste wood fired power plant

Y. Alipour*, P. Henderson and P. Szakálos

The use of waste wood as a fuel in power plants is becoming more widespread in Europe, because it is a renewable energy source with a lower cost than forest fuel. However it is more corrosive than coal and corrosion problems have arisen in the furnace wall area of a low NOx heat and power boiler. The furnace walls are made of a low alloy steel which has been coated in some parts with a nickel alloy to reduce corrosion. In this work, furnace tubes coated with a nickel alloy were compared to the uncoated tubes of the low alloy steel 16Mo3 after 3 years of exposure in the boiler. The nickel alloy coating and uncoated material were also compared with more controlled testing on a corrosion probe lasting for about 6 weeks. The corrosion rates were measured and the samples were chemically analysed by SEM/EDS/WDS and XRD methods. The corrosive environment was also modelled with Thermo-Calc software. The corrosion rates measured from the probe and tube samples of 16Mo3 agreed well with each other, implying linear corrosion rates. The results also showed that the use of nickel alloy coatings changes the corrosion mechanism, which leads to a dramatic reduction in the corrosion rate. The results are discussed in terms of the corrosion mechanisms and thermodynamic stability of the corrosion products.

1 Introduction

The combustion of fossil fuels enhances the greenhouse effect by raising the amount of carbon dioxide emitted into the atmosphere. The combustion of waste wood (or recycled wood) is becoming more widespread in Europe, because it is carbon dioxide neutral, but with a lower cost than forest fuel. Waste wood is said to be a renewable energy source. However it is a heterogeneous fuel with a high amount of chlorine, alkali and heavy metals (Table 1) which leads to more corrosion in boilers than with fossil fuel or forest fuel combustion [1].

A part of the boiler which is subjected to a high corrosion risk is the furnace wall which is formed of tubes welded together, so-called waterwalls as they contain water. Waterwalls are made of ferritic low alloyed steels, due to the low price, low stress corrosion cracking risk, high heat transfer properties and low thermal expansion. However ferritic low alloy steels corrode quickly when burning waste wood in a low NOx environment (i.e. an environment with low oxygen levels to limit the formation of NOx) [3].

Power plant owners wish to reduce the costs associated with high temperature corrosion. One method suggested to decrease the corrosion, is coating the furnace wall tubes with a more corrosion resistant material, for example a nickel alloy [4]. Corrosion mechanisms are usually investigated in laboratories, where interpretation of the results is easier. In power plants corrosion studies are more complicated. Several factors such as deposit composition, flue gas flow, boiler design, combustion characteristics and flue gas composition cause difficulties in the study of corrosion mechanisms. Therefore, the corrosion varies from plant to plant and laboratory experiments should complement field ones. In this work we have performed corrosion studies in a power plant, but have also performed thermodynamic modelling.

2 Experimental

2.1 Exposure

Test panels of the low alloy steel 16Mo3 were welded into the furnace wall of a bubbling fluidised bed power station boiler firing waste wood. Some of the tubes were arc-weld overlay coated with the nickel-based alloy IN625 and some were left uncoated.

Y. Alipour, P. Henderson, P. Szakálos
Surface and Corrosion Science Division, Department of Chemistry, School of Chemical Science and Engineering, KTH Royal Institute of Technology, Drottning Kristinas väg 51, 10044, Stockholm (Sweden)
E-mail: yousefa@kth.se

P. Henderson
Vattenfall Research and Development A.B, 169 92 Stockholm (Sweden)

Table 1. Mean value of key elements of waste wood [2]

Parameter	Waste wood	Waste wood spread
Total moisture (wt%)	23	11–39
Total ash (wt% dry)	5.8	3.2–15
C (wt% dry ash-free)	52	50–56
N (wt% dry ash-free)	1.2	0.12–1.5
S (wt% dry ash-free)	0.08	0.04–0.3
Cl (wt% dry ash-free)	0.06	0.04–0.22
K (wt% in ash)	2.0	1.0–2.6
Na (wt% in ash)	1.4	0.6–1.9
Zn (mg/kg in ash)	10393	2420–184,167
Pb (mg/kg in ash)	544	140–28,611

After 3 years service samples of coated and uncoated tubes were removed and examined. Final steam parameters for the power plant were 140 bar/540 °C. The pressure of 140 bar gives a maximum water temperature of 340 °C and the tubes are assumed to have a metal temperature of 390 °C. Sample P1 was a coated sample and sample P4 was an uncoated EN 16Mo3 low alloy steel reference tube. The chemical compositions of the low alloy steel and the Ni-alloy coating are given in Tables 2 and 3.

Some deposits were scratched from the top surface of other tubes close to the investigated tubes. They were then ground by hand and investigated by X-ray diffraction (XRD) (see Fig. 1).

To compare the results with more controlled samples probe testing was also performed for 934 h. Samples of 16Mo3 and IN625 were attached to air-cooled probes which were inserted into the fin wall between two tubes. One probe (A2) containing 16Mo3 and IN625 was installed in the back wall where the corrosion was known to be greatest. The other probe (B2) contained only 16Mo3 and was installed in the right wall, close to the test panels, where the corrosion was thought to be less severe. The probe with specimens after removal from the boiler is shown in Fig. 2. There is room for four specimens on each probe, only some of the results are reported here. The 16Mo3 specimen on probe A2 (back wall) was denoted A2-2 and the IN625 A2-3. The 16Mo3 specimen on probe B2 (right wall near test panels) was denoted B2-2. The probe specimens were 48 mm long, 7 mm wide and 6 mm thick. The temperature was measured by a thermocouple placed centrally at the back of each specimen and controlled to 400 °C to simulate the temperature of the tube wall.

2.2 Sample preparation and metallography

Before exposure in the boiler, the thickness of each probe specimen was measured with a micrometer at four equally spaced distances along the centre line. After testing the specimens were sectioned at the measuring positions without water. Four parts were used for metal thickness measurement using an optical microscope with a micrometer measuring gauge after mounting and polishing. The other part was left unmounted.

The front part (facing the combustion gases) of the tubes were cut out after 3 years of exposure. The tubes were sectioned without water and the wall thickness measured at eight equally

Table 2. Nominal chemical composition of 16Mo3 [5]

Element	C	Mn	Si	P	S	Cr	Mo	Ni	Cu	N	Nb	Fe
wt%	0.12–0.2	0.4–0.9	0.00–0.35	0.000–0.025	0.00–0.01	0.00–0.30	0.25–0.35	0.00–0.30	0.00–0.30	0.00–0.012	0.00–0.020	Balance

Table 3. Nominal chemical composition of IN625 [6]

Element	Ni	Cr	Fe	Mo	Nb + Ta	C	Mn	Si	P	S	Al	Ti	Co[a]
wt%	58.0 min	20.0–23.0	5.0 max	8.0–10.0	3.15–4.15	0.10 max	0.50 max	0.50 max	0.015 max	0.015 max	0.40 max	0.40 max	1.0 max

[a]If determined.

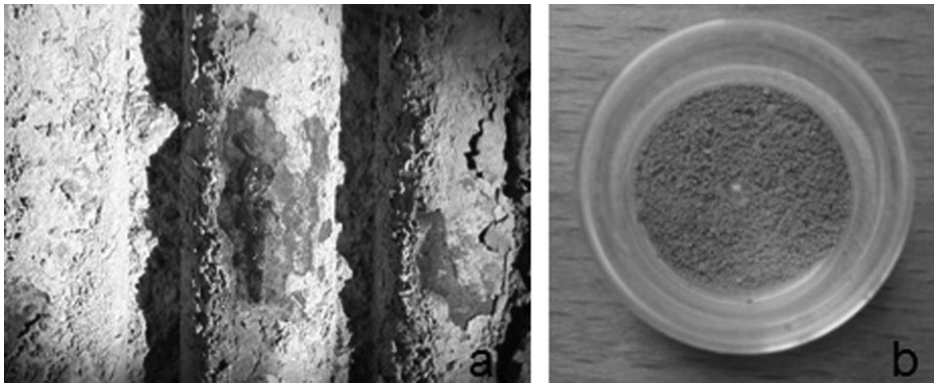

Figure 1. (a) Deposits (and corrosion products) were scraped from the tubes and (b) were ground to make XRD samples

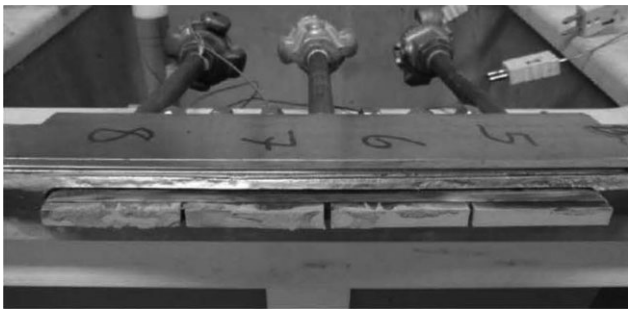

Figure 2. The fin wall probe after exposure inside the boiler

spaced positions after mounting and polishing. One part of the tubes was left unmounted.

The unmounted tube and probe sections were dry polished as follows:

The samples were dry polished by papers with grit P800, P1200, P2500 and P4000 respectively. A polishing machine was used in a dry manner to avoid washing away the corrosion product on the surface of tubes, especially chlorine which is soluble in water. Polishing in this way facilitated the investigation of the substrate base metal, oxide and interface between oxide/substrate.

The tube samples were polished according to Fig. 3 and the probe samples according to Fig. 4.

Then scanning electron microscopy (SEM) with energy dispersive X-ray spectroscopy (EDS) or with wavelength dispersive spectroscopy (WDS) was employed to analyse all three areas. The SEM conditions were 15 keV and 16 A. Mapping, point analyses and area analyses were carried out on different areas of the samples. The QuantMap software application was used to distinguish between elements such as sulphur, molybdenum and lead.

2.3 Equilibrium thermodynamic modelling

Thermodynamic modelling was performed with Thermo-Calc software using the substance database (SSUB) and the solution database (SSOL). Thermo-Calc is a software package used for phase diagram and thermodynamic computations for multi-component systems of practical importance. The modelling is based on thermodynamic databases produced by expert evaluation of experimental data [7].

Figure 3. Schematic drawings of tube samples before and after polishing

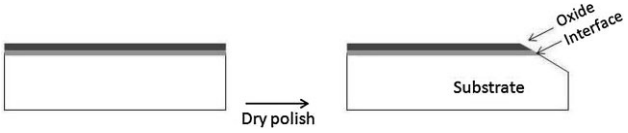

Figure 4. The polishing method of probe samples

3 Results

3.1 Metal loss results from probe testing

The thicknesses of the probe samples were measured at four points along each specimen before and after exposure to evaluate the metal loss (see Table 4). Measurements are normalized to 1000 h. The results show 16Mo3 corroded faster as one might expect.

3.2 Metal loss results from test panels

The original thickness of the IN625 welded coating on the tube samples was about 4 mm, but being a welded structure it was difficult to measure accurately and may have been greater than 4 mm in a number of areas. After 3 years exposure (about 20,000 h) the average thickness of the examined section was 3.8 mm (average of eight equally spaced measurements) and the minimum thickness 3.4 mm. This gives an estimated maximum metal loss rate of 30 μm per 1000 h.

The original wall thickness of the 16Mo3 test panel tubes was 7 mm and after 3 years exposure the average thickness of the examined section was 5.35 mm and the minimum 5.0 mm. This gives an estimated maximum loss rate of 100 μm per 1000 h, about three times greater. These values are of course, only approximate. These values are included in Table 4.

3.3 Metallography of nickel-alloy coated tube (P1) and uncoated reference tube of 16Mo3 (P4)

Figure 5 shows the element mapping for the nickel-alloy coated tube sample. The results showed concentrations of lead, and some potassium in the oxide at the substrate/deposit interface, but no chlorine. Low amounts of chlorine (less than 1 wt%) were found in the deposit adjacent to the oxide layer.

XRD results showed the presence of potassium lead chromate in the deposit, implying that lead together with potassium had reacted with the protective chromia layer and

Table 4. Metal loss from probe and tube samples

Sample	Average (μm/1000 h)	Maximum (μm/1000 h)	Position in boiler
16Mo3 (A2-2) probe	116	133	Back wall
16Mo3 (B2-2) probe	78	97	Right wall
16Mo3 (P4) tube	82 (approx)	100 (approx)	Right wall
IN625 (P1) tube	10 (approx)	30 (approx)	Right wall
IN625 (A2-3) probe	47	55	Back wall

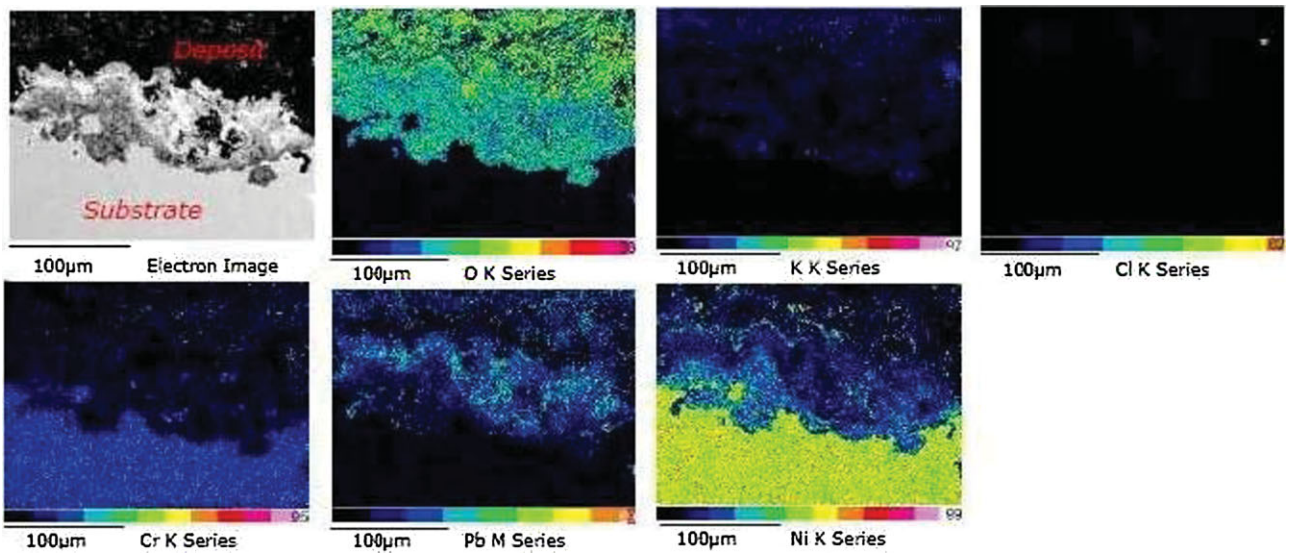

Figure 5. SEM QuantMaps of key elements on the nickel-alloy coated tube sample

formed chromate, which is unprotective. Table 5 shows compounds identified in the deposit sample.

SEM/WDS results showed that high levels of lead were frequently observed at the corrosion front; see Fig. 6 along with some point analyses (Table 6).

Figure 6 and Table 6 show that lead was highly concentrated at the interface in the pits. Only a small amount of chlorine was found in the corrosion product. Sulphur and potassium were also found in the deposit and at the interface.

Figure 7 shows the element mapping analysis for the uncoated 16Mo3 tube. The level of chlorine found was much higher in the corrosion product and interface compared with the coated sample, P1. Lead and zinc were not found at the interface or deposit.

Area analysis by the SEM clarified that corrosion products were predominantly chlorine, iron and oxygen. Table 7 shows the average chemical composition of the deposit and interface in three different areas in Fig. 7. Some iron chlorides were found at the metal interface.

Table 5. Results of XRD on deposit sample taken from IN625 coated tube

	Compound
Strong intensity/high concentrations	KCl
Medium intensity/medium concentrations	NaCl, $K_3Na(SO_4)_2$, NiO, $K_2Pb(CrO_4)_2$

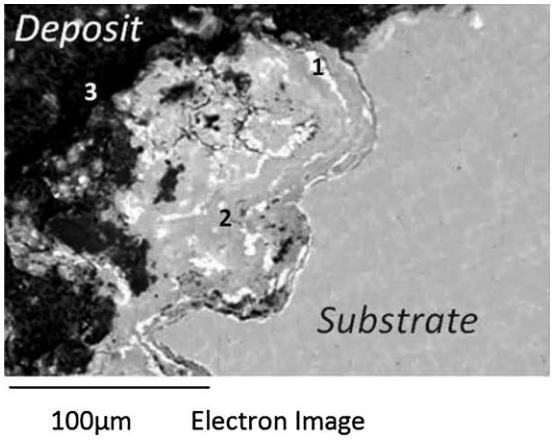

Figure 6. White areas at the deposit/substrate interface in nickel-alloy coated tube indicates high amount of lead (up to 33 wt%). Three spot analyses are also shown in the figure

3.4 Metallography of 16Mo3 probe sample (A2-2) and nickel-alloy probe sample (A2-3)

Figure 8 shows QuantMaps for the nickel-alloy probe sample, which are similar to those of the coated tube sample. It can be seen that there is a concentration of lead in the oxide layer on top of the nickel-rich substrate. The oxide layer is mainly free of chlorine (apart from an isolated area under the oxide).

SEM/EDS point analyses confirmed that lead was present, but not in connection with chlorine (Fig. 9). The oxide layer was mainly free of chlorine (Table 8).

The same procedure was performed for the 16Mo3 sample and QuantMaps for this sample are shown in Fig. 10. It can be seen than the amount of chlorine is much higher than in the IN625 coated sample. Both iron and chlorine were found at the interface and in the deposit. No heavy metals, such as lead were present in the sample. Sulphur is not found at the corrosion front.

Table 9 shows the chemical compositions of the two spot analyses in Fig. 11.

The results from the probe specimens were in agreement with the results from the tube samples.

Table 6. Chemical analysis (atomic %) of three spot analyses related to Fig. 6

Element	O	Mg	S	Cl	K	Ca	Ti	Cr	Fe	Ni	Zn	Nb	Pb
Spectrum1	53.59	–	4.70	–	4.29	0.54	1.17	8.80	0.29	14.34	1.73	6.49	7.19
Spectrum2	51.68	–	7.23	0.54	5.39	–	–	3.91	0.30	24.88	0.63	–	5.43
Spectrum3	13.79	0.85	3.29	–	2.12	1.37	–	3.45	0.76	66.14	7.16	–	1.07

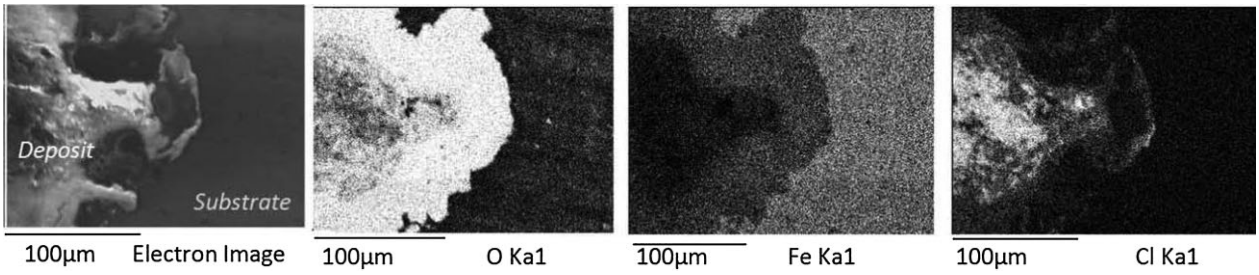

Figure 7. Mapping of the uncoated 16Mo3 tube

3.5 Modelling by thermo-calc software

Thermo-Calc modelling was performed regarding corrosion and flue gas composition at 400 °C on pure iron and pure nickel, respectively (see Figs. 12 and 13). For simplification, chromium and molybdenum were excluded in both cases.

Table 7. Average chemical composition results in weight and atomic percent for the oxide/interface of the uncoated sample (from Fig. 7)

Element	wt%	at%
O	36.38	65.84
S	0.27	0.24
Cl	3.40	2.78
K	0.30	0.22
Fe	59.65	30.93

The modelling was performed with increasing amounts of oxygen, sulphur, potassium and lead whereas iron or nickel, hydrogen and chlorine were kept constant. (It was not possible to perform the modelling with more than four elements as variables. Chlorine was especially problematic and was therefore kept at a constant amount.) The total amount of species was set to 1 mol with nitrogen as balance. The gas species in equilibrium with the solid phases is not shown in the diagrams. The gas phase mainly contains nitrogen, water vapour and small amount of hydrogen chloride. At high oxygen partial pressures the gas phase also contains oxygen gas and at lower oxygen partial pressures it also contains hydrogen gas, basically controlled by the

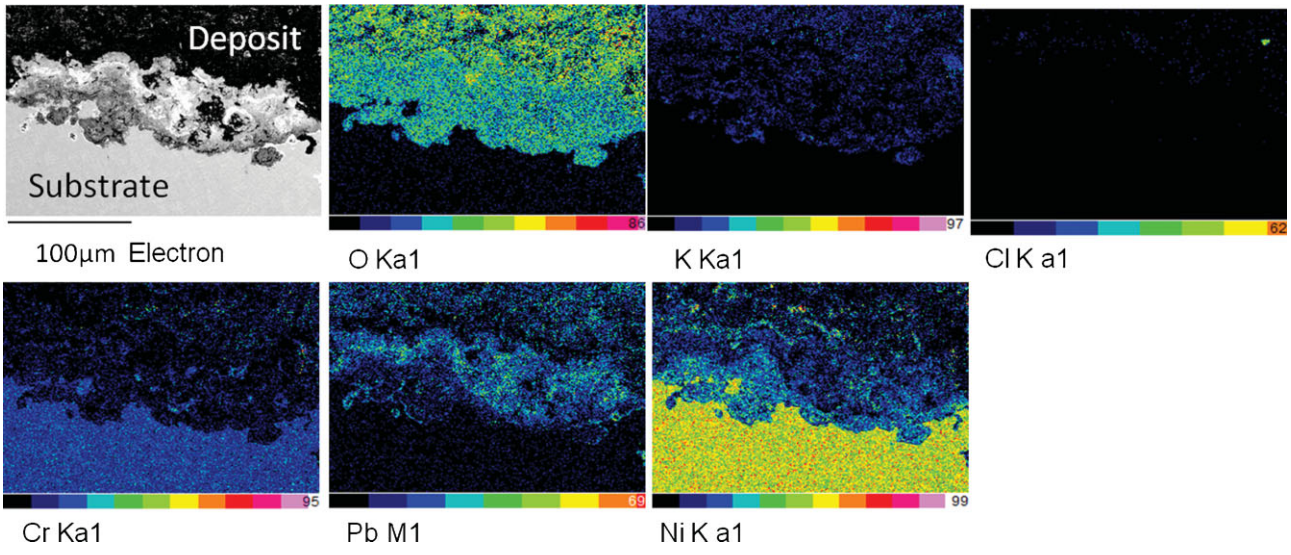

Figure 8. SEM QuantMaps of key elements on the nickel-alloy probe sample

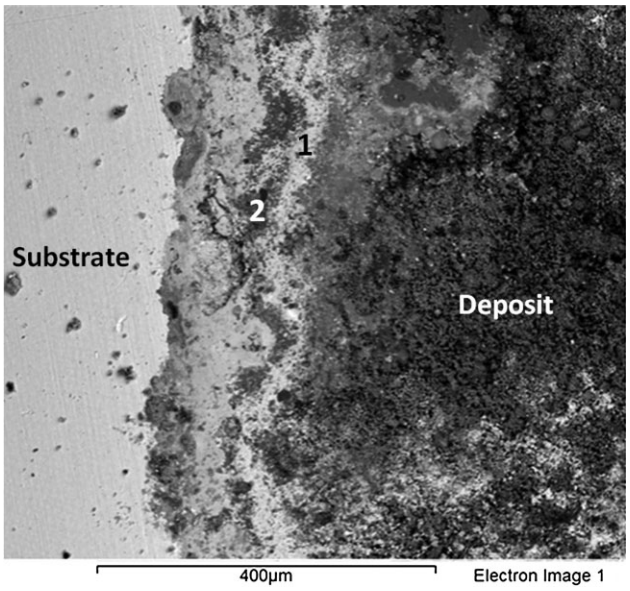

Figure 9. A section through the surface of nickel-alloy probe specimen with two marked spots

hydrogen–oxygen–water equilibrium. Only the oxygen gradient (partial pressure) is shown at the *x*-axis as seen in the figures. The exact amount of species/phases is of no importance, the modelling just shows what stable phases could be expected in a corrosion product/deposited layer.

4 Discussion

Comparison of the corrosion rates measured on the right wall with those on the back wall (see Table 4) shows that the rates on the back wall are 30–50% higher, which is in agreement with the experience of the plant. No difference in deposit chemistry or flue gas chemical composition has been detected so far between these positions although extensive measurements have been performed at the plant. The average oxygen levels at both positions were less than 1% although temperature measurements showed that the gas temperature varied between 855 and 895 °C at probe A on the back wall and 667 and 766 °C at probe B on the right wall. (The measuring points for the flue gas were 10 cm from the walls, measuring time 8 min, sampling interval 5 s.) Metal loss in a power boiler furnace depends on a wide range of factors, for example gas flow rate, particle flows, flue gas chemistry, deposit chemistry and gas temperature or heat flux.

Table 8. Chemical composition (atomic %) of two spot analyses related to Fig. 9

Element	O	Na	Mg	Al	Si	S	Cl	K	Ca	Ti	Fe	Ni	Pb
Spectrum1	69.91	4.41	1.35	–	0.82	9.17	–	6.12	3.27	0.38	–	0.77	3.78
Spectrum2	65.17	10.81	1.17	0.70	1.00	9.45	0.62	7.08	1.22	–	0.42	2.36	–

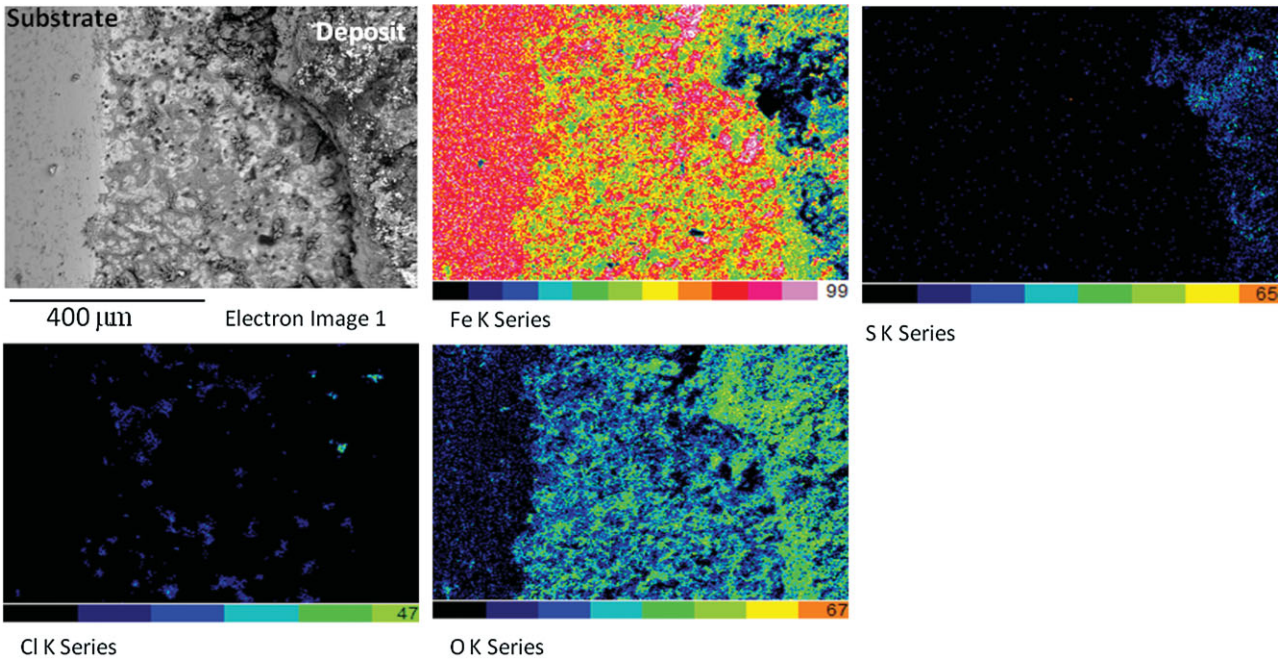

Figure 10. QuantMaps of the 16Mo3 probe sample

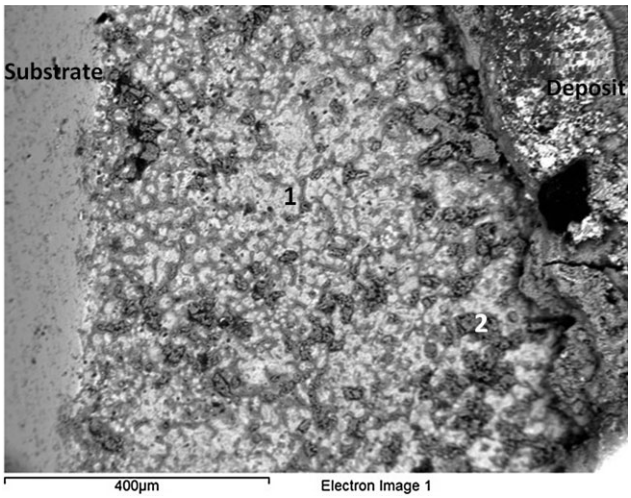

Figure 11. A section through the surface of 16Mo3 probe specimen with two marked spots

Table 9. Chemical composition (atomic %) of two spot analyses related to Fig. 11

Element	O	Si	S	Cl	K	Cr	Fe
Spectrum1	26.10	0.48	0.30	1.02	0.09	0.25	71.76
Spectrum2	61.21	0.70	0.24	7.66	–	–	29.94

In this case the increase in flue gas temperature may account for the difference, in the absence of any other factors.

The corrosion rate measured over a 20,000-h period on the 16Mo3 tube on the right wall (P4) agreed well with the rate measured over a much shorter period of only 934 h by probe testing (B2-2) (see Table 4). This indicates that the corrosion rate is linear and the oxide formed non-protective and that it is possible to extrapolate results from shorter term probe testing to

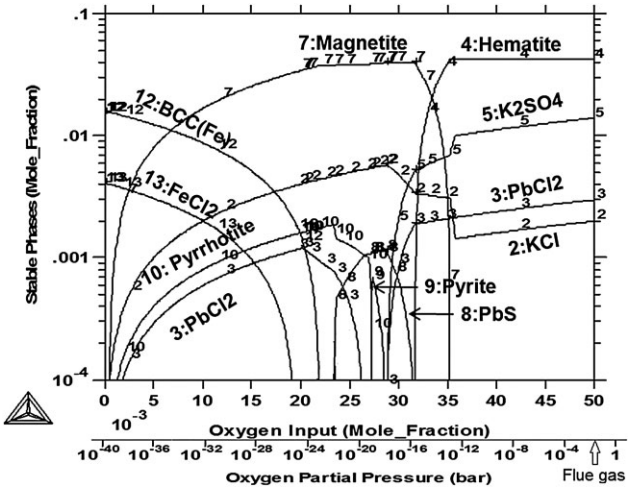

Figure 12. Modelling of iron in flue gas at 400 °C (input in 1 mol: 0.017Fe, 0.003Cl, 0.01H, balance N and gradient of O, K, Pb and S). The amount of K, Pb and S are related to the oxygen amount by factors 0.1, 0.02 and 0.04, respectively

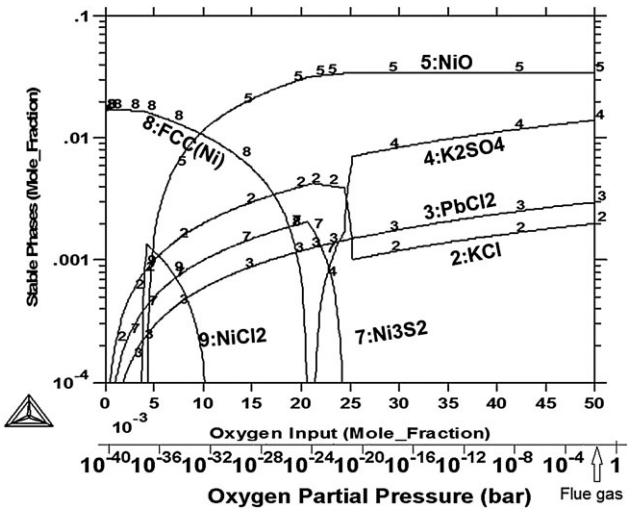

Figure 13. Modelling of nickel in flue gas at 400 °C (input in 1 mol: 0.017Ni, 0.003Cl, 0.01H, balance N and gradient of O, K, Pb and S). The amount of K, Pb and S are related to the oxygen amount by factors 0.1, 0.02 and 0.04, respectively

longer term measurements on this material in this environment. It is more difficult to draw any such conclusions for the nickel alloy, no probe testing was made on the right wall and the uneven surface of the weld overlay on the tube meant that no accurate initial thickness measurements could be made. However, the very low average corrosion rate for the tube exposed for 20,000 h may be representative and indicate a parabolic corrosion rate and a protective oxide.

Two forms of attack are thought to occur in waste environments: chlorine corrosion and alkali corrosion, both initiating from the alkali- and chloride-rich deposits and flue gas. It has been suggested that chlorine corrosion may occur by diffusion of gaseous chlorine through the oxide scale via pores and cracks and reaction with metal iron at the oxide-metal interface where the oxygen activity is low. Iron (II) chloride then diffuses outwards and oxidises, according to the following equations [8].

$$3FeCl_2(g) + 2O_2(g) \rightarrow Fe_3O_4(s) + 3Cl_2(g) \quad (1)$$

$$2FeCl_2(g) + {}^3/_2O_2(g) \rightarrow Fe_2O_3(s) + 2Cl_2(g) \quad (2)$$

Chlorine is released which is then able to participate again in the corrosion process. This is the so-called chlorine cycle. (However, according to our Thermo-Calc modelling, chlorine gas exists at extremely low levels (less than 0.1 ppm); instead the hydrated form is thermodynamically favoured, i.e. gaseous hydrogen chloride. This is a smaller molecule than chlorine which could easily diffuse through a defective oxide of the type formed on 16Mo3.)

Chlorine may also diffuse as chloride ions instead of in the gas phase [9]. In this mechanism the chloride ions diffuse along the oxide grain boundaries. It is postulated that the iron chloride

formed at the grain boundaries increases the rate of transport of oxygen and iron ions [9].

Low melting point or liquid chloride-containing salts in the deposits increase the corrosion rate because of increased reaction kinetics and transport of ions [10, 11]. For example a potassium chloride–iron chloride eutectic mixture has a melting point in the range 340–393 °C and the presence of zinc chloride and lead chloride in an alkali chloride deposit can depress the first melting temperature to 200 °C [12]. The salts attack the oxide by a fluxing mechanism whereby protective oxides dissolve in the salt. Table 1 shows that all these elements are present in waste wood.

Nickel alloys are known to be corrosion resistant in chlorine containing environments because the Gibbs free energy of formation of nickel chloride is less negative than that of chromium chloride and iron chloride and therefore nickel is more resistant to chloride formation than chromium or iron [13]. Alkali metals such as potassium and sodium can also attack the protective chromia scale and form the unprotective chromates, potassium chromate and sodium chromate [14, 15]. In addition, it has long been known that lead oxide attacks nickel–chromium alloys and reduces the corrosion resistance by the formation of lead chromate [16]. Lead chloride was more recently found to have a similar effect on stainless steels [12].

The results of our investigations are in agreement with the mechanisms outlined above. The XRD confirmed the presence of potassium–lead chromate and Fig. 5 shows the presence of potassium and lead in the deposit and the oxide on the nickel alloy coating. A protective chromia layer does not appear to have formed in this case and the nickel is spreading from the oxide into the deposit which might suggest a fluxing mechanism. High amounts of lead at the corrosion front on the nickel alloy coated tube are measured by the spot analyses shown in Table 6 (and relate to Fig. 6). In Fig. 8, the nickel-alloy probe specimen also shows a concentration of lead in the nickel oxide, an area which is devoid of chlorine. By contrast, chlorine was present in the oxides on the 16Mo3 steel tube and probe specimen, but we were unable to detect any lead, and very little potassium (see Figs. 7 and 10 and Table 9).

It appears then that the 16Mo3 steel is attacked by the diffusion of a chloride containing species, for example chloride ions or gaseous hydrogen chloride while the nickel alloy is attacked by potassium and lead and possibly by fluxing of molten salts.

As shown in the Thermo-Calc modelling the stable phases in contact with the flue gas are metal oxides, i.e. hematite and nickel oxide. In the presence of chromium, spinel oxides containing chromium, iron and nickel are thermodynamically expected. In the presence of heavy metals like zinc and lead, heavy metal chlorides may form as indicated in the modelling by lead chloride. However, at sufficiently high oxygen partial pressures other lead containing phases may form as shown by XRD data from the nickel-alloy coated tube, i.e. lead potassium chromate. This phase is unfortunately not included in the Thermo-Calc data bases. Alkali chlorides such as potassium chloride are also expected unless the sulphur and oxygen content is high enough to convert potassium chloride to potassium sulphate [17]. This conversion tendency towards potassium sulphate can be observed in the modelling at higher oxygen partial pressures than 10^{-16} in the case of iron and 10^{-21} in the case of nickel, i.e. this process is thermodynamically more favoured in the case of nickel.

At lower oxygen partial pressures (i.e. closer to the metal surface) the stability area of iron chloride is much larger than with nickel chloride. Obviously, nickel base alloys are expected to be less prone to chlorine induced corrosion from a thermodynamic point of view.

5 Conclusions

The results from this work showed that coating furnace tubes with a nickel-based high chromium containing alloy reduces the corrosion rate of the waterwalls dramatically.

The dominant mechanism in the low alloy steel probe and tube samples was chlorine/chloride corrosion, while attack by a potassium–lead combination appeared to be the dominant mechanism in the nickel-alloy coated samples. The corrosion rate of the 16Mo3 steel was linear.

The simplified thermodynamic modelling fitted well with the identified phases in the deposit/corrosion product, although thermodynamic data for some complex phases was missing in the databases.

Acknowledgements: Financial support from Vattenfall and the Swedish national KME programme is gratefully acknowledged. The authors thank *Peter Viklund*, Swerea KIMAB for the XRD results, *Mattias Mattsson*, Vattenfall Research and Development AB for the probe specimen thickness measurements, other colleagues at Vattenfall who have helped us with the plant testing and *Pingfang Shi*, Thermo-Calc Software AB. The work was carried out within the Surface and Corrosion Science Division, KTH Royal Institute of Technology, Stockholm together with Swerea KIMAB and Vattenfall AB.

6 References

[1] P. Henderson, P. Szakalos, R. Pettersson, C. Andersson, J. Högberg, *Mater. Corros.* **2006**, *57*, 128.
[2] B. Strömberg, S. S. Herstad, *Bränslehandboken*, **2012**, Available at: http://www.varmeforsk.se/rapporter?action=show&id=2782 Accessed June 10, 2012.
[3] R. M. Deacon, J. N. DuPont, A. R. Marder, *Mater. Sci. Eng.* **2007**, *460–461*, 392.
[4] B. Adams, K. Peeters, D. Earaets, H. Diederen, J. P. F. Wijnhoven, Presented at 12th North American Waste-to-Energy Conference, Savannah Georgia, USA, May 17–May 19, **2004**, pp. 229–240.
[5] http://www.springermaterials.com/docs/pdf/978-3-540-44760-3_145.html. Accessed August 12, **2012**.
[6] http://www.specialmetals.com/documents/Inconel%20alloy%20625.pdf. Accessed August 12, **2012**.
[7] http://www.thermocalc.com/. Accessed August 19, **2012**.
[8] H. J. Grabke, E. Reese, M. Spiegel, *Corros. Sci.* **1995**, *37*, 1023.
[9] N. Folkeson, T. Jonsson, M. Halvarsson, L. G. Johansson, J. E. Svensson, *Mater. Corros.* **2011**, *62*, 606.
[10] H. P. Nielsen, F. J. Frandsen, K. Dam-Johansen, L. L. Baxter, *Prog. Energy Combust. Sci.* **2000**, *26*, 283.

[11] P. Kofstad, *High Temperature Corrosion*, Elsevier Applied Science, New York **1988**.
[12] S. Enestam, *Ph.D. Thesis, Åbo Akademi, Finland, 2011.*
[13] A. Zahs, M. Spiegel, H. J. Grabke, *Corros. Sci.* **2000**, *42*, 1093.
[14] J. Pettersson, H. Asteman, J. E. Svensson, L. G. Johansson, *Oxid. Met.* **2005**, *64*, 23.
[15] S. Karlsson, J. Pettersson, L. G. Johansson, J. E. Svensson, *Oxid. Met.* **2012**, *78*, 83.
[16] D. Chatterji, D. W. McKee, G. Romeo, H. S. Spacil, *J. Electrochem. Soc.* **1975**, *122*, 941.
[17] H. Kassman, M. Broström, M. Berg, L. E. Åmand, *Fuel*, **2011**, *90*, 1325.

(Received: March 15, 2013) W7118
(Accepted: April 7, 2013)

VATTENFALL

MEMO NO U 13-66

2013-12-13

Department:

Author: Pamela Henderson, Yousef Alipour and Mattias Mattsson

Security class: Medium [C2]

Attention: KME 508 Project Group and Critical corrosion phenomena

CORROSION OF LOW-ALLOY FURNACE WALL STEEL AT DIFFERENT TEMPERATURES IN A BFB BOILER FIRING 100% WASTE WOOD

Abstract

The combustion of waste wood (recycled wood) leads to corrosion problems of furnace walls for an increasing number of waste-firing power plants. Waste wood is typically more corrosive than virgin wood fuel and the corrosion is often accelerated by reducing conditions. The furnace walls are usually made of the low alloy steel 16Mo3, due to its high heat transfer properties, low thermal expansion and low cost.

It was thought that one way of reducing the corrosion is to lower the temperature of the furnace wall by reducing the boiler pressure. To test this, four coupons of 16Mo3 were exposed on an air-cooled probe inserted in the furnace wall of a waste wood-fired boiler. The exposure time was 1075 hours and the temperature of the four samples were individually controlled in the temperature range 280 ˚C-410˚C. The corrosion rates and corrosion mechanism were investigated. The samples were chemically analysed by XRD and SEM/EDS. The corrosion fronts of two samples were studied by FIB/EDS method.

As expected, the corrosion rate decreased with decreasing metal temperature. The amount of K and Cl in the deposit decreased with decreasing temperature, but the amount of Pb peaked at about 360℃ The FIB sections showed that a distinctive iron chloride layer exists at the corrosion front, with an outer layer of iron oxide. No oxygen/chlorine overlap was observed.

Experimental

An air-cooled probe with a temperature gradient containing four specimens of 16Mo3 was exposed at the back wall of the furnace of the Idbäcken plant, boiler 3, which is a bubbling fluidised bed power station boiler firing waste wood. The probe, which is long and thin (as can be seen in Figure 1) was inserted vertically into a gap made in the fins between two tubes. The wall probe was exposed during the spring of 2013 and the average temperatures of the specimens were 285, 358, 398 and 409˚C.

The probe specimens, which were made by machining from tube, had dimensions of 48 mm length, 7 mm width and 6 mm thickness. The temperature was measured

by a thermocouple placed centrally at the back of each specimen. The total exposure time at temperature was 1075 hours.

The specimens were made of 16Mo3. The nominal chemical composition in weight % was :-
Mn0.55, Si0.22, Mo0.3, Cu0.3, C0.16, Fe Balance .

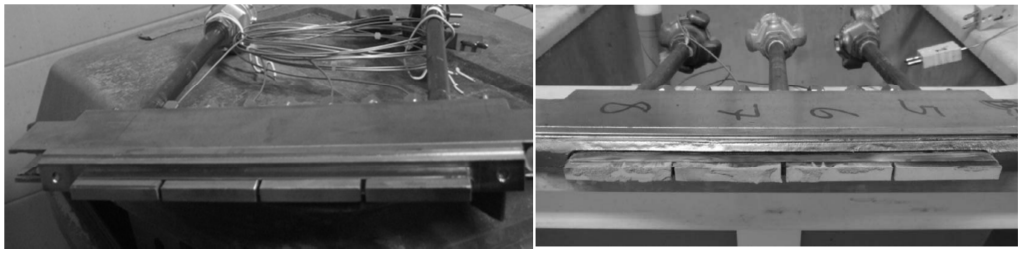

Fig. 1 The probe left) before and right) after exposure inside the boiler

Before exposure in the boiler, the thickness of each probe specimen was measured with a micrometer at four equally spaced distances along the centre line, (see Figure 2, positions 1-4). After testing, the specimens were cut, without water, at the measuring positions. Four parts of each sample were mounted in phenolic resin and used for metal thickness measurement by light optical microscope with a micrometer measuring gauge. The fifth section , the top part of each sample, (on the left in Figure 2) was left unmounted for advanced analysis.

After exposure, five thickness measurements were made on each section making a total of 20 thickness measurements for each probe specimen.

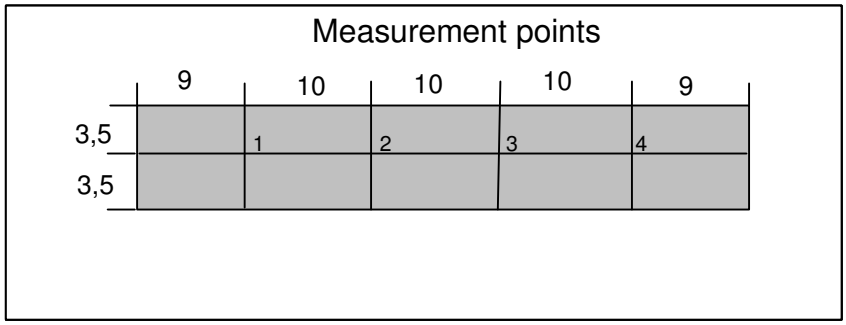

Fig. 2 Probe sample showing measurements points, 1-4. The left of the sample was uppermost in the boiler and was left un-mounted. Each probe sample was 48 mm long and 7 mm wide.

The deposit on each specimen (uppermost section of each probe sample measuring 7x9 mm) was analysed in three places near the centre of the specimen by EDS in an SEM. Each analysis area was 1 x 1.3 mm.

X-Ray diffraction was performed on one sample (sample 3 358°C) with a D8 Bruker AXS, using Cu Kα X-Rays with an energy dispersive detector.

Two samples, at the highest and lowest temperatures had sections cut out of them using FIB (Focussed ion bean) and the cross-section was immediately analysed with EDS.

Results

The variation of corrosion rate (in µm per 1000 h) with temperature is shown in Figure 3. The corrosion rate increases steeply with temperature at the higher temperatures (above about 390°C)

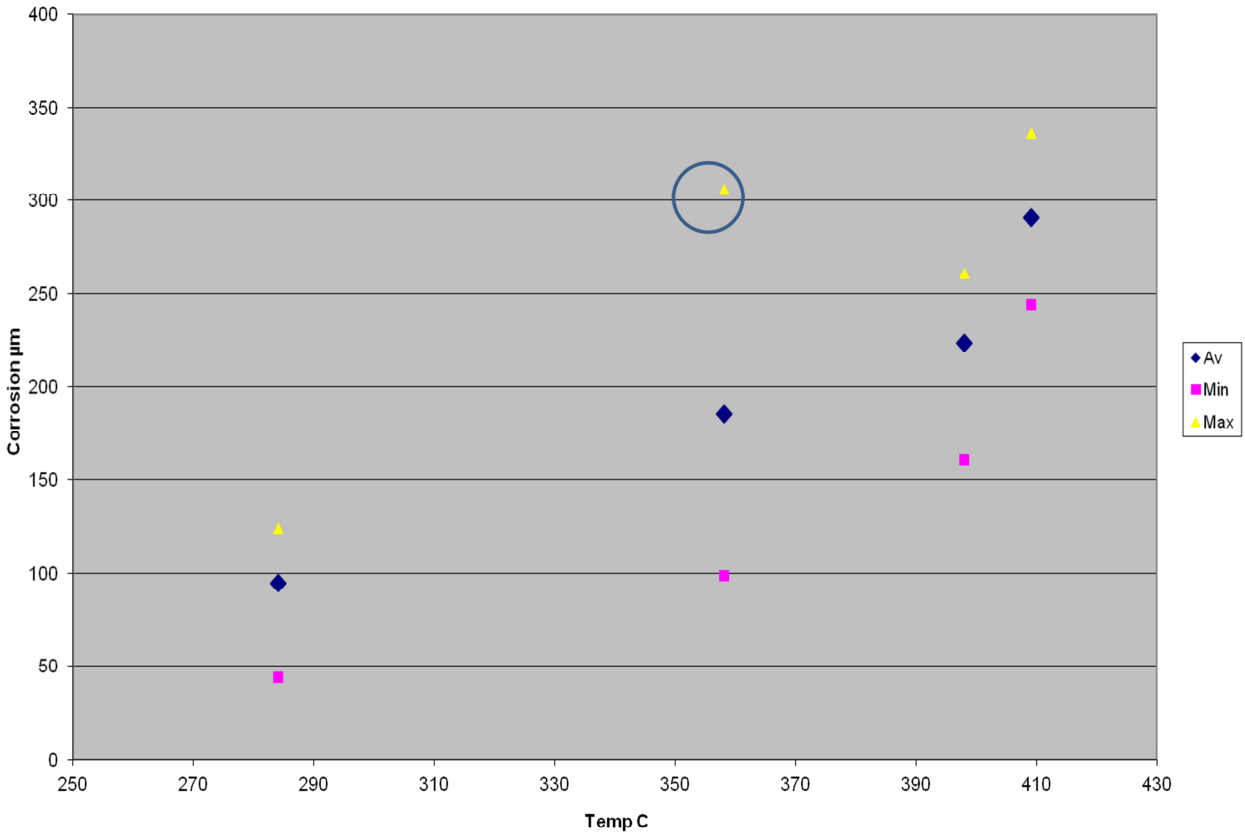

Fig. 3 Variation of corrosion rate in µm per 1000 h with metal temperature in °C. The average, maximum and minimum of the 20 measuring points are shown.

The sample exposed at 358°C showed very high corrosion rates at the upper measuring points (corresponding to section 1 in Fig. 2), which is where the maximum corrosion rate was seen. It was the top part of each specimen that was reserved for chemical analysis and so it was possible to correlate this high corrosion rate with chemical composition of the deposit, as follows.

The variation of chlorine in the deposits is shown in Figure 4. It can be seen that the amount of Cl increases with increasing temperature, but high values of Cl were measured in the 358℃ specimen.

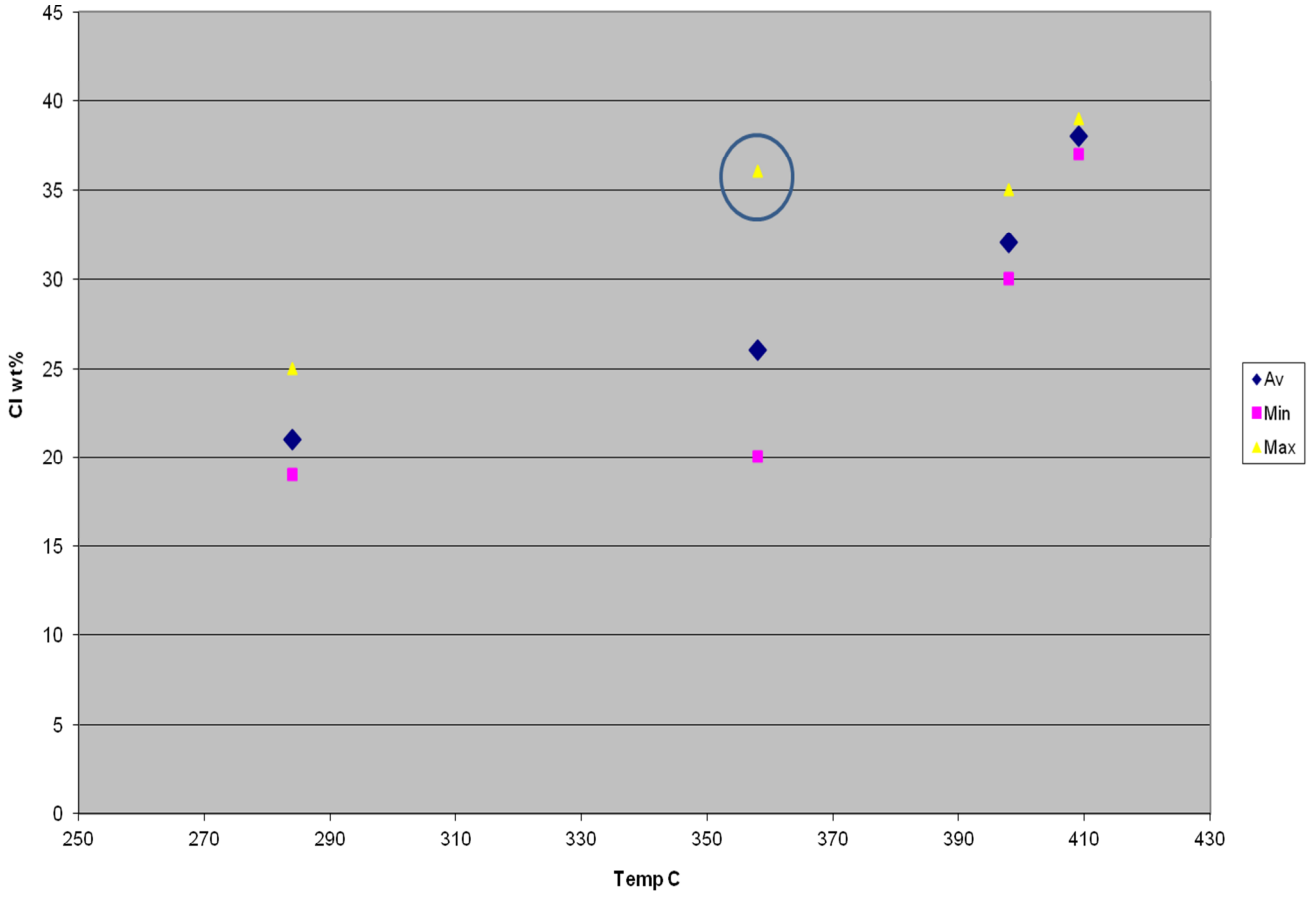

Fig. 4 Variation of Cl (in weight %) in the deposit with temperature.

The variation of potassium in the deposits is given in Figure 5. It shows the same trend as chlorine, and corrosion rate. There is also a sharp increase in the potassium level at the higher temperatures. Similar trends were found for sodium and calcium (increasing with temperature). The opposite trends were found for sulphur and oxygen (implied sulphate), which generally decreased with increasing temperature.

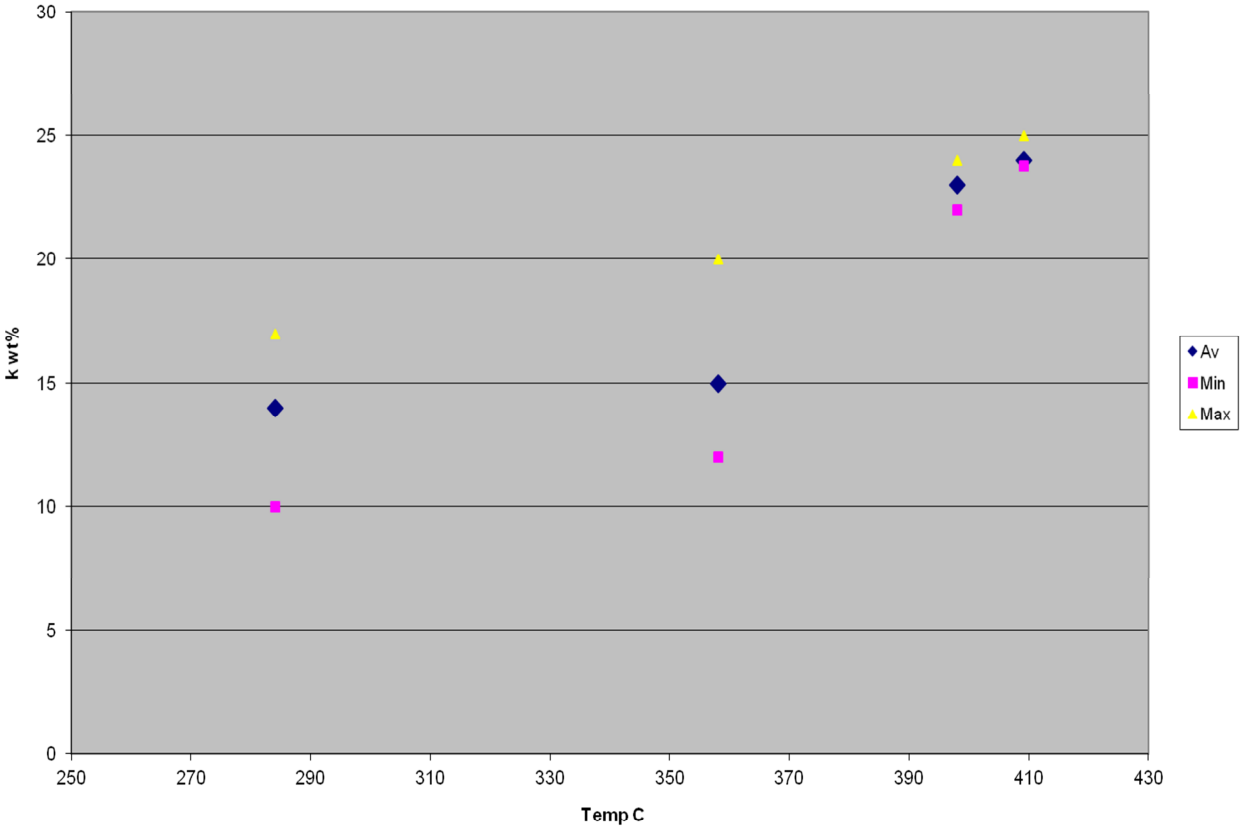

Fig. 5 Variation of K (in weight %) in the deposit with temperature

The variation of lead was more complex, (see Fig. 6). A very large amount of lead was found in the 358℃ sample.

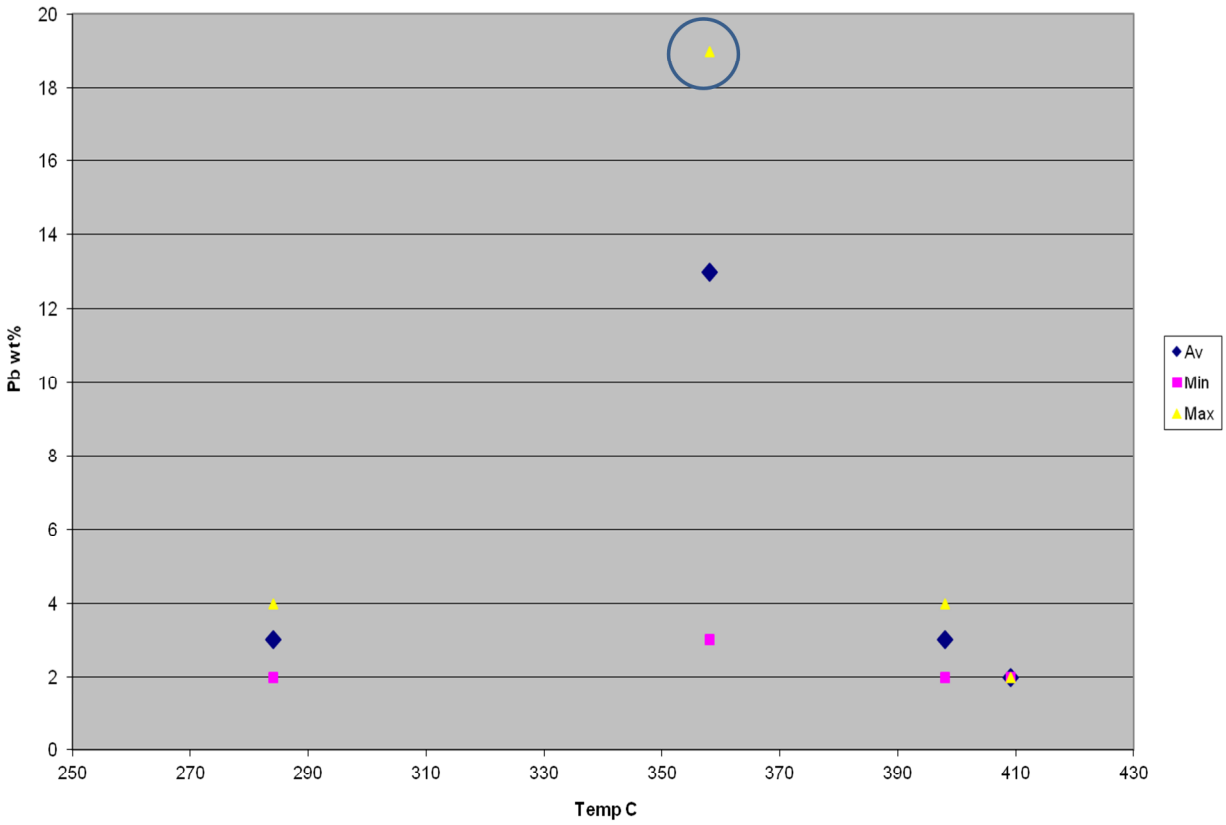

Fig. 6 Variation of Pb (in weight %) in the deposit with temperature

Because the 358℃ sample seemed to deviate from the others, especially in the amount of lead found in the deposit, the deposit was examined by x-ray diffraction to find out what phases were present. The phases are shown in Table 1.

Table 1 . Phases detected by XRD in the deposit of the 358℃ sample

Strong	KCl, NaCl
Medium	Lead
Weak	Pb2O3, Fe2O3

As expected, the chloride was associated with alkali. The deposit contains mainly KCl and NaCl. However some pure lead was detected and some lead oxide is also present.

The samples at the highest and lowest temperatures were investigated by focussed ion beam milling and EDS. A section is shown in Fig. 7. A measurement profile is shown in Fig. 8.

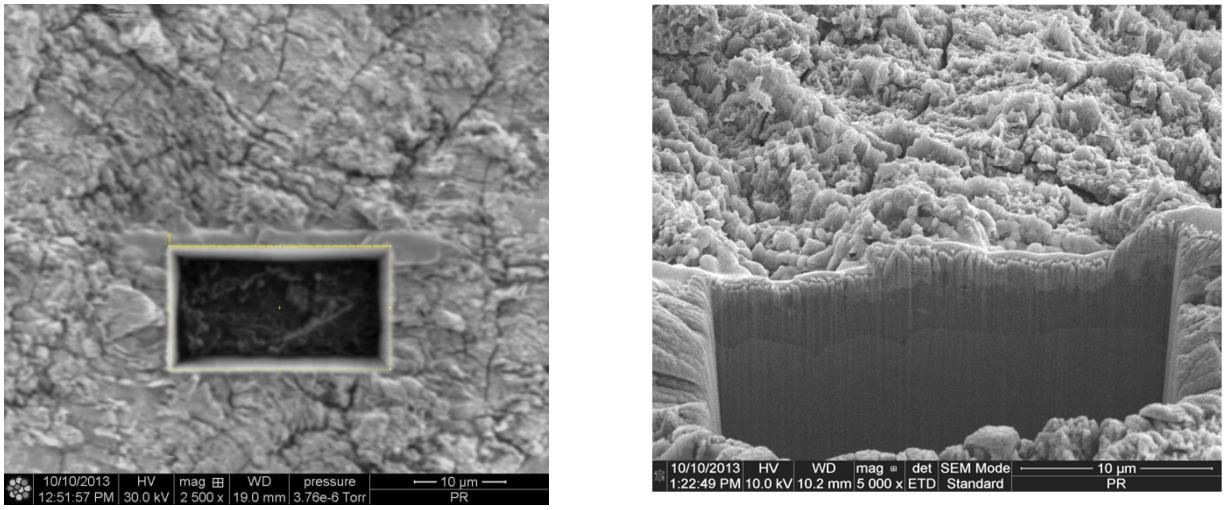

Fig. 7. (Left).Surface view of hole made by FIB. (Right) After tilting by 52 degrees to expose cross-section in the 409℃ sample.

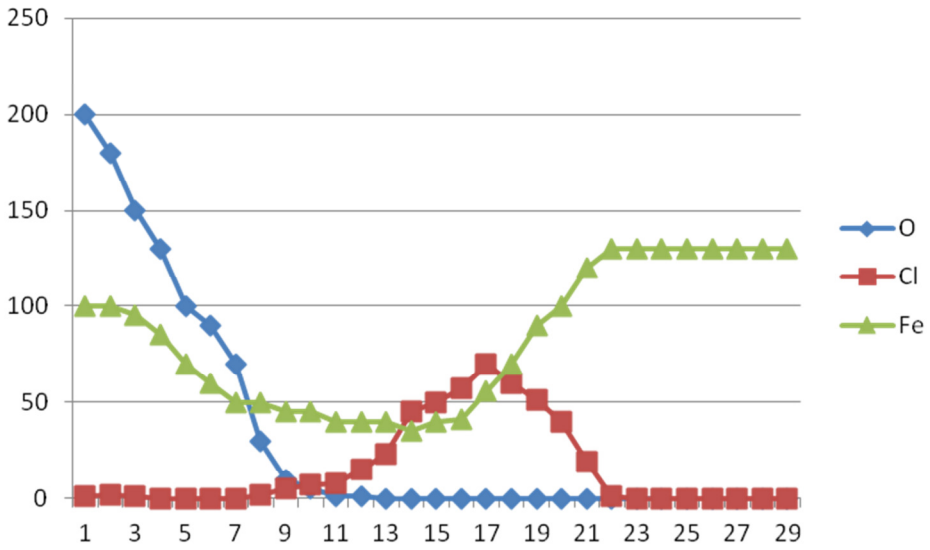

Fig. 8. Measurement profile, 5µm deep, covering 29 measurement points, from the surface of the specimen in to the metal. The iron chloride band is 2µm wide. From 409℃ sample. There is no overlap of oxygen and chlorine, i.e oxychlorides are not seen. The intensities of Fe, Cl and O are related to weight %, but have not been calibrated.

The 285℃ and 409℃ samples showed very similar results. A band of iron chloride 2 µm wide was found next to the metal and no overlap of oxygen and chlorine signals was observed.

Discussion

The steam parameters of the Idbäcken power plant are 140 bar/540°C, which means that the outgoing steam/water temperature and pressure from the boiler is 343°C/151 bar. The temperature of the furnace walls in a boiler is usually taken as the water temperature plus 50°C so the furnace walls are assumed to have a temperature of 393°C. Increasing the steam parameters to 190bar/600°C will mean that the outgoing steam temperature and pressure from the boiler will increase to 368°C/205 bar, so the furnace wall have an assumed temperature of 418°C, an increase of 25°C. It is clear from Fig. 3 that at metal temperatures over 390°C the corrosion rate increases rapidly.

The amount of Cl and K in the deposit increased with increasing temperature, which indicates a more corrosive environment. Locally, though, the highest amounts of Cl and Pb were seen on the 358°C sample, which also corresponded to a very high corrosion rate. Corrosion occurred by chloride attack leading to the formation of iron chloride

Even at the lowest temperature, 285°C, the average corrosion rate was 100µm/1000 h, which is about 0.6 mm per firing season. This indicates that 16Mo3 is not suitable for use as a furnace wall material when burning waste wood, even at very low boiler pressures.

Conclusions

The corrosion rate of 16Mo3 increased with increasing temperature in the furnace region of a boiler burning recycled wood. The amount of Cl and K increased with increasing temperature. At temperatures of 350-360°C, large amounts of lead were found in the deposit in the form of lead or lead oxide.

The corrosion mechanism was found to be similar at the lowest and highest temperatures of 285 and 409°C, that is, chloride attack leading to the formation of iron chloride.

Even at the lowest temperature the corrosion rate exceeded 0.5 mm per firing season.

Development of embrittlement resistant FeCrAl alloys

J. Ejenstam[1], M. Thuvander[2], F. Rave[3], J.N. Olovsjö[3] & P. Szakalos[1]
1. Kungliga Tekniska Högskolan, Surface and Corrosion Science
2. Chalmers Tekniska Högskola, Materials Microstructure
3. Sandvik Heating Technology AB

Introduction

The limiting factor in many energy-producing techniques, such as waste-fired power plants, is closely related to materials. Often, one is interested in increasing the power plants efficiency, and therefore the process temperature is increased. A number of issues arise from this, with corrosion often being the main one. Classical structural steels, such as AISI 316L, are close to its temperature limit already, and therefore may not be applicable at higher temperatures (> 400 °C), hence the plant operator has to look for new materials.

At really high temperatures, above 1000 °C, oxidation kinetics is fast and therefore only a few alloys can be used. The aluminium containing FeCrAl alloy is such an alloy. Due to the aluminium content, the alloy forms protective alumina (Al_2O_3), which is highly corrosion resistant. Such alloys have also been shown to be candidate materials for corrosive environments at lower temperatures, similar to a waste-fired boiler [1, 2]. However, there are some critical issues.
The typical composition of conventional FeCrAl alloys is about 20 wt. % Cr, 5 wt. % Al, with Fe as base. At high temperatures, the alloys is single phased, whereas at lower temperatures, around 500 °C, the material is known to separate into two phases, α (Fe- rich ferrite) and α' (Cr-rich ferrite). This phenomenon is also known as spinodal decomposition or 475-degree embrittlement, and occurs due to the miscibility gap present in the Fe-Cr phase diagram [3, 4]. Phase separation causes severe embrittlement of the steel, making it practically inapplicable for use at these temperatures.

In order to avoid phase separation in this type of alloy, the composition has to be drastically changed. In theory, an FeCrAl alloy containing only 10 wt. % of chromium would be immune to spinodal decomposition and therefore a candidate material for use on waste-fired boilers.

In this work, theoretical and experimental work has been carried out to show that FeCrAl alloys, containing only 10 wt. % chromium, in fact are resistant to embrittlement in the temperature interval 350 °C to 600 °C

Materials and methods

Materials

The rough chemical composition of the alloys studied in the Fe10CrAl project is presented in table 1. From now on the alloys will be referred to as XCr-YAl, i.e. Fe10Cr6Al will be called 10Cr-6Al. The experimental alloys, produced in collaboration with Sandvik Heating Technology AB, were made in an induction-melting furnace. Roughly 1 kg was made per alloy. The ingots were cut into 20 x 70 mm rods and hot-rolled at 1100 °C into 4 mm wires in 5 steps. A 5 min heat treatment at 1100 °C was carried out after each step.

Aging samples were made from 4 mm wires, which were hot-rolled into 8 x 1 mm strips in 3 steps. Heat treatment at 1100 °C was carried out between each step. Samples for electrical resistance measurement were made from 0.7 mm wires, which were produced by reduction of the 4 mm wires by means of dry (5 steps) and wet drawing (10 steps).

Table 1. Chemical composition, in wt. %, of studied materials

Alloy	Fe	Cr	Al	Si	C	Ti	Zr
21Cr-5Al	Bal.	21	5.3	0.07	0.03	0.07	0.08
10Cr-8Al	Bal.	10	8	0.07	0.03	0.07	0.08
10Cr-6Al	Bal.	10	6	0.07	0.03	0.07	0.08
10Cr-4Al	Bal.	10	4	0.07	0.03	0.07	0.08

Methods

Theoretical

All theoretical simulations were carried out by means of Thermo-Calc software. For these particular calculations, the TCFE5 (Thermo-Calc software steels/Fe-alloys database, version 5) database was used.

Experimental

Aged samples were analyzed using a Mitutoyo MKV-H1 micro Vickers hardness tester, applying 0.5 kg indentation force.

The electrical resistance measurement was carried out using a Keithley 2010 low noise digital multimeter. In order to log the data, the instrument was connected to a PC running Lab View software.

A LEAP 3000X HR atom probe (AP) microscope was used to analyze aged material. Current and laser pulse modes were used.

Experimental

Thermo-Calc modeling

In order to study phase separation in the interval 350 ° to 450 °C in a time-limited project, theoretical work had to be carried out. The reason is that phase separation kinetics exponentially decrease with decreased temperature, hence thermodynamical modeling tools (Thermo-Calc) have been used.
Calculations were carried out for two systems, the Fe-21Cr system and the Fe-10Cr system. Phase maps were constructed, where Al content was plotted against present phases in the alloy systems. Three temperatures were considered, 350 °C, 400 °C and 450 °C. The pressure of the system was set to 1 bar, and the whole system size was 1 mole.

Experiments

Thermal aging was carried out at 450 °C, 475 °C, 500 °C, 550 °C and 600 °C in air. Temperatures were controlled by means of thermocouples (type K), and kept within ±5 °C of working temperature. After the aging was completed, the samples were cooled in air.
In order to evaluate hardness, the samples were molded into bakelite and polished. Fine polishing was carried out in several steps using 9 to 1 µm SiC particles, and finalized with an OP-U (chemical polishing containing colloidal silica, product of Struers) step. Hardness tests were carried out at 4 different places on the samples in order to give a more statistically sound result.
Electrical resistance samples were made from 400 mm long 0.7 mm wires, which were spiraled. The Keithley multimeter was connected to each end of the samples, and the resistance was recorded using a PC. The spiraled samples were heated up using a Fibrothal lab furnace, and the temperature was kept within ±5 °C by means of a thermocouple (type K) running through the spiraled samples.
Needle sharp atom probe tips were prepared by means standard two-step electrochemical polishing [5].

Results and discussion

Theoretical

Modeling of the FeCrAl system at embritteling temperatures showed that there is a beneficial effect of Al-addition with respect to phase separation. In theory, if enough aluminium is added, spinodal decomposition can be suppressed at all temperatures. However, this is would cause solution hardening instead, making the alloy practically impossible to process further.

When studying the Fe-21Cr system it is clear that phase separation occurs at all temperatures in the study, depending of Al content, Fig. 1. If the reference alloys, with 5 wt. % Al is considered, Thermo-Calc suggests that at 450 °C and above the alloy is immune to α-α' phase separation. Now, this is not correct as thermal aging experiments have shown that such an alloy is readily embrittled at 475 °C, hence it clear that Thermo-Calc (TCFE5) overestimates the influence of aluminium.

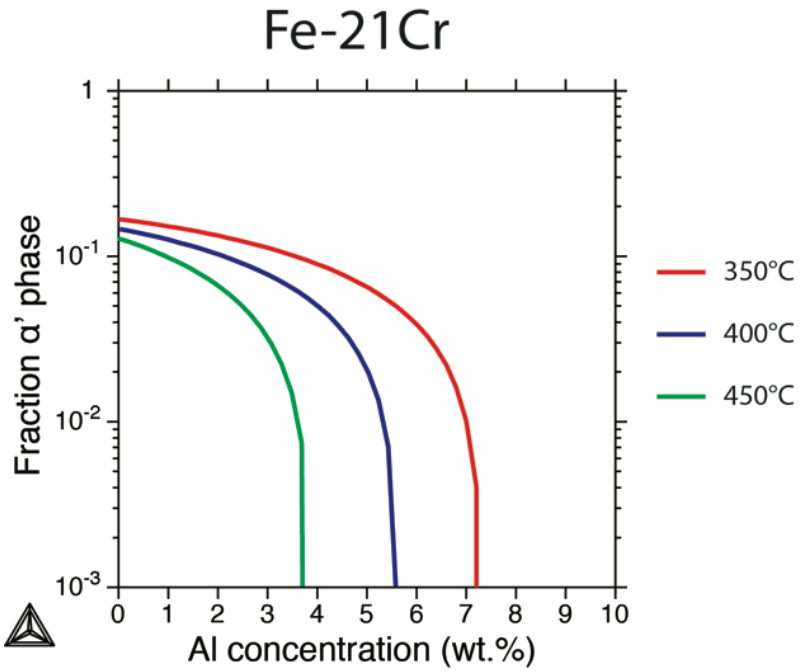

Fig. 1.Thermo-Calc simulation showing expected amounts of α' phase, as function of Al concentration, in a Fe-21Cr alloy at different temperatures

Modeling of the Fe-10Cr system showed that spinodal decomposition can theoretically be suppressed by lowering the chromium content to 10 wt. %. An effect of Al-addition is also observed, and only small Al-additions are needed to suppress spinodal composition, even at 350 °C, Fig. 2. Although Thermo-Calc (TCFE5) does not suggest large amounts of α' present in a pure Fe-10Cr alloy at either temperature, recent studies in literature have shown that this is wrong. In a study by Giovanni et. al. [6], the Fe-Cr diagram is corrected at the α' phase boundary, indicating that a Fe-10Cr alloy would not be affected by phase separation at the temperatures studied in this work.
Nevertheless, although presented calculations indicate that Thermo-Calc seems to overestimate the impact of Al for the Fe-21Cr system, and underestimate the behavior of the Fe-10Cr system at the low range temperature interval, it shows that a Fe-10Cr alloy containing some aluminium (> 1 wt. %) should be immune to spinodal decomposition at all temperatures.

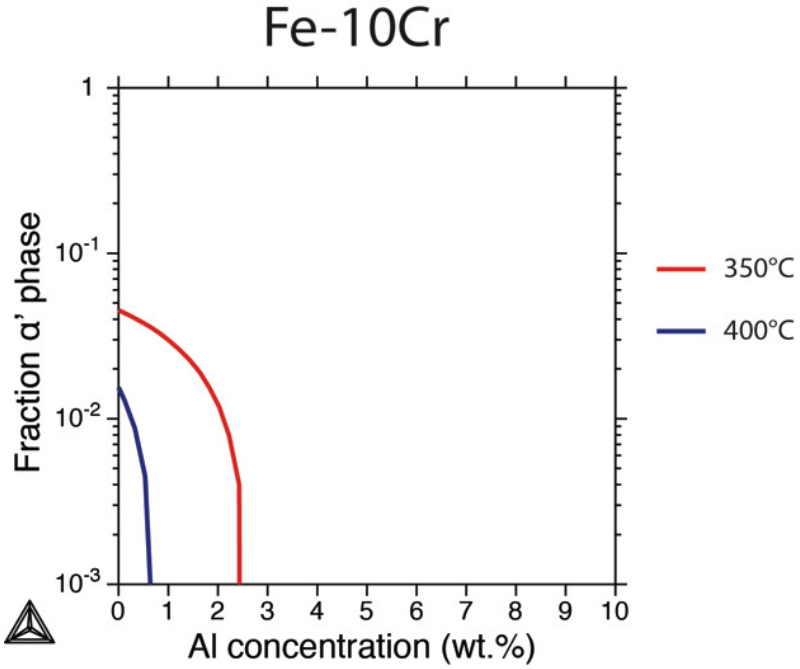

Fig. 2. Thermo-Calc simulation showing expected amounts of α' phase, as function of Al concentration, in a Fe-10Cr alloy at different temperatures

Experimental

Micro-Vickers harness testing

The following results have so far been obtained. 10,000 h aging was completed for alloys aged in 500 °C, 550 °C and 600 °C. For the alloys aged in 450 °C and 475 °C, 5,000 h aging was completed. Aged samples were initially evaluated by means of Vickers hardness testing, results are shown in table 2 and Fig. 3.

Table 2. Vickers hardness results for all alloys and temperatures, showing the change in hardness after aging at the different temperatures. The reference alloys, 21Cr-5Al, is clearly hardened in the interval 450-500 °C. All hardness values are in HV0.5

Aging time & temperature	10Cr-4Al	10Cr-6Al	10Cr-8Al	21Cr-5Al
As received	312 ± 8.9	305 ± 6.6	351 ± 5.2	313 ± 9.5

450 °C, 5,000 h	252 ± 6.7	276 ± 4.1	259 ± 5.6	380 ± 18.3
475 °C, 5,000 h	245 ± 9.0	274 ± 2.8	289 ± 5.9	386 ± 3.5
500 °C, 10,000 h	254 ± 9.0	267 ± 1.2	250 ± 6.0	361 ± 6.6
550 °C, 10,000 h	172 ± 2.6	209 ± 2.1	230 ± 4.5	221 ± 4.3
600 °C, 10,000 h	176 ± 4.5	209 ±1.7	232 ± 2.5	225 ± 3.5

The results show clearly that the reference alloy, 21Cr-5Al, is readily hardened in the interval 450 °C to 500 °C, which was expected. The 10Cr-alloys show a decrease in hardness with time in the same interval. At 550 °C and 600 °C, all alloys show a decrease in hardness, which also is expected as the temperature is too high for α-α' phase separation. The decrease in hardness is also larger, which is due to the higher temperature and the longer aging time. The general decrease in hardness, except for the hardened 21Cr-5Al alloy is believed to be due to the ongoing normalization of the alloys, as the staring material was not normalized prior to the evaluation.

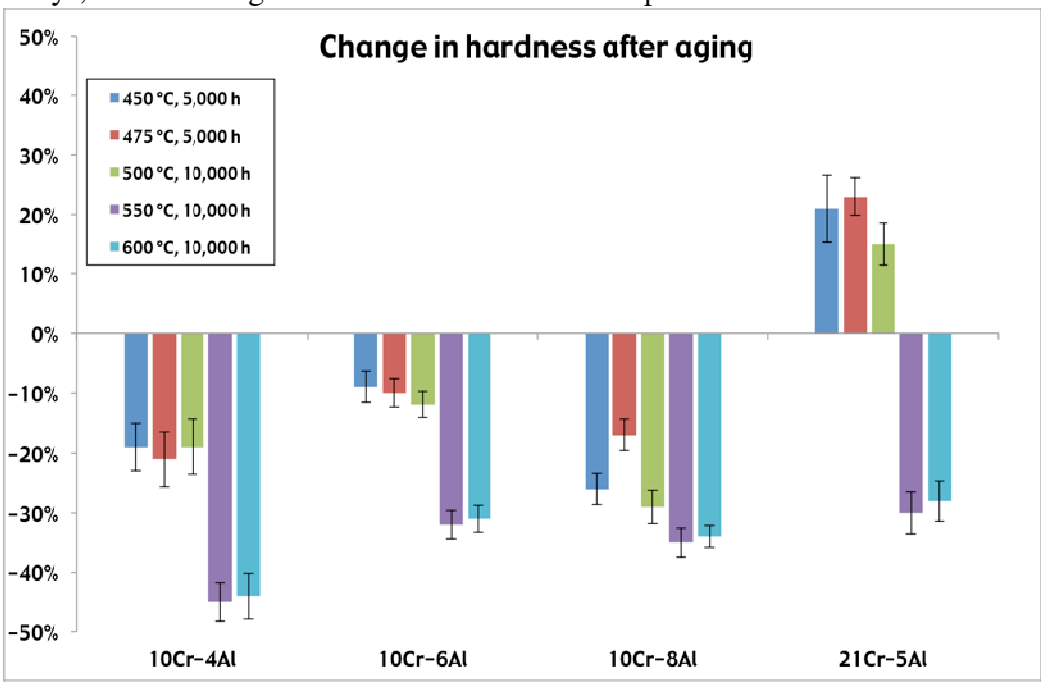

Fig. 3. Change in hardness (in %) of the aged alloys. The 21Cr-5Al alloy is clearly hardened in the interval 450-500 °C

Electrical resistance measurement

The electrical resistance measurement was carried out for all alloys at 475 °C and 500 °C up to 48 h. The method is highly sensitive to macroscopic changes in the microstructure, hence if phase separation occurs at these temperatures it would be noted instantly. Resistivity results from 475 °C and 500 °C are presented in Fig. 4.

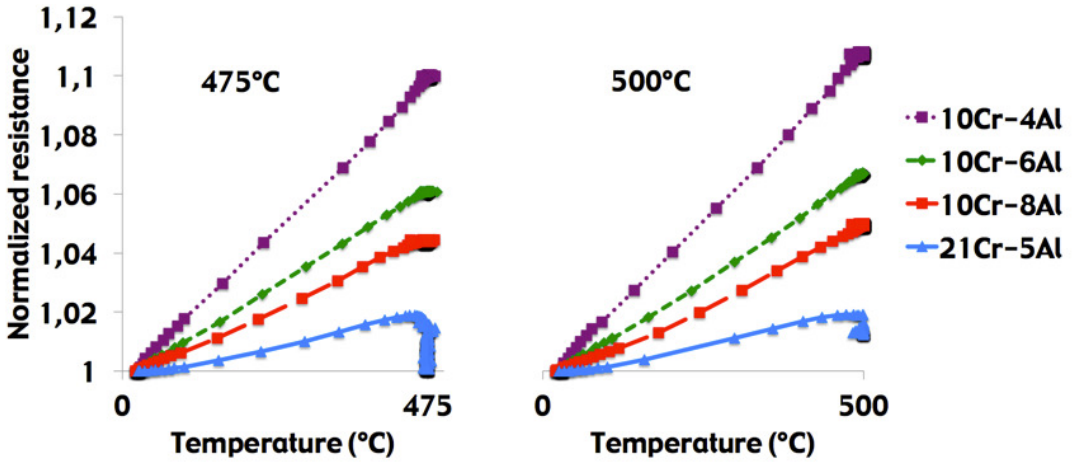

Fig. 4. The graphs show the results from the electrical resistance measurements at 475 °C and 500 °C. The temperature was ramped up to working temperature, where the resistance was measured during 48 h. Resistance values were normalized with measured resistance at room temperature, and plotted against temperature

While the resistance of the 21Cr-5Al alloy decreases rapidly at both temperatures, the 10Cr-alloys are unaffected. The resistance drop was more pronounced at 475 °C, which is expected as α-α' phase separation is known to have its maximum around this temperature.

Atom probe tomography

Two aged samples (10Cr-8Al & 21Cr-5Al) have so far been analyzed with the AP microscope in order to study the homogeneity of the microstructure. The 10Cr-8Al was aged at 500 °C for 10,000 h, whereas the 21Cr-5Al-alloy sample originated from the 48 h electrical resistance measurement at the same temperature. By studying the 48 h sample, the drop in electrical resistance could be proven to originate from a phase separation. No indications of phase separation had been observed for the 10Cr-alloys in previous tests, hence the AP would provide the ultimate answer. If any phase separation would have occurred, the kinetics must have been slow, thus the sample aged for 10,000 h was chosen. The 21Cr-5Al alloy (Fig. 5a), aged for 48 h in 500 °C, show clear signs of phase separation. Chromium rich regions have been formed, and are evenly spread throughout the analyzed volume. The result clearly shows the fast phase separation at 500 °C for the 21Cr-5Al alloy.

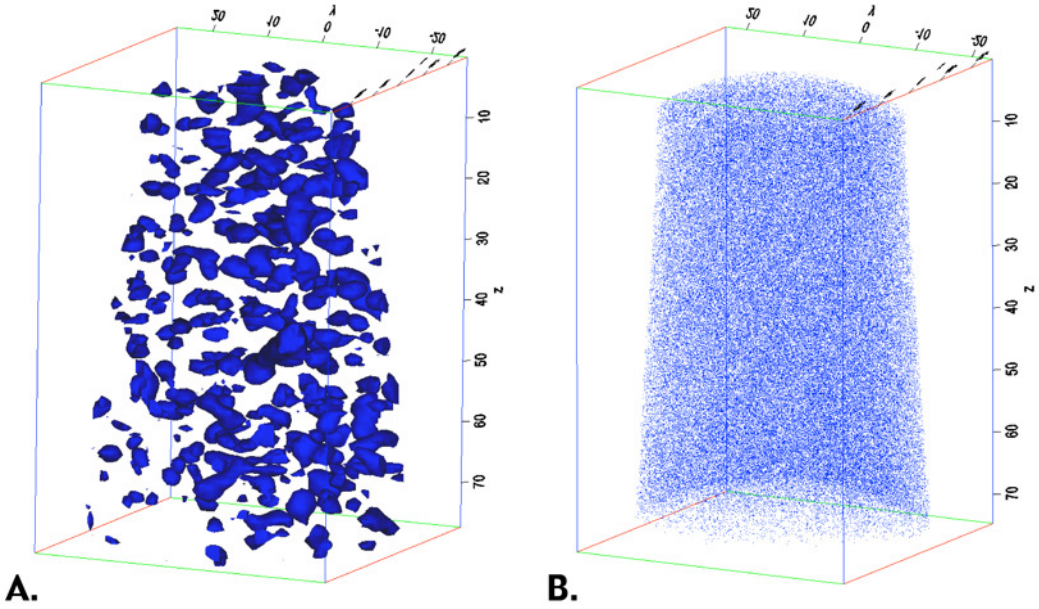

Fig. 5. Computer reconstruction of analyzed volumes (50 x 50 x 75 nm^3). The reconstruction of the 21Cr-5Al alloy aged for 48 h at 500 °C (A), show isosurfaces containing at least 30 % ^{52}Cr atoms. The formation of Cr-rich α' clusters is typical for the phase separation. The 10Cr-8Al alloy (B), aged for 10,000 h at 500 °C show a perfectly homogeneous structure, i.e. Cr atoms are evenly spread throughout the volume

It also shows that electrical resistance measurement is a powerful tool when studying this kind of phase separation process.
Perfectly homogeneous microstructures were observed for 10Cr-8Al alloy, Fig. 5b. This result was expected from the theoretical pre-evaluation of the project, however has now been experimentally proven up to 10,000 h as well.
All in all, the AP results complement the hardness testing and the electrical resistance measurement very well. While hardness tests show clear hardening of phase separating alloys, the onset is longer than for the electrical resistance measurement. The results are in good agreement with other studies on the phase separation of FeCrAl alloys [3, 7, 8].

Conclusions

The study presented in this report showed that Fe10CrAl-RE alloys are immune to α-α' phase separation at 450-600 °C. While the 21Cr-5Al alloy was clearly hardened at embritteling temperatures (450-500 °C), no signs of hardening or phase separation were observed for the Fe10CrAl-RE alloys, at least up to 10,000 h.
At lower temperatures, 350-400 °C, the Thermo-Calc modeling showed no indication of phase separation in the Fe10CrAl-RE alloy system. However, experimental results from this study in combination with recent theoretical findings in literature imply that the thermodynamic database does not give a completely correct picture of reality.

In order to use FeCrAl alloys in structural components in energy producing applications, such as waste-fired boilers, the microstructure has to completely stable at the process temperature of the plant. The work presented in this study have shown that this may be possible by reducing the chromium content, in FeCrAl alloys, to 10 wt. %.

Acknowledgements

Thanks to KME and Vattenfall Research and Development AB for funding and supporting this work, which is a part of the KME-508 project. A special thanks is given to P. Henderson for support and fruitful discussions.
Sandvik Heating Technology AB is thanked for alloy production, materials characterization, know-how, and general support of the project. A special thanks is presented to our Sandvik colleagues P. Byhlin, F. Jämtefors, D. Chandrasekaran, B. Jönsson and R. Berglund.

References

[1] M. Del Giacco, A. Weisenburger, A. Jianu, F. Lang, G. Mueller, J. Nucl. Mater., 421 (2012) 39-46.
[2] J. Ejenstam, M. Halvarsson, J. Weidow, B. Jönsson, P. Szakalos, J. Nucl. Mater., 443 (2013) 161-170.
[3] C. Capdevila, M.K. Miller, K.F. Russell, J. Chao, J.L. Gonzalez-Carrasco, Mat Sci Eng a-Struct, 490 (2008) 277-288.
[4] R.O. Williams, H.W. Paxton, The journal of the Iron and Steel Institute, 185 (1957) 358-374.
[5] M.K. Miller, Vacuum, 45 (1994) 819-831.
[6] G. Bonny, D. Terentyev, L. Malerba, J Phase Equilib Diff, 31 (2010) 439-444.
[7] S. Kobayashi, T. Takasugi, Scripta Mater, 63 (2010) 1104-1107.
[8] W. Li, S. Lu, Q.-M. Hu, H. Mao, B. Johansson, L. Vitos, Comp Mater Sci, 74 (2013) 101-106.

VATTENFALL

Owner	Changed by	Latest change	Revision	
Michal Glazer		**22 October 2013**	**1.3**	**Page 1 (24)**
Subject **HSC MODELLING RESULTS FOR KME – 508 PROJECT**		Project no **PR.263.1.9**		Memo no **U 13-57**

Distribution List:
Annika Stålenheim
Lennart Gårdman
Nader Padban
KME 508 Project group

Receiver:
Pamela Henderson

HSC MODELLING RESULTS FOR KME – 508 PROJECT

SUMMARY:

In the frame of the KME-508 project chemical equilibrium calculations have been performed. The calculations have been done using the HSC modeling software. The goal was to validate assumptions regarding the impact of Zn and Pb on water wall corrosion at increased boiler electrical efficiency/increased steam data when burning biomass and waste wood mixes. The simulations performed by Vattenfall have been compared with the similar calculations done by Metso within the KME-508 project. It was found that similarities for the reducing conditions were substantial, the oxidizing conditions showed some differences.

The Thermodynamic equilibrium calculations were performed using the chemical composition of the fuel to predict condensation behavior of Cl, Zn and Pb compounds at different temperatures. Four different fuel cases were simulated. Finally, the calculations were compared with the experimental results from the Idbäcken power plant. The HSC calculations were in qualitative agreement with the experimental results.

TABLE OF CONTENTS

1 BASIC INFORMATION

The combustion of biomass and waste is making an increasing contribution to Europe's energy production and reduces the dependence on non-renewable sources. Water wall corrosion is already a major problem in combined heat and power plant burning low quality wood fuels (like demolition wood) in low NOx environments. For example, in Idbäcken, Nyköping, operating at 140 bar, the furnace walls were replaced in 2008 for the first time since the plant was built in 1994, but recent measurements showed that wall corrosion rates have now risen to 1.5 mm a year in some places, giving a lifetime of only 3 years if nothing is done. A new furnace wall for a 100MWth BFB boiler like Idbäcken costs around 20 MSEK (2 MEuro) and ways are being sought to reduce the corrosion rate in the project KME 508.

This dramatic increase in corrosion rate has coincided with an increase in the amount of waste wood in the fuel mix from 50% to nearly 100% (as the use of forest fuel has been reduced to reduce the operating costs.) Wider use of waste wood for fuel, in combination with the requirements of reduced NOx emissions, makes it much more difficult to avoid corrosion in a reducing atmospheres adjacent to the furnace walls (water walls). Waste wood has a high content of alkali metals and chlorine, as well as heavy metals like lead and zinc, which increases the risk for corrosion. The fuel chemistry and operating conditions are specifically addressed in this report.

1.1 Overall goals of KME-508 "Furnace wall corrosion" and background to the work performed.

The overall goal of the whole project is to give recommendations about how to avoid water wall corrosion at increased boiler electrical efficiency/increased steam data when burning biomass and waste wood mixes. This will be achieved by performing a number of different tasks. For example : reviewing wall corrosion experiences and ways of reducing corrosion in other boilers, analyzing/measuring flue gas chemistry and deposits formed at the walls of boilers burning waste wood with and without fuel additives, performing short and long-term corrosion tests with a number of different materials or coatings and performing thermodynamic equilibrium calculations to compare theoretical/modelled results with the experimental ones.

This last task of thermodynamic equilibrium modelling is the subject of the work presented in this report. Thermodynamic equilibrium calculations have been performed using the actual chemical composition of fuel to evaluate the condensation behaviour of Cl, Zn and Pb compounds at different temperatures and the results are compared to the experimental ones from deposit analyses.

2 GOALS AND METHODOLOGY

2.1 Goals for the thermodynamic equilibrium calculations

Thermodynamic equilibrium calculations using the chemical composition of fuel to evaluate the condensation behavior of Cl, Zn and Pb compounds at different temperatures were performed and the calculation results compared to the experimental ones from deposit analyses at Idbäcken power plant.

2.2 Objectives

The objective was to find a correlation between the equilibrium calculations and the collected deposits in order to use the chemical equilibrium calculations to predict potentially corrosive fuel mixtures and operational conditions.

2.3 Methodology

HSC Chemistry software has been used to perform the calculations. HSC Chemistry offers powerful calculation methods for studying the effects of different variables on the chemical system at equilibrium. The software calculates the defined state at equilibrium for gas/liquid/solid compounds.

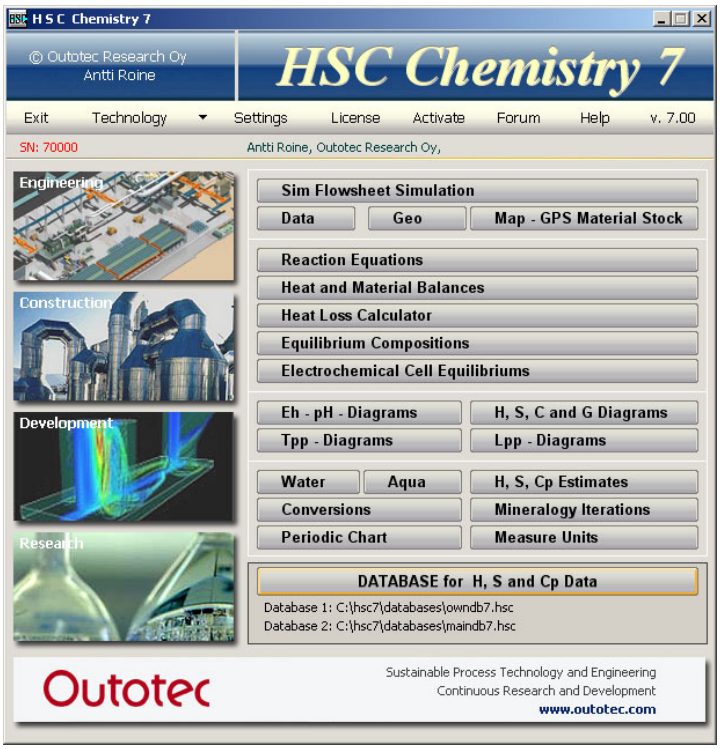

Figure 1 – HSC Chemistry 7

3 METSO

Metso performed within KME-508 similar calculations using the FACTSage software and their proprietary database modification and expertise. The report refers partially to the Metso calculations and tries to compare and analyze the differences. The full analysis was although not possible due to proprietary limitations at Metso.

3.1 Fuel composition and calculation cases

The fuel composition is presented in Figure 2. The fuel composition has been obtained from Metso and this fuel composition was used within the KME 508 project. The project used 4 different fuels varying in composition.

Boiler		Idbäcken	Ref	RPP	EON SC Lockerbie	
		Customer analyses, average values	Ref Fuel	RPP Fuel "Wide" Avg (KME601) 2011-02-03	Stevens Craft (Metso)	Customer data
Proximate analysis						
moisture	wt-%	25,30	17,10	45,00	31	46,10
ash (ashing temp 815 °C)	wt-% (d.s.)	3,90	3,10	3,10	5,3	4,80
Ultimate analysis (dry solids)						
C	wt-% (d.s.)	49,10	50,00	51,70	47,1	N
H	wt-% (d.s.)	6,00	5,60	6,25	6	N
S	wt-% (d.s.)	0,10	0,05	0,05	0,1	0,04
O (diff.)	wt-% (d.s.)	39,80	39,40	38,27	38,9	N
N	wt-% (d.s.)	1,00	1,70	0,60	2,52	
Cl	wt-% (d.s.)	0,10	0,17	0,03	0,1	0,09
Heating values						
HHV, dry	MJ/kg	19,30		20,50	19	10,50
HHV, wet	MJ/kg	14,42		11,28	13,1	
LHV, dry	MJ/kg	17,98		19,13	17,7	
LHV, wet	MJ/kg	12,81		9,42	11,4	
LHV, ash free, dry	MJ/kg	18,71		19,74	18,7	
LHV, ash free, wet	MJ/kg	13,20		9,58	11,9	
Element concentrations in the dry substance						
Al	g/kg ds.	1,41	1,20	0,80	2,20	1,24
Si	g/kg ds.	5,99	6,20	2,00	11,00	
Ti	g/kg ds.	1,13		0,10	1,70	
Na	g/kg ds.	0,92	0,69	0,30	1,30	0,65
Mg	g/kg ds.	0,07	0,58	1,00	0,68	
K	g/kg ds.	1,01	0,93	2,00	1,20	1,19
Ca	g/kg ds.	3,77	2,90	5,00	8,80	
Fe	g/kg ds.	1,08	0,93	0,50	2,60	
P	g/kg ds.	0,11	0,08	0,40	0,57	
Mn	g/kg ds.	0,11		0,50	0,11	0,14
SUM	g/kg ds.	15,59		12,60	30,2	
Heavy metals concentrations in the dry substance						
Cadmium Cd	mg/kg	0,60		0,50	0,25	0,05
Chromium Cr	mg/kg	48,30		5,00	15,00	11,90
Copper Cu	mg/kg	50,90		5,00	24,00	12,50
Lead Pb	mg/kg	58,20	17,00	4,00	120,00	127,00
Mercury Hg	mg/kg	0,10		0,05	0,06	0,03
Nickel Ni	mg/kg	2,60		1,00	8,70	4,73
Vanadium V	mg/kg	2,40		1,00	7,70	2,10
Zinc Zn	mg/kg	621,90	260,00	100,00	92,00	83,50

Figure 2 – Fuel composition used in calculations

In the first part of this report the results of chemical equilibrium calculations for above mentioned 4 different fuels are presented. The fuels were simulated at 2 different conditions each. The first part of the calculations was performed to fine tune the system and compare the modeling findings with the calculations from Metso.

The calculations have been done for:

- Idbäcken fuel at lambda 0.8 and 1.2
- Reference (REF) fuel at lambda 0.8 and 1.2
- RPP Reference Power Plant fuel (as defined in KME 601) at lambda 0.8 and 1.2
- Steve's Croft fuel at lambda 0.8 and 1.2

The conditions represent oxidizing and reducing conditions present in real boiler. The reducing conditions simulate the conditions experienced at boiler walls and the oxidizing conditions at superheaters further downstream in the boiler. This report will focus mainly on the reducing conditions and the Zn and Pb based system.

3.2 Idbäcken at lambda 0.8 and 1.2

Figures 3 and 4 present the equilibrium results for the Idbäcken fuel. Figure 3 presents the results for reducing conditions, Figure 4 presents the result for the oxidizing. It can be seen that in case of reducing conditions the Zn compounds are dominant in the gas phase in the analyzed range between 800°C – 1000°C. The gaseous Zn was found to be the most stable together with $ZnCl_2$.

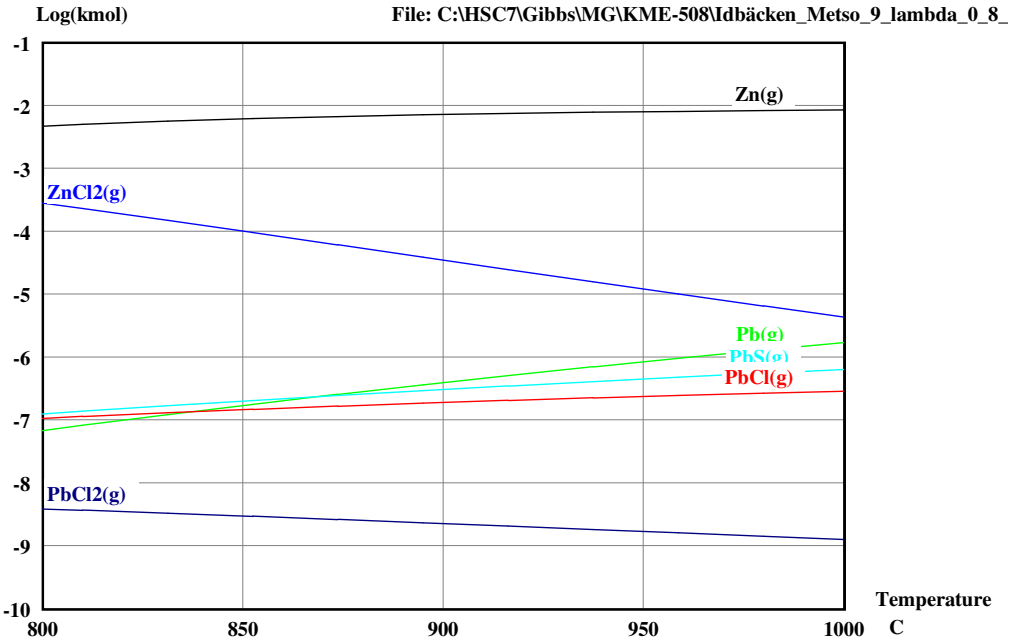

Figure 3 – HSC results – Fuel Idbäcken - at lambda 0.8, temperature range 800-1000°C

In case of oxidizing conditions Zn and Pb chlorides were the dominant compounds with the stable concentration in the whole temperature range. The concentration for the PbO(g) was also increasing with temperature.

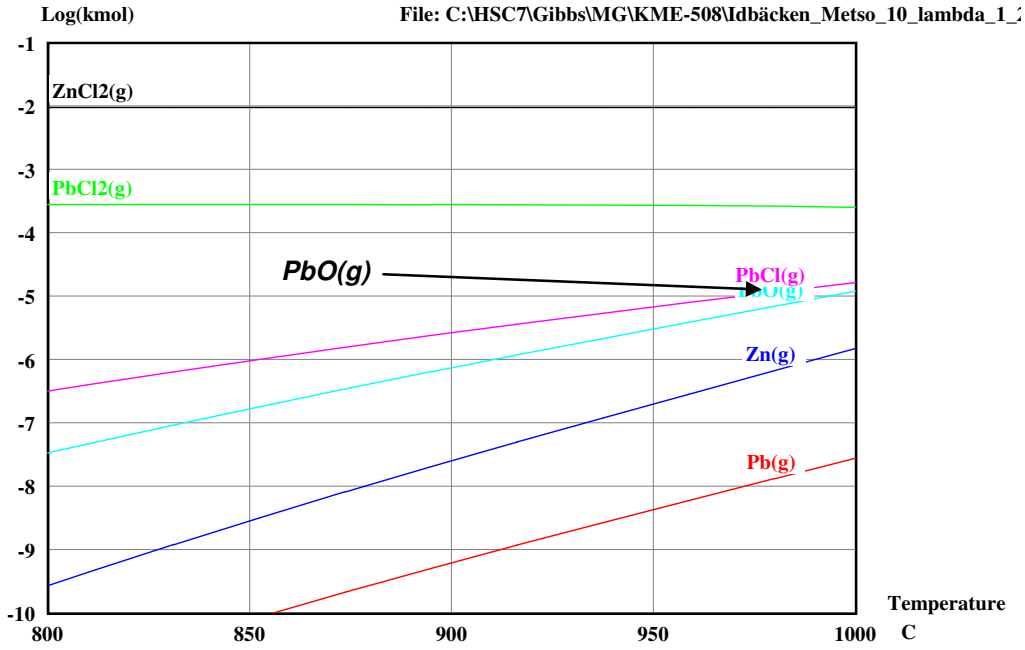

Figure 4– HSC results – Fuel Idbäcken - at lambda 1.2 - temperature range 800-1000°C

Comparing the Vattenfall simulation results with Metso (Figure 5) one can see that the results for the reducing conditions are similar (not taking $ZnCl_2$ into account, which is much more dominant in the Vattenfall case) while the oxidizing conditions differ from each other (Figure 5). For Metso calculations the PbO(g) was found to be dominant almost in the whole temperature range while for Vattenfall it was present only in lower concentrations.

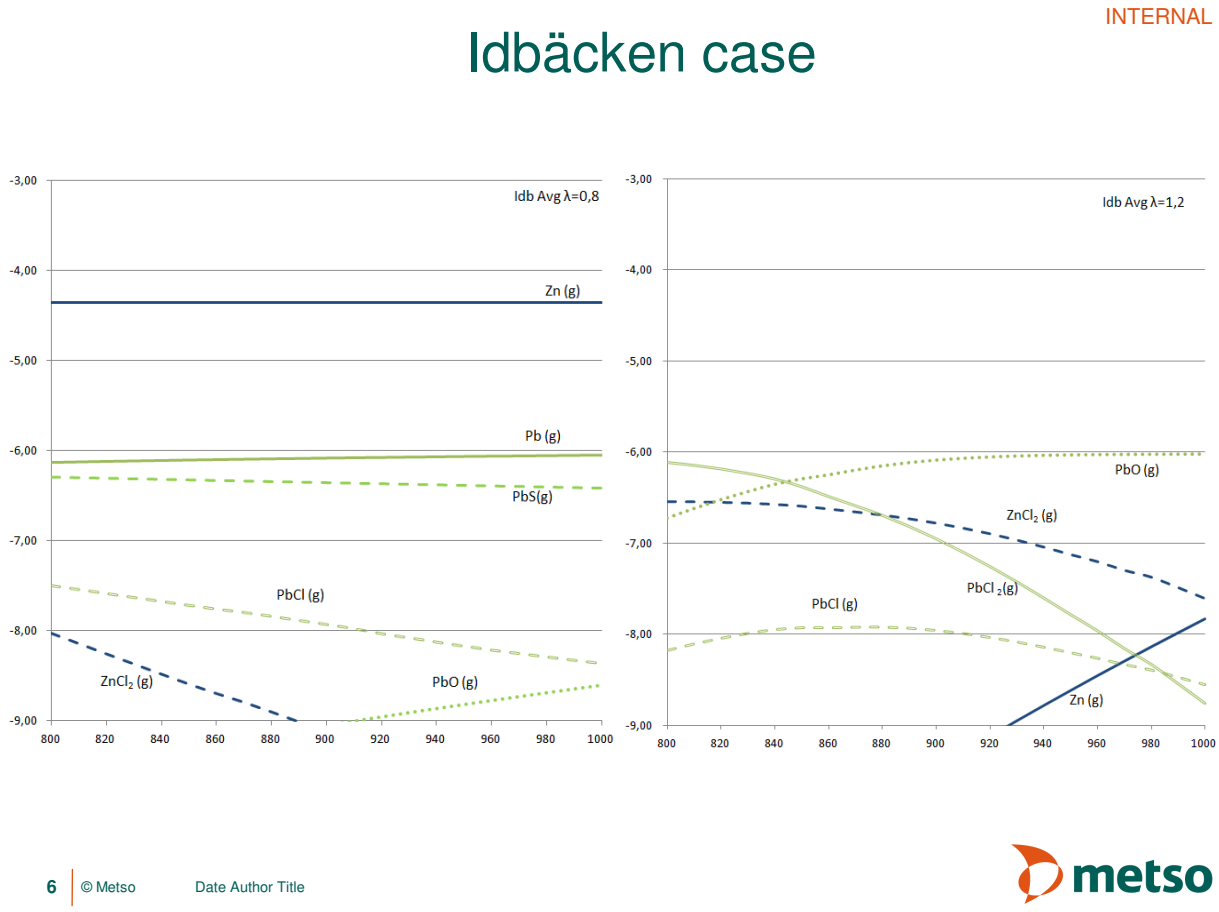

Figure 5 – Metso results – Fuel Idbäcken - lambda 0.8 (left) and 1.2 (right) - temperature range 800-1000°C

3.3 Reference fuel (REF) at lambda 0.8 and 1.2

Figures 6 and 7 present the equilibrium results for REF fuel. Figure 6 presents the results for reducing conditions. Figure 7 presents the results for the oxidizing case. It can be seen that in case of reducing conditions (Figure 6) the Zn compounds were dominant in the equilibrium system calculated with HSC Chemistry. As for the Idbäcken fuel (number 1 case) the dominant and preferred equilibrium compound was Zn(g). $ZnCl_2$ is the second most important component predicted by HSC chemistry to be present at the equilibrium.

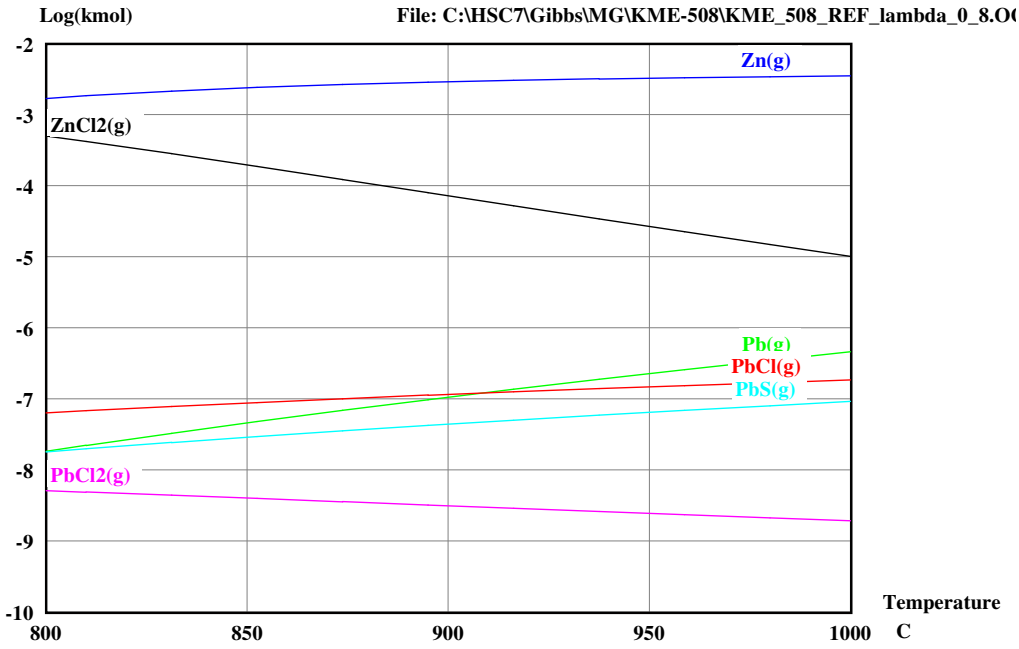

Figure 6 – HSC results – Reference Fuel (REF) - at lambda 0.8 - temperature range 800-1000°C

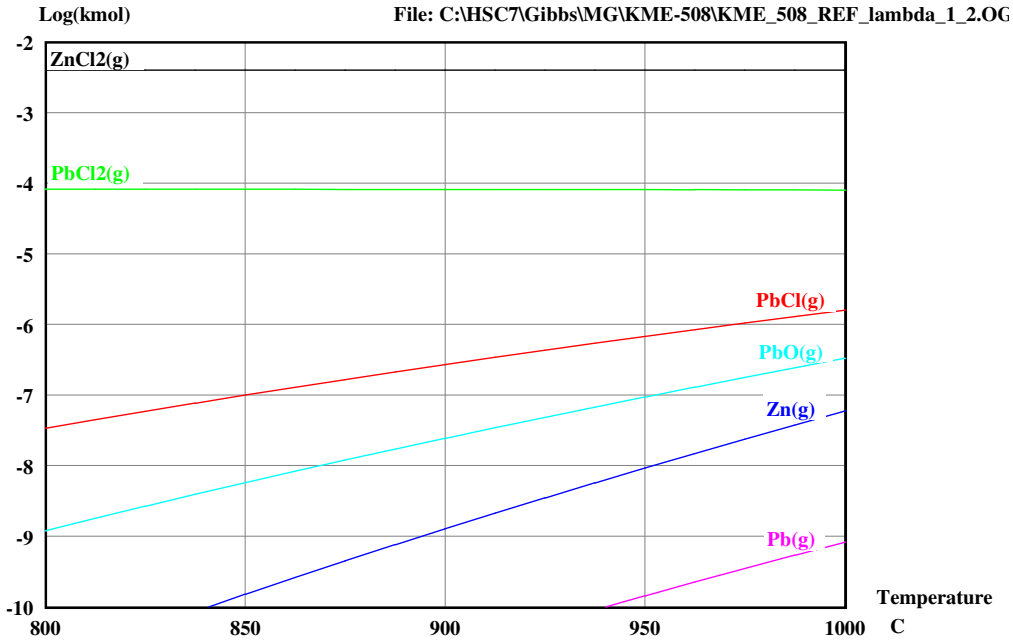

Figure 7 – HSC results – Reference Fuel (REF) - at lambda 1.2 - temperature range 800-1000°C

Comparing the Vattenfall results with Metso one can see that the reducing conditions are similar (not taking $ZnCl_2$ into account). For the oxidizing conditions HSC predicts the chlorides to be dominating the system (Figure 7) while for Metso calculations at lambda 1.2 PbO(g) is the most dominant compound in

the temperature range above 880°C. The Idbäcken and REF fuels are similar in composition so one can expect they react in a similar way which is reflected in the very similar modeling cases.

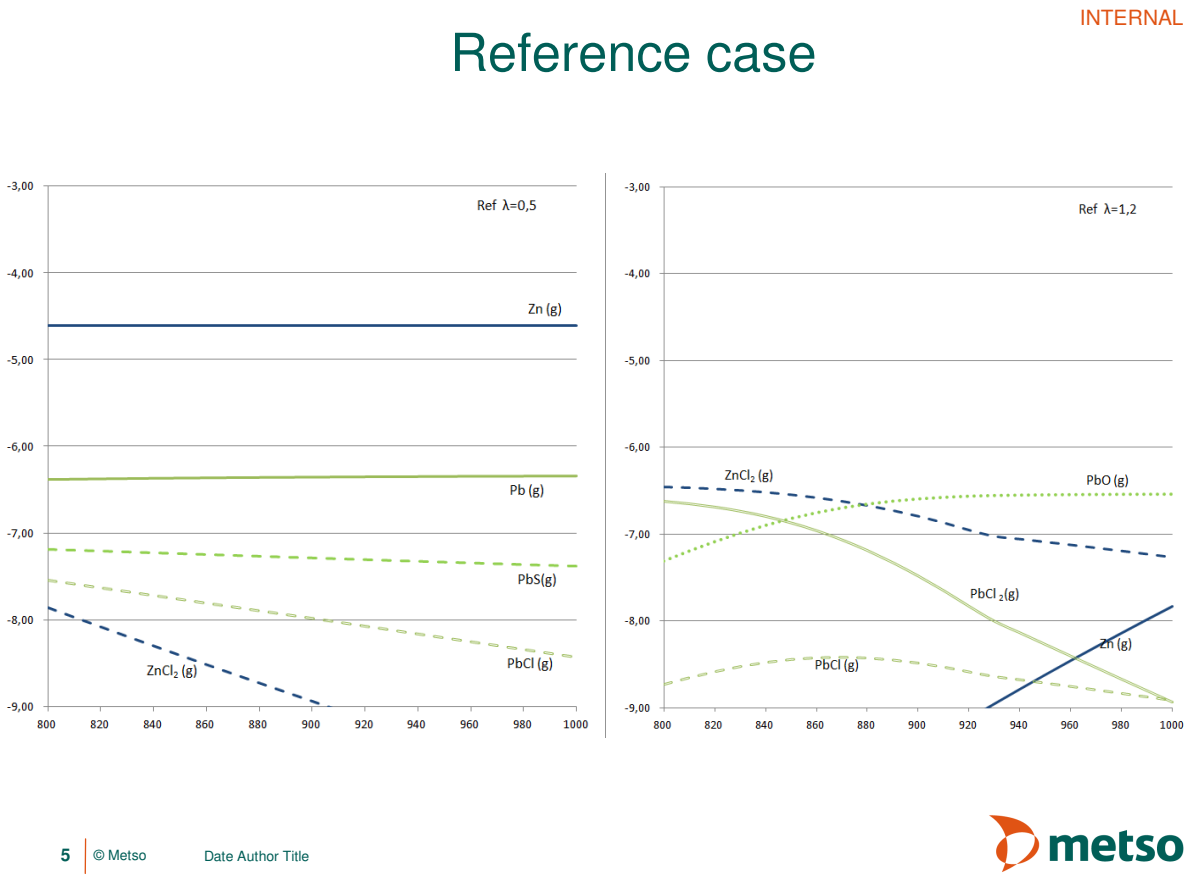

Figure 8 – Metso results – Reference Fuel (REF) - lambda 0.5 (left) and 1.2 (right) - temperature range 800-1000°C

3.4 RPP fuel at lambda 0.8 and 1.2

Figure 9 and 10 present the equilibrium results for the RPP fuel. Figure 9 presents the results for reducing conditions and Figure 10 for oxidizing. It is can be seen that in case of reducing conditions the Zn compounds are dominant. Gaseous Pb(g) and PbS(g) were the second most important components predicted by HSC chemistry to be present at equilibrium but the concentrations were much lower. The RPP fuel contains much less Cl than the Idbäcken or REF cases which can be the reason the chlorine based compounds are not dominant for the reducing case. For the oxidizing case (Figure 10) $ZnCl_2(g)$ was predicted to be the dominant component and PbO(g) the second - almost in the whole temperature range.

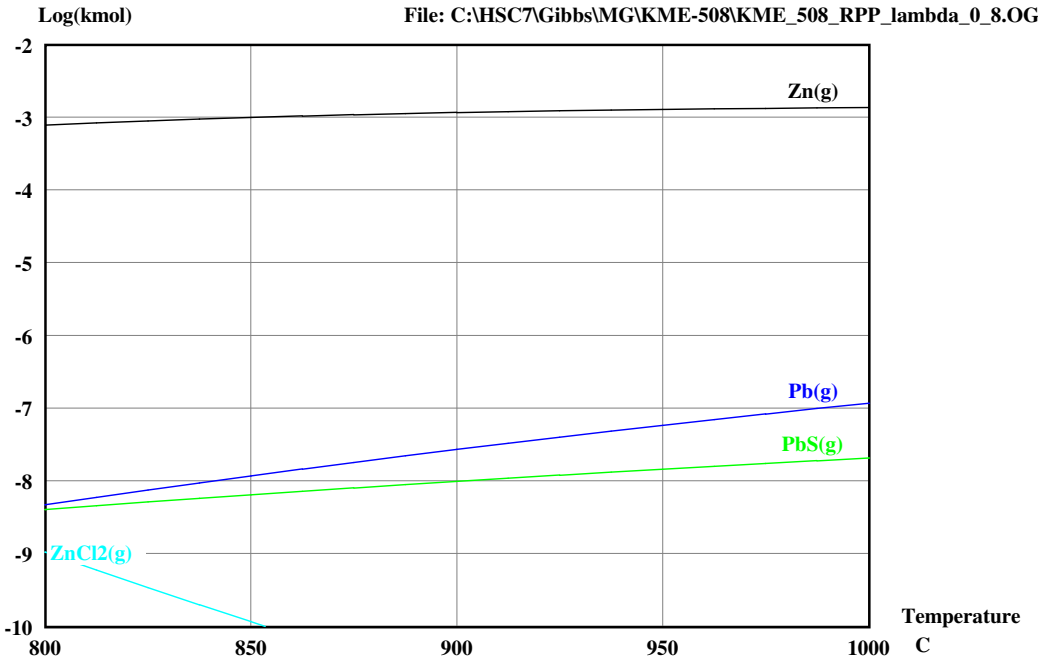

Figure 9 – HSC results – Fuel RPP - at lambda 0.8 - temperature range 800-1000°C

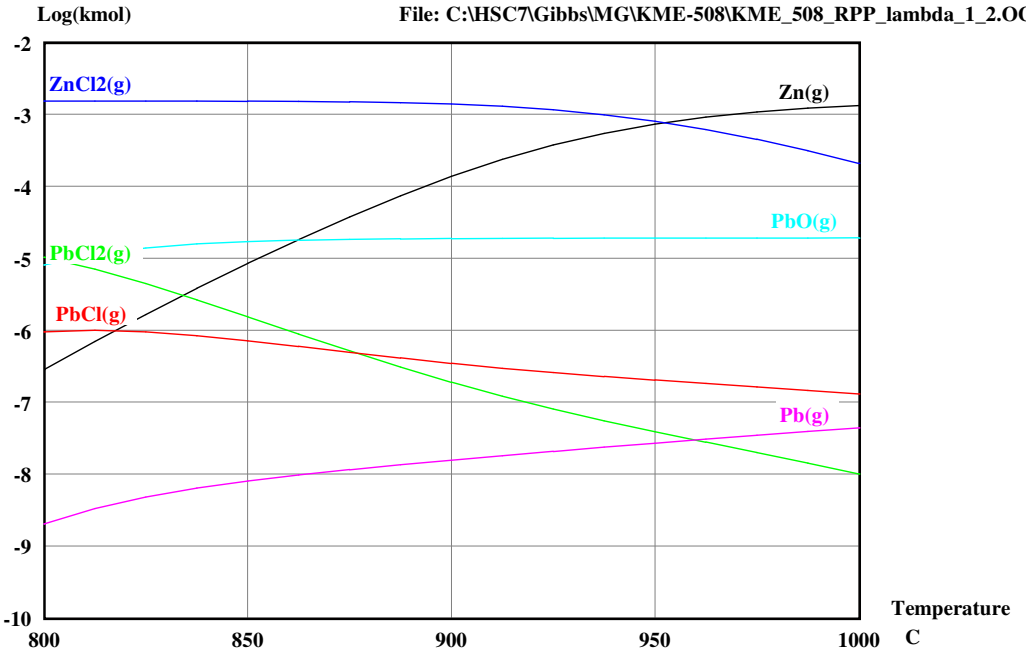

Figure 10 – HSC results – Fuel RPP - at lambda 1.2 - temperature range 800-1000°C

Comparing the Vattenfall results with Metso one can see that the reducing conditions are dominated by gaseous elemental Zn(g) and Pb(g) while for Metso calculations at lambda 1.2 PbO(g) is the most dominant compound in the temperature range above 800°C. One can observe that for the reducing conditions the concentration of Zn(g) and Pb(g) were almost constant through the whole temperature range. While the amounts of corrosive metal chlorides were decreasing with increasing temperature. The temperature near the boiler walls was at the range between 800-1000°C while the temperature of

the wall approx. 400°C. The corrosive metal chlorides will condense at the colder walls (see discussion and comparison with the experimental results).

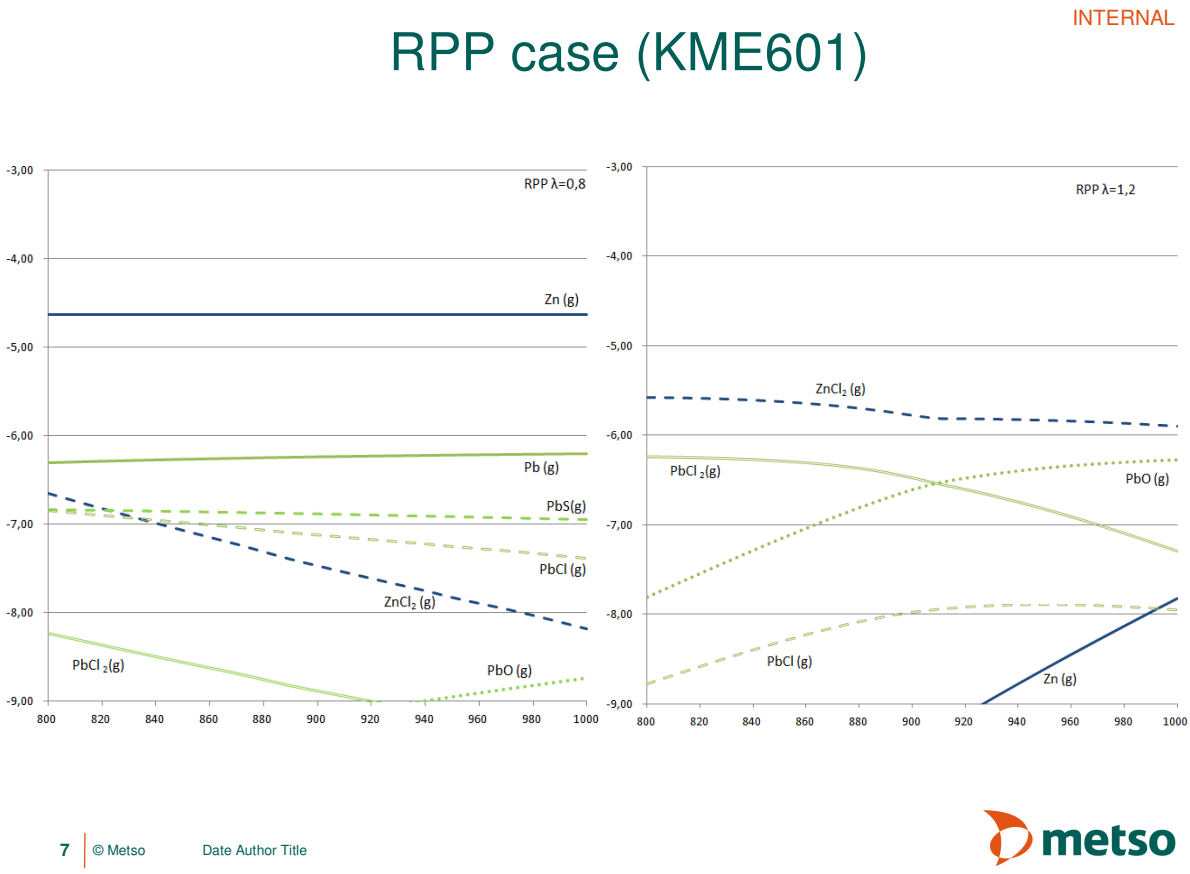

Figure 11 – Metso results – Reference Fuel (REF) - lambda 0.8 (left) and 1.2 (right) - temperature range 800-1000°C

3.5 Steve's Croft fuel at lambda 0.8 and 1.2

Figure 12 and 13 present the equilibrium results for the Steve's Croft fuel. Figure 12 presents the results for reducing conditions and Figure 13 for the oxidizing. It can be seen that in case of reducing conditions the Zn compounds are dominant. Gaseous Pb(g) and ZnCl2(g) were the second most important component predicted by HSC chemistry to be present at the equilibrium but the concentrations were much lower. This fuel contains the same amount of Cl as the Idbäcken fuel so the picture here for the reducing conditions is very similar. For the oxidizing case (Figure 13) $ZnCl_2$(g) together with $PbCl_2$(g) were predicted to be dominant.

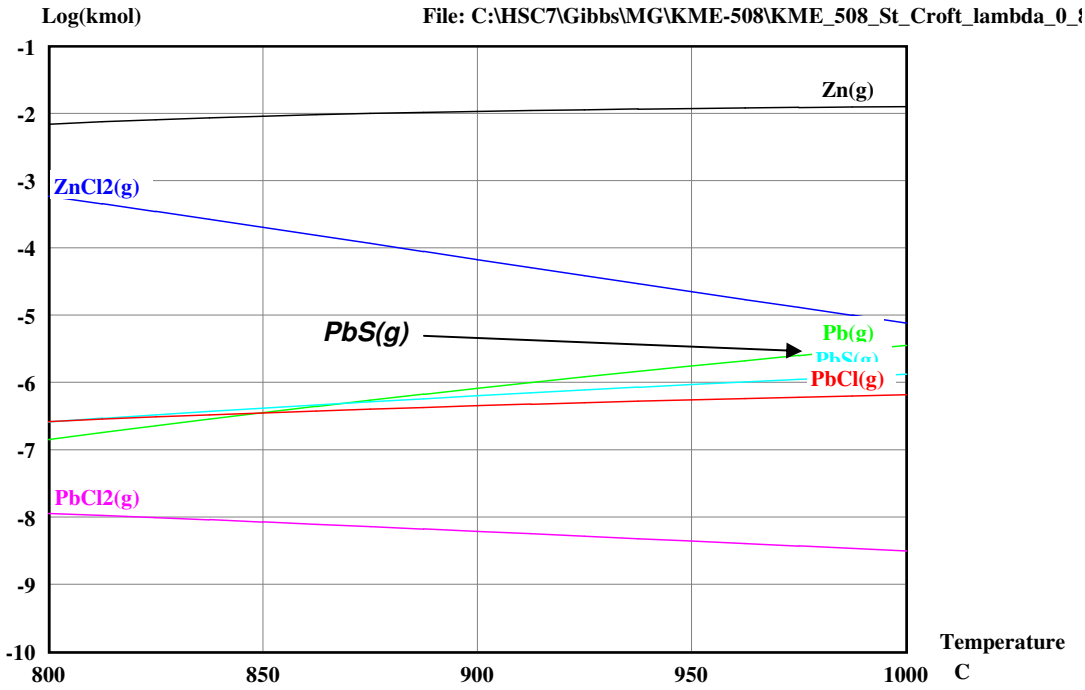

Figure 12 – HSC results – Fuel Steve' Croft - at lambda 0.8 - temperature range 800-1000°C

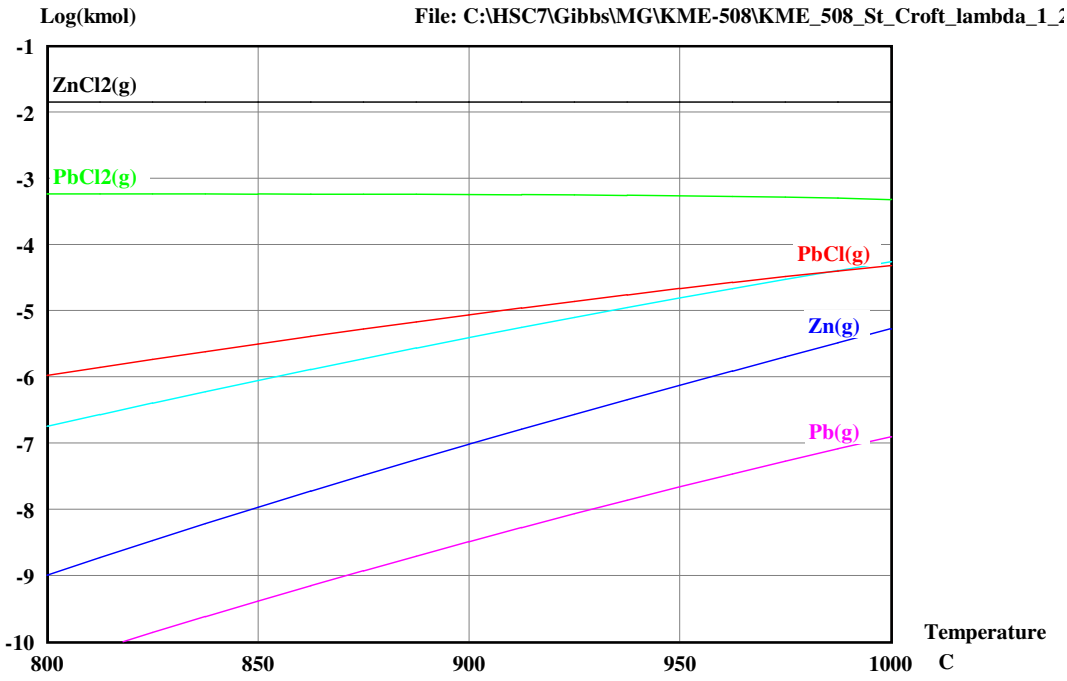

Figure 13 – HSC results – Fuel Steve' Croft - at lambda 1.2 - temperature range 800-1000°C

Comparing the Vattenfall results with Metso one can see that the reducing conditions are dominated by gaseous elemental Zn(g) and Pb(g) while for Metso calculations at lambda 1.2 PbO(g) is the most dominant one in the temperature range above 840°C. One can observe that for the reducing conditions the concentration of Zn(g) and Pb(g) were almost constant through the whole temperature range. While the amounts of corrosive metal chlorides were decreasing with increasing temperature. The temperature near the boiler walls was at the range between 800-1000°C while the temperature of the wall is approximately 400°C. The corrosive metal chlorides will most probably condense at the colder walls.

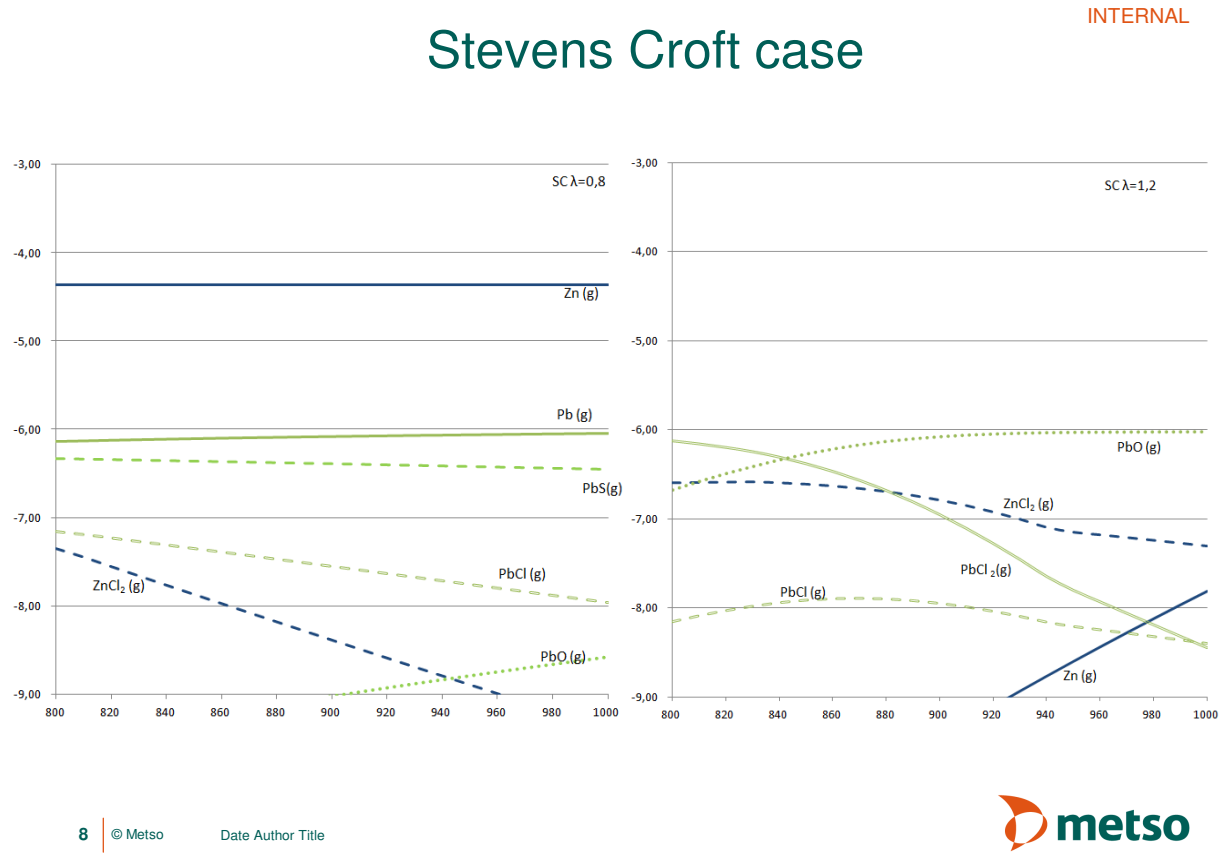

Figure 14 – Metso results – Fuel Steve' Croft - lambda 0.8 (left) and 1.2 (right) - temperature range 800-1000°C

3.6 Summary

The comparison between the Metso calculations (FactSage) and Vattenfall calculations (HSC) reveals that the reducing conditions cases were characterized in a similar way by both calculation tools. The system is dominated with the pure elements of Zn and Pb or with their chlorides, apart from the case of the RPP fuel, which had a lower Cl content. The chlorides are believed to be responsible for the corrosion of the boiler walls. More differences between Metso and Vattenfall were visible for the oxidizing conditions. Here the systems don't match each other. For Vattenfall the system was dominated by chlorides, for the Metso calculations the lead oxides were the main components. It was tried to increase the lambda much above the level of 1.2 but the calculations with lambda much higher than 1.2 did not change the results observed for the oxidizing conditions.

The main conclusions then can be summarized:

- There are differences for oxidizing conditions observed between Vattenfall results and Metso results
- The reducing system was similar, some smaller differences were observed.
- With varying the oxygen content (lambda =1.2 + lambda max.) no differences were observed.

4 RESULTS DEPOSITS IDBÄCKEN

Within KME 508 a measurement campaign was performed at Idbäcken with waste wood in November 2011. The measurements were made during the period 8-10 November with the boiler running at 65-80% of full load.

The lower waterwall region of a boiler, where the main devolatilization and combustion takes place is a difficult region to make tests. The combustion conditions fluctuate rapidly leading to a heterogeneous distribution of flue gases and particles landing on the furnace walls. Additionally, the operating conditions are not constant with time leading to a variation in bed and flue gas temperature in the furnace over the measurement period [Stålenheim and Henderson , VRD MEMO U13-03}.

Table 1 – Measurements at Idbäcken plant – the gas compositions as measured in the boiler together with near the wall temperature (in red) (From VRD MEMO U13-03)

Pos	Distance from wall	FTIR										Sick	
		CO	NO	SO2	NH3	HCl	HF	CH4	NOx	H2O	CO2	O2	Temp
	(m)	(ppm)	(ppm)	(ppm)	(ppm)	(ppm)	(ppm)	(ppm)	(ppm)	(%)	(%)	(% tg)	(°C)
A	0,1	17436	50	24	277	7,9	0,8	931	51	18	3	0,7	**873**
	0,8	18760	10	15	207	9,0	0,7	876	11	17	3	1,1	**1089**
B-C	0,1	19035	88	76	438	0,1	1,2	2497	85	26	5	0,6	**701**
	0,8	19179	88	67	408	3,7	1,1	2544	86	24	5	0,2	**968**

Very low O_2 levels were detected, sometimes below 0.5%, (Table 1). The fluctuation over time was also large (VRD MEMO U13-03). The fluctuation was greatest at the back wall (position A) and least on the right wall (side wall - position B-C). The temperatures were lower close to the wall than 1 m into the furnace. The CO levels were high. Cl, Pb and Zn were found in the deposits. The levels varied considerably and in a seemingly random manner.

The chlorine content varied between 2 and 14 wt % , zinc 5-15 wt%, lead up to 6.8 wt%, potassium 2-9 wt% , sodium up to 6.6 wt% and sulphur 4-11 wt%. There was no correlation between Cl content, measuring position (back wall or side wall), substrate temperature or alloy, but a high S content correlated with a low Cl content [VRD MEMO U13-03].

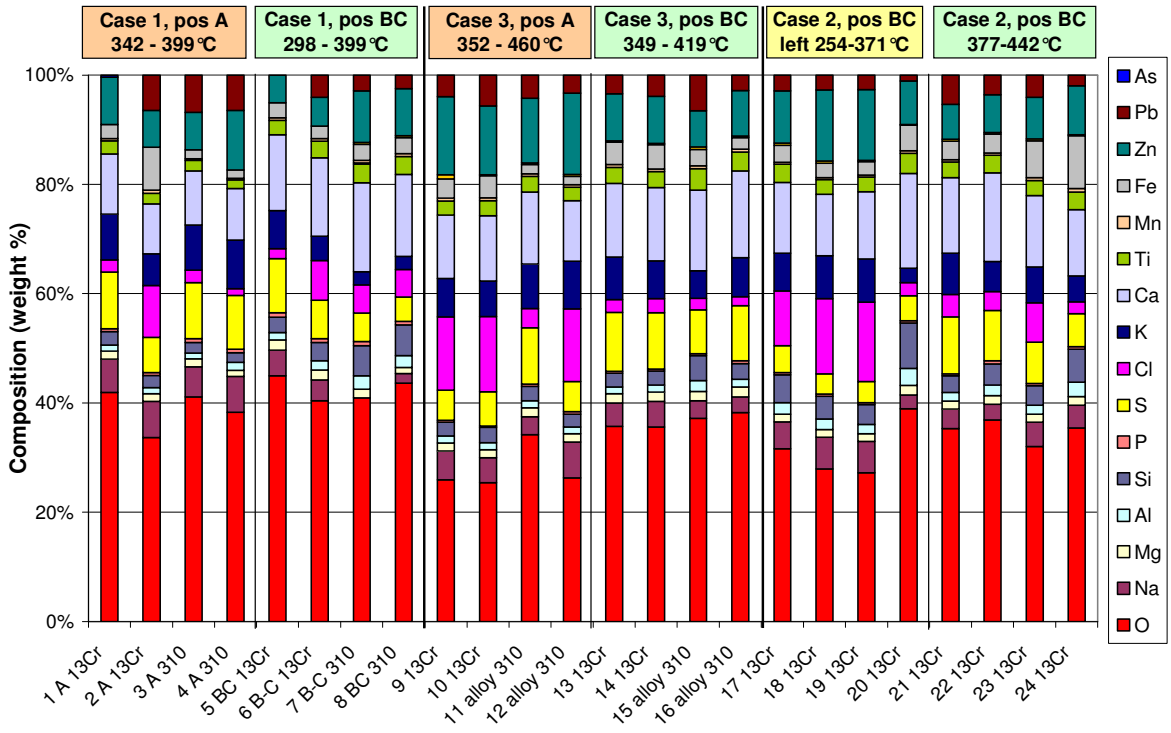

Figure 15 – Idbäcken deposits – composition of the deposits collected on probes at the different position on the wall, the temperature at the collection point is given as well (from VRD U13-03)

The deposits were collected from probes inserted in the water walls where the conditions lambda below 1 prevails. The composition of the deposits is given in the Figure 15. The gas temperature range near the collection point was between 800-1000°C (Table 1) but the temperature at the collection spot was in the range of approx. 350 – 450°C (Figure 15). One can observe from the figure 15 that Zn and Pb are a substantial part of the deposits taking into account their low content in the fuel itself.

Deposits were collected from the actual walls during the summer shut down in 2011 and the results published [Alipour, VGB PowerTech,, 2012]. Zn and Pb were found in most of the deposits and crystals of $ZnCl_2$ were observed. Areas of pure lead or Pb-Cl-O and Pb-K-S-O mixtures were also observed. (Oxidation of these mixtures might have occurred after the deposits were removed from the boiler).

Only the Idbäcken system will be considered here for comparing the collected deposits with the equilibrium calculations. The main Zn and Pb based components to be present in the system for lambda 0.8 and the temperature range between 800-1000°C are listed in the Table 2 together with their melting and evaporation temperatures:

Table 2 – The main equilibrium components and their melting/evaporation temperatures.

Compund	Melting	Evaporation
	°C	°C
Zn(g)	**419**	**907**
ZnCl2(g)	**290**	**732**
Pb(g)	**327**	**1749**
PbS(g)	**1114**	**1280**
PbCl2(g)	**501**	**952**

5 DISCUSSION

5.1 Zinc and Lead – the source of Zn and Pb in fuels

Zinc

Galvanizing is one of the largest industrial applications of Zn. Galvanized fastening systems are considered as a potential source of heavy metals, particularly of Zn. Another common source of Zn in waste fractions is brass (Cu-Zn alloy) as well as other alloys. Tinted glassware, apart from Si and Cu, also contains Zn. Zn is also used in plastics as an acid scavenger and filler in the form of ZnO. In recovered waste wood mainly surface treatments, such as white pigment in paints, contribute to an increase in the amounts of Zn. Zn is also a plant nutrient and is naturally present in small amounts in wood. Moreover Pb- and Zn-containing compounds are widely used in PVC as stabilizers [Frandsen et al. 2006].

Lead

Nakamura et al. [1996] found that up to 90% of the Pb in waste originates from batteries, glassware and electric appliances and light bulbs etc. If the highly contaminating items (batteries, glass, light bulbs) are excluded from waste the main sources of Pb are most likely to be plastics, textiles, rubber and leather, present as lead oxide (white pigment) and lead stearate [Nakamura et al. 1996]. Also, as mentioned already above, Pb is a common metal stabiliser used in PVC. In RWW, Pb typically originates from different surface treatments such as siccatives (additives which promote drying) and colouring pigments.

5.2 Chemical equilibrium modeling, input data and databases

Chemical equilibrium analysis is a useful tool in the study of a variety of processes, and it has been widely used to evaluate many environmental, geochemical, and technical processes. Moreover, equilibrium studies have proven valuable in verifying and understanding the chemistry of heavy metals in combustion systems.

Equilibrium predictions are highly sensitive to the input data. All relevant species of the system must be taken into account, and the numerical values of the constants must be correct and consistent. If some important species are omitted from the calculations or the data is not correct, the results can be very misleading. In practice, investigators often attribute the discrepancies between the experimental data and the results of calculations to the absence of chemical equilibrium in the system or to incorrect parameters in the model used, while the actual reason may be errors in the thermodynamic data. Even in cases where equilibrium is not actually reached, equilibrium analysis might still be the best approximation possible since kinetic data are not always available for the chemical systems that occur in combustion systems [Talonen, 2008].

There appear to be significant differences in the thermodynamic values of compounds in different databases. Figure 16 shows all the gaseous molybdenum compounds that are formed under oxidizing conditions according to the HSC and FACT databases. It can be clearly seen that there are far more gaseous compounds formed according to HSC than according to FACT. While most of the compounds are also present in the FACT database, their thermodynamic values are so different that they do not become stable.

a)

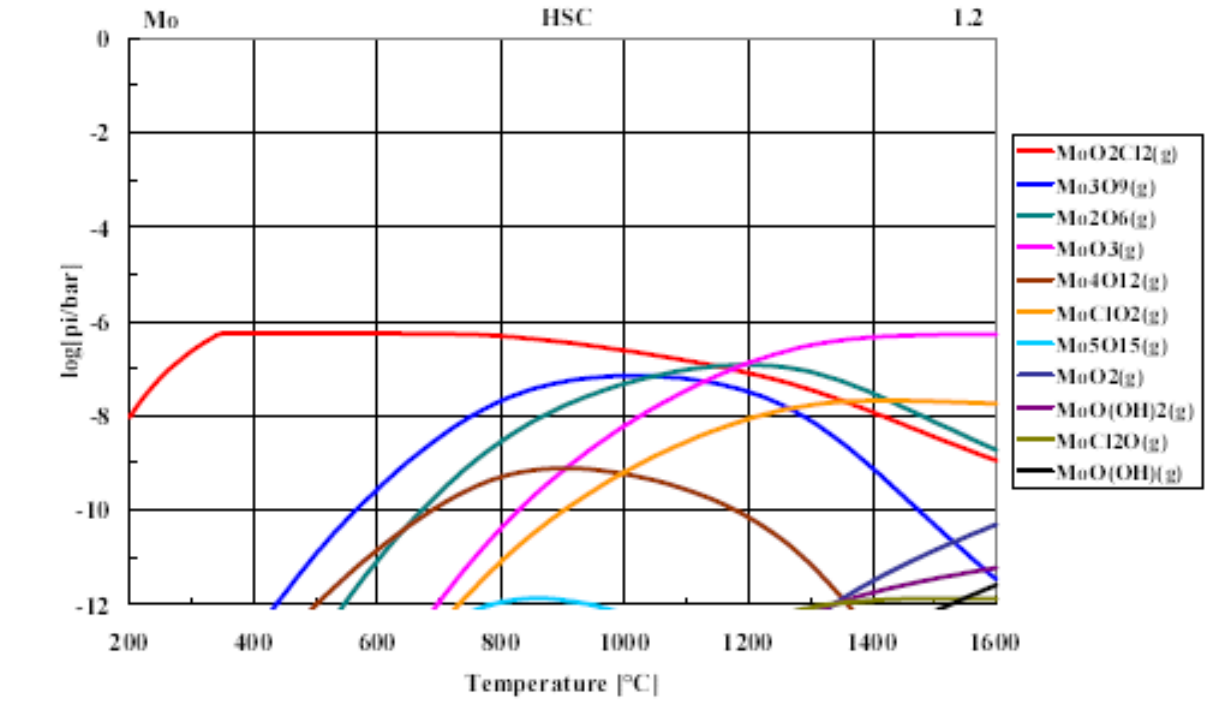

b)

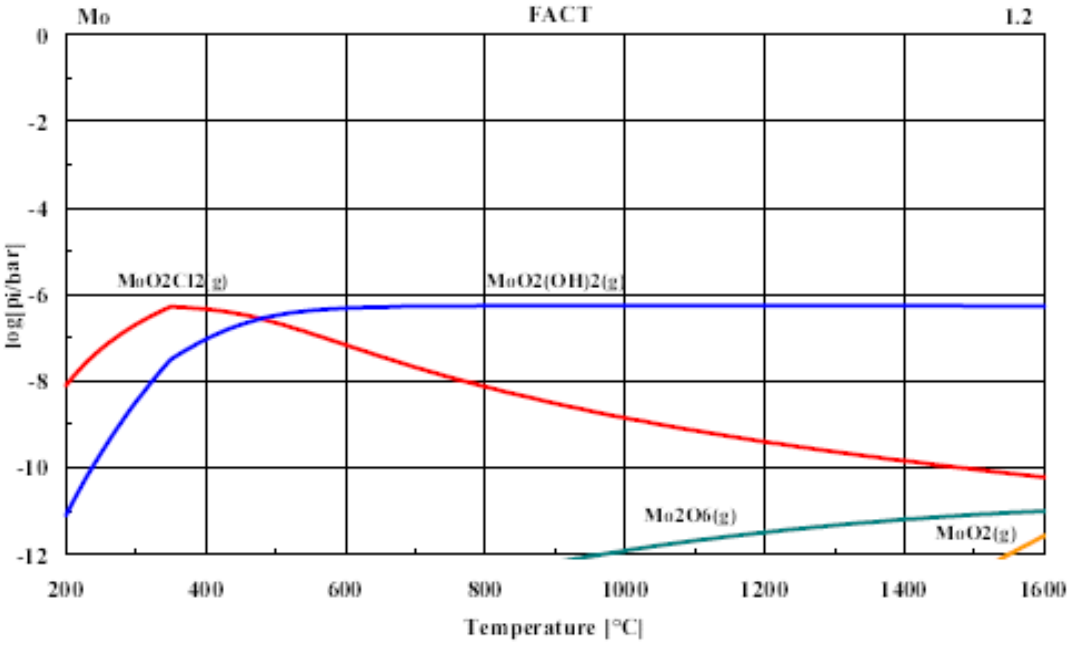

Figure 16 – Comparison between HSC and FactSage and their ability to predict the equilibrium for Mn compounds. The Figure illustrates the possible significant differences between the results

5.3 HSC results and the Idbäcken deposit data – discussion

Only the Idbäcken based system (Idbäcken Fuel) will be considered here for comparing the collected deposits with the equilibrium calculations. The experimental findings (deposits collected) do not exist for the other conditions. The deposits were collected from water walls where the conditions lambda below 1 prevails. The temperature range was between 800-1000°C. One can observe from the Figure 17 that between 10-20% weight compounds of the deposits were Zn and Pb based compounds. It means that although Zn and Pb are not the biggest part of the fuel/ash composition they are present in deposits in substantial mounts. Also a lot of chlorine is present in the deposits. This is also shown from the HSC calculations for the gas temperatures of 800-1000°C

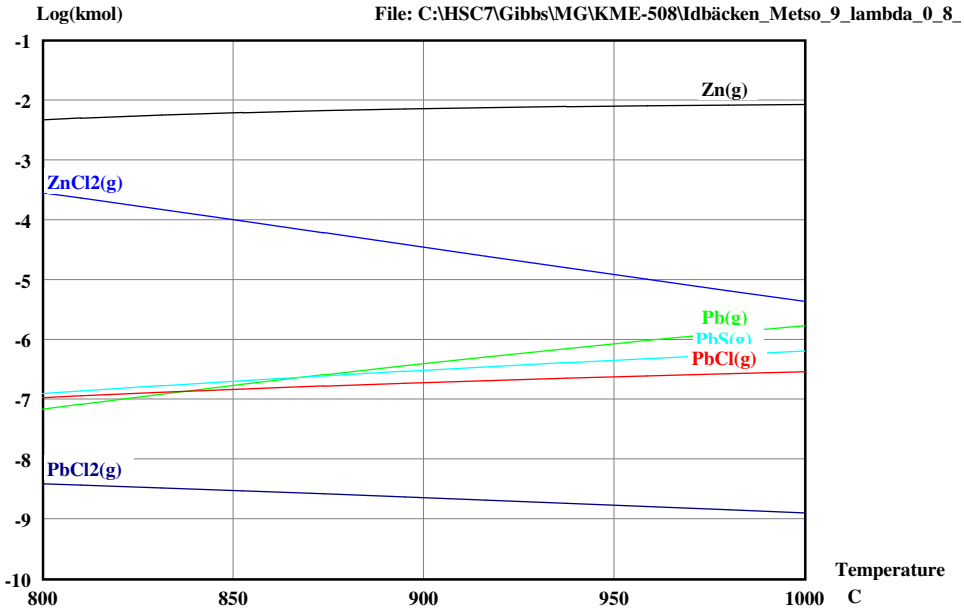

Figure 17 – Repeated - The HSC equilibrium system for Zn + Pb compounds at lambda 0.8 conditions and the temperature range 800-1000°C for Idbäcken fuel

Looking at the equilibrium calculations the main Zn and Pb components present in the calculated equilibrium system for lambda 0.8 and the temperature range between 800-1000°C were:

Table 2 – Repeated - The main equilibrium components and their melting/evaporation temperatures.

Compound	Melting	Evaporation
	°C	°C
Zn(g)	419	907
ZnCl2(g)	290	732
Pb(g)	327	1749
PbS(g)	1114	1280
PbCl2(g)	501	952

Table 2 lists also the melting and evaporation temperatures. The surface temperature at the spots were the deposits were collected was approx. 400°C. This means that the Zn and Pb compounds present in

the gaseous form in contact with the boiler walls could condense. From the list of the compounds it can be seen that only PbS will not be present in the system due its high melting/evaporating temperatures. The system conditions make it possible for all the others to be present at least in the liquid form. The most probable would be formation of Zn and Pb chlorides in the gaseous form and then subsequent condensation of these compounds on the boiler walls. For ZnCl2 it would be present on the boiler walls in a liquid form which can accelerate the corrosion phenomena on the boiler walls even more.

In this sense the chemical equilibrium software can be helpful to predict the gas composition and the deposit formation propensity. In the real system the Zn and Pb will compete with K and Na and form potassium and sodium chlorides and sulfides as well. Already at the boiler wall temperatures (Figure 18) one can observe that $ZnCl_2$ and PbS are the dominant compounds. This near-wall condensation phenomena and subsequent deposition of Zn and Pb compounds in the form of chlorides and sulfides is responsible for the corrosion. In order to have the complete picture of the situation one should simulate the system at the gas temperature to learn the components present in the gas form and also simulate the system at the sampling position temperature (Figure 18) to learn the chemical equilibrium at the point of interest. For the temperature range between 300-500°C condensed Zn chlorides are dominant.

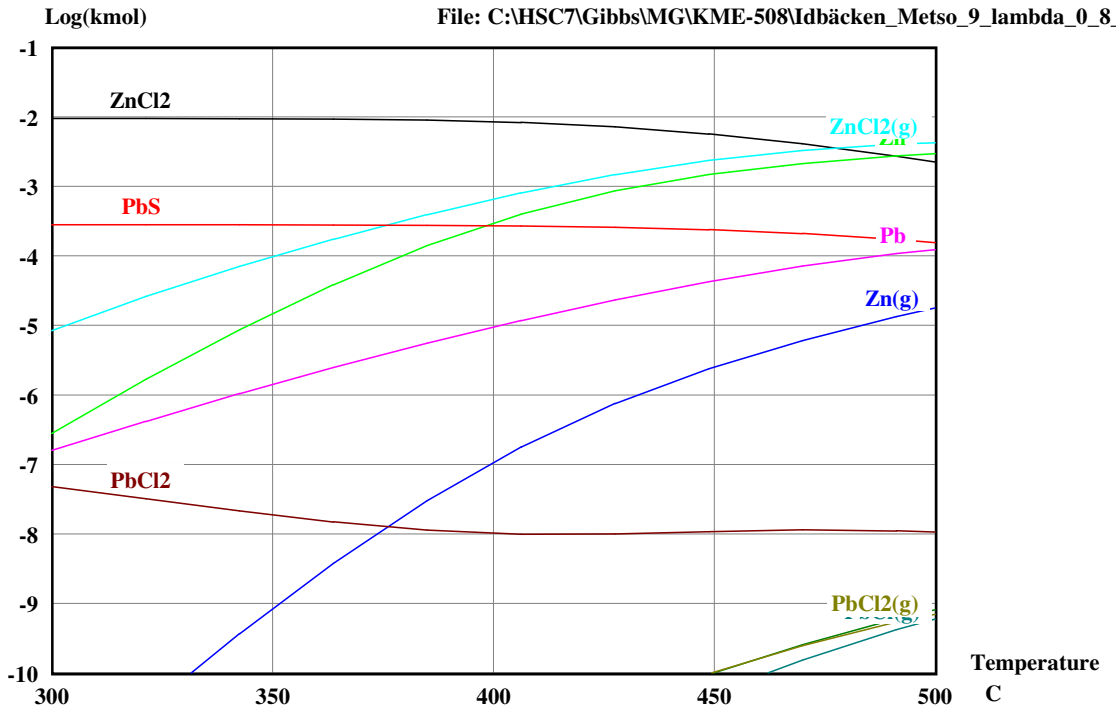

Figure 18 - The HSC equilibrium system for Zn and Pb compounds at lambda 0.8 conditions and the temperature range 300- 500 °C for Idbäcken fuel. The equilibrium composition at the deposition temperatures is shown.

5.4 Chemical equilibrium calculations – applicability and limitations

The chemical equilibrium calculations can be a useful tool for the R&D and operational engineers when dealing with new (biomass) fuel types and mixtures and helping with the operational issues like corrosion or deposit formation. Of course the method will not provide all answers but may indicate problem areas. The equilibrium calculation itself takes into account only the chemistry of the system and

based on the mathematical calculations tries to minimize the Gibbs free energy of the system to check at which composition the system is at equilibrium. The equilibrium calculation process assumes the infinite amount of time available for the chemical formation reactions to happen which is in contrary to the situation in real boilers. In reality some reactions will happen faster and some slower, all of them controlled by kinetics. One has to be careful analysing the results. The classical example is the sulfation reaction of metal chlorides which happens in two steps and one step is kinetically slow. That's the reason also the sulfation of deposits takes place when there is enough time available [Aho et. al 2010, Ferrer 2005]. Another limitation of the chemical equilibrium method is that it does not take into account anything related to the flow conditions in the boiler and boiler geometry which may influence the deposits formation and composition. Summarizing HSC software is a great tool for some initial analysis of any new fuel and its influence on the boiler. It can be also use to help analyze the operational problems experienced at the site. Process optimization like optimal fuel mix for a certain specific type of boiler is also possible application. Nevertheless one has to be careful and always an expert knowledge needs to be applied when analyzing the results. The results need to be supported by experimental findings when needed.

6 CONCLUSIONS

The equilibrium modeling using the HSC Chemistry software has been successfully performed. The results were compared and analyzed with the results of the other project partner Metso. Similarities for the reducing conditions were substantial, the oxidizing conditions showed some differences. For KME 508 and the investigation of the boiler wall corrosion the reducing conditions are of the most importance. The discussion on the differences between the HSC and Factsage databases based on the work of Talonen was performed in order to obtain some critical look at the software features.

The HSC data reveal that for the temperature range 800 – 1000°C Zn(g) and Pb(g) are dominant while for the wall temperatures (350°C – 450°C) chlorine based and sulfur based compounds were present at the highest concentration. Comparing the results with the deposits one could speculate that the Zn, Pb based compounds condense at the walls in the form of chlorides and sulfides creating high risk of corrosion. In the deposits collected from the boiler walls substantial levels of chlorine were measured.

7 REFERENCES:

Tarja Talonen, Chemical Equilibria of Heavy Metals in Waste Incineration: Comparison of Thermodynamic Databases, Abo Akademi, report 08-02, 2008

Frandsen F., Pedersen A.-J., Hansen J., Madsen O.-H., Lundtorp K., Mortensen L. Deposit formation in the FASAN WtE boiler as a function of feedstock composition and boiler operation. Energy Fuels 23 (2009) 3490–3496.

Nakamura K., Kinoshita S., Takatsuki H. The origin and behavior of lead. Cadmium andantimony in MSW incinerator. Waste Manage 16 (1996) 509–517.

Alipour Y., Viklund P., Henderson P., The analysis of the furnace wall deposits in a low NOx waste-wood fired bubbling fluidized bed boiler. VGB PowerTech 2012

M. Aho, “Reduction of superheater corrosion by co-firing risky biomass with sewage sludge” Fuel 89 (2010)

Project meeting - knowledge exchange Abo Akademi Vattenfall – April 2013

X. Wei “Behaviour of gaseous chlorine and alkali metals during biomass thermal utilization, Fuel 84 (2005) 841–848

E. Ferrer, “Fluidized bed combustion of refuse-derived fuel in presence of protective coal ash”, Fuel Processing Technology, Volume 87, Issue 1, December 2005, Pages 33-44

.Jensen, P., Frandsen, F., Dam-Johansen, K., and Sander, B. (2000b). Experimental investigation of the transformation and release to gas phase of potassium and chlorine during straw pyrolysis. Energy & Fuels, 14:1280–1285.

Stålenheim A and Henderson P. VRD Internal MEMO U13-03 “Measurement campaign November 2011, within KME 508. “

Memo KME508

GD-OES analysis of deposit probes

Investigator:	Annika Talus
Department:	Corrosion in aggressive environment
Phone:	084404838
E-mail:	annika.talus@swerea.se
Date:	2014-01-15

Swerea KIMABs Ref No: 702006

Approved by:

Rikard Norling

swerea | KIMAB

Swerea KIMAB
P O Box 7047
SE-164 07 Kista, Sweden

Isafjordsgatan 28A
SE-164 40 Kista, Sweden

Phone +46 (0)8-440 48 00
Telefax +46 (0)8-440 45 35

2012-03-27/bb
kimab@swerea.se
www.swereakimab.se

1. Background

A measuring campaign with waste wood was performed in boiler P3 at Idbäcken in November 2011. The materials exposed were 16Mo3 and 310S, for chemical composition of the exposed alloys see Table 1. Totally 24 deposit probe samples was exposed in the campaign, see Table 2. The exposure time for the campaign was 12-14 hours and the metal temperatures were between 250 and 460°C. For further details regarding the exposures see the memo written by A. Stålenheim and P. Henderson [1].

Table 1. Chemical composition of alloys used for deposit probe samples in the waste wood campaign November 2011.

Alloy	Fe	Cr	Ni	Mn	Mo	Si	C
13CrMo4-5	Bal.	0.7-1.15	<0.3	0.4-1.0	0.4-0.6	≤0.35	0.08-0.18
310S	Bal.	25	20	1.5	<0.5	<0.5	<0.08

Four of the expose deposit probes were selected to be analysed with Glow Discharge Optical Emission Spectroscopy (GD-OES) in order to study the oxide thickness and element distribution in the deposit. The selected samples are marked with grey in Table 2.

Table 2. Details for exposed deposit probes. Marked samples were selected for GD-OES anlaysis.

Exposure	Position	Sample #	Material	Average temp [°C]	Temp std dev [°C]	Weight gain [mg/mm^2/h]
1	A	1	13CrMo4-5	399	2	0.0116
1	A	2	13CrMo4-5	342	17	0.0108
1	A	3	310S	344	35	0.0071
1	A	4	310S	398	25	0.0077
1	B-C	5	13CrMo4-5	399	6	0.0075
1	B-C	6	13CrMo4-5	298	22	0.0118
1	B-C	7	310S	317	25	0.0169
1	B-C	8	310S	375	15	0.0110
3	A	9	13CrMo4-5	420	1	0.0104
3	A	10	13CrMo4-5	352	28	0.0172
3	A	11	310S	405	27	0.0093
3	A	12	310S	460	24	0.0085
3	B-C	13	13CrMo4-5	419	2	0.0074
3	B-C	14	13CrMo4-5	395	10	0.0120
3	B-C	15	310S	349	30	0.0135
3	B-C	16	310S	418	9	0.0155
2	B-C left	17	13CrMo4-5	254	16	0.0263
2	B-C left	18	13CrMo4-5	334	21	0.0242
2	B-C left	19	13CrMo4-5	371	14	0.0443
2	B-C left	20	13CrMo4-5	370	5	0.0544
2	B-C	21	13CrMo4-5	377	13	0.0112
2	B-C	22	13CrMo4-5	412	10	0.0106
2	B-C	23	13CrMo4-5	425	9	0.0112
2	B-C	24	13CrMo4-5	442	15	0.0140

Before GD-OES analysis the sample surfaces had been analysed with SEM/EDS in order to study the deposit composition at the surface. An illustration of how the deposit probes were mounted and exposed in the furnace is shown for some chosen samples in Figure 1 such as the areas of SEM-analysis. In Table 3 the results from SEM/EDS for the specific GD-OES samples are shown.

Exposed deposit probes

(a)

Areas of analysis in SEM/EDS

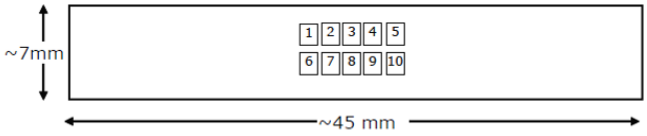

Area: 2*2,5mm
Magnification: 50X
Accelerating Voltage: 20kV

(b)

Figure 1. Illustration of exposed deposit probes (a) and areas for the SEM-analysis (b).

Table 3. Results from surface analysis for the samples in SEM/EDS, weight%.

	O	Na	Mg	Al	Si	P	S	Cl	K	Ca	Ti	Mn	Fe	Zn	Pb	Total
11(2012)	38.21	4.96	1.50	1.16	2.28	0.55	9.23	3.42	6.87	11.34	2.53	0.29	1.62	9.97	5.96	100
12(2012)	32.06	5.35	1.60	1.30	2.39	0.58	5.48	12.42	6.56	10.55	2.29	0.72	4.05	12.60	1.42	100
15(2012)	41.84	3.23	1.58	1.71	3.84	0.51	6.94	4.38	4.13	12.68	3.21	0.50	3.93	5.33	5.71	100
16 (2012	43.18	2.03	0.90	1.64	4.54	1.12	6.30	1.95	5.67	11.63	3.28	0.38	2.71	5.17	9.42	100

2. Aim

The main aim with the investigation was to study the possibilities of using GD-OES as analysis method for samples exposed in short term tests where thin oxides is expected. Another scope was to study the distribution of elements in the deposit and if possible draw some conclusions regarding the initial corrosion. As a complement and for further development for studying the oxide thickness also minor analysis with FIB (Focused Ion Beam) was aimed to be performed.

3. Method

The GD-OES technique is based on the principle that optical emission is achieved when sputtering a sample surface with ions and atoms formed due to glow discharges in a low pressure Argon-plasma. By performing spectral analysis of the optical emission achieved when sputtering a sample the composition of the sample can be determined. Most GD-OES instrument is equipment with up to 60 individual photomultiplier detectors which record a specific wave length representing a specific material, see Figure 2a. All elements have a certain wave length that describes it and by evaluating the light spectra given from the GD-OES the distribution of different elements in the sputtered area can be achieved.

The technique can be used to study bulk or depth profiles (intensity of emission versus sputtering time) of both conducting and non-conducting materials, see example in Figure 2b.

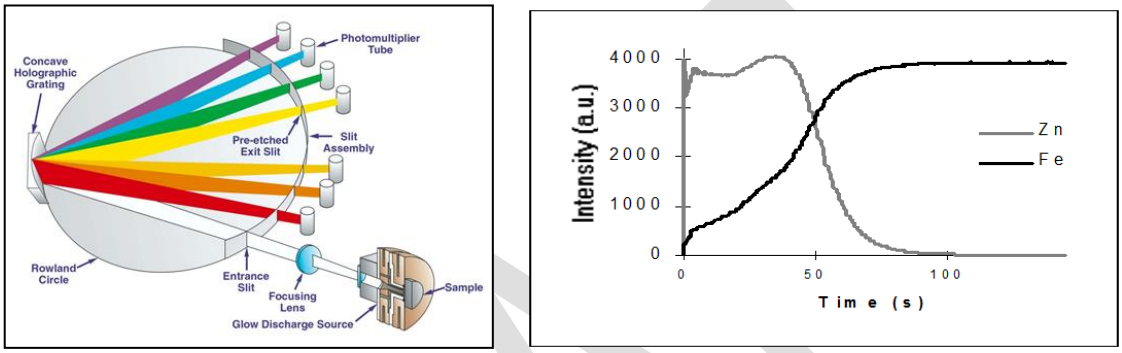

(a) (b)

Figure 2. Illustration of the principal of the GD-OES-technique (a) and an example of a depth profile achieved (b).

Quantifications can be made based on the amount of emitted light at the certain wave length for each element. In the Leco GDS 850A equipment used in this case, one detector for each element is installed to only register the wave length of a certain element. To be able to quantify the different elements a calibration of the instrument is performed before the analysis. However, one problem with this particular equipment is that no detector for the wave lengths of potassium are installed which means that no information regarding potassium can be achieved. Since potassium is an important and central element, another technique was used to also get data of how potassium was distributed in the deposit. To also get information of the potassium distribution in the deposit a complementary CCD (charged coupled device)-detector was used which collected the whole light spectra. The light spectra was manually recorded every 15s and when the analysis was ended the specific wave lengths for potassium was manually evaluated and plotted in excel next to the GD-OES spectra achieved. To confirm that this complementary technique gave comparable results two extra elements was plotted and compared with the data achieved from the GD-OES spectrum.

4. Experimental

4.1 Sample preparation

The samples were cut to a dimension of 7*7mm without any lubricant in order to preserve the elements in the deposit. To achieve maximum hit area in the GD-OES the samples were also ground at the edges to an octagon shape, see Figure 3a. After cutting, the samples were mould in a 50/50 Sn/Bi-metal mixture to be able to fit the sample in the GD-OES-equipment, see Figure 3b. In Figure 3c one sample after GD-OES-analysis is shown.

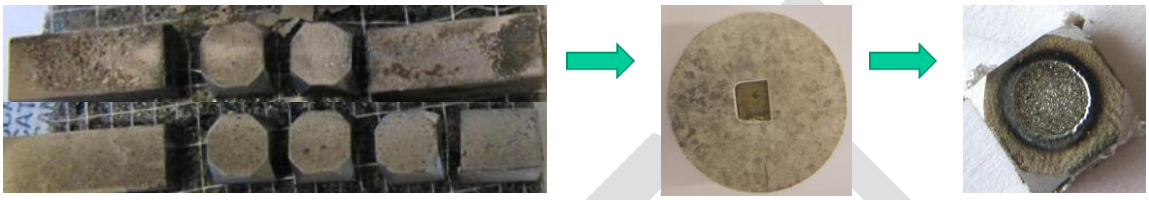

(a) (b) (c)

Figure 3. Sample preparation prior to GD-OES analysis (a, b) and sample after GD-OES analysis (c).

4.2 GD-OES analysis

The samples were mounted in the GD-OES equipment and since the deposit was non-conductive a radio frequency lamp was used for the analysis. The analysis was performed until the live signal showed that the bulk metal was reached. When the analysis was started the operator also started to collect the CCD-spectra as fast as practically possible aiming on every 15s.

Since these kinds of deposits are very complex and the GD-OES technique has not been used for these kinds of deposits before a lot of effort was put in to the analysis of the results. The most important issue in these first trials was to study the relative distribution of the element in the deposit and where they were located. To get a relation to quantitative data the first sputtered outer layers were correlated to the performed surface analysis in SEM.

However, it needs to be kept in mind that some of these elements do not have good quantitative reference samples for calibration and due to that the data has to be considered as semi quantitative.

Another thing that can be added to the complexity of the samples is the porous structure of the deposit. The porosity of the deposit most probably results in that the depth profile cannot be totally reliable.

4.3 FIB analysis

Analysis with FIB was performed for some of the samples mainly to verify the oxide thickness. In addition also the thickness of the deposit was evaluated and could be used as a complement to the GD-OES measurements. Same sample that had been exposed in the GD-OES measurement was analysed but an area outside of the sputtering spot was used.

5. Results

5.1 Correlation between CCD-detector and GD-OES spectra

When comparing the results from the GD-OES spectra with the spectra given using the CCD detector for the selected elements Cl and Na, a very good correlation between the used techniques is shown, see Figure 4. This result implies that the potassium spectra from the CCD-detector can be used in addition with the GD-OES spectra in order to study the element in the deposit. However, there is a difference in intensity between the GD-OES spectra and the CCD-detector so the results should mainly be used to study the distribution of potassium in the deposit.

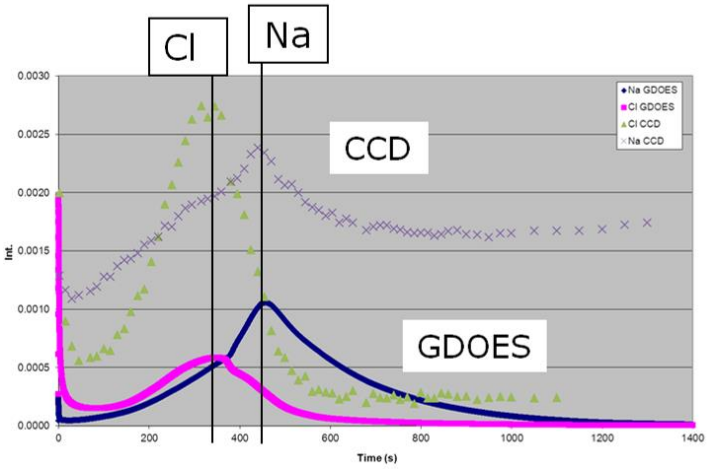

Figure 4. Comparison of Cl and Na spectrum from GD-OES and CCD-detector.

By comparing the signal of Na, K and Cl it was also shown that the potassium signal for this sample is following the signal of sodium and reaches its max at the same place. This result showed that the location of the potassium maximum could be read also from the GD-OES-spectra if combined with the CCD-detector results. No quantitative data was achieved but the distribution of potassium in the deposit could from this be evaluated, see Figure 5. This was performed for each sample in order to verify the location of the potassium.

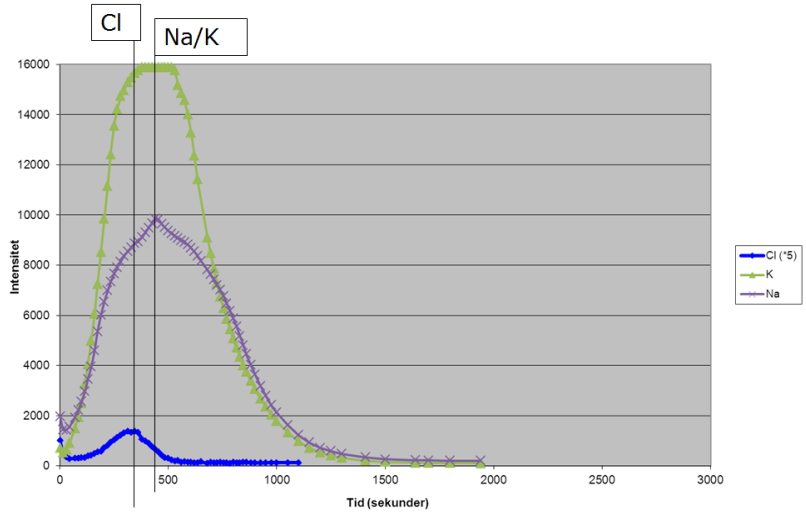

Figure 5. Comparison of location of the potassium peak compared to Na and Cl.

5.2 Waste wood campaign 2011

5.2.1 GD-OES

Commonly the interface between metal and oxide is generally referred to the place where Fe and O have its intersection, see mark with black line in Figure 6. However, it cannot be concluded that this is the interface in this case since there is an uncertainty due to several factors such as for example porosity and uneven surfaces but to simplify this is assumed also in this case.

The GD-OES results from position A, showed increased levels of Na close to the interface. Also Zn showed somewhat high levels but slightly further out in the deposit compared to Na. It was not possible to draw any conclusions about oxide thickness from these results but a slight tendency for oxide is seen for sample 11, (see mark in the figure) since a plateau of Fe is seen. Regarding Cl It can be seen that the highest values can be seen quite far out in the deposit. Most other elements are also highest further out in the deposit and decreasing when approaching the metal surface. No clear trend could be seen regarding temperature dependence.

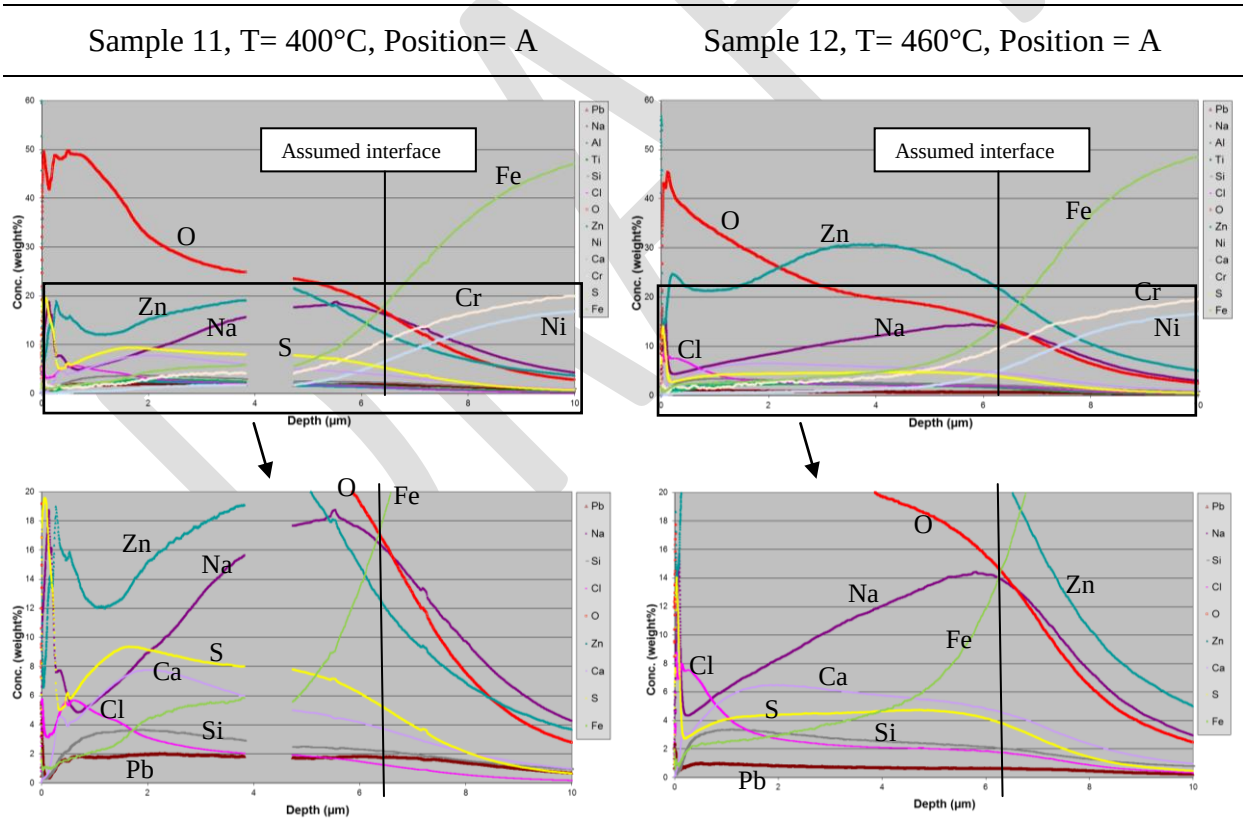

Figure 6. GD-OES results from position A, weight%. For sample 11, some data points are deleted from the spectra since some errors occurred in the measurement at this position.

The GD-OES results from position B-C also showed increased levels of Na close to the interface. For this position not as high levels of Zn was seen compared to position A but still the Zn was enriched relatively close to the metal surface. For this position also increase levels of Pb and Cl was noticed (at least for sample 15). It was not possible to draw any conclusions about oxide thickness from these runs. Opposite from position A, a lot of element is increasing when approaching further in in the deposit and then decreases closer to the metal surface again. No clear trend could be seen regarding temperature dependence.

Sample 15, T= 350°C, Position= B-C	Sample 16, T= 420°C, Position = B-C

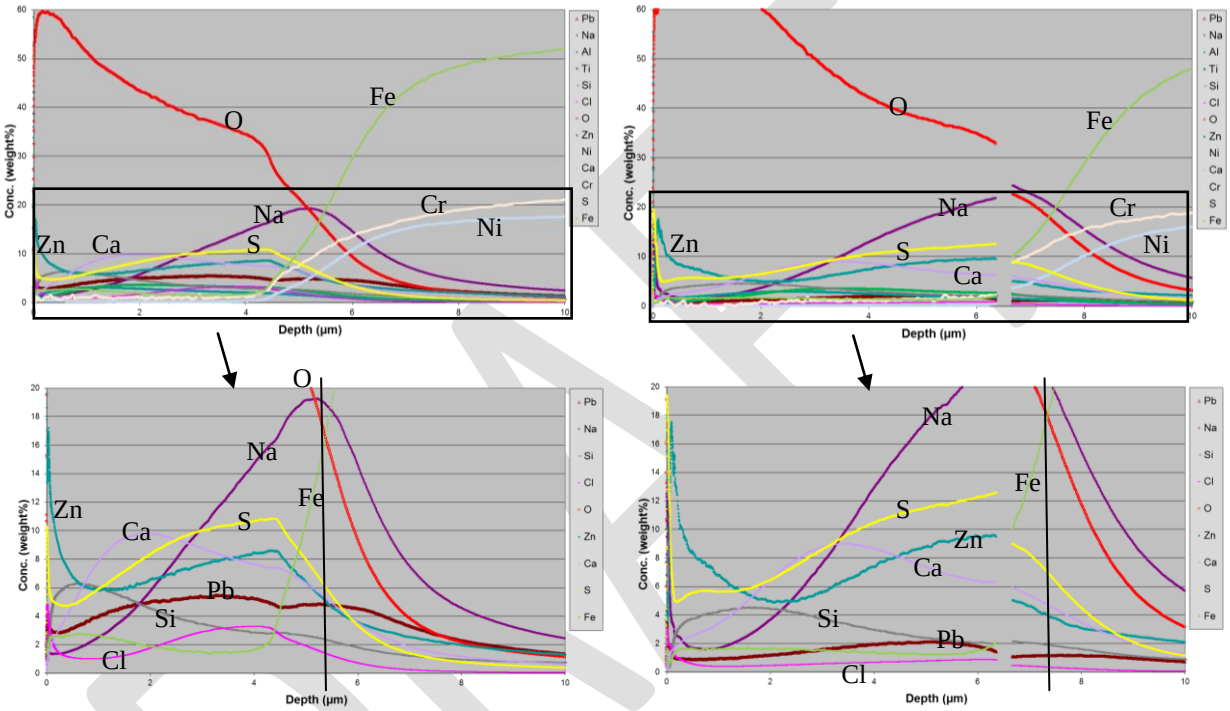

Figure 7. GD-OES results from position B-C, weight%. For sample 16, some data points are deleted from the spectra since some errors occurred in the measurement at this position.

5.2.2 FIB

Some additional FIB-analysis was performed and showed very thin oxides for all samples, see example for sample 15 in Figure 8. It could be seen that there was a difference in deposit thickness and porosity for the two positions which could possibly be connected also to the differences seen with GD-OES.

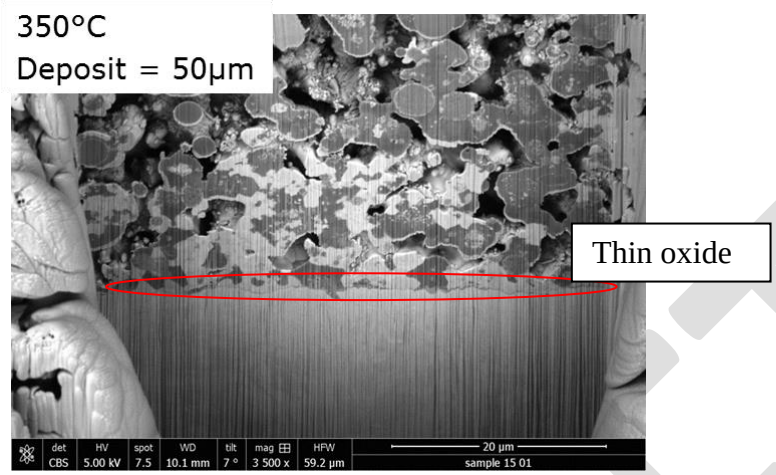

Figure 8. Oxide thickness evaluation using FIB.

5.3 Sludge campaign

Some GD-OES analysis was also performed for samples where sludge had been used together with waste wood. One of the samples showed very nice correlations between the element mapping from SEM and GD-OES regarding chloride distribution, see

Figure 9. In SEM it was clearly seen that chlorides was enriched at the metal surface. In the GD-OES spectra chlorine showed a clear peak at the interface which is in very good correlation to what was seen in the SEM.

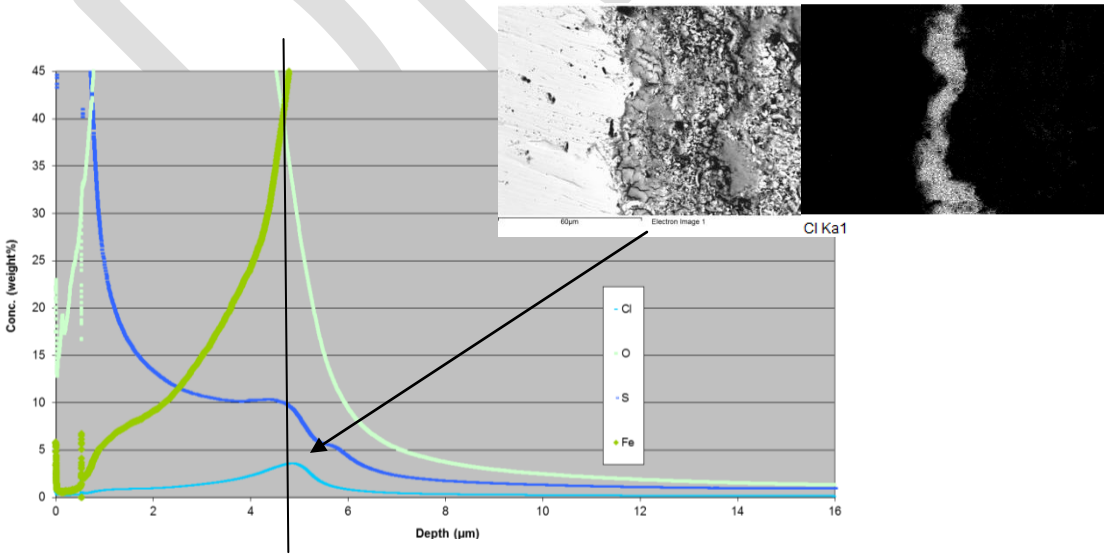

Figure 9. Correlation between GD-OES and SEM-mapping of chlorine distribution.

6. Discussion and conclusions

No clear conclusions could be made regarding the oxide thickness of the samples exposed in the campaigns. Due to the complex and porous structure of the deposits it is rather difficult to get the depth information and sensitivity from only the GD-OES-analysis. One problem with these kinds of samples is that there is no element that only appears in the oxide. If there would have been one element only appearing in the oxide it would have been easier to tell the thickness of the oxide. However, by combining the analysis with some FIB-analysis it was possible to tell that the oxide thickness was very thin. It could also be seen that the deposits were porous and showed differences depending on position. However, this was not further investigated but would be of great interest to work further with in upcoming project.

The results in the study show that GD-OES is an analysis method that can be used in order to study the element distribution in deposit and oxide of a sample. However, due to the complexity of these kinds of samples it is not used for quantitative analysis today. The analysis could though be useful when studying for example corrosion mechanisms since the distribution of elements close to the metal surface can be detected. By developing the method further this technique could be a very useful tool. Since the analysis with this equipment is rather fast and give good information of the deposit composition it is a tool that preferably could be used in the future when it comes to these kinds of samples.

7. References

[1] Memo U13-03, A. Stålenheim & P. Henderson, Vattenfall AB

KME508, Chemical equilibrium calculation

Table of Contents

1 The overall goal of the KME 508 project

The goal is to give recommendations about how to avoid water wall corrosion at increased boiler electrical efficiency/increased steam data when burning biomass and waste wood mixes.
A review of experiences in biomass boilers will be made which includes additives and current measures for reducing wall corrosion – design, operation and materials.
The environment near the furnace wall will be characterised for a variety of fuels and the deposits formed at different wall temperatures will be collected by using wall probes. The chemical composition of deposits, compounds present and initial corrosion will be analysed. Thermodynamic equilibrium calculations using chemical composition of fuel to evaluate the condensation behaviour of Cl, Na, K, S, Zn and Pb compounds at different temperatures will be performed and the theoretical results compared to the experimental ones from deposit analyses. Tests of water wall corrosion with different fuel mixes and different materials/coatings will be performed with probes to evaluate at which temperatures there is increased risk for corrosion and for which material and fuel.
The mechanism of waterwall corrosion will be studied by analysis of deposits, corrosion probes and tubes from different boilers.
Modified FeCrAl alloys will be evaluated with respect to corrosion resistance and mechanical properties

1.1 Metso's contribution to the project

Metso's main task in this project was to perform a evaluation of the chemical environment in the furnace, based on chemical equilibrium analysis. The analysis method uses the chemical composition of the fuel as input and estimates the equilibrium composition of the ash forming matter in the fuel as a function of temperature at a given air to fuel ratio. The method also includes an estimation of condensation of ash forming matter relevant for corrosion, that is, alkali chlorides and sulphates as well as lead and zinc salts.

2 Thermodynamic equilibrium calculation

In this work, global multi-phase, multi-component equilibrium calculations were used to study the chemistry of zinc and lead in BFB combustion of Recovered Waste Wood (RWW). Special emphasis was put on the formation of gaseous zinc and lead species and their condensation behavior in different parts of the boiler. Different locations in the boiler are described by the temperature profile (800 – 1000 °C) and by dividing the boiler into a reducing part (λ=0,8) and an oxidizing part (λ=1,2). The calculation method and procedure is described in detail in Enestam et al.

2.1 Calculation procedure

The software used (SteaMax) is a tailor-made calculation routine based on the thermodynamic equilibrium program ChemSheet (Koukkari, Penttilä, Hack and Petersen 2000). The thermodynamic data base used is based on data from Fact (Bale, Bélisle, Chartrand, Decterov, Eriksson, Hack, Jung, Kang, Melançon, Pelton, Robelin and Petersen 2009) with additions from backman (Backman 2005). The database includes 16 elements (C, H, N, O, S, Cl, Ca, Mg, Na, K, Al, Si, Fe, P, Pb, and Zn), 1 gas phase, 1 liquid solution, 2 solid solutions ((Na, K)(Cl) and (Na, K)(SO_4,CO_3)), 18 pure liquid compounds, and 269 pure solid compounds. The liquid solution is a molten salt phase consisting of the system (K, Na, Pb, Zn)(Cl, CO_3, SO_4).
The input to the calculations was the elemental composition of the fuel and the output gave the equilibrium composition of the gas phase and the amount and composition of condensed phases as functions of temperature. Formation of zinc- and lead silicates was inhibited in this work since the heterogeneous reactions involving solid silicate are considered to be significantly slower than the gas phase reactions involving na, K, Zn, Pb, S, Cl and O. Some interaction between zinc and silicon in the bed material or in the fuel ash are however likely to occur in the boiler.
The output of the calculations was the amount of the thermodynamically stable gaseous, solid and liquid compounds in the two calculation zones (λ<1 or λ>1). The condensation temperature for the gaseous lead and zinc compounds was then calculated based on the saturation pressure for each gaseous compound. This approach was chosen in order to describe the fast condensation of gaseous compounds meeting a significantly cooler metal surface. Secondary reactions that might take place on the surface of the tube were not considered.

2.2 Fuel Data

The elemental composition of the fuel used in this work were from Enestam et al. (Reference fuel), Idbäcken (Vattenfall), Stevens Croft (SC Lockerbie, E.ON), and RPP (Reference Power Plant fuel data for KME601 project). The compositions of the fuels are shown in Table 1.

Boiler		Idbäcken	Reference	RPP	EON SC Lockerbie
		Customer analyses, average values	Ref Fuel	RPP Fuel "Wide" Avg (KME601) 2011-02-03	Stevens Craft (Metso)
Proximate analysis					
moisture	wt-%	25,30	17,10	45,00	31
ash (ashing temp 815 °C)	wt-% (d.s.)	3,90	3,10	3,10	5,3
Ultimate analysis (dry solids)					
C	wt-% (d.s.)	49,10	50,00	51,70	47,1
H	wt-% (d.s.)	6,00	5,60	6,25	6
S	wt-% (d.s.)	0,10	0,05	0,05	0,1
O (diff.)	wt-% (d.s.)	39,80	39,40	38,27	38,9
N	wt-% (d.s.)	1,00	1,70	0,60	2,52
Cl	wt-% (d.s.)	0,10	0,17	0,03	0,1
Heating values					
HHV, dry	MJ/kg	19,30		20,50	19
HHV, wet	MJ/kg	14,42		11,28	13,1
LHV, dry	MJ/kg	17,98		19,13	17,7
LHV, wet	MJ/kg	12,81		9,42	11,4
LHV, ash free, dry	MJ/kg	18,71		19,74	18,7
LHV, ash free, wet	MJ/kg	13,20		9,58	11,9
Element concentrations in the dry substance					
Al	g/kg ds.	1,41	1,20	0,80	2,20
Si	g/kg ds.	5,99	6,20	2,00	11,00
Ti	g/kg ds.	1,13		0,10	1,70
Na	g/kg ds.	0,92	0,69	0,30	1,30
Mg	g/kg ds.	0,07	0,58	1,00	0,68
K	g/kg ds.	1,01	0,93	2,00	1,20
Ca	g/kg ds.	3,77	2,90	5,00	8,80
Fe	g/kg ds.	1,08	0,93	0,50	2,60
P	g/kg ds.	0,11	0,08	0,40	0,57
Mn	g/kg ds.	0,11		0,50	0,11
SUM	g/kg ds.	15,59		12,60	30,2
Heavy metals concentrations in the dry substance					
Cadmium Cd	mg/kg	0,60		0,50	0,25
Chromium Cr	mg/kg	48,30		5,00	15,00
Copper Cu	mg/kg	50,90		5,00	24,00
Lead Pb	mg/kg	58,20	17,00	4,00	120,00
Mercury Hg	mg/kg	0,10		0,05	0,06
Nickel Ni	mg/kg	2,60		1,00	8,70
Vanadium V	mg/kg	2,40		1,00	7,70
Zinc Zn	mg/kg	621,90	260,00	100,00	92,00

Table1, The elemental composition of the fuel used in this work were from Enestam et al. (Reference fuel), Idbäcken (Vattenfall), Stevens Croft (SC Lockerbie, E.ON), and RPP (Reference Power Plant fuel data for KME601 project).

3 Results

Thermodynamically stable gaseous lead, zinc, potassium and sodium compounds for the two calculation zones (λ=0,5 or λ=1,2) for the four fuel cases are presented in Figure 1 to 4 as functions of temperature (800 - 1000°C). The condensation temperatures of the gaseous zinc, lead, potassium and sodium compounds were calculated from the saturation curves for each compound, presented in Figure 5. For each compound the maximum concentration within the studied temperature interval was used in order to describe the worst-case scenario. The condensation temperatures of gaseous lead, zinc, potassium and sodium compounds are presented in Table 2.

3.1 Thermodynamically stable gaseous lead, zinc, potassium and sodium compounds

In all cases, KCl (g) and NaCl (g) are the predominating alkali species in the gas phase in both oxidizing and reducing conditions. Lower amounts of K_2SO_4 (g) and Na_2SO_4 (g) are formed under oxidizing conditions.

Zinc is totally vaporized under reducing conditions in the temperature interval. The thermodynamically most stable form of zinc is Zn (g), in all cases. In addition to Zn (g) a small amount of $ZnCl_2$ (g) is formed in all cases.
Under oxidizing conditions, the major portion of the zinc is in the form of solid ZnO in all cases. The only gaseous zinc compound formed is a small amount of $ZnCl_2$ (g) and, at high temperatures, Zn (g).

Under reducing conditions, lead is fully volatized in the investigated temperature range. Minor lead compounds formed in the reducing part of the furnace are PbS (g), PbCl (g) and very low concentrations of $PbCl_2$ (g)
Also under oxidizing conditions, lead is fully volatized in the investigated temperature range. Lead forms PbO(g) at temperatures above approximately 840 °C and $PbCl_2$ (g) below 840 °C except in RPP case the temperature is about 900 °C.

Volatile compounds of lead and zinc can condense on surfaces in the boiler when the surface temperature is below its condensation temperature. Lead- and zinc-containing deposits are known to be potentially low-melting and corrosive. However, both the melting behavior and the corrosivity of the deposits depend on the speciation of lead and zinc and therefore it is of great importance to know, not only at which locations in the boiler lead and zinc will condense, but also as which chemical compounds.

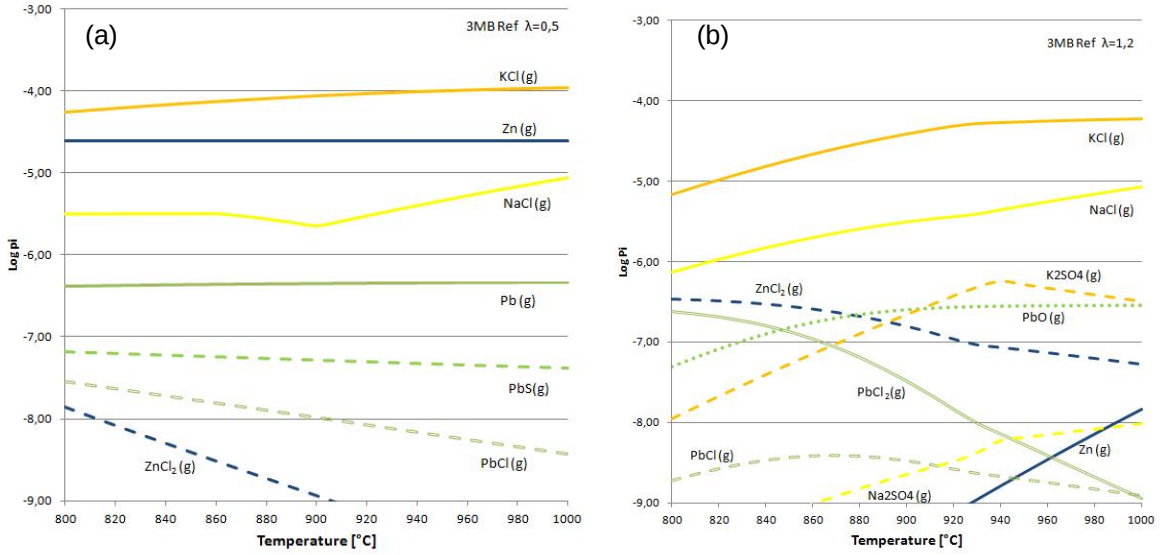

Figure 1, The partial pressure of the thermodynamically stable gaseous lead, zinc, potassium and sodium compounds for the two calculation zones ((a) λ=0,5 and (b) λ=1,2) for the reference case as functions of temperature (800 - 1000 °C).

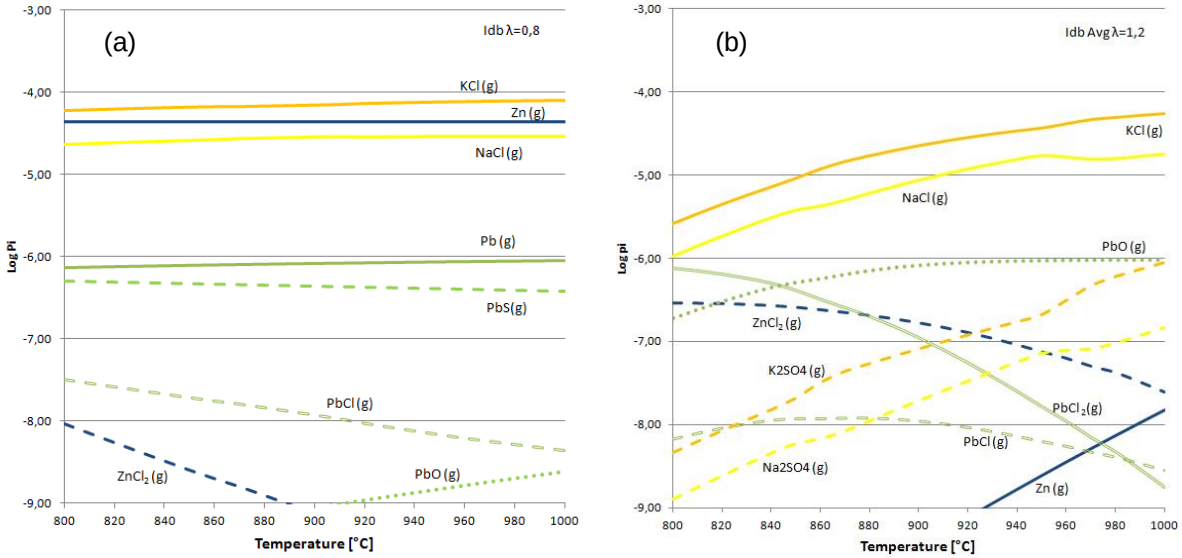

Figure 2, The partial pressure of the thermodynamically stable gaseous lead, zinc, potassium and sodium compounds for the two calculation zones ((a) λ=0,8 and (b) λ=1,2) for the Idbäcken case as functions of temperature (800 - 1000 °C).

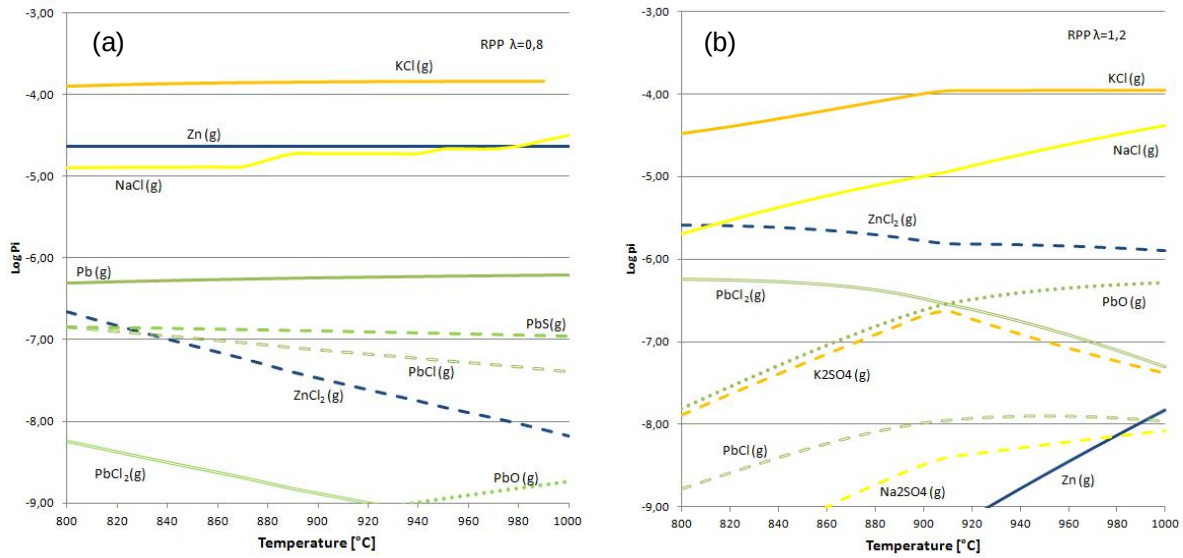

Figure 3, The partial pressure of the thermodynamically stable gaseous lead, zinc, potassium and sodium compounds for the two calculation zones ((a) λ=0,8 and (b) λ=1,2) for the RPP (KME601) case as functions of temperature (800 - 1000 °C).

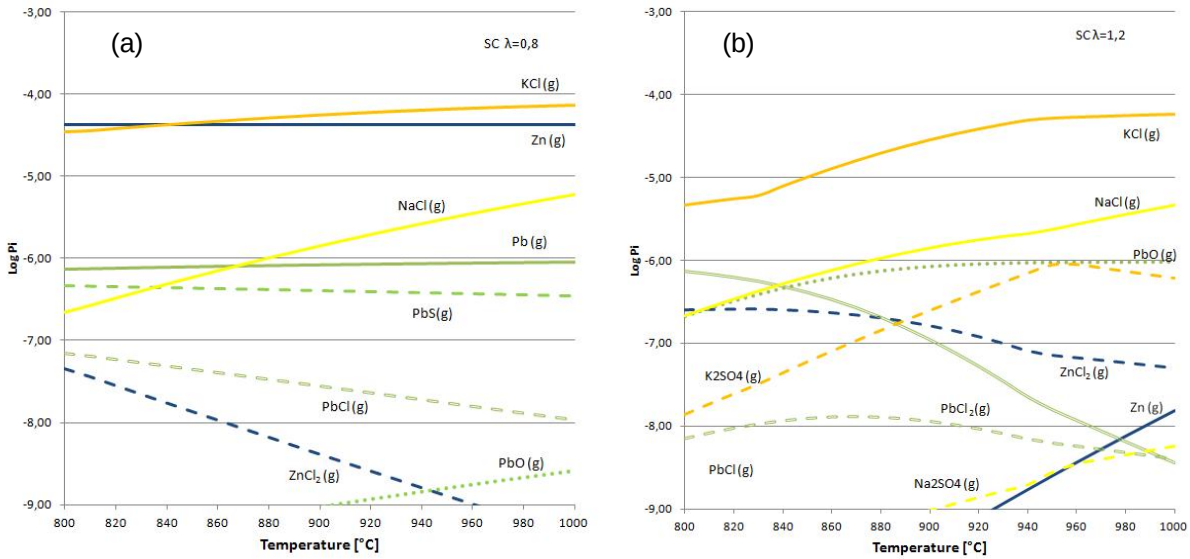

Figure 4, The partial pressure of the thermodynamically stable gaseous lead, zinc, potassium and sodium compounds for the two calculation zones ((a) λ=0,8 and (b) λ=1,2) for the Steven's croft case as functions of temperature (800 - 1000 °C).

3.2 Condensation of gaseous lead, zinc, potassium and sodium compounds

The condensation temperatures of the gaseous zinc, lead, potassium and sodium compounds were calculated from the saturation curves for each compound, presented in Figure 5.

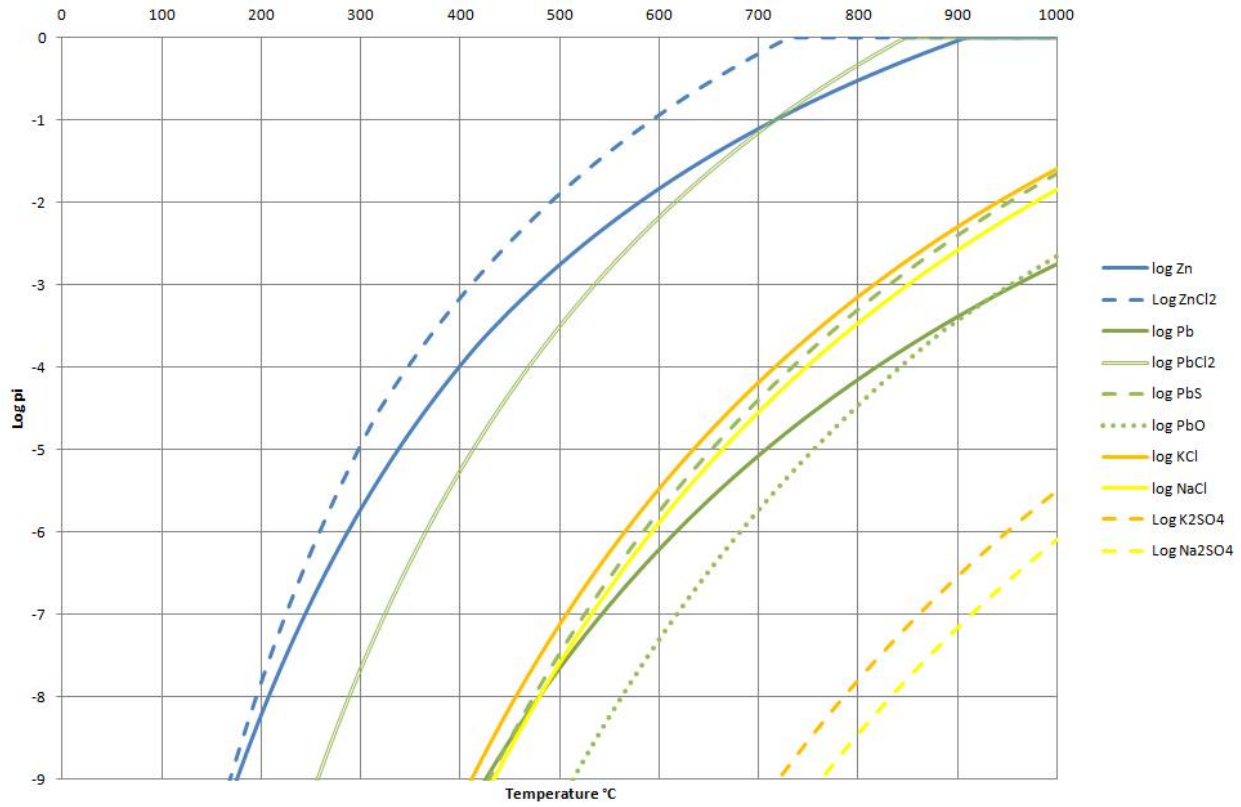

Figure 5, Saturation curves of stable gaseous lead, zinc, potassium and sodium compounds

For each compound, the maximum concentration within the studied temperature interval was used in order to describe the worst-case scenario. The condensation temperatures of gaseous lead, zinc, potassium and sodium compounds are than estimated from Figure 5. The condensation and melting temperature are shown in Table 2.

In reducing conditions, the condensation temperatures for Zn are in the studied cases between 358 - 374 °C, depending on the amount of zinc in the fuel. The melting point of Zn is 420 °C, which means that Zn will deposit as solid Zn. The condensation temperature of $ZnCl_2$ is varies between 193 – 235 °C in the studied cases, which are lower than melting temperature, 318 °C, $ZnCl_2$. The condensation temperature for $ZnCl_2$

is however lower than any surface temperatures typically found in the furnace and hence condensation of $ZnCl_2$ is unlikely to occur. Similar result for Zn and $ZnCl_2$ in oxidizing conditions.

	p(i) max	T(cond)	Tm
Zn ref 0,5	2,4E-05	359	420
Zn ldb 0,8	4,3E-05	374	
Zn RPP 0,8	2,3E-05	358	
Zn SC 0,8	4,3E-05	374	
Zn ref 1,2	1,5E-08	212	420
Zn ldb 1,2	1,5E-08	212	
Zn RPP 1,2	1,5E-08	212	
Zn SC 1,2	1,5E-08	212	
ZnCl2 ref 0,5	1,4E-08	198	318
ZnCl2 ldb 0,8	9,2E-09	193	
ZnCl2 RPP 0,8	2,2E-07	235	
ZnCl2 SC 0,8	4,5E-08	213	
ZnCl2 ref 1,2	3,4E-07	241	318
ZnCl2 ldb 1,2	2,9E-07	239	
ZnCl2 RPP 1,2	2,6E-06	273	
ZnCl2 SC 1,2	2,6E-07	237	
Pb ref 0,5	4,6E-07	589	328
Pb ldb 0,8	8,9E-07	611	
Pb RPP 0,8	6,2E-07	599	
Pb SC 0,8	9,1E-07	612	
Pb ref 1,2	1,6E-10	387	328
Pb ldb 1,2	5,5E-10	412	
Pb RPP 1,2	3,1E-10	400	
Pb SC 1,2	5,7E-10	412	
PbS ref 0,5	6,5E-08	513	1113
PbS ldb 0,8	5,1E-07	564	
PbS RPP 0,8	1,4E-07	532	
PbS SC 0,8	4,7E-07	562	
PbS ref 1,2	4,3E-21	145	1113
PbS ldb 1,2	2,3E-20	156	
PbS RPP 1,2	7,5E-21	149	
PbS SC 1,2	3,2E-20	159	

	p(i) max	T(cond)	Tm
PbCl2 ref 0,5	2,8E-10	240	501
PbCl2 ldb 0,8	1,9E-10	235	
PbCl2 RPP 0,8	5,8E-09	279	
PbCl2 SC 0,8	9,3E-10	255	
PbCl2 ref 1,2	2,4E-07	338	501
PbCl2 ldb 1,2	7,6E-07	359	
PbCl2 RPP 1,2	5,7E-07	354	
PbCl2 SC 1,2	7,4E-07	359	
PbO ref 0,5	2,7E-10	487	886
PbO ldb 0,8	2,5E-09	531	
PbO RPP 0,8	1,8E-09	525	
PbO SC 0,8	2,6E-09	532	
PbO ref 1,2	2,9E-07	644	886
PbO ldb 1,2	9,5E-07	679	
PbO RPP 1,2	5,3E-07	661	
PbO SC 1,2	9,5E-07	679	
KCl ref 0,5	1,1E-04	719	771
KCl ldb 0,8	8,1E-05	707	
KCl RPP 0,8	1,5E-04	731	
KCl SC 0,8	7,4E-05	704	
KCl ref 1,2	6,0E-05	696	771
KCl ldb 1,2	5,5E-05	693	
KCl RPP 1,2	1,1E-04	720	
KCl SC 1,2	5,7E-05	694	
K2SO4 ref 0,5	4,3E-17	418	1069
K2SO4 ldb 0,8	1,4E-13	532	
K2SO4 RPP 0,8	1,4E-15	463	
K2SO4 SC 0,8	2,2E-14	502	
K2SO4 ref 1,2	5,7E-07	925	1069
K2SO4 ldb 1,2	9,0E-07	943	
K2SO4 RPP 1,2	2,3E-07	890	
K2SO4 SC 1,2	8,8E-07	943	

	p(i) max	T(cond)	Tm
NaCl ref 0,5	8,8E-06	658	801
NaCl ldb 0,8	2,9E-05	699	
NaCl RPP 0,8	3,2E-05	703	
NaCl SC 0,8	5,9E-06	645	
NaCl ref 1,2	8,4E-06	656	801
NaCl ldb 1,2	1,8E-05	682	
NaCl RPP 1,2	4,1E-05	712	
NaCl SC 1,2	4,6E-06	637	
Na2SO4 ref 0,5	4,1E-19	385	884
Na2SO4 ldb 0,8	2,7E-14	534	
Na2SO4 RPP 0,8	9,9E-17	451	
Na2SO4 SC 0,8	2,1E-16	461	
Na2SO4 ref 1,2	9,7E-09	830	884
Na2SO4 ldb 1,2	1,5E-07	927	
Na2SO4 RPP 1,2	8,3E-09	825	
Na2SO4 SC 1,2	5,8E-09	814	

Table 2, The condensation temperatures of gaseous lead, zinc, potassium and sodium compounds. All meting temperature except K_2SO_4 and Na_2SO_4 were taken from Enestam 2011.

Under reducing conditions, lead is fully volatized in the investigated temperature range. The main lead compound formed is Pb (g). The calculated condensation temperature for Pb (g) is 589 – 612 °C. The melting point of metallic lead is 328 °C, so there is a risk of condensation of molten metallic Pb on surfaces in the range 328 – 612 °C. Under reducing conditions lead can also form PbS (g). The calculated condensation temperature for PbS (g) is 513 – 564 °C. The melting point of PbS is 1118 °C, and therefore PbS is deposited in solid form. The condensation temperature of $PbCl_2$ is between 240 - 279 °C. The melting point for $PbCl_2$ is 501 °C and hence $PbCl_2$ will deposit in solid form.

In oxidizing conditions, the condensation temperature of PbO is between 644 - 679 °C. This means that deposition of PbO can occur at surface temperatures lower than 644 - 679 °C and flue gas temperatures above 870 °C. The melting point of PbO is 886 °C, so PbO is deposited in solid form. At flue gas temperatures below approximately 870 °C,

$PbCl_2$ is predicted to be the most stable lead compound. The condensation temperature of $PbCl_2$ is around 338 – 359 °C. This means that deposition of $PbCl_2$ can occur at surface temperatures lower than 338 – 359 °C and flue gas temperatures below 870 °C. The melting point of $PbCl_2$ is 501 °C, so $PbCl_2$ will be deposited in solid form.

The condensation temperature of KCl is around 693 – 720 °C in oxidizing conditions and 704 – 719 °C in reducing conditions. Since the melting temperature of KCl is 770 °C, KCl can deposit in solid form. In oxidizing conditions, the condensation temperature of the K_2SO_4 is between 890 – 943 °C for oxidizing conditions. Since the melting temperature of K_2SO_4 is 1069 °C, K_2SO_4 may deposit as solid.

The condensation temperature of NaCl is around 637 – 712 °C in oxidizing conditions and 645 – 712 °C in reducing conditions. Since the melting temperature of KCl is 801 °C, NaCl can deposit as solid. In oxidizing conditions, the condensation temperature of Na_2SO_4 is between 814 – 927 °C. Since the melting temperature of K_2SO_4 is 884 °C, K_2SO_4 may deposit as molten or solid phase.

3.3 Discussion and comparison of results with measured data

It is difficult task to exactly describe the furnace environment. In the lower part of the furnace, reducing condition is expected while oxidizing condition is expected in higher parts of the boiler (after secondary and tertiary air system). The different part of the boiler environment may be simplified by regarding as more or less (fluctuating) reducing and oxidizing conditions and described by calculating the equilibrium compositions of given fuel mixture in reducing and oxidizing conditions. In table 3, the results of the O_2 measurement with SICK instrument are shown in different boiler wall positions from Idbäcken. The level of O_2 differs a lot even when the positions of the measurement were at about the same height of the boiler.

Pos	Distance from wall	FTIR										Sick	
		CO	NO	SO2	NH3	HCl	HF	CH4	NOx	H2O	CO2	O2	Temp
	(m)	(ppm)	(ppm)	(ppm)	(ppm)	(ppm)	(ppm)	(ppm)	(ppm)	(%)	(%)	(% tg)	(°C)
A	0,1	17436	50	24	277	7,9	0,8	931	51	18	3	0,7	873
	0,8	18760	10	15	207	9,0	0,7	876	11	17	3	1,1	1089
B-C	0,1	19035	88	76	438	0,1	1,2	2497	85	26	5	0,6	701
	0,8	19179	88	67	408	3,7	1,1	2544	86	24	5	0,2	968
D	0,1	37702	81	74	1090	42,2	1,1	2578	104	22	26	0,3	792
	0,8	35811	21	53	876	16,8	1,0	2838	22	25	-3	0,4	1055
D	0,1	39663	42	56	1182	47,2	2,0	2497	62	18	25	0,2	910
	0,8	29793	10	17	845	12,4	1,5	2963	9	18	0	0,2	1058
F	0,1	6991	126	46	102	7,5	0,7	401	127	22	9	0,6	829
	0,8	22279	7	26	440	1,0	0,4	1896	7	21	3	0,2	1024
F	0,1	874	167	58	35	22,7	0,9	38	171	16	11	1,7	875
	0,8	1393	175	74	56	20,2	1,1	65	178	17	11	1,6	1115
G	0,1	1862	170	30	80	4,4	0,9	135	173	21	13	1,8	823
	0,8	3723	188	52	59	7,3	0,8	269	190	21	11	0,9	1049
G	0,1	315	179	76	14	21,5	1,0	29	182	16	11	2,2	888
	0,8	1524	181	92	15	23,8	1,0	119	184	17	10	1,3	1125
J	0,1	20941	45	33	400	3,7	1,0	1618	46	18	2	0,3	910
	1,2	23234	2	18	462	2,7	1,1	2153	1	19	1	1,4	1002
K	0,1	35	184	26	50	8,7	0,7	0	188	18	16	4,1	923
	1,2	155	169	39	42	22,1	0,5	8	174	20	15	3,8	973
K	0,1	38237	42	55	1178	44,1	2,0	2626	59	18	23	2,2	943
	1,2	30233	7	13	822	10,9	1,4	2884	4	18	-1	2,6	1007

Table 3, FTIR result from Idbäcken, taken from Appendix D, Vattenfall Memo U13-03

In table 4 below, the expected condensed components in both reducing and oxidizing conditions are listed.

	Component expected	~~Component expected in small amount~~
Reducing conditions	Zn (s), Pb (l), PbS (s), KCl (s), NaCl (s)	~~$ZnCl_2$ (s), $PbCl_2$ (s), PbO (s)~~
Oxidizing conditions	ZnO (s), PbO (s), $PbCl_2$ (s), KCl (s), NaCl (s),	K_2SO_4 (s), Na_2SO_4 (s)

Table 4, The expected condensed components in reducing and oxidizing conditions

In the lower, reducing part of the furnace K, Na, Zn and Pb are all volatilized, according to the equilibrium calculations. Potassium and sodium are mainly found as chlorides in the gas phase and the alkali chlorides are expected to condense in solid form on the furnace walls. Zinc is volatilized as Zn (g) and lead mainly as Pb (g) and PbS (g). Zinc is predicted to condense as Zn (s) and lead as Pb (l) and PbS (s).
Small fractions of PbCl (g), PbO (g) and $ZnCl_2$ (g) are also predicted to form but PbCl is not stable in condensed form, PbO (g) exists in very small concentrations (ppb level) and the condensation temperature of $ZnCl_2$ is very low (around 250 °C), and hence the condensation of these compounds on the furnace wall is not expected to be of great significance.

Under oxidizing conditions and furnace temperatures (> 800 °C), the main part of both potassium and sodium are found in the gas phase as KCl (g) and NaCl (g), a smaller part of the alkali metals are found as gaseous sulphates. Under oxidizing conditions condensation of alkali metals can be expected mainly as alkali chlorides, but possibly to some extent also as sulphates. Zinc will under oxidizing conditions mainly be found as ZnO (s), with a small fraction (a few percent) forming $ZnCl_2$ (g). The solid ZnO will obviously not cause condensation and the condensation temperature of $ZnCl_2$ is low (approximately 250 °C), hence condensation of zinc in the oxidizing part of the furnace is not expected to be significant.

The prediction of condensation of alkali chlorides and sulphates is supported by the deposit analyses from Idbäcken where chlorine, potassium and sulphur were found in all deposit samples and sodium in most. KCl, NaCl and $(K,Na)SO_4$ were identified by XRD. $(K,Na)SO_4$ might have been formed in the deposit through a reaction between Na_2SO_4 and K_2SO_4. Also XRD analyses of deposits colledted on corrosion probes in Idbäcken confirmed the prescence of KCl and NaCl in the deoposits.

Pb was found in a third of the long term deposit samples collected in Idbäcken, at low average concentrations, but high concentrations locally. Scanning electron microscopy showed that lead, when present in a deposit, was heterogeneously distributed and could be observed as “islands” of pure lead or in mixtures containing oxygen, for example Pb-Cl-O mixtures or Pb-K-S-O mixtures. In the XRD analysis lead was identified as Pb_2OSO_4 and $K_2Pb(CrO_4)_2$. The potassium lead chromate is most probably a corrosion product. The finding of pure lead in the deposits is in good agreement with

the calculations, the other experimental findings do not clearly support the calculations. Since the deposits analysed were longtime deposits collected from the boiler it is impossible to know in which form lead originally has bee deposited on the walls and what reactions have taken place in the deposits.
In the impactor measurements done in Idbäcken, lead was found in sub-micron particles together with Cl, K, Na, Zn and S which indicates that laed has been in the gas phase, which is in consictency with the calcualtions.
In the depoists from the corrosion probe exposed in Idbäcken lead was found as pure lead and lead oxide which is in very good agreement with the calculations.

Zn was found in three-quarters of the long term deposit samples from Idbäcken in low concentrations, zinc could not be identified by XRD but chrystals of $ZnCl_2$ were occasionally observed by SEM-EDX. Formation of $ZnCl_2$(g) was predicted in small concentrations under both oxidizing and reducing conditions. Condensation of $ZnCl_2$ was not predicted to occur in the furnace due to the low condensation temperatures, but the finding of $ZnCl_2$ in the deposits indicate that condensation of $ZnCl_2$ has taken place.
As for lead, the finding of zinc in the sub-micron particle fraction in the impactor measurements indicates that zinc has been in the gas phase in the furnace.
Analyses of long term deposits from Stevens croft showed higher amounts of zinc in samples collected below the tertiary air level (level 1) than above the tertiary level (level 5). This could possibly be explained by the equilibrium calculations that predict condensation of Zn under reducing conditions but not (significantly) under oxidizing conditions.

3.4 Differences in output data and databases

The differences in results between Metso and Vattenfall can partly be explained by differences between data bases. The database used by Metso is a tailor made database, based mainly on data from FACT whereas Vattenfall has used the HSC database. Thermodynamic data for zinc and lead in FACT and HSC have been compared in detail in the licentiate thesis of Tarja Talonen. However, the database used by Metso is not based solely on FACT data but contains additional data for the liquid solution of the system (K, Na, Pb, Zn)(Cl, CO_3, SO_4). This might also cause discrepancies between the results. Moreover, the reactivity of other ash forming elements, such as calcium, aluminum and silicate will influence on the formation of alkali, zinc and lead compounds. The assumptions used by Vattenfall and Metso have not been compared in detail due to proprietary rights.

Below some major differences between HSC and FACT data bases, described by Talonen, are listed for the temperature range 800 - 1000 °C.

3.4.1 Lead

Oxidizing Conditions
Talonen describes that the phase distributions of lead according to the HSC, and FACT databases resemble one other. $PbCl_2$ (g) is dominant within temperature range 700-1100 °C. PbCl (g) begins to form above 800 °C. PbO (g) is, however, slightly more stable according to FACT-data, which, at least partly, can explain the difference between the Metso and Vattenfall results where PbO (g) was formed under oxidizing conditions in the Metso calculations but not in the Vattenfall calculations (see Appendix I).

Reducing Conditions
Under reducing conditions, the main lead compounds formed are the same with both databases but $PbCl_2$(g) and PbS are more stable in FACT than in HSC, wheras Pb(bl)[1] is more stable in HSC.

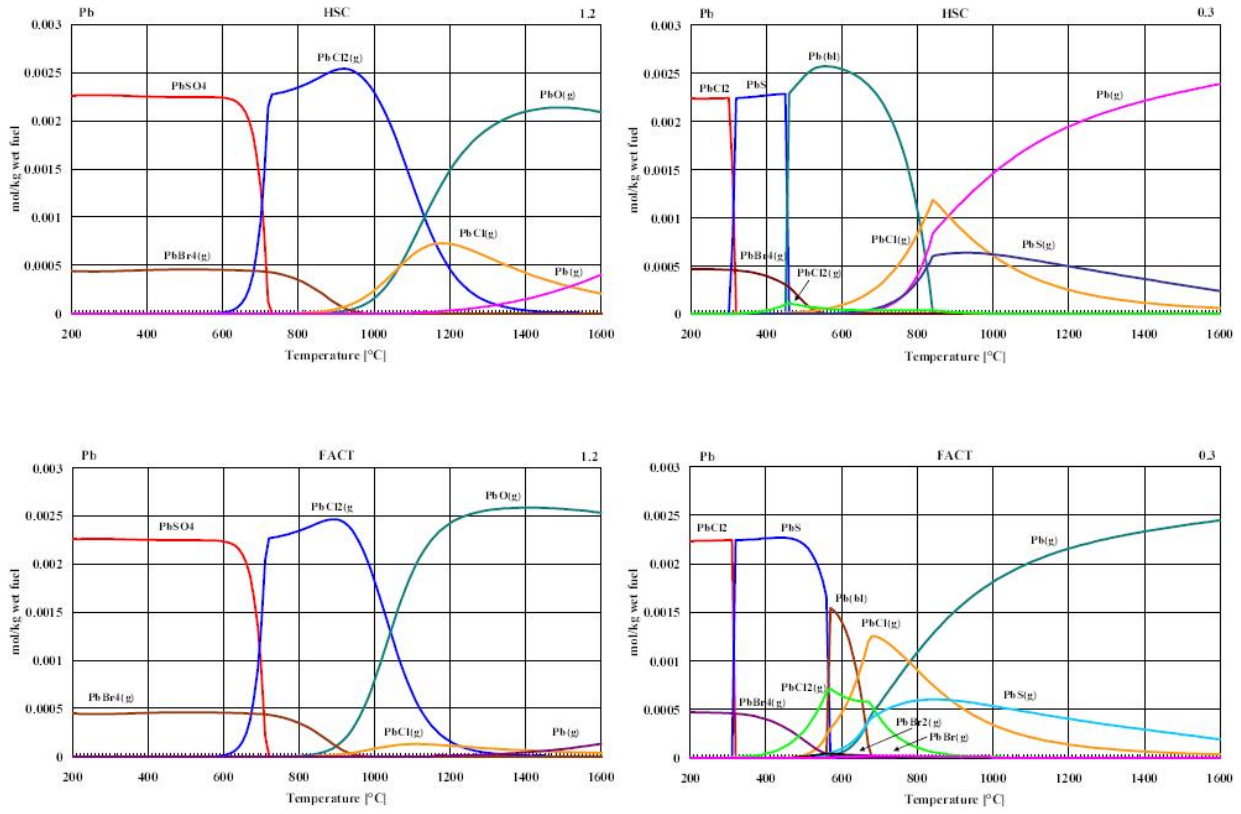

Figure 6, Comparison of the HSC and FACT results of the equilibrium calculations of Pb compounds in both oxidizing and reducing conditions, taken from Talonen 2008.

[1] *The notation (bl) means that the thermodynamic values of the liquid in the database have been extrapolated to room temperature (298.15 K)*

3.5 Zinc

Oxidizing Conditions

Under oxidizing conditions, the phase distribution reported by the FACT database is very similar to that reported by HSC, but $ZnCl_2$ (g) is has a higher stability according to the FACT data. For example, the higher concentration of $ZnCl_2$ (g) in the Vattenfall results compared to Metso results in oxidizing conditions may be explained by Figure 7, where $ZnCl_2$ (g) is more dominating spice in HSC compared to FACT.

Reducing Conditions

Under reducing conditions, HSC and FACT give nearly identical phase distribution for zinc.

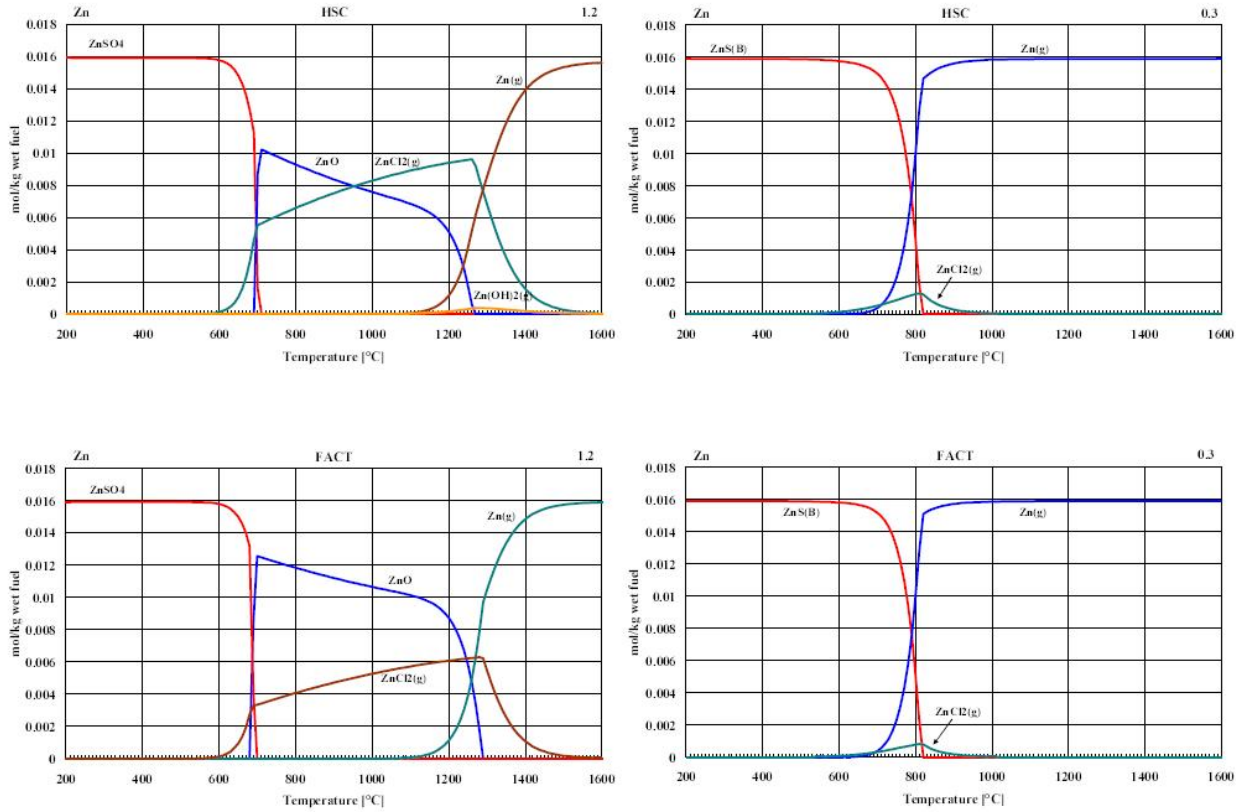

Figure 7, Comparison of the HSC and FACT results of the equilibrium calculations of Zn compounds in both oxidizing and reducing conditions, from Talonen 2008

4 References

S. Enestam, R. Backman, K. Mäkelä, M. Hupa, ”Evaluation of the condensation behavior of lead and zinc in BFB combustion of recovered waste wood”, Fuel Processing technology 105 (2013) 161-169

S. Enestam, “Corrosivity of hot flue gases in the fluidized bed combustion of recovered waste wood”, Åbo Akademi, report 11-04, 2011

M. Glazer, “HSC modeling results for KME – 508 project” Vattenfall report 2013, PR.263.1.9

T. Talonen, “Chemical equlibria of heavy metals in waste incinerations: Comparison of thermodynamic databases, Åbo Akademi, report 08-02, 2008

Backman, R., Skrifvars, B-J., Yrjas, P., Ed. (2005). The influence of aerosol particles on the melting behavior of ash deposits in biomass fired boilers. Aerosols in biomass combustion, Thermal biomass combustion. Graz.

Bale, C. W., et al. (2009). "FactSage thermochemical software and databases -- recent developments." Calphad **33**(2): 295-311.

Koukkari, P., et al. (2000). ChemSheet - an efficient worksheet tool for thermodynamic process simulation. Weinheim, Wiley-VCH Publishers.